

International Journal of Computational and Engineering

DECEMBER 2018 VOLUME3 NUMBER4

Publisher: ACADEMIC PUBLISHING HOUSE
Address: Quastisky Building, Road Town, Tortola, British Virgin Islands
UK Postal Code: VG1110

E-mail: editorial@ij-ce.com
www.ij-ce.com



ACADEMIC PUBLISHING HOUSE

CONTENTS

RESEARCH ON MECHANICAL BEHAVIOR DURING WARM DEFORMATION OF GCR15 BEARING STEEL.....	1
APPLICATION OF BIG DATA TECHNOLOGY IN SMART TOURISM PROJECTS IN HENAN.....	5
OVERVIEW OF MOVING TARGET DETECTION ALGORITHMS.....	8
RETURN OF NOKIA: THE CALL OF CRAFTSMAN SPIRIT IN THE INTERNET ERA.....	11
CONVERTER ENDPOINT PREDICTION MODEL BASED ON GA-BP NEURAL NETWORK MODEL.....	14
RESEARCH ON OPTICAL CHARACTER RECOGNITION BASED ON BP NEURAL NETWORK...17	
IDENTIFICATION BASED ON COLOR AND SUBSTANCE CONCENTRATION.....	21
VEHICLE BRAKE AIR ENERGY STORAGE AND ENERGY CONVERSION DEVICE.....	25
DESIGN OF URBAN DOMESTIC WASTE TREATMENT CHARGE SCHEME BASED ON FACTOR ANALYSIS.....	29
SLEEP DISEASE RESEARCH BASED ON SVM AND FUZZY COMPREHENSIVE EVALUATION..33	
OVERLAY TRAJECTORY OPTIMIZATION OF SPRAY GUN SPRAYING.....	36
BASED ON IMPROVED CPSO-LSSVM BLAST FURNACE HOT METAL TEMPERATURE PREDICTION MODEL.....	41
BASED ON DIFFERENTIAL EQUATION HOT WATER BATH MODEL.....	45
RESEARCH ON INFLUENCE FACTORS OF BATHTUB HEAT DISSIPATION BASED ON HEAT CONDUCTION EQUATION.....	51
MULTI-HOP HF RADIO PROPAGATION.....	56
PREDICTION OF REFLECTIVITY OF COAL-FIRED VITRINITE BASED ON KNN ALGORITHM64	
SOLUTION TO CT SYSTEM PARAMETER BASED ON SINUSOIDAL TRIGONOMETRIC FUNCTION.....	67
RECOGNITION OF COLOR AND MATTER CONCENTRATION BASED ON REGRESSION ANALYSIS.....	71
DESIGN OF SPECIAL SERVICE FOR HIGH TEMPERATURE OPERATION BASED ON PARTIAL DIFFERENTIAL EQUATION.....	74
COURSE SELECTION MODEL BASED ON 0-1 PROGRAMMING.....	78
TEMPERATURE DISTRIBUTION OF HIGH TEMPERATURE CLOTHING UNDER UNSTEADY HEAT CONDUCTION.....	82
RESEARCH ON LOGISTICS FINANCIAL SUPERVISION RISK BASED ON BP NEURAL NETWORK ALGORITHM.....	86
RESEARCH ON A RESOURCE SCHEDULING ALGORITHM BASED ON CLOUD TASK.....	90
SHADOW LOCALIZATION BASED ON SPHERICAL TRIANGLE.....	93
DYNAMIC SCHEDULING STRATEGY OF INTELLIGENT RGV BASED ON OPTIMAL PATH.....	98
SWARM INTELLIGENCE APPLICATION IN COGNITIVE RADIO.....	103

MULTI-SHIP COLLISION AVOIDANCE OPTIMIZATION BASED ON SHIP COLLISION AVOIDANCE SYSTEM.....	108
DYNAMIC MODELING OF AERIAL REFUELING.....	114
DECOUPLING KERNELS FROM HASH TABLES IN SYMMETRIC ENCRYPTION.....	117
DISCUSSION ON APPLICATION VALUE OF DI-RECTDIGIT RADIOGRAPHY(DR) PHOTOGRAPHY TECHNOLOGY IN RADIOLOGY.....	121
EXPONENTIAL STABILITY CONTROL OF NONLINEAR STOCHASTIC NETWORKED SYSTEMS	124
SIMULATING RED-BLACK TREES AND ACCESS POINTS.....	129
THE ENLIGHTENMENT OF US ARMY EQUIPMENT EMERGENCY MAINTENANCE TRAINING TO OUR ARMY TRAINING.....	133
A CLOUD COMPUTING LOAD BALANCING FORECASTING MODEL.....	138
EXPLORE THE APPLICATION OF MATHEMATICS IN PHYSICS.....	142
FINITE-TIME TRACKING CONTROL OF QUANTUM SYSTEMS WITH TARGET FUNCTION... 	146
RESEARCH ON THE EFFECTS OF DME’S TEMPERATURE ON POWER PERFORMANCE OF A TURBOCHARGED DME ENGINE.....	150
PROFESSIONAL MODELS IN DESIGNING CLOUD-BASED DISTRIBUTED STORAGE SYSTEMS	153
RESEARCH AND CONSTRUCTION OF PRACTICAL TEACHING SYSTEM OF SOFTWARE ENGINEERING SPECIALTY BASED ON CDIO.....	159

Research on Mechanical Behavior during Warm Deformation of GCr15 Bearing Steel

Wang Sufen*, Li Zhijie, Wu Mingming

College of Mechanical Engineering, Quzhou University, Quzhou, Zhejiang, 324000, China

*E-mail: wangsufen09@163.com

Abstract: GLEEBLE-3500 thermal simulation test machine was used to study the warm deformation process of GCr15 bearing steel. Besides, the influence rules of deformation temperature and deformation rate on mechanical behaviors of deformation of the test steel, and its microstructure were investigated. The results show that, there is obvious working softening phenomenon when the steel deforms under 600 °C ~700 °C; the deformation temperature rises, m value increases and flow stress value presents exponential decline; significant fracture and crush happen to cementite sheet and presents granular distribution during deformation under 650 °C.

Key words: GCr15 bearing steel; warm deformation; flow stress; microstructure.

1. INTRODUCTION

With high requirements for hardness, abrasive resistance, toughness and contact fatigue strength, GCr15 bearing steel is used to manufacture ferrule, pin roller and other parts of bearings. In order to gain excellent performance, proper strengthening and toughening treatment is usually done on the basis of favorable alloy composition and metallurgy process control so as to get the good working stability and mechanical property. Thus, many scholars studied heating processing technology of bearing steel [1-3]. Xiao Maoguo et al.[4] explored strengthening and toughening mechanism of high-temperature bearing steel, and secondary tempering hardening after secondary tempering. Cao Xin et al. [5] researched the mathematical model of high-temperature austenite grain growth of bearing steel. Wang Yanshan et al. [6] investigated double refining process of GCr15 bearing steel, and drew the conclusion that various performance indexes of bearing steel improve greatly through refining grain size and carbide of bearing steel. All of their studies show that, the proper process refining can effectively enhance mechanical properties of bearing steel and obtain favorable toughness so as to promote mechanical properties of bearing steel[7]. Moreover, many scholars also studied structure refining process in quantity. The research results indicate that, low-temperature deformation process can effectively refine material structure and enhance mechanical properties. However, rheological behaviors of low-temperature molding of metal materials are different from conventional temperature, and their mechanical behaviors, microstructure

evolution and influence mechanism are too complex. In this paper, rheological behavior and microstructure evolution of GCr15 bearing steel in the warm deformation process are studied, and the influence rules are analyzed.

2. EXPERIMENTAL METHOD

2.1 Experimental material

The chemical components of test samples include C: 0.95~1.05 Mn: 0.20-0.40 Si: 0.15-0.35 S: ≤ 0.020 P: ≤ 0.027 Cr: 1.30-1.65. Mono-axle warm compression experiment was conducted on GLEEBLE-3500 thermal simulation test machine, and the test samples were processed into the cylinders with the size of $\Phi 10\text{mm} \times 15\text{mm}$ and $\Phi 8\text{mm} \times 12\text{mm}$. Wire electric discharge machine was applied to cut the sample from the center and sample as shown in Fig.1. After inlaying, polishing, burnishing and cleaning of the test samples, 4% nital was used to etch the samples. Microstructure observation was carried out under Hitachi S-4800 scanning electron microscope (SEM), and the analysis software was applied to measure ferrite grain size and carbide particle size.

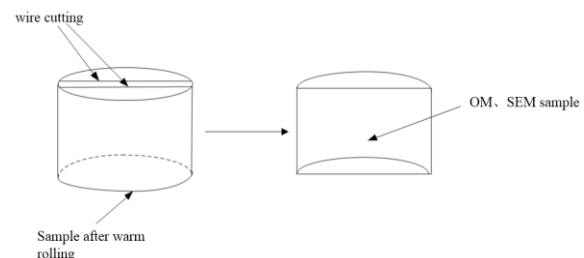


Figure.1 Sketch of cutting the sample

2.2 Process route of experiment

The deformation process is shown in Fig.2. Complete austenitizing was first conducted for the test samples. Then, the test samples were cooled to certain temperature to gain the required structure property for the convenience of thermal treatment or thermal deformation of materials. The test samples were heated to certain temperature and kept isothermy for 3min. Then, the test samples were cooled to the deformation temperature at the speed of 10 °C/s. After heat preservation for 3min, warm deformation was conducted, and then water quenching for cooling was carried out.

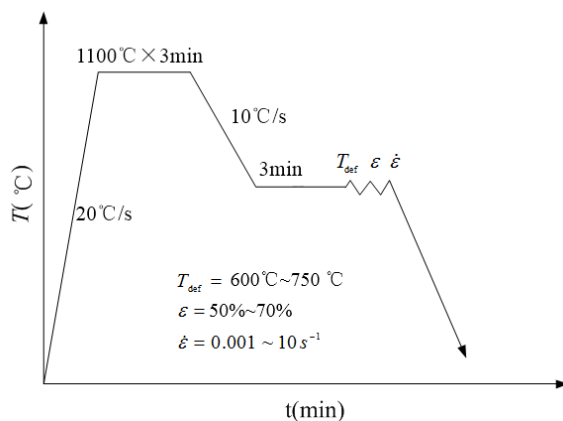


Figure.2 Technology of GCr15 steel warm deformation

3. EXPERIMENTAL RESULT AND DISCUSSION

3.1 Analysis of flow stress curve

Flow stress curves of warm compression deformation of GCr15 bearing steel are shown in Fig.3. After deformation starts, the test steel presents sharp work-hardening, and the stress increases quickly. Then, work-hardening weakens. After the peak stress appears, the material presents fast and strong softening. With the continuous increase of strain, flow stress declines. Finally, deformation reaches the stable stage, and internal hardening and softening of the material reach balance. The deformation increases, while flow stress almost does not change.

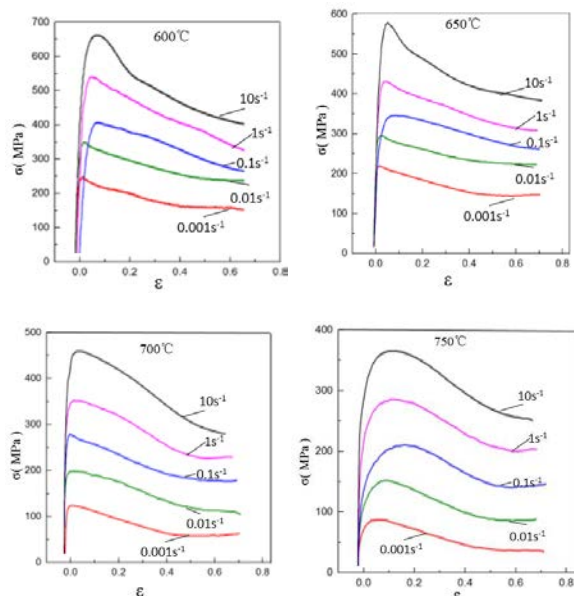


Figure.3 Flow stress curve of steel warm deformation
Characteristic value of flow stress curve can be confirmed by work-hardening rate θ .

$$\theta = \frac{d\sigma}{d\varepsilon} \approx \frac{\Delta\sigma}{\Delta\varepsilon}$$

Fig.4 shows work hardening rate curves of GCr15 bearing steel. It can be seen from the figure that, working softening is not obvious when deformation happens under 750 °C. There is obvious working

softening when deformation happens under 600 °C ~ 700 °C. When the deformation is close to peak strain, θ value has an inflection point.

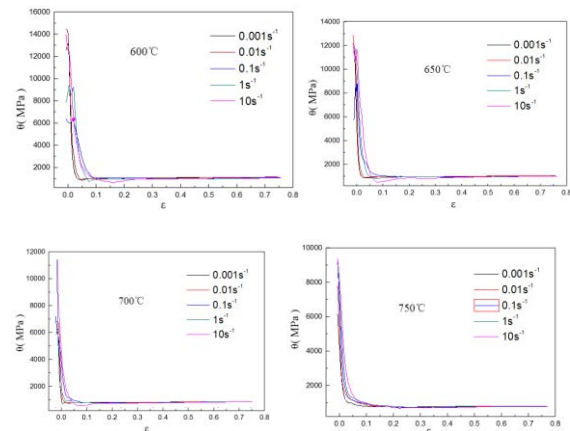
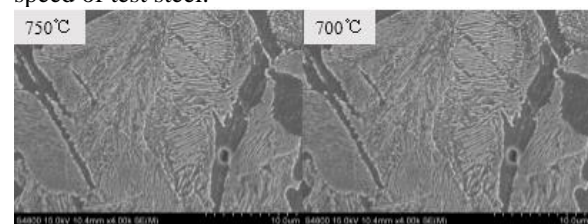


Figure.4 Work-hardening rate curves

3.2 Microstructure evolution in deformation process

Based on flow stress curves and work-hardening rate curves under different deformation temperatures, after warm compression deformation starts, deformation presents strong work-hardening. After the peak stress reaches, strong softening begins. Finally, the steady-state process of flow stress is achieved. The microstructure evolution of warm deformation is shown in Fig.5. According to the figure, pearlite sheet structure is intact during deformation under 750 °C, and the orientation of pearlite colony changes. The deformation process mainly leads to orientation change of partial pearlite colony and large F plastic deformation. Hardening happens to both P and F. During deformation under 700 °C - 650 °C, cementite sheet twisting and fracture happen to P structure in the material, and dynamic recrystallization happens to F structure. In this process, stress concentration appears to partial cementite sheet with the slow increase of deformation, thus resulting in sheet crush. Since sheet structure is partially destroyed, restraint intensity of F in the degraded P decreases, which leads to certain degree of softening. Meanwhile, deformation of each part in the internal is coordinated to generate large plastic deformation. During deformation under 600 °C, metallographic phase presents quicksand shape due to refining, and cementite sheet is crushed in quantity and presents granular distribution, as shown in the figure. This will be beneficial for accelerating spheroidizing speed of test steel.



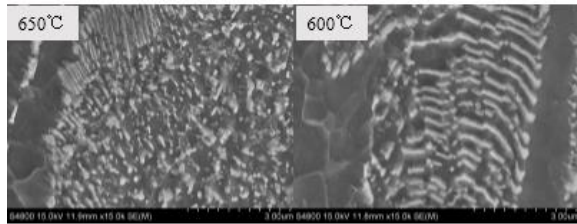


Figure.5 SEM of the microstructure of GCr15 steel warm deformation

3.3 Influence of temperature

Fig.6 shows the effect of temperature on flow stress under different rate. According to the figure, flow stress value presents exponential reduction with temperature rise under each deformation rate. But, the warm deformation process of carbon steel cannot be simply described by the linear relation between \ln and T . The effect of temperature on flow stress changes with deformation.

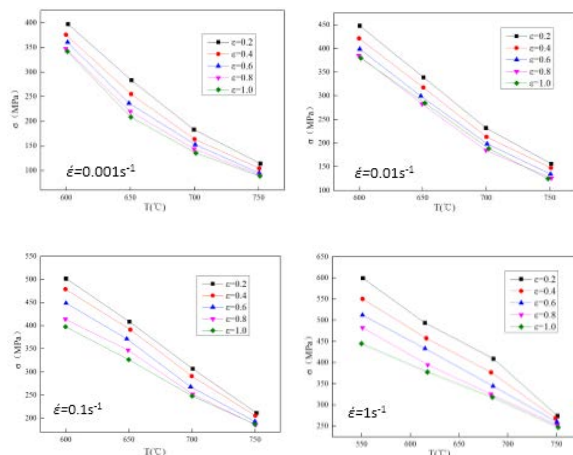


Figure.6 Influence of temperature on flow stress

3.4 Influence of deformation rate

Fig.7 shows the influence rules of deformation rate on flow stress. According to the figure, when temperature remains unchanged, flow stress increases with the rise of deformation rate. This is because hardening rate will increase with the rise of deformation rate, and lots of dislocation, vacancy and other defects happen in a short time. Meanwhile, dislocation tangle happens in quantity, and thus obvious work-hardening forms. In addition, the increase of deformation rate leads to insufficient time for softening process or insufficient softening process in the deformation process. At this moment, warm deformation shows significant work-hardening phenomenon, and flow stress increases. When steel deforms under the constant temperature, the logarithm of strain rate and the logarithm of flow stress present the linear relation, and the relational expression is

$$\sigma = \sigma_0 \left(\frac{\dot{\epsilon}}{\dot{\epsilon}_0} \right)^m$$

Where, σ_0 , standard flow stress (MPa); m , strain rate sensitivity index; $\dot{\epsilon}$, standard strain rate, $1s^{-1}$ or $10s^{-1}$. The logarithm was taken, and the following can be

gained:

$$\ln \sigma = \ln \sigma_0 - m \ln \dot{\epsilon}_0 + m \ln \dot{\epsilon}$$

$\ln \dot{\epsilon}$ and $\ln \sigma$ are used as the coordinate axis to draw, Strain rate sensitivity index is the straight slope m . It can be seen from the figure that, m value increases with the rise of deformation temperature. The higher temperature will bring more significant influence of deformation rate on flow stress.

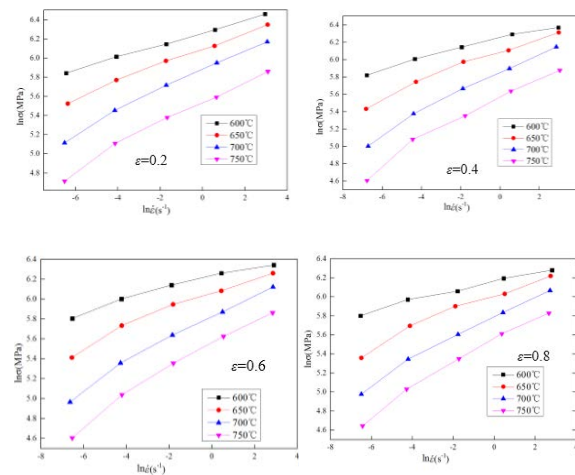


Figure.7 Sensitive exponent of strain rate (m)

4. CONCLUSION

(1) The structure of pearlite sheet is intact when deformation happens under 750°C . The deformation process mainly leads to orientation change of partial pearlite colony and large F plastic deformation. Hardening happens to both P and F. During deformation under 700°C - 650°C , cementite sheet twisting and fracture happen to P structure in the material, and dynamic recrystallization happens to F structure. During deformation under 600°C , cementite sheet is crushed in quantity and presents granular distribution. This will be beneficial for accelerating spheroidizing speed of test steel.

(2) Work-softening is not obvious when deformation happens under 700°C . There is obvious work-softening when deformation happens under 600°C ~ 700°C . When the deformation is close to peak strain, θ value has an inflection point.

(3) Temperature rise and flow stress present exponential reduction relation. The influence of temperature on flow stress changes with deformation. m value increases with the rise of deformation temperature. The higher temperature will bring more significant influence of deformation rate on flow stress.

ACKNOWLEDGEMENT

QuZhou of Science and Technology Plan Projects(2015Y006); QuZhou of Science and Technology Plan Projects(2014Y002) The Talented Projects of Quzhou University(BSYJ201403)

REFERENCES

[1] Yi Zhang, Zhe Chai, Huili Sun. Research Progress

on Heat Treatment Technology of GCr15 Bearing Steel for High-speed Railway. *Nonferrous metal materials and engineering*. 2017(06): 356-362.

[2]Guojong Zhang, Zhicheng Zhang, Kaiming Wu. Progress of Research on Composition Design and Heat Treatment Process of High Carbon Chromium Bearing Steel. *Special steel*. 2015(03): 9-13.

[3]Yeqing Chen, Yiwen Wu, Ziwei Qing. Influence on Structure and Mechanical Properties of GCr15 Bearing Steel with Cryogenic Treatment. *Journal of material guide*. 2018(05): 55-58.

[4]Maoguo Xiao, Donghui Li, Xinyang Lu. Effects of heat treatment on microstructure and properties of a high Cr-Co-Mo alloyed heat resistant bearing steel. *Transactions of materials and heat treatment*. 2018(08):

75-81.

[5]Xin Cai, Mingyue Sun, Wei Wang. Mathematical Model of Austenite Grain Growth of 8Cr4Mo4Ni4V Aviation Bearing Steel at High Temperature [J]. *Journal of Material Engineering*. 2018(09): 131-137.

[6]Yanshan Wang, Xiaochao Chen, Leilei You. Research on Double Refining Process of GCr15 Bearing Steel. *Metal processing (thermal processing)*. 2018(09): 52-54.

[7]Yuelin Yao, Suhui Deng, Liping Wang. Effect of temperature on microstructure of GCr15 bearing steel in low-temperature rolling. *Heat treatment of metals*. 2014(04): 68-71.

Application of Big Data Technology in Smart Tourism Projects in Henan

Yazi Wang¹, Aijv Lei^{2*}, Yu Zhao¹

¹Zhoukou Normal University, Henan, 466001, China

²Zhoukou Central Hospital, Henan, 466000, China

*E-mail: 215771666@qq.com

Abstract: With the rapid development of Internet information technology, the world has entered the era of big data. The application fields of big data technology are becoming more and more extensive, and the influence is bigger and bigger. Intelligent tourism project is the latest product of the development of tourism industry informatization, which has a very great impact on the development of the tourism industry. In view of this situation, this paper starts with the Henan Intelligent Tourism Project, and makes a thorough study and analysis of the problems existing in the application of large data technology in Henan Intelligent Tourism Project, and puts forward some suggestions for improvement on this basis. It is hoped that this study can play a guiding role in the application of large data technology in China's Intelligent Tourism projects.

Key words: Henan province; intelligent tourism project; big data technology; Application Research

1. INTRODUCTION

With the rapid development of global information technology, large data technology has become an important strategic resource of the country, and it has a great impact on all fields. The same is true for tourism industry. Intelligent tourism is also coming into being. But what is smart tourism? Where does the wisdom lie? The author thinks that the wisdom of wisdom tourism is mainly embodied in three aspects as shown in Figure 1. At the same time, Intelligent Tourism as a tourism industry by big data technology and the emergence of a new thing, its development is relatively immature, and there are great defects, the provinces are also groping forward. Therefore, this paper analyzes the development of Henan Intelligent Tourism project, not only has a vital role in the application of large data technology of Henan Intelligent Tourism project, but also has a very important reference for other provinces.

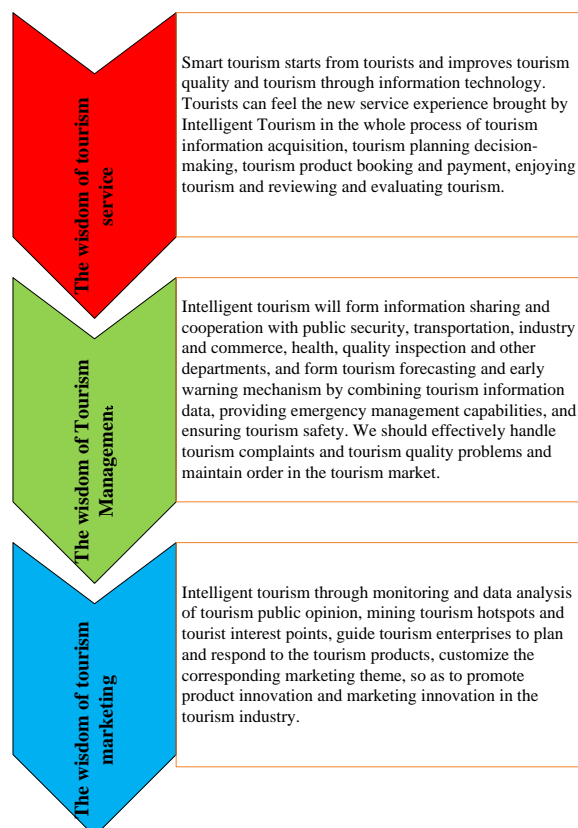


Figure. 1. The embodiment of wisdom Tourism

2. THE PROBLEMS IN THE APPLICATION OF BIG DATA TECHNOLOGY IN SMART TOURISM

2.1 The lack of innovation in smart tourism products

At present, the tourism products in Henan Province are mainly traditional products, and lack of attention to tourists' tourism experience and on-line and off-line interaction in the tourism process. Tourists often go to places to play, play enough to go, lack of attention to the tourism situation, the product does not have enough added value. In order to cope with the increasingly fierce competition and diversified tourism market, the most important and severe task of Henan Intelligent Tourism Project in the application of large data technology is how to complete the innovation of tourism products, and how to develop more interactive and attractive according to the actual needs of tourists. The tourism products will contribute more to the economic development of Henan province.

2.2 The Information data update and collection speed

is slow.

Because of the vacancy in technology and capital investment, Henan Province still has not established a unified and efficient platform for filling in tourism information, mainly relying on the way to print out the spreadsheet to fill in the data by hand. And the data sharing has also been greatly hindered by the inconsistency of data exchange rules among various departments in Henan Province. It is precisely because of this reason that many intelligent tourism platforms in Henan Province have not issued comprehensive information, and even the various platforms have appeared inconsistent information, update slowly. And the platform is difficult to interact with tourists in a timely and close manner, the service efficiency of scenic spots is relatively slow and can not be effectively improved. Careful research has proved that no matter what level of tourism information data platform, to be able to play an effective role, it must be the first time to complete the data update collection, so as to provide tourists with the best quality and comprehensive services. Therefore, one of the key problems in the application of Henan Intelligent Tourism Big Data is how to build a more efficient data update collection channel, and on this basis to speed up the pace of information update.

2.3 Technology application and project development are superficial.

Now, with the rapid development of smart tourism projects, many regions are aware of the business opportunities contained in this project, began to develop related projects, the same is true in Henan Province. However, due to the lack of understanding of wisdom and the lack of technological strength, Henan Province in the development of intelligent tourism projects appeared in the application of technology and project research and development superficial situation. And many of the plans simply can not be effectively implemented, and there is not a full understanding of the market prospects for development. Therefore, one of the key problems in the application of large data technology in intelligent tourism projects in Henan Province is how to formulate high-quality intelligent tourism projects according to their own actual tourism resources, and effectively avoid unnecessary waste of resources.

2.4 There is a big gap in talents.

With the passage of time, now a large number of enterprises have chosen to participate in the research and development of Henan Intelligent Tourism projects, these enterprises also have specialized personnel. But there are few comprehensive talents who can effectively use the Internet information technology and have a clear understanding of the actual situation of tourism projects and tourism projects in Henan Province, even there is a big gap. Therefore, in order to promote the further development of intelligent tourism projects in Henan

Province, it is necessary to establish a mechanism of selecting, cultivating and transferring enough outstanding talents, and lay a solid foundation for the application of big data technology in Intelligent Tourism projects.

3. THE COUNTERMEASURES FOR FURTHER APPLICATION OF BIG DATA TECHNOLOGY IN HENAN INTELLIGENT TOURISM PROJECT

3.1 The development of experiential intelligent tourism products

With the development of the times and the progress of society, the types and quantity of tourism products are more and more, and the homogenization phenomenon is more and more serious, and the competition situation faced by the tourism market is more and more intense. Therefore, the most important means to promote the further application of large data technology in Henan intelligent tourism project is to innovate the frequency of tourism and enhance the competitiveness of its products. And with the rapid development and progress of the times, people are increasingly pursuing personalization, and often choose to share their travel experience on the Internet platform. Henan Province should develop excellent experiential tourism products through the application of information technology according to the actual needs of tourists. On this basis, we can break the barrier of traditional tourism products and develop more interactive and attractive Intelligent Tourism products, so that tourists can enjoy more in the process of tourism and develop intelligent tourism products with unique Henan characteristics.

3.2 Speed up the update and perfection of intelligent terminals

Travel intelligent terminal is the implement tool and carrier of intelligent tourism project which integrates Internet information technology and Internet of Things technology. It has the most direct impact on the service efficiency and service quality of Intelligent Tourism project. Therefore, in order to promote the further development of Intelligent Tourism projects, Henan Province should make full use of modern Internet information technology to build intelligent terminals according to the actual situation of its own economic development. And according to the actual situation of the tourism project is divided into A, B, C three levels, the higher the level of intelligent tourist attractions related infrastructure and intelligent terminals will be about perfect. At the same time, it can publish the corresponding rating results on the platform to the public, so that not only can tourists more quickly and conveniently complete the tourist attractions, surrounding hotels and traffic queries, more autonomous destination selection. Moreover, the intelligent terminal can be upgraded and perfected on the basis of this, thus contributing more to the rapid development of Henan Intelligent Tourism project.

3.3 Strengthening the overall planning of technological application research and development

At present, the intelligent tourism project in Henan Province is in the stage of starting to develop in an all-round way, and the choice of the project plays a vital role in this stage. First of all, Henan Province should according to its own actual situation of the corresponding development planning of Intelligent Tourism projects, in-depth analysis of the actual situation in the region, and on this basis, the feasibility of the project and the corresponding technology in-depth analysis, to complete the overall planning of Intelligent Tourism projects. In addition, Henan Province should also promote the further development and integration of new industrialization, urbanization and Intelligent Tourism industry, so that intelligent tourism projects can play their service role to the extreme, and achieve the coordinated and sustainable development of intelligent cities and intelligent tourism.

3.4 Strengthening the cultivation and introduction of talents

In order to promote the further development of the Intelligent Tourism Project, the Henan Provincial Government must combine with colleges and universities and social institutions to train the existing staff and build a diversified and all-round talent training system while introducing complex talents. Real-time more advanced and outstanding technology, speed up the pace of personnel training, so that we can train a sufficient number of composite tourism talents in line with the actual needs. It will contribute more to the further development of Henan Intelligent Tourism Project, and let people get more excellent tourism enjoyment in Henan Province, and then make greater contributions to the economic development of Henan Province.

4. CONCLUSION

Generally speaking, big data technology has made great changes in people's work, life and way of thinking. The age of big data is a great revolution in

the way of life, mode of production and way of thinking. With the continuous development and progress of big data technology, the online tourism market will inevitably grow rapidly. Enterprises will inevitably promote the further development of Henan's smart tourism industry, effectively change the backward development level of Henan's tourism image, so as to further enhance its economic growth rate, and thus contribute more to the great rejuvenation of the Chinese nation and the construction of a socialist modernization power.

ACKNOWLEDGMENT

This work is supported by the Key Project of Guangxi Social Sciences, China (No.gxsk201424), the Education Science fund of the Education Department of Guangxi, China (No.2014JGA268), and Guangxi Office for Education Sciences Planning, China (No.2013C108).

REFERENCE:

- [1]Lu Yi, Yin Changying, Huang Ya. The Development Status and Countermeasure of Intelligent Tourism in Guizhou Province in the Big Data Era [J].Guizhou Agricultural Science, 2017,45(04): 157-162.
- [2]Zhang Jing. Internet+thinking boosts the development of Kaifeng's wisdom tourism development [J]. tourism overview (second half month), 2016 (10): 181-182.
- [3]Wang Shiyun, Tian Xingyan, Wu Zhenxing. Intelligent Tourism Information System Tourism Data Integration [J].Electronic Technology and Software Engineering, 2016 (24): 194-195.
- [4]Xu Bolin, Li Donghe, Qian Yalin, Liu Yantao. Intelligent tourism: a new trend of tourism development-a review based on existing research results [J].Resource development and market, 2013, 29 (07): 781-784.

Overview of Moving Target Detection Algorithms

Yang Yufeng

Guangdong University of Science & Technology, Dongguan 523083, China

*E-mail: 294054110@qq.com

Abstract: Target detection is an important part of human beings moving towards the era of intelligence, and has attracted the attention of many experts and scholars. However, due to the influence of various targets and complex scenes, the reliability and robustness of tracking of moving targets are severely limited. In this paper, the common methods and steps of target tracking are discussed. The difficulties of common algorithms in target tracking are analyzed. At the same time, the development status at home and abroad is summarized and the future development of technology is prospected.

Keywords: target detection; robustness; occlusion

1. INTRODUCTION

Moving target detection is the process of finding a target in a specific environment. With the development of machine intelligence and image processing technology, moving target detection has also achieved rapid development and wide application, and has high practical value in intelligent transportation system, intelligent human-computer interaction and robot navigation. Target detection becomes a more complicated task due to changes in target state and changes in target scenes. The main difficulty is that the appearance, color and texture of the target are subject to change at any time; the scene in which the target appears is also subject to change at any time, and external factors such as occlusion and changes in illumination intensity that affect the tracking effect may occur at any time. Therefore, the current target detection technology can not fully achieve the effect of demand, and it is subject to further research by experts and scholars from various countries.

Moving target detection is the process of extracting the tracking target from the motion background, which is the premise of target tracking. The accuracy of the detection directly affects the final tracking effect. The complexity of the background and the variability of the target are two major challenges in the detection of moving targets. Currently commonly used algorithms for moving target detection are interframe difference method, background difference method and optical flow method.

2. INTERFRAME DIFFERENCE METHOD

The interframe difference method [1] is to perform a difference operation on two consecutive frames of a video image, and then perform binarization

processing to determine a moving target. This method is more practical for monitoring places with large differences between adjacent frames when there is an abnormality such as warehouse monitoring and home security. The main advantages of the interframe difference method are: the algorithm is simple, the program implementation complexity is low; there is no problem of background acquisition, update and storage; it is not sensitive to the change of light in the scene, and the real-time performance is good. However, in the actual environment, when the target moving speed is too fast, it is easy to generate voids, or it is possible to divide one moving target into two or more, and the moving target has problems such as blurred edges.

In view of the above problems in the interframe difference method, an improved method such as a three-frame difference method and the addition of color information for discrimination is proposed. For example, Shahinfard et al. proposed differential processing for adjacent five-field video sequences, and integrated RGB component signals of the video sequence for motion detection [2]. This method is not only suitable for low-speed moving targets, but also has a good effect on high-speed moving targets.

3. BACKGROUND DIFFERENCE METHOD

The background difference method is a commonly used method in target detection. The principle is to obtain the moving target area by performing the difference between the current frame and the background image. Compared with the inter-frame difference method, this method can better detect high-speed moving targets. The difficulty of this method lies in background modeling, and the accuracy of background image modeling directly affects the detection effect. When constructing background modeling, three issues need to be considered. First, the background image that needs to be constructed needs to be free of moving targets, and can be continuously updated according to the current background changes. Second, it is necessary to consider the background and video noise problems to obtain video images. Video noise is often incorporated in the process, especially in outdoor situations where natural factors such as light and wind are greatly affected. Different filters are needed to eliminate noise. Third, choose the appropriate threshold and threshold. Directly affect the accuracy of the test results. In addition, the shadow of the target

has a greater influence on the background difference method, and is often misdetected as a target.

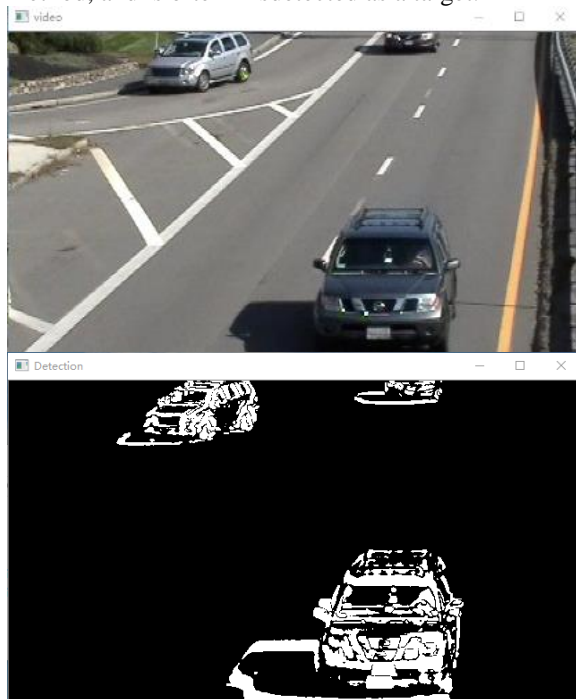


Figure.1 The result of Background difference of mixed Gaussian model

Commonly used background construction methods are: background construction based on a single Gaussian model, background construction based on mixed Gaussian model, background construction based on Kalman filter, and background model construction based on kernel function density estimation. In order to solve the problem of mode and shadow elimination, many scholars have proposed an improved method. Elgammal et al. used a Gaussian kernel to nonparametrically estimate the probability density of the same pixel, and proposed a parameterless kernel density estimation method, which greatly improved the accuracy of background construction. The target shadow is usually removed by transforming the color space.

4. OPTICAL FLOW METHOD

The optical flow method [3] determines the shape and position of a moving target by temporal variation and correlation of pixel data in a video sequence, that is, the shape of the moving object is determined by studying the temporal change of the image gradation.

The concept of optical flow was first proposed by Gibson in 1950. It is the instantaneous velocity of the pixel motion of the moving object in the observation plane, and the correspondence between the previous frame and the current frame is calculated by the change of the pixel in the image sequence in the time domain and the correlation between adjacent frames. Further, a method of obtaining motion information of an object between adjacent frames is obtained. Generally, the optical flow is produced by the motion of the moving target itself in the scene, the motion of

the camera, and the simultaneous movement of both.

In 1981, Horn and Schunck creatively combined the two-dimensional velocity field with grayscale and introduced the optical flow constraint equation to obtain the basic algorithm for optical flow calculation. Based on different theoretical foundations, various optical flow calculation methods have been proposed, and the performance of the algorithms is different. Barron et al. classify them into four categories according to their theoretical basis and mathematical methods: gradient-based methods, matching-based methods, energy-based methods, and phase-based methods. In recent years, neurodynamic methods have also received attention from scholars.

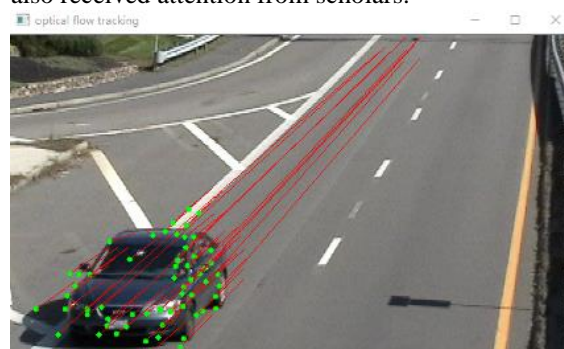


Figure. 2 The result of optical flow method

In an ideal situation, the optical flow method can accurately detect the moving target without predicting any scene information method, even if the camera motion still has a good effect. However, the optical flow method also has serious shortcomings. In areas where the gray level does not change much, the moving target is often not detected. In addition, when the external illumination changes, the optical flow method can detect even if no motion occurs. Optical flow, causing misjudgment; in actual situations, when three-dimensional objects are projected into two-dimensional graphics, due to partial information loss, the optical flow method is difficult to achieve a high accuracy level when dealing with aperture and occlusion; Accuracy, optical flow method usually needs to use features such as gray and edge to improve the segmentation accuracy. At the same time, the optical flow method adopts an iterative method, and the calculation amount is large. In reality, it is difficult to detect real-time.

5. RESEARCH STATUS

Countries such as the United States and Europe, with their own technical and financial advantages, have taken the lead in conducting research on intelligent video surveillance systems since the 1990s, including: Video Security and Control (VSAM) led by Carnegie Mellon University. Research plan. According to the plan, the researchers developed an end-to-end test system that integrates many advanced video security monitoring technologies, such as real-time target detection and tracking in stationary backgrounds and motion backgrounds, and classification of common targets (such as people, cars, trucks). Identification,

classification of special objects (such as school buses and other specially marked objects), target pose estimation, camera autonomous control, multi-camera coordinated tracking, human footwork analysis, etc.; US Defense Advanced Research Agency (DARPA) and Joint Services Commission (JSG&CC) co-sponsored and established the Automatic Tracing and Identification Working Group (ATRWG) . It is mainly responsible for the standardization of image data, formulating uniform specifications for automatic target recognition and tracking, and holding three meetings every year. Many international publications such as IEEE on AES, IEEE on PAMI, IEEE on AC, Pattern Recognition and Proceedings of SPIE have become important fields for academic exchanges among many experts and scholars. It has provided a good environment for image tracking research in the world and has made gratifying achievements. In addition, the University of Maryland's real-time monitoring system W4 can use a single camera to track the human body and various parts of the human body in real time. The so-called W4 refers to Who, When, Where and What, which means that the system can determine who the target is, when, where and what. And large companies such as IBM are also funding related research in this field, hoping to apply research results to the business field.

6. CONCLUSION

This paper systematically introduces the practical significance and development prospects of target detection. The steps of target detection and common methods of target detection and target tracking are discussed. The advantages and disadvantages of the classical method are summarized. The reason why the target tracking effect is not ideal is because the target characteristics and the external environment are constantly changing, so to achieve the desired effect. It is necessary to join the learning mechanism. Only enough samples for the target training can better cope with the changes in the target shape and color, so as to achieve better tracking results.

REFERENCES

- [1]Collins R,Lipton A,Kanade T.Introduction to the Special Section on Video Surveillance.IEEE Tans.Pattern Analysis and Machine Intelligence. 2013,22(8):745-746.
- [2]Narendra P.M.,Westover B.L.Advanced target tracker concepts.2008, AD-A101845.
- [3]Haritaoglu I,Harwood D,Davis L.W4:Real-time surveillance of people and the iractivities.IEEE Transations on Pattern Analysis and Machine Intelligence.2010,22(8):809-803.

Return of NOKIA: the Call of Craftsman Spirit in the Internet Era

Deran Bei

School of Management, Shanghai University, Shanghai, 200444, China

E-mail: 893341256@qq.com

Abstract: Nokia has successfully recovered from the bottleneck of smartphone innovation by virtue of its craftsmanship of product excellence. This also reflects the return of customer demand for product quality from the side, the enterprise only has the craftsman spirit, can meet the increasing demand for quality of consumers. Therefore, how to cultivate the spirit of craftsmen has become the focus of attention of enterprises, in addition, no innovative spirit of craftsmen is to build cars behind closed doors, no spirit of craftsmen is the innovation of the castle in the air. How to combine Internet thinking with artisan spirit has become a problem that enterprises must solve.

Keywords: Internet thinking; Innovation; Craftsman spirit

1. THE RETREAT OF SMARTPHONE WAVE

Speaker Zhao Xiaoguang's judgment on the smartphone industry was greeted with a scene of applause at a summit of Chinese listed company leaders hosted by the Daily Economic News. Zhao Xiaoguang's long-term tracking of the electronics industry, has won many times the best analyst of new wealth, including the successful excavation of the Apple industry chain and other investment themes has laid his position in the industry. In his view, the big wave of smart phones has ended, so far 80% of the world's people have smartphones[1-2].

There is a general view in the electronics industry that electronic consumption is about a five-year cycle, such as the 1994-1999 desktop, 1999-2004 functional phones, according to the cycle law, the tide of smartphones has faded, real life people feel as if it coincides with this law. In September 2012, Apple launched a 4-inch iPhone 5 to meet customers' demand for large screens, reaching 5 million units in the first week of launch, and a new generation of iPhone 6 was launched in 2014, with screen sizes upgraded from 4 inches to 5.5 inches. The iPhone 6S was released on September 10, 2015, but sales were flat because it had no more surprising innovations. At this point, smartphones seem to have reached a bottleneck in functional innovation, rarely creating new features that refresh customers, and people seem to be less sensitive to the pursuit of mobile phone functions. It is urgent for enterprises to discover new pain spots and itch points.

2. THE RETURN OF NOKIA

Nokia 6 was launched in China with a brand new look and signed a strategic cooperation agreement with Jingdong, which sells exclusively for China at 1,699 yuan. On the day of microblogging, many users paid close attention to it. As the king of the mobile phone industry, there were many classics that were unforgettable. Nokia manufactured its first mobile phone in 1982, overturning Nokia's first portable GSM handset, NOKIA 1011, which was listed in New York in 1990, surpassed its rival MOTO in 1998, Nokia launched Nokia's Shenji 1100 in 2003, the N-series handset in 2005, and Nokia's handset has dominated the world since then, and Nokia in 2011. The Kia N9 sang the slogan "Don't Follow"; the Nokia Lumia 800 let the world know what a beautiful phone is in 2012; the Nokia Lumia 1020 let mobile photography into a new chapter in 2013; and Nokia left us in 2014 with fewer mobile phone owners.

Nokia's return has attracted a lot of attention. Users have been looking forward to the return. Numerous related analyses suggest that Nokia is using emotional brand to achieve its marketing purpose. But this view is only superficial, and the deeper reason lies in the return of consumers' demand for the fundamental attributes of the product.

Since the launch of Apple's smartphone, people's demand for the quality of mobile phones has gradually been replaced by functional diversity. The traditional quality-based mobile phone industry has gradually declined. People are more willing to get more services and experience from mobile terminals. In this case, consumers for the basic attributes of mobile phone demand regression trend, a moderate function, high quality mobile phone has become the ideal product of the majority of consumers. Nokia is the endorsement of quality in the hearts of the majority of users, it once for the spirit of product quality excellence has become the best memories of consumers, so the success of Nokia's return to stimulate consumer interest in buying[3].

3. WHAT IS CRAFTSMAN SPIRIT?

Nokia's pursuit of excellence in quality is one of the manifestations of the craftsmanship of the enterprise. It is precisely because of the existence of this craftsmanship that the hegemony was able to make a comeback. Then what is craftsman spirit? Dong Zhiyong, a professor at Peking University's School of Economics, puts forward his view that craftsmanship can be summarized in four aspects: excellence,

perseverance, devotion to work, integrity and innovation. One of the most praised parts of the craftsman's spirit is to strive for perfection. People with craftsman's spirit have unremitting pursuit of the quality of craftsmanship. Persistence is the most touching part of the craftsman's spirit, with which people are willing to dedicate all their own to a skill. Aigang dedication is the source of strength of craftsmanship, "ask the canal so clear, for the source of living water," is precisely the spirit of Aigang dedication to inspire craftsmen to realize their dreams. Keeping up with innovation shows the spirit of the craftsman. Craftsmanship enriches the existing skills through continuous learning, improvement and innovation, innovates on the basis of excellence, and realizes the double leap of product function and quality.

4. HOW TO CULTIVATE CRAFTSMAN SPIRIT

How to train craftsmen's spirit has become a hot topic of current scholars. Building a good market environment and insisting highly respect the labor market economy system are the top priority. It is also necessary to establish a good social and cultural atmosphere, and we should do well in four advocates: first of all, advocate labor. Today, the lack of craftsmanship is largely due to people despising front-line employees, thinking that this dirty work, hard work is done by inferior people, it is the breeding of this misconception that leads to the lack of front-line employees in enterprises. Due care, which greatly reduces their enthusiasm for labor, is not conducive to the healthy development of the organization, so respect for their work is an important step to achieve a comprehensive craftsman spirit. The second is to advocate skills, craftsmanship employees often use their full energy to study a certain craft. The third advocates innovation, craftsmanship is not equal to making cars behind closed doors, but through a large number of practices to weed out the old and bring forth the new, and constantly combine labor and wisdom to achieve a higher leap. Fourthly, we advocate perseverance. As the saying goes, good things go on and on. Any success is not achieved overnight. It is through constant failure and repetition to sum up experience. Only those who devote themselves wholeheartedly can obtain happiness from perseverance.

5. HOW TO COMBINE INTERNET THINKING WITH CRAFTSMAN SPIRIT

The spirit of craftsmen without innovation is the creation of a closed door and no craftsman spirit is a castle in the air. Only by combining the two together can we get twice the result with half the effort. Internet thinking is the source of enterprise innovation inspiration, it specifically refers to the Internet, big data, cloud computing technology in the context of the continuous development of the market, users, products to re-examine the way of thinking. The key to the combination of Internet thinking and craftsman

spirit lies in the following three points:

Firstly, enterprises grasp consumer demand through Internet thinking. Internet is an equal and open virtual network platform. Compared with the traditional mode, the uncertainty of information is bridged. Users can give timely feedback to the enterprise. Enterprises build relevant prediction models by accumulating data. These models can well feed back the core needs of consumers. Enterprises can transform the core needs into products or services by understanding the core needs. Of course, after the products or services are put into the market, the enterprises will make suggestions to them. A series of monitoring and tracking, in order to evaluate the new product, and then according to user feedback information to make corresponding improvements, optimize the user experience, provide personalized, differentiated services.

Secondly, the spirit of craftsmen should be carried out in every link: when the enterprise determines the products and services according to the needs of consumers, the production process becomes the most important, which requires that every staff involved in production design can face up to their own responsibility, devote themselves to their work, for each skill, each. We must strive for excellence in every detail and do our best to achieve the ultimate goal. In addition to the higher requirements for craftsmanship in the production process, the same need for craftsmanship in the R&D process and sales process, because craftsmanship not only refers to the accuracy and reliability of production and processing, but also refers to the entire enterprise R&D, production, sales process of all personnel can love the post, dedication, selflessness. Only by carrying out the spirit of craftsmen can enterprises remain invincible in the fierce market competition.

Finally, the Internet thinking and craftsmanship promote each other, harmony and unity: Internet thinking for enterprises to open the fog, to find consumer pain, itch, with it the enterprise has a way forward, craftsmanship for enterprise product quality escort, it will become a reality, with real products, services to go Satisfying customer needs and creating enterprise value. Internet thinking provides a driving force for craftsmanship, and craftsmanship provides support for Internet thinking. They promote and develop each other while checking and balancing each other.

Nokia's new Nokia 6 today is pre-installed with Android 7.0. Its main hardware parameters are Qualcomm 430, 4GB memory, 64GB storage, and support for external memory cards. Judging from these mainstream configurations, the former king has finally bowed his head to innovation, turning from solipsism to the present-day Haina River. Perhaps only after experiencing the depression can he feel the joy of rebirth. I believe that Nokia, with its craftsmanship, can revive the flag and drum under the impetus of Internet thinking. Retrieve the lost once.

REFERENCE

[1]Chen Hao: craftsman spirit: Advanced Handbook for learning workers [M]. China Industrial and Commercial Union Press, 2016.

[2]Alex Foggy: Craftsman Spirit: An Important Force in Creating Great Legends [M]. Zhejiang People's Publishing House, 2014.

[3]Zhao Dawei: Internet thinking alone Gu Jiu Jian [M]. Machinery Industry Press, 2014.

Converter Endpoint Prediction Model based on GA-BP Neural Network Model

Yulu Fu^{1,2}, Shuo Zhang^{1,2}, Xinbo Yan^{1,2}, Lu Liu^{3,*}

¹Engineering Computing and Simulation Innovation Lab, North China University of Science and Technology, Tangshan 063210, China

²Mathematical Modeling Innovation Lab, North China University of Science and Technology, Tangshan 063210, China

³College of Science, North China University of Science and Technology, Tangshan 063210, China

*E-mail: 93665397@qq.com

Abstract: The pressure of small and medium sized transfer stations in China has led to the intelligent steelmaking of small converters. In order to get a high hit rate prediction model of converter end point, a prediction model of converter end point based on BP neural network was established. Firstly, a BP neural network model consisting of four input neurons, three hidden layer nodes and two output neurons is established. Then the weights and thresholds of the neural network model are optimized. Finally, the model is validated and analyzed with the existing sample data, and the conclusion that the prediction model of converter end point has small error and high hit rate is effective and feasible is obtained.

Keywords: Converter-steelmaking; BP neural network; Converter end point forecast

1. INTRODUCTION

The purpose of end point control of converter steelmaking is to meet the requirement of carbon content in molten steel. At the end of steelmaking, the temperature of molten steel can meet the basic temperature of the process after successful completion. The content of phosphorus and sulfur in steel shall be lower than the lower limit of specification.

Steps for end control of converter:

Control the starting point and refine the raw materials to obtain more pure materials.

2.A static model is used to calculate the amount of oxygen and other materials needed for the blowing process.

The dynamic control of the blowing process is mainly used for standard track tracking of metallurgical reactions.

In the middle of the process, the steel is directly tested and corrected.

Perform feedback calculation at the end of the blowing.

The end point control of converter steelmaking adopts the approach step by step method. Then the control precision is improved by the dynamic model of blowing. Finally, the end goal hit rate of high accuracy is achieved through intermediate detection and late correction model.

BP neural network model

There are many factors influencing end control of converter, among which there are very complex nonlinear relations. BP neural network is a highly parallel nonlinear system composed of many simple processing elements, which is known for dealing with nonlinear problems [1].

BP neural network is a forward network without feedback. It reduces the error rate by reverse-transmitting the error. In BP neural network, different neurons are arranged in layers, and the output of the neurons in the upper layer are all transmitted to the neurons in the next layer, and this transmission is achieved by the connection weight [2]. The work process is divided into two parts: learning period and working period. The calculation key lies in the error back propagation process in the learning period, which minimizes the objective function to be completed [3].

BP neural network is mainly divided into three parts: input layer, hidden layer and output layer, as shown in Figure 1.

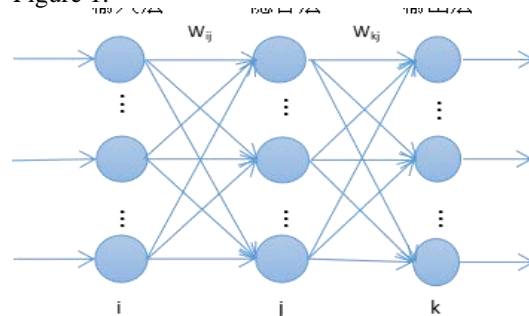


Figure 1 Basic structure diagram of BP neural network

FIG. 1 basic structure of BP neural network

I, j and k represent the input layer, hidden layer and output layer respectively. W_{ij} and W_{jk} respectively represent the weight value of the input layer to the hidden layer and the weight value of the hidden layer to the output layer.

The input of each neuron in the hidden layer and output layer is:

$$net_j = \sum_i w_{ij} o_i \quad (1)$$

$$\text{net}_k = \sum_i w_{jk} o_j \quad (2)$$

The output of each neuron of the hidden layer and the output layer are respectively

$$o_j = g(\text{net}_j) \quad (3)$$

$$o_k = g(\text{net}_k) \quad (4)$$

Use the unipolar s-type function as the activation function:

$$g(x) = \frac{1}{1 + e^{-x}} \quad (5)$$

When the output o_k of the network is not equal to the actual output y_k (expected value), the model has training error, so the model needs to be analyzed for error.

The average error of the model is:

$$e = \frac{1}{2} (o_k - y_k)^2 \quad (6)$$

The total error of the model is:

$$E = \frac{1}{2} \sum_k (o_k - y_k)^2 \quad (7)$$

The key of BP neural network lies in the determination of weights and thresholds. As it is sensitive to the selection of initial weights, the selection of initial weights is particularly important. Genetic algorithm is a global search and optimization algorithm based on nature and heredity, which can adaptively control the search process to obtain the optimal solution, and has high efficiency [4].

2. PARAMETER DETERMINATION AND MODEL ESTABLISHMENT

As the common BP neural network model is divided into three layers: input layer, hidden layer and output layer. The number of input layers is determined by the number of factors into model learning and the number of target predictive factors is determined by the number of output layers. In this paper, the input layer node is 4, as oxygen consumption ratio -PQ, total oxygen consumption -Q, CO content -[CO] in flue gas and -[CO₂] in flue gas are four factors that enter into model learning. The data predicted by the model are the carbon content in the molten steel [C] and the temperature value of molten steel [T], then the output node is 2. The number of nodes in the hidden layer should be more than half of the number of neurons in the input and output layer and less than the sum of the number of neurons in the input and output layer [4-8].

$$\begin{cases} m = \sqrt{n+l} + \alpha \\ m = \log_2 n \\ m = \sqrt{nl} \end{cases} \quad (8)$$

Where m denotes the number of hidden layer nodes, n denotes the number of input layer nodes, l denotes the number of output layer nodes, and α is a constant between 1 and 10.

In this equation, n is 4 and l is 2 are substituted into the empirical formula, and the optimal formula is selected to obtain the number of hidden layer nodes is 3.

The Sigmoid differentiable function and linear function are usually adopted as the excitation function of BP neural network [9]. In this paper, tensing of s-type tangential function is selected as the excitation function of hidden layer neurons. As the output of the network is within the range of [-1, 1], the prediction model selects the s-type logarithmic function tensing as the excitation function of the output layer neurons [10].

Through the determined number of neural nodes in the hidden layer, the gaussian distribution was used to initialize the weight, and the learning rate of the first layer was 0.81, the learning rate of the second layer was 0.07, and the training times were 2,000. In order to reduce the random probability, the entire training process was repeated for 10 times.

3. SIMULATION EXPERIMENTS AND ERROR ANALYSIS

At present, some converter furnaces in China use flue gas analysis system to control the steelmaking terminal. According to the basic principles of the above model, data samples that can be collected by the smoke analysis system are collected in this paper.

First, the original data is analyzed preliminarily. It is known that data sample sets of oxygen consumption proportion -PQ, total oxygen consumption -Q, CO content -[CO] in flue gas, -[CO₂] in flue gas, carbon content in molten steel [C] and temperature value of molten steel [T] are obtained by the flue gas analysis system. The model is established according to the three hidden layer nodes, and some data in the existing data samples are used for machine learning, and the rest are used for predictive test.

To prevent overfitting, the network model USES the method of dividing the data into three parts, training, validation, and test. Only the training data will participate in the training, and the other two parts will not participate in the training, which will be used for testing. In the process of training, the error between the target and the training data target will be smaller and smaller [9] (because the network is trained according to these data). At the beginning, the error between the verification and the verification target will be smaller, but with the increase of training, the error of the test will continue to decrease, and the error of verification will increase. The training stops when the error of verification increases 6 times in a row, because there is a tendency for overfitting, as shown in Figure 2.

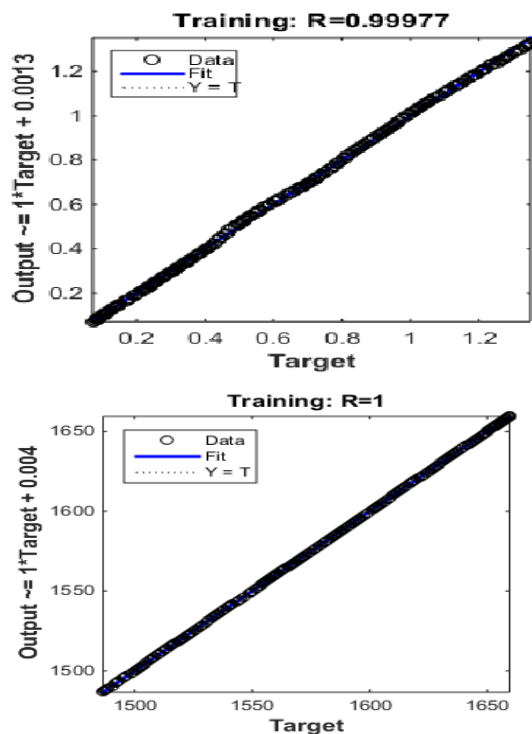


Figure 2 The training stops

In figure 1, the black part is the actual value of the carbon content in the fresh water corresponding to the data, and the straight line is the figure formed by the predicted value of the carbon content in the steel water based on the values of the four factors input by the learned model. According to the four comparison graphs, the predicted carbon content is highly consistent with the actual value.

In figure 2, the black part is the actual output value of the fresh water temperature corresponding to the data, and the straight line is the figure formed by the prediction of the steel water temperature based on the values of the input four factors of the model after learning. It can be seen from the four comparison figures that the predicted value of the steel water temperature is highly consistent with the actual value. The prediction accuracy of the network prediction model optimized by genetic algorithm is high, that is, the converter endpoint prediction based on ga-bp neural network model is feasible.

4. CONCLUSION

At present, most end point control of converter

steelmaking in China still USES artificial experience control or static control, but end point control has been replaced by artificial intelligence. According to the test results, ga-bp based terminal prediction model has small error, and the predicted carbon content and the precise high temperature of molten steel can be put into actual production development. Intelligent converter steelmaking will be more and more widespread.

REFERENCES

- [1] Sun lingfang, zhou jiapo, Lin weijian, hou shilu, xu feng. A study on online public opinion crisis early warning based on BP neural network and genetic algorithm. *Intelligence journal*, 2014, 33(11):18-24.
- [2] Xu xingjun, yan gangfeng. Stock price trend analysis based on BP neural network. *Zhejiang finance*, 2011(11):57-59+64.
- [3] Chang xiang xiang chiung, Chien Yuehone. The Application of Genetic Algorithm in bead flow Prediction. *Environmental Geology*, 2007, 53(2): 339-347.
- [4] Guo gang, li fazhi, Lin zhongyuan. Prediction of edm boring and grinding effect based on genetic neural network. *Henan science & technology*, 2014(12):90-91.
- [5] Wang shangfeng. Study on power performance matching of hybrid electric vehicles [D]. Lanzhou university of technology, 2010.
- [6] Tan hua. Study on optimization of field pipe network of drip irrigation in different plot shapes [D]. Lanzhou university of technology, 2009.
- [7] Zhu wenyu. Fault location of distribution network based on BP neural network optimized by cloud genetic algorithm. *Hubei university of technology*, 2016.
- [8] Zhu zhenxing. Evaluation of urban livability based on BP artificial neural network. *Modern business and trade industry*, 2011, 23(23):15-17.
- [9] Cui bo. Application of neural network in GDP prediction. *Information technology*, 2011, 35(02):103-105.
- [10] Zhang Lin. Prediction and analysis of weibo topics based on neural network. *Digital technology and application*, 2017(03):82-83.

Research on Optical Character Recognition based on BP Neural Network

Kangkang Jin^{1,2}, Reixuan Zhao², Kaili Xu², Bin Bai^{2,*}

¹Engineering Computing and Simulation Innovation Lab, North China University of Science and Technology, Tangshan 063210, China

²College of Science, North China University of Science and Technology, Tangshan 063210, China

*E-mail: 956201990@qq.com

Abstract: OCR recognition technology can make the text in the image into computer text, so that the storage of the image data can be reduced, the recognized text can be reused and analyzed, and the manpower and time input by the keyboard can be saved. Optical character recognition is the core of OCR technology. Studying its recognition technology and improving the correct rate of recognition have greatly promoted the development of OCR technology. Based on this meaning, this paper conducts centralized data statistical description, denoising, binarization and other preprocessing on the collected UCI optical character recognition data, and establishes BP neural network model by selecting the appropriate features by principal component analysis to study the optical character recognition problem and the law.

Keywords: Optical character recognition; BP neural network; Principal component analysis; Confusion matrix

1. INTRODUCTION

OCR refers to the process in which an electronic device checks characters printed on paper, determines its shape by detecting dark and bright patterns, and then translates the shape into characters by character recognition [1,2]. In other words, it is to analyze the text data that is mastered into an image file for comprehensive information. At the same time, optical character recognition is the core of OCR. The

Table 1 Data Description Statistics

	Character	Horizontal position	Vertical position	Width	Height
Number of cases	20000	20000	20000	20000	20000
Effective deficiency	0	0	0	0	0
Average value		4.02	7.04	5.12	5.37
Mean standard error		.014	.023	.014	.016
Standard deviation		1.913	3.305	2.015	2.261
Variance		3.660	10.920	4.059	5.114
Skewness		.715	-.228	.235	-.278
Skew standard error		.017	.017	.017	.017
Kurtosis		.883	-.421	.304	-.249
Kurtosis standard error		.035	.035	.035	.035
Minimum value		0	0	0	0
Maximum		15	15	15	15

According to the result of the description statistics, it is possible to obtain no missing values in the optical character recognition data set, and the data are

non-electronic version of the text information is converted into a picture format by scanning, shooting, etc., and then the image is output as an electronic version of the text information by the recognition technology [3-5].

In this paper, the SPSS is used to analyze the image data in the UCI optical character recognition data set according to the letters. However, since the image data is often noise data, wavelet denoising is applied to the data, and the denoised data is passed. SPSS is standardized; After the principal component analysis, the obtained 16 independent variables are subjected to dimensionality reduction, and the best data simplification is performed with the least loss of information data. Five new variables are selected in combination with the cumulative contribution rate of variance. Accurately identify characters; Finally, the BP neural network model is established to identify the optical characters, and the functional relationship between the input layer and the output layer is extracted. The function relationship is used to perform optical character recognition

2. DATE PROCESSING

(1) Statistical description of the data

A simple statistical analysis was performed on the obtained UCI optical character recognition data set, and the data characteristics of the average value, standard deviation, kurtosis, skewness, maximum and minimum values of 16 variables were realized by SPSS software, as shown in Table 1.

distributed between 1 and 15. The standard deviation is mostly distributed between 2 and 3, and the data is more scattered, as shown in Figure 1.

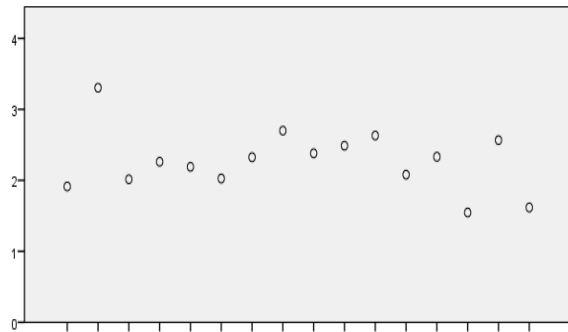


Figure 1: Variable standard deviation distribution marker map

(2) Data preprocessing

Since the image data is noise data, it is necessary to use MATLAB to perform wavelet denoising on the image data. Wavelet transform has good time-frequency localization characteristics, and its linear representation is $W_x = W_f + W_e$, the wavelet coefficients, which are mainly controlled by the signal, are retained, and the wavelet coefficients controlled by the noise are found and removed. The remaining wavelet coefficients are inverse transformed to obtain a denoising signal, and the data can be smoothed by denoising, as shown in Figure 2.

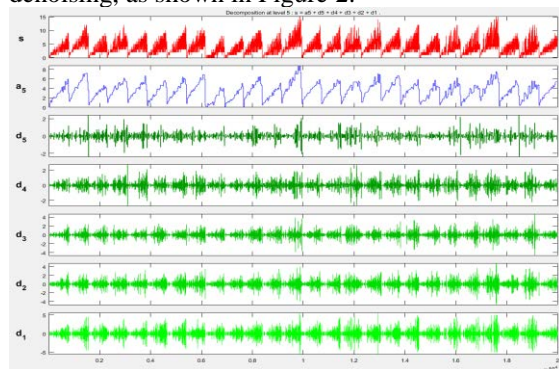


Figure 2: Image of black pixel number wavelet

Table 2: Principal Component Analysis Total Variance Interpretation

Ingredient	Initial eigenvalue			Extract the sum of squared loads		
	Total	Percentage of variance	Accumulation%	Total	Percentage of variance	Accumulation %
1	6.400	39.997	39.997	6.400	39.997	39.997
2	3.347	20.916	60.914	3.347	20.916	60.914
3	2.144	13.398	74.311	2.144	13.398	74.311
4	1.400	8.751	83.063	1.400	8.751	83.063
5	.719	4.496	87.559	.719	4.496	87.559
6	.526	3.288	90.846			

denoising in rectangular area

Because the UCI optical character recognition data set given by the annex includes 20,000 data, and the data is distributed between 1 and 15, in order to remove the unit limitation of the data, the influence of the dimension is eliminated, and to accelerate the optimization of the optimal solution, therefore, the data is standardized using SPSS. Here z-score using a standardized method.

$$Z_{ij} = \frac{X_{ij} - X_j}{S_i} \quad (1)$$

X_{ij} is the actual variable value, X_j is the arithmetic standard deviation, S_i is the standard deviation, and Z_{ij} is the normalized variable value.

3. PRINCIPAL COMPONENT ANALYSIS

(1) Principal component extraction

Since the obtained optical character recognition data set has 16 independent variables and the data dimension is too large, data dimensionality reduction processing is required. In order to better recognize characters, a principal component analysis method is adopted, which aims to use the idea of dimensionality reduction to transform multiple indicators into a few comprehensive indicators, as shown in Figure 3.

Each of the principal components can reflect most of the information of the original variables, and the information contained therein is not repeated. This method combines complex factors into several principal components while introducing multi-faceted variables, simplifies the problem, and at the same time obtains more scientific and effective data information, as shown in Table 2.

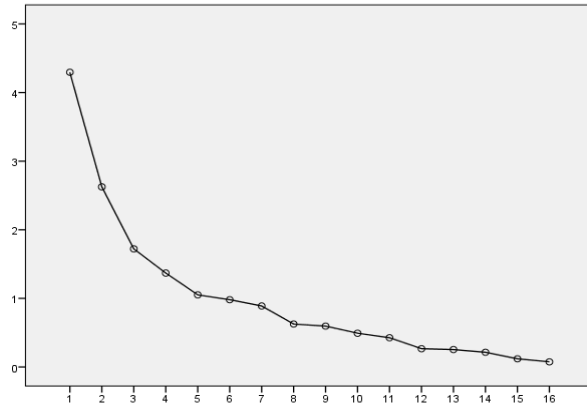


Figure 3: Crushed stone diagram obtained by principal component analysis

4. CHARACTER RECOGNITION BASED ON BP NEURAL NETWORK ALGORITHM

(1) Neural Network Principle, as shown in Figure 4.

The neural network is a complex network system formed by many simple processing units interconnected. It reflects many basic features of human brain function and is a highly complex nonlinear dynamic learning system.

Neural networks have massively parallel, distributed storage and processing, self-organizing, adaptive, and self-learning capabilities, and are particularly well-suited for handling inaccurate and ambiguous information processing problems that require many factors and conditions to be considered simultaneously. Using the extracted five variables and training through the obtained data, a BP neural network model is established, in which the model topology map is:

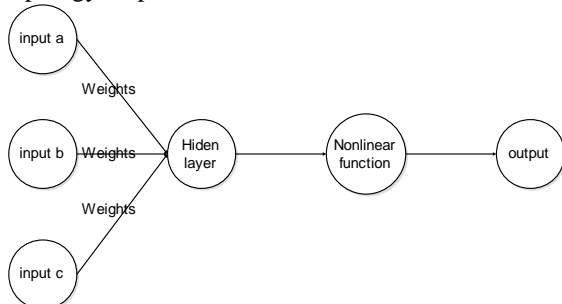


Figure 4 BP neural network topology map

The neural network model is constructed by using the extracted five variables. The model is divided into input layer, hidden layer and output layer. According to the neural network principle, the relationship is obtained as follows:

$$S_1^{(1)} = W_{11}^{(1)}x_1 + W_{21}^{(1)}x_2 + \cdots + W_{51}^{(1)}x_5 + b_1^{(1)}$$

$$S_1^{(1)} = W_{12}^{(1)}x_1 + W_{22}^{(1)}x_2 + \cdots + W_{52}^{(1)}x_5 + b_2^{(1)}$$

$$S_1^{(1)} = W_{13}^{(1)}x_1 + W_{23}^{(1)}x_2 + \cdots + W_{53}^{(1)}x_5 + b_3^{(1)}$$

Table 3 confusion matrix

The true situation	Forecast is positive	Forecast is reverse
--------------------	----------------------	---------------------

Where W_{ij}^l denotes the weight between the i th node of the l th layer and the j th node of the $l+1$ th layer; b_i^j denotes the offset term of the i th node of the $l+1$ th layer; and S_j^l denotes the j th node of the $l+1$ th layer with the input value, and when l is equal to 1, there is:

$$S_j^l = \sum_{i=1}^m \quad (2)$$

Use $\theta(S_j^l)$ to indicate the output value of the j th node of the $l+1$ th layer after the activation function $\theta(x)$. Finally, the output value can be obtained:

$$hw, b(x) = \theta(S_1^{(2)}) = \theta(W_{11}^{(2)}\theta(S_1^{(1)})) + \cdots \quad (3)$$

$$(W_{41}^{(2)}\theta(S_4^{(1)})) + (W_{51}^{(2)}\theta(S_5^{(1)})) + b_1^{(2)}$$

(2) BP neural network performance evaluation

This paper establishes a typical machine learning model. Through a large amount of data learning and training, the model can obtain the ability to identify optical characters through data. Therefore, the confusion matrix can be used to evaluate the performance of the established neural network model. The confusion matrix, also called the error matrix, is a standard format used to represent the accuracy evaluation, and is represented by a matrix of n rows and n columns. The specific evaluation indicators have overall accuracy, drawing accuracy, user accuracy, etc. These precision indicators can reflect the accuracy of classification from different sides. The confusion matrix is used as a visualization tool, especially for supervised learning. In the image accuracy evaluation, it is mainly used to compare the classification result with the actual measured value, and the accuracy of the classification result can be displayed in a confusion matrix. The confusion matrix is calculated by comparing the position and classification of each measured pixel with the corresponding position and classification in the classified image.

The correct rate calculation formula is

$$accuracy = \frac{TP + TN}{N}$$

Among them $N = TP + FP + FN + TN$

The true positive rate is calculated as

$$TPR = \frac{TP}{(TP + FP)}$$

The false positive rate is calculated as

$$FPR = \frac{FP}{(FP + TN)}$$

Among them, some necessary definitions of the confusion matrix are shown in Table 3.

positive	TP	FN
Anti	FP	TN

5. CONCLUSION

In this paper, the BP neural network model based on many sample spaces is constructed. The obtained matrix can calculate the correct rate of about 81.36%. Of course, the recognition rate of OCR is impossible to reach 100%. To a large extent, this is a good, high-quality training result that improves the efficiency and accuracy of recognition.

REFERENCES

- [1] Li Zhan. Design and implementation of optical character recognition application based on Android platform. Nanjing University, 2016.
- [2] DONG Tianyu, CHEN Zhikun, LI Wei. An Improved Method of License Plate Character Recognition Based on BP Neural Network. Journal of Chengde Petroleum College, 2017, 19(04): 53-58.
- [3] Wang Na. A License Plate Character Recognition Algorithm Based on BP Neural Network. Computer Knowledge and Technology, 2017, 13(32): 201-202.
- [4] Li Jun, Zhang Weiyuan. Study on heat insulation value distribution of multi-layer clothing system. Journal of donghua university (natural science edition), 2003(03): 11-14.
- [5] Yan Lin, Xia Yiya. Testing and analysis of clothing insulation performance. Journal of hefei university of technology (natural science edition), 1998(S1): 72-78.

Identification based on Color and Substance Concentration

Mingze Wang^{1,2}, Chen Fan^{1,2}, Jiaqi Zhang^{1,2}, Bin Bai^{3,*}

¹Engineering Computing and Simulation Innovation Lab, North China University of Science and Technology, Tangshan, 063210, China

²College of Electrical Engineering, North China University of Science and Technology, Tangshan, 063210, China

³College of Science, North China University of Science and Technology, Tangshan 063210, China

*E-mail: 956201990@qq.com

Abstract: In this paper, we obtain the concentration of the substance to be measured by establishing the quantity relation between the color reading and the substance concentration. In this regard, linear regression model and nonlinear regression model are established to study the quantitative relationship between them, and correlation coefficient, DW and other methods are used to evaluate the model. By using correlation analysis, it is found that there is a multiple linear relationship between the five color readouts, and it is impossible to establish a multiple linear regression model. Through literature review, it is known that there is a functional relationship between hue and saturation and the primary colors. Therefore, the regression model is established with the primary color as the independent variable. The effects of data volume and color reading on the model were investigated. Select two representative substances whose data amount varies greatly. Based on question 1, the data amount of each substance is gradually reduced. By fitting the trend and evaluation criteria, the data amount model is analyzed, and finally, the influence relation of data amount to the model can be obtained.

Keywords: Substance Concentration; Regression model; Compensation measures

1. INTRODUCTION

At present, the method of measuring the concentration of substances is usually by colorimetric method, which is to determine the concentration of substances to be measured by making the substances to be measured into solution and then dropping them on the surface of a specific white test paper, and changing them into colored test paper after they are fully reacted [1-3]. Due to the color sensitivity and observation error, this method is greatly affected in accuracy. With the improvement of photographic technique and color resolution, it is hoped to establish a quantitative relationship between color reading and material concentration. The color reading is to use the idea of dimensionality reduction, reduce the color index, re-fit the model, to observe the accuracy of the model [4,5]. Therefore, the effect of color index on the model is obtained.

2. ESTABLISHMENT AND SOLUTION

In order to obtain the relationship between the color reading and the concentration of the substance, the linear regression model should be established to find the relationship between them. However, when applying linear regression analysis, the existence of collinearity of independent variables should be checked. If the collinearity between the independent variables is large, the established model will have certain error. SPSS was applied to conduct colinear analysis of the five data sets, and the following results were obtained, as shown in Table 1:

Table 1 color reading and VIF diagram

species	histamine	Potassium bromate	Industrial base
B	900.92	38433.98	43.13
G	370.69	28.17	6330.07
R	51.69	5.21	24.90
H	93.80	4.72	158.97
S	760.89	19.13	4800.65

species	Aluminium potassium	urea
B	195.00	453.55
G	18.92	24.33
R	82791.81	66.64
H	139.20	8.68
S	443.57	441.99

The variance expansion factor VIF refers to the ratio of variance between explanatory variables with multicollinearity and variance without multicollinearity. It's the inverse of tolerance, and the bigger the VIF, the more collinearity. By observing the table information, it can be seen intuitively that VIF in these five sets of data is basically greater than 10. In combination with the judgment method of VIF, when 0 When 10 is less than or equal to $VIF < 100$, there is strong multicollinearity. Serious multicollinearity occurs when VIF is greater than or equal to 100. Therefore, strong collinearity exists between independent variables. Therefore, the established regression equation has a large error, which is not desirable.

Through literature review, it is known that there is a

functional relationship between hue and saturation and the primary colors. As follows:

$$H = 0.1687 \times R - 0.3313 \times G + 0.5 \times B + 128$$

$$S = 0.5 \times R - 0.4187 \times G - 0.0813 \times B + 128 \quad (1)$$

Therefore, the influences of R, B and G on the concentration of substances will be selected as follows.

The multivariate linear regression model is a dependent variable affected by multiple independent variables. The remaining three variables are used for collinearity analysis and the table below is obtained in SPSS, as shown in Table 2.

Table 2: the relationship between the three variables and the concentration

species	histamine	Potassium bromate	Industrial base
B	900.92	38433.98	43.13
G	370.69	28.17	6330.07
R	51.69	5.21	24.90
species	Aluminium potassium	urea	
B	195.00	453.55	
G	18.92	24.33	
R	82791.81	66.64	

It can be seen from the table that the collinearity between the concentrations of B, G, R and 5 substances is strong, so a relatively accurate multiple linear regression model can be established.

Next, multiple regression models were established for the five substances given in annex data1.xls. The following five functional relationships are obtained.

Partial data of the multiple regression model established by histamine are as follows, as shown in Table 3:

Table 3 histamine composition analysis

color reading	B	Partial regression	95%CI
B	-0.172	0.398	(-1.14,0.80)
G	-2.289	0.458	(-3.40,-1.16)
R	0.651	0.907	(-1.56,2.87)
coefficient	F	F variation	DW
0.995	415.75	0.00	2.15

The function expression of histamine can be obtained from the table as follows:

$$y_1 = -0.172x_B - 2.289x_G + 0.651x_R + 182.387 \quad (2)$$

The coefficient of determination is 0.946, indicating that the regression equation is significant. And the probability of F is rejected, so the regression model holds.

Function of potassium bromate, as shown in Table 4.

Table 4 potassium bromate composition analysis

color reading	B	Partial regression	95%CI
B	-1.36	0.39	(-2.32,-0.40)
G	7.46	5.53	(-6.08,1.00)
R	-7.18	4.41	(-7.99,3.61)
coefficient	F	F variation	DW
0.941	31.771	0.000	1.357

The expression of potassium bromate can be obtained from the table as follows:

$$y_2 = -1.366x_B + 7.462x_G - 7.187x_R + 152.291 \quad (3)$$

The coefficient of determination is 0.941, indicating that the regression equation is significant. And the probability corresponding to F rejects H. Therefore, the regression model is established, as shown in Table 4.

Table 4 Function of industrial alkali

color reading	B	Partial regression	95%CI
B	0.06	0.13	(-0.37,0.49)
G	-0.04	0.05	(-0.22,0.14)
R	-0.10	0.25	(-0.89,0.69)
coefficient	F	F variation	DW
0.482	0.931	0.523	0.894

The functional expression of industrial alkali can be obtained from the table as follows:

$$y_3 = 0.06x_B - 0.04x_G - 0.10x_R + 15.538 \quad (4)$$

Function of aluminum potassium sulfate, as shown in Table 5:

Table 5 composition analysis of aluminum and potassium sulfate

color reading	B	Partial regression	95%CI
B	-0.23	-1.96	(-3.89,3.43)
G	-0.19	-0.77	(-2.28,1.90)
R	-0.12	-1.83	(-2.61,2.36)
coefficient	F	F variation	DW
0.521	0.725	0.624	2.210

The function expression of aluminum potassium sulfate can be obtained from the table as follows:

$$y_4 = -0.231x_B - 0.19x_G - 0.124x_R + 63.451 \quad (5)$$

The coefficient of determination is 0.521, indicating that the regression equation is not significant. But the probability that F corresponds to H is rejected. However, the accuracy of the model is not high.

Correlation function of urea, as shown in Table 6.

Table 6 urea composition analysis

color reading	B	Partial regression	95%CI
B	-0.17	-0.89	(-152.42,-72.18)
G	-2.28	-0.01	(-235.83,235.41)
R	0.65	-0.01	(-254.40,249.99)
coefficient	F	F variation	DW

0.795	14.251	0.000	1.906
-------	--------	-------	-------

The function expression of urea in milk can be obtained from the table as follows:

$$y_5 = -112.304x_B - 0.209x_G - 2.203x_R + 13891.006 \quad (6)$$

The coefficient of determination is 0.795, indicating that the regression equation is more significant. And the probability corresponding to F rejects H. Therefore, the regression model is established.

To further analyze whether the five functional relations are accurate, we should look at the VIF and the autocorrelation coefficient between the three-color readings and the substance concentration. The following table can be obtained, as shown in Table 7:

R^2	0.94	0.99	0.48	0.52	0.79
-------	------	------	------	------	------

The observation table shows that the correlation coefficient between aluminum potassium sulfate and industrial alkali is small, which indicates that the accuracy of model establishment is not high. At the same time, according to F, it was determined that the industrial alkali could not establish a multiple linear regression model. However, the model fitting degree of histamine, potassium bromates and industrial alkali is good, and the multiple linear regression model can be established.

Evaluation criteria and results: through the establishment of the above five models, it is found that the determination coefficient, P value (Sig) and F test can determine whether the multiple linear regression equation can be established. Therefore, take these three quantities as evaluation criteria. 5 models were established based on the color reading in 3 and the concentration of substances, and the analysis was conducted according to the evaluation criteria.

The data volume of histamine and potassium bromate was at the average level, and the data was relatively complete, with the best fitting degree of the model.

The data volume of aluminum potassium sulfate and urea in milk is large, and there may be some points with large deviation in the data, resulting in the average fitting degree of the model. However, it conforms to the multiple regression model.

3. MULTIPLE LINEAR REGRESSION

Based on the idea of establishing regression model in question 1, the influencing factors of color reading on material concentration include: R, G, B, and these three factors, and the mathematical model is established between the material concentration and the three variables. As a result, one variable is affected by multiple variables and the regression model is adopted. To analyze the data in the attached data2.xls, the linear correlation between the independent variable and the dependent variable should be judged first. Through VIF, whether there is multicollinearity between the variables can be determined, and the following table is obtained, as

shown in Table 8.

Table 8 VIF judgment

Color readings	B	G	R
VIF	63.752	696.164	73.415

Through VIF judgment, it can be known that there is a significant correlation between material concentration and color reading, so multivariate linear regression model can be used for analysis. The following results can be obtained, as shown in Figure 1:

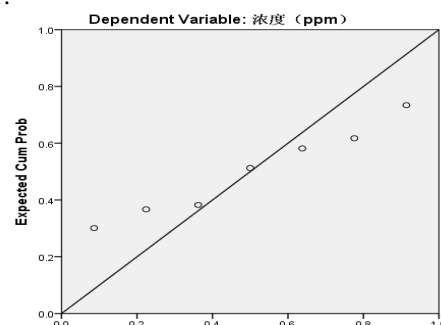


Figure 1 relation between concentration and color readings

Using SPSS to establish the regression model, the following table is obtained, as shown in Table 9:

Table 9 SPSS analysis results

color reading	B	Partial regression	95%CI
B	6.48	0.60	(-40.51,53.47)
G	-5.75	-2.27	(-19.20,7.70)
R	-5.88	-0.87	(-22.01,10.14)
coefficient	F	F variation	DW
0.811	4.280	0.132	2.087

At the same time, the multivariate linear relationship between the concentration of sulfur dioxide and the three-color readings is obtained:

$$y_s = 6.482x_B - 5.753x_G - 5.883x_R + 769.284 \quad (7)$$

The coefficient of determination is 0.811, indicating that the regression equation is more significant. And the corresponding probability rejects H. Therefore, the regression model is established. Then, the function relation expression is fitted. Take the average values of R, G and B of different concentrations first, and the results are shown in the figure below, as shown in Table 10:

ppm	R	G	B
0	153.2	146.4	157.4
20	144.33	115	170.33
30	145.25	114	175
50	141.67	99	175
80	140.67	96	181.67
100	139	96	175
150	138.75	86.25	177.5

Table 10 real concentration and fitting concentration
Then test the concentration using the linear equation

obtained, as shown in the table below; At the same time, the following line chart was made by using Excel, as shown in Figure 2:

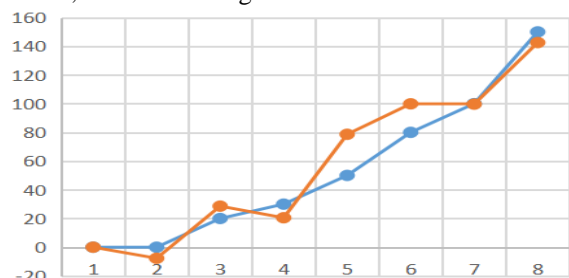


Figure 2 test the concentration

Series 1 is the original concentration and series 2 is the fitting concentration. It can be found that the fitting effect is general through the line graph, and there is room for improvement and optimization.

The multivariate nonlinear model is applicable to the dependent variable which is the function form of independent variable at least once. The linear relationship between the concentration of sulfur dioxide and the three-color readings can be found by solving model 1. Therefore, it explores the establishment of multivariate nonlinear model to analyze the problem.

SPSS was used for regression analysis to obtain the function expression:

$$y_{s2} = -0.05415x_1^2 + 0.015434x_2^2 + 0.014762x_3^2 + 514.0142$$

At this point, the correlation coefficient is 0.962, indicating that the model establishment is relatively accurate. According to the formula, the fitting data is calculated as follows, as shown in Table 11:

Table 11 comparison of actual concentration and fitting concentration

Real concentration	0	20	30
Fitting concentration	-2.5	29.	26.4

Then test the concentration using the linear equation obtained, as shown in the table below; At the same time, the following line chart was made by using Excel, as shown in Figure 3:

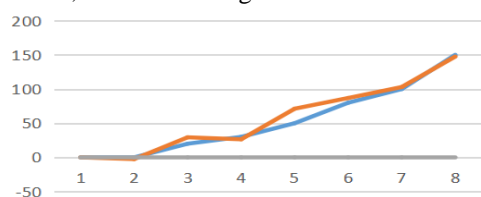


Figure 3 test the concentration

Series 1 is the original concentration and series 2 is the fitting concentration. It is found that the fitting effect is good through the line graph. The accuracy of the model has been improved.

4. THE ERROR ANALYSIS

Residual analysis refers to the difference between the observed value and the predicted value (fitting value), namely the difference between the actual observed value and the regression estimate. In regression analysis, the difference between the measured values

and those predicted by the regression equation. The residual follows the normal distribution $N(0, t1 \ 2)$. There are as many residuals as there are pairs of data. Standardized residuals, expressed as pixels. Values *comply with standard normal distribution $N(0,1)$.

Therefore, there is an optimized space for this model, which can remove the abnormal data points at 95% confidence level without participating in regression line fitting. The accuracy of the model will be improved.

The fitting degree of real data is better than that of linear model. The standard residual error is low and the model accuracy is high. However, the multivariate nonlinear model is more complex, and the data points with large errors can also fit the fitting model within a certain range. But the overall impact is low, as shown in Figure 4.

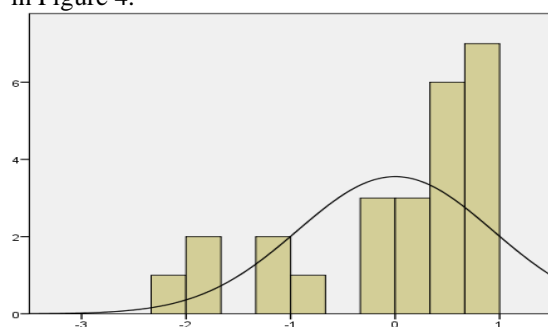


Figure 4 real data fitting

5. MODEL EVALUATION

First, the data in the attachment are processed and the fitting trend chart is made, which can reflect the trend of the data intuitively. The error shown can also be shown through the image. Some data points may have a certain deviation, without considering whether there are abnormal data points in the data, which may have an impact on the model.

REFERENCE

- [1] Dong senior colonel. Multiple nonlinear regression model based on MATLAB. Journal of yunnan normal university (natural science edition), 2009, 29(02):45-48.
- [2] Li Chunyan, Shen Jun, Li Jianhua. Determination of cyanide concentration in environmental and biological samples by digital colorimetry. Chinese inorganic analytical chemistry, 2012, 2(02):24-26.
- [3] Shen Jichen, Wang Xueqing, Liu Bangli and Zhang Weihong. Study on the determination method of concentration of colored solution based on image colorimetry. Optical instrument, 2008(02):9-12.
- [4] Zhu Xinyan, Shi Zhongke. Outlier detection and removal method based on residual characteristic analysis [J]. Flight mechanics, 2008, 26(06):79-83.
- [5] He Xiping, Zhang Qihua. Image processing and analysis based on MATLAB. Journal of chongqing technology and business university (natural science edition), 2003, 20 (2): 22-25.

Vehicle Brake Air Energy Storage and Energy Conversion Device

Jianhu Xu*, Zixuan Qiao, Jiaxuan Jiang

Engineering Computing and Simulation Innovation Lab, North China University of Science and Technology, Tangshan, 063210, China

*E-mail:1729667013@qq.com

Abstract: Based on the idea of transforming the energy consumed by automobile braking into air energy storage to speed up the start of automobile, this paper puts forward the energy recovery and utilization method using one-way valve as the gas collection device and pneumatic motor as the driving device.

Keywords: One-way valve, air motor; AMESim; simulation; Energy recovery and utilization

1. INTRODUCTION

Gas collecting device model is established through the thermodynamic analysis, the main principle of the model for the pneumatic transmission system to transfer the motion of the vehicle due to loss of braking energy is converted to gas pressure can be stored in the storage tanks, complete energy recovery and auxiliary braking process, the final will be stored in a storage tank of high pressure gas in the car to start by pneumatic motor driven will air the potential energy into mechanical energy to drive wheel running. A mathematic model of the air storage gas collecting device, and the mathematical model of vehicle of energy recycling formula and AMESim simulation analysis, the selection of different speed and comparison between the simulation training and the results get automobile brake air energy storage energy conversion device on the degree of auxiliary brake vehicles have a tend to be asymptotically stable process [1-3]. At this point, the energy recovery rate is about 34.33%. Braking energy recovery technology refers to the process of braking, on the one hand, the system makes the driving speed of the vehicle gradually reduce to the required speed, and even decelerate to the state of parking [4,5]. On the other hand, the lost kinetic energy during the deceleration process can be recovered, that is, the heat energy generated during braking can be converted into mechanical energy and stored in the energy storage device for use by other systems of the vehicle. It can not only reduce the friction loss of transmission braking, but also reduce the consumption of fuel, thus reducing the emission of exhaust, improving the energy utilization rate and ultimately achieving the goal of energy saving and emission reduction. At present, the most widely used hybrid electric vehicle is that when the vehicle is braking, the motor is controlled to operate in the power generation mode to

charge the battery and convert the energy into electricity. This braking energy recovery effect is greatly affected by the battery state, and frequent charging and discharging of the battery will reduce its service life. In addition, a new way of reclaiming brake energy based on air energy storage is proposed. Compared with hybrid electric vehicles, pneumatic energy storage system and flywheel energy storage system have the advantages of light weight, low cost, high reliability and high efficiency. Hydraulic energy storage system requires high performance seal. Leakage will not only affect its own performance, but also seriously pollute the environment, bringing expensive maintenance costs to people. Air pressure energy storage system does not need complicated pneumatic circuit, and takes common air as the working medium. It is not only clean and green, but also requires less components. Compared with hydraulic energy storage system, the cost is lower and the electrochemical energy storage is longer. Therefore, the air pressure energy storage scheme is the best choice for vehicle braking energy recovery system

2. BASED ON THE DOMESTIC CAR, THIS PAPER PROPOSES ANOTHER METHOD OF BRAKING ENERGY RECOVERY AND UTILIZATION, AND OBTAINS THE ULTIMATE ENERGY EFFICIENCY OF THE DEVICE THROUGH MODELING AND ANALYSIS

2.1 Air energy storage and gas collection device

2.1.1 introduction to air energy storage gas collection

1- airway; 2- brake controller; 3 - cylinder; 4 - the piston; 5- linkage mechanism; 6 - K1 valve; 7- valve K2; 8- one-way valve; 9- gas storage tank; 10- pneumatic drive motor.

Like the traditional internal combustion engine, the device is modified based on the original cylinder head. First brake controller received brake signal, and allows the gas to open the corresponding valve via the catheter 1 into the device, then open valve K1, linkage drives the piston moves down, makes full of gas in the cylinder, the piston moving up in the process of closing valve K1 K2, open the valve the air pressure into the storage tanks, has completed a cycle. It is worth noting that a one-way valve must be added between the cylinder and the storage tank to prevent the gas body pressure in the cylinder from rising.

When it exceeds the gas pressure in the cylinder, the gas in the storage tank enters the cylinder, as shown in Figure 1.

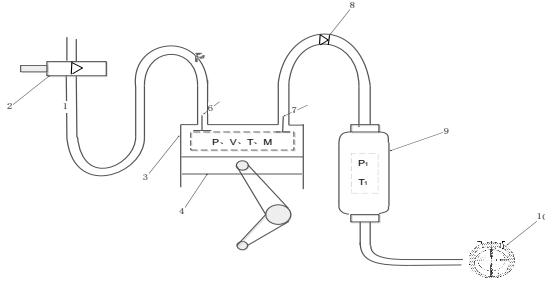


Figure 1 air energy storage gas collecting device

2.1.2 establishment of air energy storage gas collection model

The engine has no fuel injection or combustion during compressed air braking, which is simpler than traditional mode. Firstly, the motion energy of the vehicle is transmitted to the vehicle semi-axle in the form of inertia torque. Secondly, the vehicle semi-axle transmits the torque and speed to the linkage mechanism in the system, and then drives the valve to open and close and then stores the air compression in the air storage tank. When the vehicle is braking, the driving force disappears. Currently, due to the action of inertia torque, the wheel of the vehicle continues to rotate. Through the semi-axle and connecting rod mechanism, torque and speed are input to the system air energy storage and gas collection device. Therefore, the Angle (φ) of connecting rod mechanism is taken as the independent variable in the model of air energy storage and gas collection device.

In establishing the mathematical model, the following assumptions are made

- 1) the gas in the cylinder is uniform and is an ideal gas;
- 2) the gas flowing into or out of the cylinder shall be subject to steady flow, and the kinetic energy of the inlet and outlet shall be ignored;
- 3) the cylinder wall temperature is uniformly distributed and does not change with time.

On the premise of the above hypothesis, combined with the conservation law of mass and energy, the continuity equation of gas in the cylinder can be expressed as

$$\frac{dp}{d\varphi} = \frac{\alpha-1}{V} * \left(\frac{-\alpha}{\alpha-1} p \frac{dV}{d\varphi} + \frac{\delta Q_w}{d\varphi} - H_c \frac{\delta m_c}{d\varphi} - H_p \frac{\delta m_p}{d\varphi} \right) \quad (1)$$

Where: $\frac{dp}{d\varphi}$ is the gas pressure in the cylinder, V is the working volume in the cylinder, m and H are respectively the mass and specific enthalpy of the gas,

and the subscript j, c, p respectively represent the intake, inflation and exhaust. δQ_w is the heat transfer between the cylinder and the gas; α is the specific heat capacity ratio of air.

Gas mass flow through valve k_2 and one-way valve is expressed as

$$m = \mu \varphi A \sqrt{\frac{p_1}{V_1}} \quad (2)$$

Where: μ is the flow coefficient, the flow coefficient of inlet and exhaust valve is obtained through airway steady flow test, and the flow coefficient of one-way valve is obtained through aerodynamic element steady flow test; φ is the flow function; A is the theoretical flow cross-sectional area; V_1 is the specific volume of upstream gas; p_1 is the upstream gas pressure.

The heat transfer expression of the cylinder wall and the gas in the cylinder is

$$\frac{dQ_w}{dt} = h_x A_w (T_w - T) \quad (3)$$

Where: h_x is the heat transfer coefficient between the cylinder wall and the gas in the cylinder, T_w is the cylinder wall temperature, T is the gas temperature in the cylinder, A_w is the effective heat transfer area. The heat transfer coefficient is obtained by the empirical formula of turbulence in the pipe:

$$h_x = 0.1129 p^{0.8} \bar{u}^{-0.8} T^{-0.594} D^{-0.2} \quad (4)$$

Where: \bar{u} is the average speed of piston and D is the diameter of cylinder.

2.2 vehicle model establishment

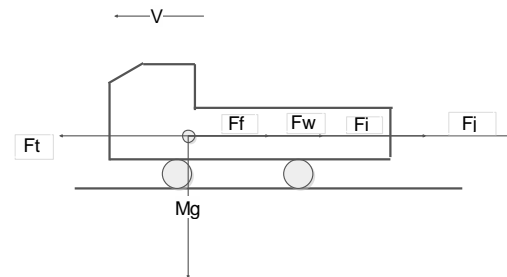


Figure 2 vehicle driving force

When the vehicle is running, as shown in Figure 2, the acceleration resistance of the vehicle is considered.

$$F_t = F_j + F_f + F_w \quad (5)$$

Where: F_t is the driving torque of the driving vehicle, F_j is the acceleration resistance, F_w is the air resistance and F_f is the rolling resistance.

2.2.1 driving torque

The torque produced by the vehicle engine is transmitted to the driving wheel via the transmission system. At this point, the torque acting on the driving

wheel produces a pair of circumferential force of the ground. The reaction force of the ground facing the driving wheel is the external force driving the car, and the force becomes the driving force of the car. Values for

$$F_t = \frac{T_{tq} i_g \eta_T}{r_r} \quad (6)$$

Where, T_{tq} torque of the engine, i_g transmission ratio of transmission, i_0 final drive ratio, η_T mechanical efficiency of drive train.

2.2.2 rolling resistance

In the process of tire rolling, the friction elements, such as tire and rubber, cord and so on, generate friction between the components of each component of heat dissipation of friction. This loss is called hysteresis loss elastic element. Due to the energy consumption of compression damping, the damping hysteresis loss in tire friction, the performance loss of this hysteresis resistance even hinders the motion of wheels. Therefore, the rolling resistance can be considered as the ratio of the thrust required to the wheel load when the wheel rolls under certain conditions, or the thrust required by the unit vehicle gravity. That is to say, the rolling resistance is equal to the product of the rolling resistance coefficient of the car and the load of the wheel, i.e

$$F_f = f M_g \cos \alpha \quad (7)$$

Where, M_g is the total gravity of the vehicle.

1.2.3 air resistance

The force of air on the vehicle the force of the vehicle in the direction of travel becomes air resistance. Air resistance is divided into pressure resistance and friction resistance. In the range of vehicle speed, air resistance is directly proportional to the dynamic pressure of airflow relative to speed, i.e

$$F_w = \frac{1}{2} C_D A \rho u_r^2 \quad (8)$$

Where, C_D is the air resistance coefficient

1.2.4 acceleration resistance

The acceleration of the translational inertia force is produced by the translational mass, and the rotational inertia force moment is produced by the rotational mass. In order to facilitate the calculation, the moment of inertia of rotating mass is generally converted into translational mass inertial force. Namely

$$F_j = \delta m \frac{d\mu}{dt} \quad (9)$$

Therefore, the expression of F_t , F_j , F_f , F_w is substituted into

$$M \frac{du_r}{dt} = i \frac{T_{tq}}{r_r} - f M_g \cos \alpha - \frac{1}{2} C_D A \rho u_r^2 \quad (10)$$

When the car brakes, you get

$$M \frac{du_r}{dt} = i \frac{T_{tq}}{r_r} + f M_g \cos \alpha + \frac{1}{2} C_D A \rho u_r^2 \quad (11)$$

2.3 calculation model of braking energy recovery efficiency of the device

For the convenience of study, the energy transfer of a moving vehicle during a continuous period after the recovery system is turned on is analyzed below. The equilibrium equation of the vehicle is:

$$\frac{\delta}{2} m (v_2^2 - v_1^2) = E_p + E_f + E_j \quad (12)$$

According to the law of isothermal change of gas, the work done by unit volume expansion in gas storage tank is:

$$W = m \int_{p_1 v_1}^{p_0 v_2} p dv = m R T_s \ln \frac{p_s}{p_0} \quad (13)$$

The formula of braking energy recovery efficiency when the vehicle is driving on the expressway is:

$$\eta = \frac{\Delta p}{\Delta E} = \frac{m R T_s \ln \frac{p_s}{p_0}}{\delta (v_2^2 - v_1^2) m / 2} \quad (14)$$

Where, η is the energy recovery efficiency, and v_1 is the speed after driving, as shown in Figure 3.

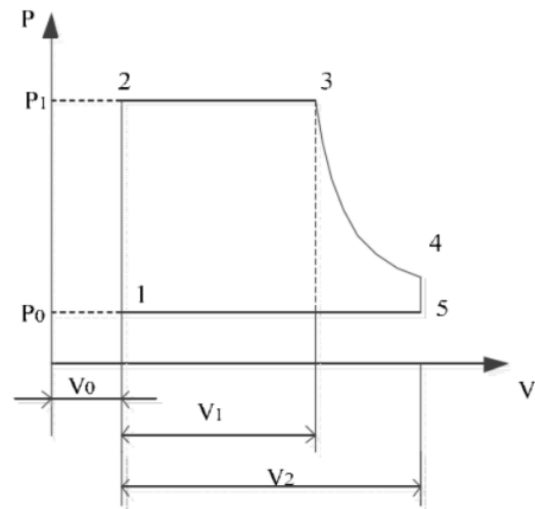


Figure 3 PV diagram of gas storage tank energy release

3. AMESIM SIMULATION TRAINING

3.1 AMESim is introduced

LMS Imagine.Lab AMESim is an integrated modeling and simulation platform for integrators, electricity, liquid and gas. It not only provides a single platform for users to establish complex multi-disciplinary system models, but also enables users to conduct in-depth simulation analysis on this basis

3.2 The AMESim simulation

In order to study the effect of deceleration and braking energy recovery of transport vehicles, namely

the feasibility of the air energy storage energy conversion device, this paper USES AMESim software to establish a simulation model of the pneumatic energy storage braking energy recovery system

3.2.1 selection of simulation parameters, as shown in Table 1

Table 1 select simulation parameters

symbol	name	unit	numerical
m_z	Curb weight	K_g	2370
m_m	Full quality	K_g	4495
V_{\max}	Top speed	m/s	90
$V_{p\min}$ $v_{p\min}$	Minimum economic speed	m/s	40
$V_{p\max}$ $v_{p\max}$	Maximum economic speed	m/s	70
V_k	Air speed	m/s	1.0
C_D	Air resistance coefficient		0.55
ρ_k	Air density	K_g/m^3	1.2
F_f	Rolling friction	N	50

Table 2. Corresponding AMESim vehicle speed

Group number	1	2	3	4	5	6
speed	40	45	50	55	60	65
Corresponding speed	11	12	13	15	16	18

The speed is set in the AMESim, as shown in the figure, the simulation time is 100s, and the slope is set to 0, as shown in Table 2. The simulation results also show the change curves of vehicle speed and air pressure in the air storage tank, as shown in Figure 4.

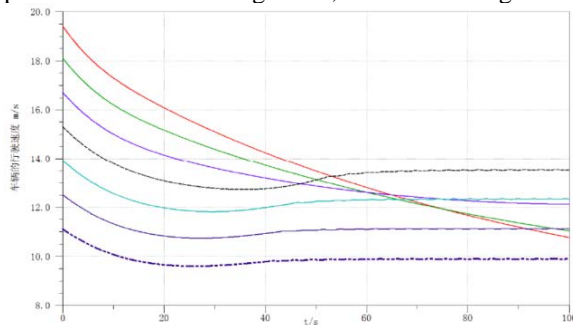


Figure 4 when the vehicle speed change curve

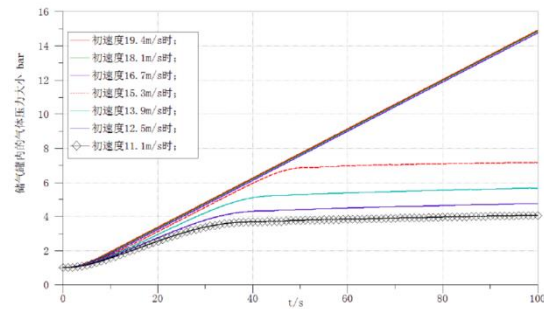


Figure 5 gas-holder in gas pressure changes Pressure, as shown in the store jar within 0 ~ 100 s, due to the speed of the car is in a declining phase, so the kinetic energy of the vehicle has also been gradually reduced, and part of the reduction of the kinetic energy into pressure of storage tanks, so the pressure rising stage, the pressure rise, no longer in the store jar calculation at this time for energy recovery efficiency, as shown in Figure 5.

$$\eta = \frac{\Delta p}{\Delta E} = \frac{mRT_s \ln \frac{p_s}{p_0}}{\delta(v_2^2 - v_1^2)m/2} = 0.32 \quad (15)$$

It can be clearly seen from FIG. 5 that, within 0 ~ 10s, the speed decrease is the largest, at 4.1%, and the speed decrease is smaller and smaller, from 4.1 to 2.2%, within 4 time periods. In the six periods between 40s and 100s, the decrease of vehicle speed remains unchanged at about 2.2%, which indicates that the air pressure energy storage braking energy recovery system has a process of asymptotically stable braking degree for vehicles. At this point, the energy recovery rate is about 34.33%.

REFERENCES

- [1] Li Guoqing, He Qing, Du Dongmei, Liu Wenyi. New variable pressure ratio compressed air energy storage system and its operation mode. Power system automation: 1-7.
- [2] Guo Huan, Xu Yujie, Zhang Xinjing, Guo Congsheng, Chen Haisheng. Variable operating characteristics of regenerative compressed air energy storage system. Chinese journal of electrical engineering: 1-13.
- [3] Liu Hui, Zhang Lei, Zhang Junjie, Wang Shunsen, Xie Yonghui. Thermodynamic analysis of distributed energy system based on compressed air energy storage. Energy saving technology, 2008, 36(04):325-330.
- [4] Wang Yunliang. Study on dynamic coordination optimization control of miniature compressed air energy storage system. Shandong university, 2018.
- [5] Dai Li. Energy storage determines the development level of renewable energy. Energy conservation and environmental protection, 2018(05): 26-27.

Design of Urban Domestic Waste Treatment Charge Scheme based on Factor Analysis

Guoqing Wang^{1,2}, Honglei Lin^{1,2}, Donghao Jin², Cuihuan Ren^{3,*}

¹Engineering Computing and Simulation Innovation Lab, North China University of Science and Technology, Tangshan, 063210, China

²North China University of Science and Technology, Tangshan 063210, China

³College of Science, North China University of Science and Technology, Tangshan 063210, China

*E-mail: 979624482@qq.com

Abstract: The basic idea of the factor analysis method is to classify the observed variables and use the sum of the linear functions of the common factors and special factors to describe each component of the original observation. This article takes the urban residential waste treatment and charging standards as the research object which has proposed the design of fee plan based on factor analysis and embodies the advantages of factor analysis in the application of urban waste processing and billing processing. This article also carried out a Logistic population forecast on the growth of the number of urban residents, and made a test based on the grey theory prediction analysis of the corresponding municipal solid waste production.

Key words: Factor Analysis; Logistic population forecast; Grey theory prediction analysis; Urban Domestic Waste Billing

1. INTRODUCTION

With the rapid development of urban economy and rapid population growth, domestic waste has also rapidly increased and has become a new source of pollution. Therefore, it is imperative to formulate a reasonable and effective classification standard for domestic garbage. For this issue, Factor analysis was used to extract common factors from a large number of garbage disposal data groups. Based on the correlation coefficient matrix, principal component analysis was used to extract components with a cumulative contribution of 80%. According to principal component analysis, After deciding to retain the n principal components, we then find the sum of the squares of the n feature vectors as commonalities, and use this value instead of the diagonal of the correlation matrix to form the approximate correlation matrix. On the basis of the correlation coefficient matrix, the number of factors and the coefficient of factors are further determined by the method of repeatedly finding eigenvalues and eigenvectors, is shown in Figure 1.

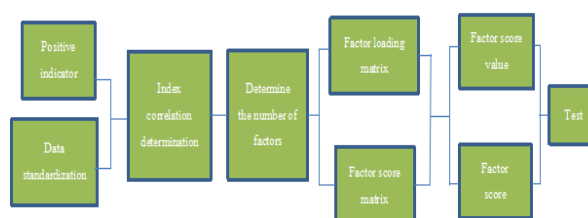


Figure.1 Flow chart of factor analysis model solution
2. URBAN WASTE ACCOUNTING PROCESSING MODE

(1) Manage temporary fees

The urban waste treatment model needs to go through transit stations, collection and transportation stations, garbage disposal points and other processes. Based on this process, urban domestic waste is classified into the following payment items, is shown in Figure 2:

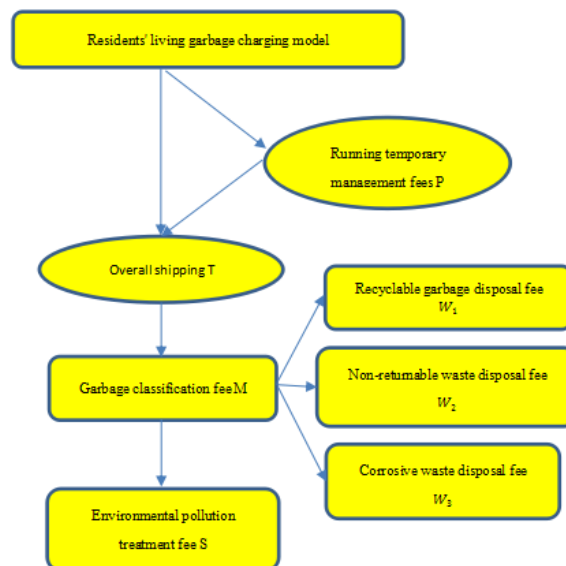


Figure.2 Residents' living garbage charging model
Residues of household garbage shall be set in temporary storage sites within a small area, and environmental protection measures such as anti-corrosion and anti-fungal protection shall be carried out at the temporary storage point. When the amount of domestic garbage reaches a certain amount, a unified garbage loading and transportation will be carried out. The temporary management fee for kilograms of domestic garbage is:

$$P = Ma + Ca \quad (1)$$

(2) Overall freight

The overall distribution costs are related to the actual transportation costs. Different waste classification or treatment modes correspond to different waste disposal centers. Such as incineration plants, landfills, kitchen waste disposal centers, etc. Therefore, the transportation cost will change according to the number and location of the corresponding end processing centers according to different classification processing modes. The cost conversion rate per kilogram charge and actual transport cost is β .

$$T = \beta C \quad (2)$$

The majority of urban garbage collections follow the path model of "waste transfer station collection-total collection of collection points — delivery to end-of-site waste treatment plants". Transportation costs are mainly composed of fuel costs, total car value, and driver labor costs, which are denoted as C_f , C_r , and C_s , respectively. The total cost of transporting domestic waste can be expressed as:

$$C = C_f + C_r + C_s \quad (3)$$

The fuel cost is related to the total length of the route:

$$C_f = PY \times LC \quad (4)$$

The total length of the route is related to the total amount of garbage removal, the capacity of garbage trucks and the average distance of single transportation:

$$L = \left(1 + \frac{H}{D}\right) S \quad (5)$$

The car value C_r is the current value of the car:

$$C_r = V \times m \times fn \quad (6)$$

The quantity of transport vehicles is usually fixed value. When the growth of garbage is stable, it will not be suddenly purchased in large quantities, and the total amount of garbage production does not dynamically float during calculation. The driver's labor cost C_s is the driver's insurance fee, monthly salary, and various tax items:

$$C_s = Ta \times L \quad (7)$$

(3) Garbage classification fees

The collected large amount of urban domestic garbage is classified into two categories. The first smart machine assembly line sorting, and the second time the artificial assembly line sorting. The intelligent machine assembly line employs optical technology [1] to control the nozzles mounted on the conveyor belt by computer, and use the high-pressure gas to blow various useful materials on the conveyor belt into the collection container placed beside the conveyor belt. This process is very fast because the conveyor belt operates at 2.7 meters per second and each system can sort 14 tons of trash per hour.

The garbage sorting efficiency of this project should be 1.8-2.6 tons/person/day. In accordance with the manual sorting of garbage components, the

requirements for bag breakage will be increased, and the sorting amount of recyclables will be increased, and the sorting efficiency will be reduced correspondingly. If each person works 8 hours per day, the manual sorting efficiency is revised to approximately 1 ton/person/day according to the survey practice [2].

According to sampling and analysis standards, the per-kg garbage collection fee is:

$$M = d \left(\frac{Q}{v} \right) + d' \left(\frac{Q'}{v'} \right) \quad (8)$$

(Q' is the number of garbage after sorting for the first time, v' is the number of sorting garbage during manual unit time, and d' is the sorting cost for manual unit time)

(4) All kinds of garbage disposal fees

Recyclable waste mainly refers to waste paper, waste plastics, used furniture, scrap metal, waste glass, etc., which can be directly recycled or reused and recycled. In the initial classification of domestic waste, perishable organic foods can be separated from domestic waste. Perishable garbage is mainly composed of organic substances such as starches, dietary fibers, and animal fats. The content of perishable garbage is between 60% and 85% of the total waste output. Non-returnable waste refers to heavy or toxic waste that poses a real or potential hazard to human health or the environment.

At present, there are three methods for sanitary waste disposal, composting, and incineration. China's landfill disposal, composting, and incineration accounted for 79.3%, 1.5%, and 18% of the total (other disposals were 1.2%) which accounted for 56.6%, 1.1%, and 12.9% of the volume of garbage transported [8], is shown in Figure 3.

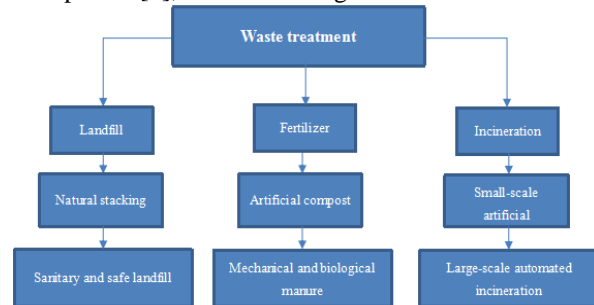


Figure.3 Waste treatment

The advantage of the sanitary filling method is that the amount of garbage is large and convenient. U1 per kilogram of landfill waste disposal fee is:

$$U1 = LA(b) + BU(b) + OP(b) \quad (9)$$

Two kinds of grate burning furnaces and fluidized beds for waste incineration treatment process are on the market in China. However, grate furnace technology is the main method (most of which are imported equipment or imported technology). The market share of grate furnaces and fluidized bed incinerators is 64:36. The waste disposal cost per kilogram is:

$$U2 = LA(c) + BU(c) + OP(c) \quad (10)$$

That is, the fee U per kilogram of garbage disposal method is:

$$U = 0.75U_1 + 0.25U_2 \quad (11)$$

In addition, the weight of all kinds of domestic garbage weight W is:

$$W = W_1 + W_2 + W_3 \quad (12)$$

(5) Environmental pollution treatment fee

In addition, leachate produced by precipitation soaking or degradation of domestic wastes enters the soil to pollute groundwater, or directly into rivers, lakes and seas, causing water pollution. The fine particles and dust in the living garbage float in the wind and enter the air to pollute the environment. After biodegradation, some organic solid wastes release biogas, consume oxygen from the upper space, and rot the plants. The chemical reaction of the household waste produces toxic gases that pollute the atmosphere^[3].

$$S = WL + LE + PO \quad (13)$$

(6) Comprehensive fees

$$K = U + M + T + P \quad (14)$$

$$K = 0.75U_1 + 0.25U_2 + z + z' + \beta C + Ma \quad (15)$$

3. FEES STANDARD

Two standard pricing methods are used for the charging standards of urban domestic landfills. The two pricing methods consist of two parts: One part is the fixed fee paid by the consumer for the right to use a certain product or service, regardless of the amount of consumption and adopts a quantitative calculation method. The other part is directly related to the consumption of user fees, which is paid at a price equal to the marginal cost. In simple terms, its composition is to make up for the basic cost of fixed costs and the amount of fees to make up for variable costs.^[4] In the urban household waste measurement and charging model, the pricing standards of the two departments are composed of basic expenses and unit use fees: The basic cost is based on the fixed investment and the corresponding capital gains of the initial construction of a municipal solid waste treatment facility, while the unit use cost is based on the daily operating costs of a municipal solid waste treatment facility. The total amount of payment for each item is summed up.

4. PREDICTION OF DAILY PRODUCTION OF DOMESTIC WASTE

The garbage system has both known and unknown information. It is an intrinsic grey system. Urban waste generation generally has the following characteristics: Monotonically increasing, and non-negative, the rate of change is non-uniform and conforms to the grey theory modeling conditions [5]. The original data is cumulatively generated for the purpose of weakening the randomness of the original time series. Let the time series $x^{(0)}$ have n observations,

then

$$x^{(0)} = \{x^{(0)}(1), x^{(0)}(2), \dots, x^{(0)}(n)\} \quad (16)$$

generated by accumulation New sequence:

$$x^{(1)} = \{x^{(1)}(1), x^{(1)}(2), \dots, x^{(1)}(n)\} \quad (17)$$

Among :

$$x^{(1)} = \sum_{k=1}^i x^{(0)}(k) \quad (i=1, 2, \dots, n) \quad (18)$$

$$x^{(0)}(k) \quad (i=1, 2, \dots, n) \quad (19)$$

Then the corresponding differential equation of the GM(1, 1) model is:

$$\frac{dx^{(1)}}{dt} + ax^{(1)} = u \quad (20)$$

Construct cumulative data matrix B and constant vector Y_n , Using the Least Square Method to Obtain Gray Parameters a, μ , Among them: a is called developing grey number; μ is called endogenous control grey number. Let a^\wedge be the parameter vector to be evaluated, which can be solved:

$$a^\wedge = (B^T B)^{-1} B^T Y_n \quad (21)$$

The grey parameters are brought into differential equations and the differential equations are solved to get the prediction model:

$$x^{(1)}(k+1) = \left[x^{(0)}(1) - \frac{u}{a} \right] e^{-ak} + \frac{u}{a} \quad (22)$$

$$(k=0, 1, 2, \dots, n)$$

Accuracy test, using the residual test, correlation test and posttest error test and other common test methods for accuracy testing. If the accuracy meets the requirements, the model can be used for prediction. If the accuracy is not satisfactory, a residual correction model is still required to improve the accuracy, and then the model is used for prediction. Using the annual average amount of 5-year domestic garbage produced in Tangshan City as the original data series, the GM(1, 1) prediction model of annual domestic garbage production in Tangshan City can be obtained through gradual calculation according to the above-mentioned modeling steps:

$$x^{(1)}(t+1) = 337.67384e^{0.6517t} - 3160917 \quad (23)$$

As shown in the table, despite the implementation of garbage charging standards, there will be a trend of decreasing human waste output in a short period of time. If it can be implemented over a long period of time, it will promote the reduction of per capita living garbage.

REFERENCES

- [1] Liu Ping, Germany adopts high-tech garbage sorting. China Packaging News, 2004-04-27(002).
- [2] Hong Chi, Lv Yong. Discussion on Artificial Sorting Cost of Domestic Waste in Guangzhou. Guangdong Science and Technology, 2016, 25(06): 61-63.
- [3] WANG Xiuchuan, DONG Yang, ZHAO Hong.

Using the concept of circular economy to manage the environmental pollution of municipal solid waste. *Environment and Sustainable Development*, 2009, 34(04):35-38.

[4]Chen Li, Research on the theoretical model of the

application of two pricing methods in toll highway, *Price Monthly*, 2007(5).

[5] Li Xiaoming, Wang Min, Chen Zhaoyi. Gray theory model for predicting urban waste volume. *Environmental Engineering*, 2002, 20(2): 70-73.8.

Sleep Disease Research Based on SVM and Fuzzy Comprehensive Evaluation

Tingting Wang^{1, 2*}, Chenshuai Liu^{1, 3}, Liyan Dong^{1, 4}, Xu Zhou^{3, *}

¹ Engineering Computing and Simulation Innovation Lab, North China University of Science and Technology, Tangshan, 063000, China

² Yi Sheng College, North China University of Science and Technology, Tangshan 063000, China

³ College of Science, North China University of Science and Technology, Tangshan 063000, China

⁴ College of Metallurgy and Energy, North China University of Science and Technology, Tangshan 063000, China

*E-mail:625525957@qq.com

Abstract: Because of the many factors affecting sleep and the great impact on health, it is especially important to study sleep problems. In this paper, cross-indicator sleep quality, daytime dysfunction and hypnotic drugs were applied to establish a multi-combined SVM classification prediction model to explore the relationship between disease classification and sleep. Secondly, 90% of the data were selected as training samples, and the most significant of the three diseases in each of the remaining 10% were selected. A total of 21 groups of data were tested, and the accuracy of the observed model was 91.53%. Finally, with reference to recent related research to develop a healthy sleep program, the fuzzy comprehensive evaluation model is established to evaluate the effectiveness, and the total score is 89.75 points.

Keywords: Sleep disease; Multiple SVM; Fuzzy comprehensive evaluation

1. INTRODUCTION

According to incomplete statistics, the insomnia rate of Chinese adults is as high as 38.2%, and the rate of insomnia among teenagers is rising, which is very unfavorable for the growth of adolescents. Since 2001, the World Sleep Medicine Association has set March 21st as the World Sleep Day every year to remind people to pay attention to sleep [1]. In general, if you fall asleep for more than 30 minutes, it is a category of insomnia. If you suffer from long-term insomnia, you will feel tired all day, and your concentration will not be concentrated, which will affect your normal work and study. Severe insomnia may even cause neurological disorders, leading to imbalances in the body system and triggering various diseases. There are many factors affecting insomnia, which can be generally divided into objective factors and subjective factors [2-3]. Objective factors are external influences, while subjective factors are generally mental factors such as life stress, emotional loss, and spiritual excitement. Because of the pressure of learning and work during growth and development, the brains of young people are extremely prone to fatigue, which affects the quality of sleep. Therefore, it is especially

important to study the factors affecting sleep in the direction of human health.

2. DISEASE CLASSIFICATION BASED ON MULTIPLE SVM

According to the international classification of sleep diseases, the sleep diseases can be classified into seven types of sleeps: organic diseases, mental diseases, neurological diseases, insomnia diseases, drug-dependent diseases, senile diseases, and other diseases [4-8]. Diseases, and the primary indicators associated with sleep disorders associated with the indicators presented herein, include sleep quality, hypnotic drugs, and daytime dysfunction. In this paper, according to the correlation between various indicators, each specific disease is classified into seven categories according to the standard, and specific diseases included in each major type of sleep diseases can be obtained. Among them, the specific steps of SVM classification are as follows:

Step1: Record that x_1-x_7 represent seven indicator variables respectively. The known observation surface is $[a_i, y_i]$. First, find a classification surface of $(\omega \cdot x) + b = 0$. Among them, $x = [x_1, \dots, x_7]^T$ the following conditions are met:

$$\begin{cases} (\omega \cdot a_i) + b \geq 1, y_i = 0 \\ (\omega \cdot a_i) + b \leq 0, y_i = 1 \end{cases}$$

Where $y_i = 0$ is a disease, $y_i = 1$ is not a disease, $y_i[(\omega \cdot x) - b] \geq 1, i = 1, \dots, n$, the sample satisfying $(\omega \cdot a_i) + b = 0, 1$ is a support vector.

Step2: Build SVM quadratic programming model is as follows:

$$\min \frac{1}{2} \|\omega\|^2$$

Step3: Define generalized Lagrange function [5]:

$$L(\omega, \alpha) = \frac{1}{2} \|\omega\|^2 + \sum_{i=1}^n \alpha_i \{1 - y_i[(\omega, a_i) + b]\}$$

Derived separately,

$$\omega = \sum_{i=1}^n \alpha_i y_i a_i, \quad \sum_{i=1}^n \alpha_i y_i = 0,$$

brought into the original Lagrange function.

Step4: It can be transformed into the following model:

$$\max \sum_{i=1}^n \alpha_i - \frac{1}{2} \sum_{i=1}^n \sum_{j=1}^n \alpha_i \alpha_j y_i y_j (a_i \cdot a_j)$$

$$\begin{cases} \sum_{i=1}^n \alpha_i y_i = 0 \\ 0 \leq \alpha_i, i = 1, 2, \dots, n \end{cases}$$

Step5: The classification function is finally obtained by the KKT complementary condition.

$$g(x) = \text{sgn}[\sum_{i=1}^n \alpha_i^* y_i (a_i \cdot x) + b^*]$$

The classical SVM only gives the algorithm of the second-class classification [6]. In the practical application of the sleep disease data mining, it is necessary to solve the classification problem of many types, so it is considered to solve by the combination of multiple two types of support vector machines. Combining the obtained important indicators of crossover, the sleep quality is classified into classification labels to deal with insomnia and other diseases; the daytime dysfunction is selected as the classification label, and the organic classification and spiritual classification are obtained; the hypnotic drugs are selected as the classification labels. The classification of drug action classification and other sleep diseases were obtained. The final SVM classification function was determined based on the classification combination of the above three types of support vector machines, and implemented by Matlab. Select 90% of the training samples, select the data of the seven types of diseases from the remaining 10% of the samples, number 1~7, and randomly select the 3 most common diseases in each category of treatment, and obtain the fitted image. As shown in Figure 1:

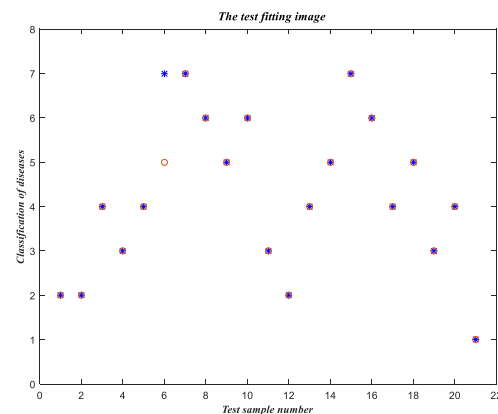


Figure 1 Test result chart

It can be obtained from Fig. 1 that the degree of fitting is good and the correctness of the model can reach 91.53%, so the model is established.

3. ESTABLISHMENT OF SLEEP PLAN AND EVALUATION SYSTEM

3.1. Sleep Plan

According to the 2017 Nobel Prize in Physiology and Medicine, Jeffrey C Hall, Michael Rosbash and Michael W. Young reveal the secrets of our biological clock and clarify its intrinsic working mechanism separates a gene that controls the normal circadian rhythm of the organism.[7-8] In the complex physiological mechanisms of human beings, the biological clock plays an important role in many aspects, so rhythmic biology has important implications for human health. Moreover, long-term staying up late can easily lead to high blood pressure, endocrine abnormalities, blood sugar and lipid metabolism disorders, etc., causing diabetes, tumors, and even dementia of the nervous system, such as the occurrence of senile dementia, this also has a certain relationship, which further suggests that we must follow the laws of nature Doing things, living sometimes, eating and eating. Therefore, we first need to develop a scientific rest schedule, as shown in Table 1:

Table 1 Schedule

Time	Matter	Result
7:00am	water	Supplement the loss of water at night
7:00~7:30am	Breakfast	Intestinal absorption of nutrients
12:30~1:30	Siesta	Restore state and energy
9:00~11:00pm	Quiet- state	Prepare for good, fast sleep
11:00+pm	Sleep	Liver detoxification, gallbladder detoxification, lung detoxification and some other self-detoxification process

Secondly, it should be noted that sleep hygiene reduces the time in bed, unless it is sleeping, especially not reading or watching TV on the bed; distracting when it is difficult to sleep; avoiding coffee, alcohol and tobacco before sleep, reducing the impact of external factors on sleep.

3.2. Effectiveness Evaluation Based on Fuzzy Comprehensive Evaluation

According to the study of the Nobel Prize in Physiology and Medicine in 2017 on the impact of

biological rhythms on human life, substances that stimulate the brain such as tobacco, alcohol, coffee, etc. have a greater impact on sleep quality, but to a certain extent, can slow depression, anxiety, etc. Mental illness caused by sleep or other various diseases or symptoms.

Form a sleep plan effectiveness evaluation index system, and then apply the AHP method to determine the weight. In this regard, from the aspects of sleep quality, physical and mental health, the establishment

of a sleep evaluation effectiveness evaluation system, the evaluation indicators are divided into two layers, one is the overall goal, that is, the effectiveness of the

evaluation of this sleep plan; The sleep plan has a direct way of being effective, as shown in Table 2.

Table 2: Effectiveness evaluation index system

Effectiveness of sleep plans	E1-Sleep quality	E11Sleep time E12Sleep latency
	E2-Healthy body	E21Hypnotic E22Daytime dysfunction

The separate test affects the influence of the factors of the criterion layer and the scheme layer. Two factors are recorded as x_i and x_j , and a_{ij} indicates the influence of the former factor on the latter factor. The scale is divided according to the former. The importance of 1 means that the importance is the same, and 2 means that the former is more important than the latter, as shown in Table 3.

Table 3: Program layer judgment matrix

E1	E11	E12	E2	E21	E22
E11	1	1/2	E21	1	3
E12	2	1	E22	1/3	1

Finally, each element, especially the ranking weight of each scheme in the lowest layer, is selected, to

Table 4: Total hierarchy and weight

Guidelines	Sleep quality	Healthy body	Sort weight
Standard layer weights			
Sleep time	0.0125	0.1987	0.3657
Sleep latency	0.1372	0.1021	0.4364
Hypnotic	0.1234	0.0921	0.1262
Daytime dysfunction	0.082	0.0934	0.0717

The actual score formula is:

$$S = 0.3657E_{11} + 0.4364E_{12} + 0.1262E_{21} + 0.0717E_{22}$$

If the score is greater than 80, it is very effective, 50~80 is more effective, 0 to 50 is slightly effective, and less than or equal to zero is completely invalid. Each score of the sleep program has a score of 10 points and a total score of 89.75 points, so the validity meets the requirements.

REFERENCES

- [1]Wu Mengda. Mathematical modeling tutorial [M].Higher Education Press, 2011.
- [2]ShiZhi liang. The Necessity of Partial Correlation Analysis in Foreign Language Teaching Research and Implementation by SPSS. Journal of Wada Teachers College, 2009, 28 (02): 169-170.
- [3]Bruna Rainho Rocha, Mara Behlau. The Influence of Sleep Disorders on Voice Quality. Journal of Voice, 2017.

select the scheme. The total ranking weight is important to synthesize the weights under the single criterion from top to bottom. The weight of the two indicators in the criterion layer is m_1, m_2 , and the weight of the four indicators in the plan layer is n_1, n_2, n_3, n_4 , the weight of the plan layer for the total target is n_{ij} ($i = 1, 2, 3, 4; j = 1, 2$). The weight of the solution layer for the total goal is

$$n_i = \sum_{j=1}^2 n_{ij} \times m_j (i = 1, 2, 3, 4).$$

The total ranking of the following index weights is as follows, as shown in Table 4:

- [4]Yongsheng Zhu, Youyun Zhang. A new type SVM—projected SVM. Science in China Series G: Physics, Mechanics and Astronomy, 2004, 47(1).

- [5]Chebotarev Sergei. Economic factorial analysis: general theory and original approaches. Acta Montanistica Slovaca, 2003, 8(4).

- [6]Hui Li, Cai-xia Hu, Ying Li. Application of the Purification of Materials Based on GA-BP. Energy Procedia, 2012, 17.

- [7]Daniel T.L. Shek, Cecilia M.S. Ma. The use of confirmatory factor analyses in adolescent research: Project P.A.T.H.S. in Hong Kong. International Journal on Disability and Human Development, 2014, 13(2).

- [8]Thomas D. Gauthier. Detecting Trends Using Spearman's Rank Correlation Coefficient. Environmental Forensics, 2001, 2(4).

Overlay Trajectory Optimization of Spray Gun Spraying

Honglei Lin¹, Donghao Jin¹, Guoqing Wang¹, Weixuan Wang^{2,*}

¹Engineering Computing and Simulation Innovation Lab, North China University of Science and Technology, Tangshan, 063210, China

²College of Science, North China University of Science and Technology, Tangshan 063210, China

*E-mail:485936252@qq.com

Abstract: Glaze spray in the process of ceramic production is a crucial link, it directly related to the final product can flow to the market, so in the spraying process required to paint the thickness of the glaze as much as possible. This is of great significance to automate the production process. The parameter matrix of the elliptic double β distribution model is computed and the specific function is obtained. Then, through the Matlab to fit, obtains the three-dimensional glaze thickness distribution diagram, the analysis obtains its parabolic chart, through calculates the accumulative situation, obtains the suitable overlap interval trajectory curve of the spray gun. Finally, the range of repetition interval is obtained in 80 ~ 90mm. An overlap interval optimization model based on simulated annealing is proposed for the spray gun spraying problem. First, it is proved that the spray interval does not apply to the surface $z = -x^2 + x - xy$. Then, the optimization model of the target function with spray paint thickness is established to solve the optimal h value. Finally, the optimal range d is solved by relationship between the local minimum spray thickness and the interval d .

Keywords: Simulated annealing algorithm; Particle swarm algorithm; Optimization model

1. INTRODUCTION

Ellipse double β distribution model in the plane of the spray is an ellipse, spray gun spray gun can move in the direction along the long axis can also be along the short axis direction [1]. However, when the direction of motion is along the short axis, the area covered by the swath is larger than when moving along the long axis. Therefore, the spray gun should be selected to spray glaze along the short axis of the swirl. An enamel trajectory can be determined by four factors: path, direction, height and velocity. When spraying glaze along a track, the spray direction is always perpendicular to the surface of the workpiece, and the spray height remains unchanged [2-5]. After determining the distance between the two tracks, the spray gun path can be obtained. Therefore, determining the gun movement rate and the distance between adjacent tracks distance to determine a glaze track.

2. CREATE A SPRAY GUN OVERLAP INTERVAL TRACE

Assuming the gun is moving at a constant speed, the speed of movement v is a fixed value. Can be drawn as shown in figure 1 spray diagram:

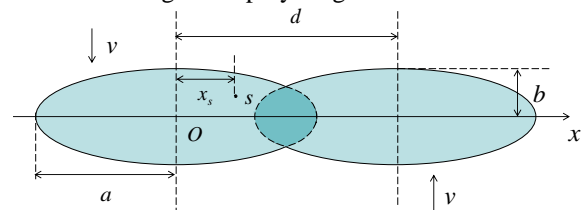


Figure 1 Schematic diagram of the plane spray

Shown in figure 1 is spray gun spray along the two adjacent tracks when the situation, x_i indicates the distance from point s to the first track in the swath area, s' is the projection of s on the first track, d is the distance between two adjacent tracks, Then the glaze layer thickness of point s is:

$$T_s(x) = \begin{cases} T_1(x) & 0 \leq x \leq d-a \\ T_1(x) + T_2(x) & d-a \leq x \leq d \\ T_2(x) & a \leq x \leq d \end{cases} \quad (1)$$

$$T_1(x) = 2 \int_0^{t_1} q(x, y_1) dt \quad 0 \leq x \leq a \quad (2)$$

$$T_2(x) = 2 \int_0^{t_2} q[(d-x), y_2] dt \quad d-a \leq x \leq d \quad (3)$$

among them

$$t_1 = b \sqrt{1 - \frac{x^2}{a^2}} / v ; y_1 = b \sqrt{1 - \frac{x^2}{a^2}} - vt$$

$$t_2 = b \sqrt{1 - \frac{(d-x)^2}{a^2}} / v ; y_2 = b \sqrt{1 - \frac{(d-x)^2}{a^2}} - vt$$

Where $T_1(x)$ and $T_2(x)$ represent the glaze thickness of the spray gun at the point of spray glaze along the trajectory 1 and the trajectory 2, respectively; t_1 and t_2 , respectively, when the spray gun along the adjacent track when the spray pattern completely through half the time s ; t is the time that the gun moves from point O to s' . From equation (1), the thickness of the glaze layer at any point along the X direction between two adjacent tracks can be obtained.

According to atomization pressure P_1 , diaphragm pump pressure P_2 and jet distance h is the main factor affecting the above parameters have the following relationship:

$$\begin{bmatrix} 129.8665 & -55.2435 & 1.7436 & -297.3908 \\ 52.5130 & -5.7480 & 0.7394 & -128.6368 \\ 59.7245 & 393.9655 & -0.1244 & 150.0184 \\ -7.0125 & 34.5045 & 0.0284 & -9.5229 \\ -4.6130 & 18.3620 & 0.0113 & -0.3924 \end{bmatrix} \times \begin{bmatrix} P_1 \\ P_2 \\ h \\ 1 \end{bmatrix} = \begin{bmatrix} a \\ b \\ z_{\max} \\ \beta_1 \\ \beta_2 \end{bmatrix}$$

According to the problem 1 given P_1 and P_2 to take 0.2Mpa, h take 225mm, calculated by the matrix can be drawn

$$\begin{bmatrix} a \\ b \\ z_{\max} \\ \beta_1 \\ \beta_2 \end{bmatrix} = \begin{bmatrix} 109.8438 \\ 47.0812 \\ 212.7664 \\ 2.3655 \\ 4.8999 \end{bmatrix} \quad (4)$$

It can be concluded that the maximum thickness of the paint film is 212.7664 μ m. Will get the result (4) into the oval double β distribution model by matlab curve fitting, can be drawn as shown in Figure 2, the three-dimensional function chart[3].

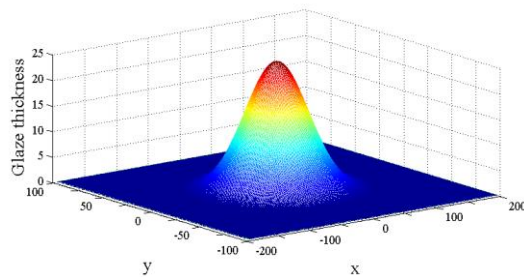


Figure 2 Overlapping interval trajectory three-dimensional map

The three-dimensional map is taken as a two-dimensional plan, and the adjacent tracks are superimposed to obtain the distribution of glaze thickness between adjacent tracks when the plane is sprayed, as shown in Figure 3 and Figure 4.

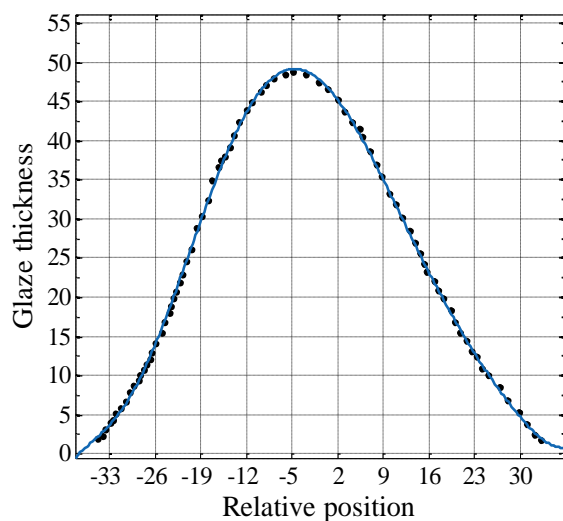


Figure 3 Plane glaze layer thickness distribution

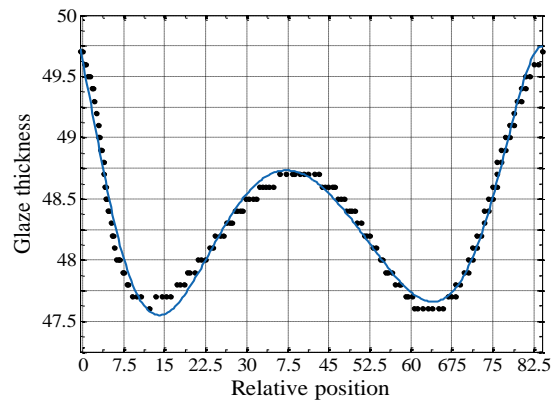


Figure 4 The distribution of glaze thickness between adjacent tracks during plane coating

By calculating the cumulative condition, it can be concluded that the suitable overlap interval trajectory of the spray gun is as shown in figure 4, and the repetition interval is in the range of about 80 to 90 mm.

3. ALGORITHM PREPARATION

Simulated annealing algorithm in the search process with the ability of sudden jump, can effectively avoid the search process into a local minimum solution. Simulated annealing algorithm in the annealing process not only accept a good solution, but also with a certain probability to accept the poor solution, while the probability of temperature parameters by the control of its size decreases with decreasing temperature [4].

- (1) Randomly initialize the position and speed of each particle in the population;
- (2) Evaluate the fitness of each particle, store the current position and fitness value of each neutrino in each neutrino, and store the positions and fitness values of all individuals in the best for the best individuals;
- (3) Determine the initial temperature;
- (4) Determine the current temperature of the fit value;
- (5) Use the roulette strategy to determine a globally optimal alternative value from all, then update the velocity and position of each particle;
- (6) Calculate the new target value of each particle, update the value of each particle and population values;
- (7) Temperature operation;
- (8) If the stop conditions (usually the default calculation accuracy or number of iterations), the search stops, the output results, do not know to return to (4) continue the search.

4. OPTIMIZATION FUNCTION ESTABLISHMENT

The optimization function is no longer the best uniformity of glaze, but the optimal function is to optimize the glaze layer with the minimum glazing time as the constraint condition. Need to optimize the two parameters(Gun rate v , adjacent track pitch d)all have an impact on the spray glaze time, that is, the faster the spray gun, the greater the distance between adjacent tracks, spraying the same workpiece the

shorter the time required, therefore, you can use these two parameters to characterize the spraying time, assuming the ideal glaze layer thickness q_d , the maximum and minimum values of the coating between adjacent tracks are q_{max} and q_{min} , The allowable deviation is $\eta(\%)$, then the optimization function can be expressed as[5]:

$$\min(v, d) \quad (5)$$

$$s.t. \begin{cases} |q_{max} - q_d| \leq q_d \cdot \eta \\ |q_d - q_{min}| \leq q_d \cdot \eta \end{cases} \quad (6)$$

This is an optimization problem with constraints, this paper uses the particle swarm optimization algorithm to find the optimal solution

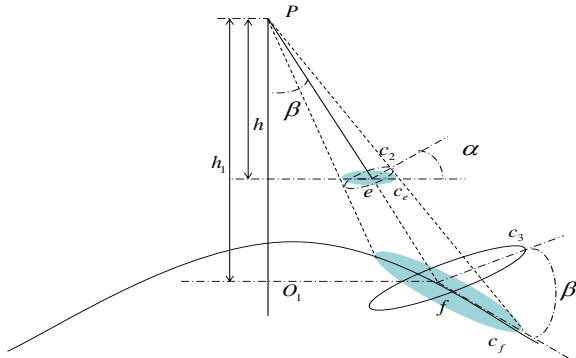


Figure 5 The relationship between the various pieces
As shown in Figure 5, β is the angle between the line connecting point f and the center point p of the lance and the axis of the lance, p point and e point, f point height were h and h_1 respectively. Assuming that the amount of glaze sprayed from the gun is the same on both the experimental plane and the curved plane, (on the plane passing through point e and perpendicular to line pf, e point as the center, for a radius of a small round face c_2 , the experimental plane and c_2 in the same cone-shaped coating under the angle of the picture is put round ce, The angle between c_2 and ce is also β , the minor axis of ellipse c_e can be regarded as the radius of circle c_2 , and the major axis is half of segment m_n . According to the geometric knowledge [6]:

$$\frac{1}{2}mn = \frac{\Delta r \times p e^2 \times \cos \beta}{p e^2 \times \cos^2 \beta - \Delta r^2 \times \sin^2 \beta} \quad (7)$$

The ratio of the area S_{e2} of c_2 to the area of ce is

$$\frac{S_{e2}}{S_{ce}} = \frac{\pi \times r^2}{\frac{1}{2} \pi \times r \times mn} = \cos \beta - \Delta r^2 \frac{\sin^2 \beta}{p e^2 \times \cos \beta} \quad (8)$$

Since Δr is very small, the last term of (8) is the infinitesimal term of Δr , which cannot be considered:

$$\frac{S_{e2}}{S_{ce}} = \cos \beta \quad (9)$$

The relationship between the thickness of the glaze on c_2 and the thickness on ce is:

$$q_2 = q_e / \cos \beta \quad (10)$$

The circular surface c_3 is parallel to the circular surface c_2 and is located under the same conical coating opening angle. According to the geometric relation, the relationship between the two circular areas is as follows.

$$S_{e3} = \left(\frac{h_1}{h} \right)^2 S_{e2} \quad (11)$$

S_{e3} and S_{e2} are the areas of c_3 and c_2 , respectively, the relation between the thickness q_3 of the glaze layer on q_3 and q_2 is:

$$q_3 = \left(\frac{h}{h_1} \right)^2 q_2 \quad (12)$$

The oval surface cf is located on the plane of point f that is tangent to the surface and is at the same conical coating opening angle as c_3 , with an angle of cf between c_3 and α . According to Eq. (8), the thickness of the glaze layer is:

$$q_f = q_3 \cos \alpha \quad (13)$$

Combined with (9) (10) (11) (12) to get the surface of the glaze f point thickness is:

$$q_f = q_e \left(\frac{h}{h_1} \right)^2 \frac{\cos \alpha}{\cos \beta} \quad (14)$$

Set the gun center p to point f distance l, then $h_1 = l \cos \beta$, and then $\alpha \geq \pi/2$, the point with glaze cover. Therefore, a point f on the surface of the glaze layer thickness accumulation rate model:

$$q_f = \begin{cases} q_e \left(\frac{h}{l} \right)^2 \frac{\cos \alpha}{\cos^2 \beta} & \alpha < 90^\circ \\ 0 & \alpha \geq 90^\circ \end{cases} \quad (15)$$

From equation (15), we know that the key to calculating the cumulative rate of glaze layer thickness on the surface is to find the accumulation rate of the corresponding point on the experimental plane and the angle between the line connecting the point and the gun center and the normal of the point. Furthermore, the cumulative rate of glaze layer thickness at any point on the sprayed surface can be obtained during the process of spray glaze, which lays the foundation for the subsequent generation and optimization of trajectories on the natural quadric surface [7-9].

5. SOLUTION OF OVERLAPPING INTERVAL OPTIMIZATION MODEL

Using matlab surface $z = -x^2 + x - xy$ 3D three-dimensional map, specific programming sees Annex 1. As shown in Figure 6. The thickness of the glaze layer on the curved surface is analyzed based on the two-dimensional surface. As shown in Figure 7, the glaze thickness difference is greater than 10%, so the spray interval calculated in problem 1 is no longer applicable.

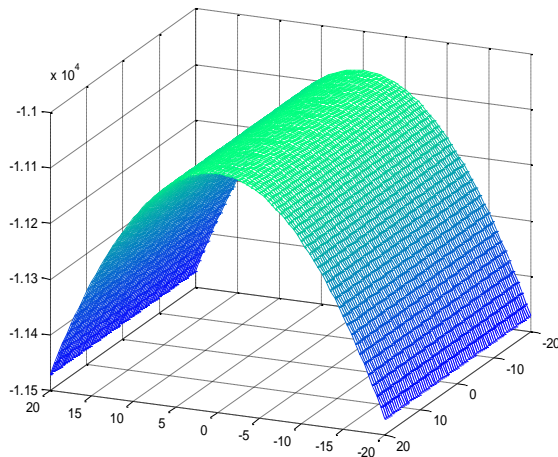


Figure 6 Surface three-dimensional perspective

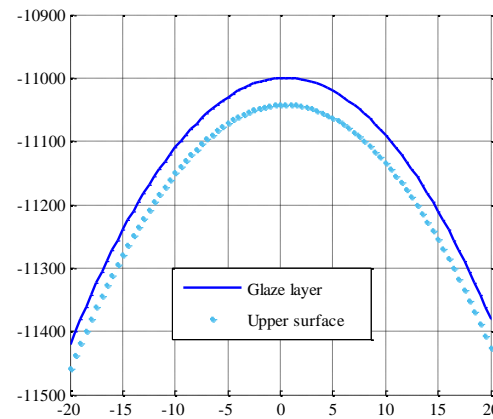


Figure 7 Surface glaze layer thickness

Bring the values of P_1 and P_2 given in the title to the matrix expression

$$\begin{bmatrix} 129.8665 & -55.2435 & 1.7436 & -297.3908 \\ 52.5130 & -5.7480 & 0.7394 & -128.6368 \\ 59.7245 & 393.9655 & -0.1244 & 150.0184 \\ -7.0125 & 34.5045 & 0.0284 & -9.5229 \\ -4.6130 & 18.3620 & 0.0113 & -0.3924 \end{bmatrix} \times \begin{bmatrix} P_1 \\ P_2 \\ h \\ 1 \end{bmatrix} = \begin{bmatrix} a \\ b \\ z_{\max} \\ \beta_1 \\ \beta_2 \end{bmatrix} \quad (12)$$

You can get the model related to the indicator expression, as shown in Table 1

Table 1 model index expression

Unknowns	Value	Reduction
a	$(4359 \cdot h)/2500 - 282.4662$	$1.7436h - 282.4662$
b	$(3697 \cdot h)/5000 - 596419/5000$	$0.7394h - 119.2838$
z_{\max}	$240.7564 - (311 \cdot h)/2500$	$240.7564 - 0.1244h$
β_1	$(71 \cdot h)/2500 - (8049/2000)$	$0.0284h - 4.0245$
β_2	$(113 \cdot h)/10000 + (11787/5000)$	$0.0113h + 2.3574$

Substituting the elliptical double- β distribution model of the elliptical distribution, a functional relation is obtained as to the height h of the lance and the thickness $z(x, y)$ of the glaze:

$$z(x, y) = (240.7564 - 0.1244h) \times \left(1 - \frac{x^2}{(1.7436h - 282.4662)^2} \right)^{(0.0284h - 3.0245)} \times \left[1 - \frac{y^2}{(0.7394h - 119.2838)^2 \left(1 - \frac{x^2}{(1.7436h - 282.4662)^2} \right)} \right]^{(0.0113h + 2.3574)}$$

The algorithm is run by Matlab, which realizes the optimal function of particle swarm optimization algorithm based on simulated annealing algorithm. The programming code is shown in Appendix 2 [8]. Finally, when the value of the time, with the minimum glaze thickness. Maintain the relative height of the gun relative to the surface h is constant, the trajectory of the gun relative to the relationship between the surface be two parallel planes. As shown in Figure 8.

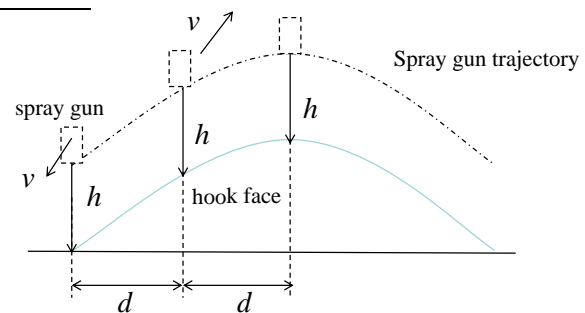


Figure 8 Gun trajectory map

From h can get the maximum glaze thickness z_{\max} , in order to make the glaze thickness difference is less than 10%, the overlap curve of the local minimum z_{\min} must be satisfied $z_{\min} \leq 0.9z_{\max}$. Different d values correspond to different local minimum z_{\min} , z_{\min} calculated from many data d decreases with increasing, so d value range of $d \leq 114.9mm$.

REFERENCES

- [1]Feng Hao, Wu Qiu, Wang Xiaoping. Optimization of spherical spray trajectory based on elliptic double β model [J]. Mechanical Design and Manufacturing, 2016 (4): 249-252.
- [2]Zhou Qian, Chen Guanlin, Liu Zuoyu. Design of

robot glaze path based on offline programming technology [J]. Mechanical and Electrical Engineering Technology, 2017, 46 (6): 16-17.

[3]Wu Qiu. Spray glaze robot gun trajectory optimization [D]. Jingdezhen Ceramic Institute, 2015.

[4]Qu Xingtian, Wang Hongyi, Fan Cheng, et al. A aspheric polishing trajectory planning with overlapping rate helix [J]. Journal of Xi'an Jiaotong University, 2015, 49 (6): 126-131.

[5]Sheng L, Cai W U, Bai Y Y, et al. Plasma homocysteine levels are independently associated with alterations of large artery stiffness in men but not in women[J]. Journal of Geriatric Cardiology Jgc, 2015, 12(3):251-256.

[6]Yan Xin, Dong Junqing, Li Qinghui, et al. Study on the structural characteristics of ancient porcelain glaze

based on OCT technique [J]. China Laser, 2014, 41 (9): 195-200.

[7]Li Shuailong, Cui Guomin, Zhou Jianwei. Synchronization optimization of heat exchange network based on two-layer algorithm of covariance of temperature uniformity [J]. Power Journal of Thermal Energy Engineering, 2017, 32 (7): 17-23.

[8]Li Shuailong, Cui Guomin, Zhou Jianwei. Synchronization optimization of heat exchange network based on two-layer algorithm of covariance of temperature difference [J]. Power Journal of Thermal Energy Engineering, 2017, 32 (7): 17-23.

[9]Zhang, B.. 110m hurdles phased performance significance research based on SPSS regression analysis and GRA model. Journal of Chemical and Pharmaceutical Research, 2014, 6(2), 649-659.

Based on Improved CPSO-LSSVM Blast Furnace Hot Metal Temperature Prediction Model

Xueyong Jia^{1,2}, Liyan Dong^{1,3}, Baorong Wang^{1,4}, Yang Han^{5,*}

¹Engineering Computing and Simulation Innovation Lab, North China University of Science and Technology, Tangshan, 063210, China

²College of Electrical Engineering, North China University of Science and Technology, Tangshan, 063210, China

³College of Metallurgy and Energy, North China University of Science and Technology, Tangshan 063210, China

⁴College of Chemical Engineering, North China University of Science and Technology, Tangshan 063210, China

⁵College of Science, North China University of Science and Technology, Tangshan 063210, China

*E-mail: 729420132@qq.com

Abstract: Based on the actual production data of a steel mill, this paper analyzes the principle of blast furnace hot metal temperature prediction and uses LSSVM to model. When constructing the LSSVM model, the Gaussian kernel width σ and the regularization penalty parameter γ are important, and the prediction accuracy of the model is affected by it. The particle swarm optimization (PSO) algorithm is used to optimize the LSSVM model parameters. And because the standard particle swarm algorithm is better than the shortcomings of individual extremes, it is improved. Finally, according to the optimization algorithm, the optimal parameters are obtained, and the optimal rolling road temperature prediction model is constructed. And the actual test data is used to test the obtained model. The simulation analysis shows that the method will strengthen the accuracy of the furnace hot metal temperature, and it has obtained a certain applicability.

Keywords: Blast furnace ironmaking; CPSO-LSSVM; Furnace temperature prediction

1. INTRODUCTION

The various control measures of the oven are to keep the temperature in the proper range. Due to the complex high-pressure and high-temperature characteristics of furnace smelting, it is almost impossible to directly measure the internal temperature through the instrument, and the two parameters that can evaluate the thermal characteristics in the furnace are the molten iron temperature and Si content [1]. For a long time, most studies have been based on the Si content to establish a furnace temperature prediction model, but the iron content of molten iron does not fully reflect the slope of the furnace temperature. In the metallurgical production process, the difference between the blast furnace capacity, the external environment and the proportioning conditions will cause different parameters of the smelting smelting. The differentiation of the prediction model will also cause

different parameters, and the furnace temperature and the molten iron Si content are not closely related. The pig iron temperature is the most intuitive parameter to measure the temperature of the furnace. Therefore, this chapter takes the temperature of the furnace molten iron as the research object, and constructs the prediction model of the furnace molten iron temperature to predict it. And forecasting its future development direction, in order to propose adjustments in a timely manner, it plays an important role in maintaining stable production of smelting, reducing the occurrence of faults and improving the quality of pig iron [2-4].

2. CHARACTERISTICS OF BALST FURNACE HOT METAL TEMPERATURE PREDICTION

There are many variables in the blast furnace ironmaking process, and the physical and chemical reactions are complicated. It is difficult to correctly describe the mechanism model and mathematical expressions, and even there may be cases where the model may be considered incomplete. If only through the experience of experts and the experience of the field foreman, the analysis may lead to the missing factors, which will affect the performance of the model [3-6]. Therefore, it is chosen to build an intelligent algorithm based on actual production data mining to establish a time series prediction model. In this way, the law and characteristics of the data itself are mined, and a high-precision prediction model of the furnace temperature of the furnace is established.

3. PRINCIPLE OF BALST FURNACE HOT METAL TEMPERATURE PREDICTION

In this paper, LSSVM is used as the main body of prediction model. This algorithm shows good characteristics in small sample data and nonlinear fitting. At the same time, LSSVM has fewer adjustment parameters and faster convergence [4]. Constructing a model with this as the main body will have excellent performance. After being selected as the model body, kernel width 1 and regularization parameter 2 in LSSVM are two important parameters

of the model. In modeling, the value of the two parameters is directly related to the effect of the model, so it needs to be iteratively optimized with intelligent optimization.

About the optimization of model parameters. In this paper, the PSO optimization algorithm is used to solve the problem. The PSO algorithm is a typical group intelligent optimization method. The related literatures all prove the superiority of the PSO algorithm in the optimization. However, the ordinary particle swarm optimization algorithm falls into the local maximum value defect. Therefore, the introduction strategy is improved, and then iterative optimization is used to finally obtain the optimal prediction model, which improves the accuracy of the model [5-6].

4. BASED ON IMPROVED CPSO-LSSVM PREDICTIVE MODEL MODELING PROCESS

(1) Application the GRA analysis method is used to determine the main influence parameters affecting the temperature of the furnace molten iron. The final selection: hot air volume, hot air pressure, oxygen enrichment, material speed, furnace permeability index, coal injection, wind temperature, iron volume difference as an input factor.

(2) Randomly select appropriate actual production data for preprocessing, which contains two aspects:

① Clear and organize errors, redundant data, and supplement residual data. The 3σ method is used for screening and redundancy, and the principle of the 3σ method is: set the sample data $X = (x_1, x_2, \dots, x_n)$, the average number is \bar{x} , and the deviation $v_i = x_i - \bar{x} (i=1, 2, \dots, n)$ can obtain the standard deviation according to the Bayesian calculation formula: $S = \sigma \left[\sum v_i^2 / (n-1) \right]^{1/2}$. When the deviation $v_i (1 \leq i \leq n)$ of a certain sample data x_i matches $|v| > 3\sigma$, x_i abnormal data can be determined and should be deleted.

② Normalized anti-normalization. Data normalization is the conversion of a sequence into a value between $[-1, 1]$. Calculated as follows:

$$x' = 2 * \frac{x - x_{\min}}{x_{\max} - x_{\min}} + (-1), x \in R^n \quad (1)$$

The anti-normalization process transforms the predicted data into ordinary values. Its formula is as follows:

$$y' = \frac{1}{2} (y_i + 1) * (y_{\max} - y_{\min}) + y_{\min}, y \in R^n \quad (2)$$

Among them, y' is the temperature value of the furnace molten iron after the conversion, y_i is the temperature of the blast furnace molten iron before the transformation, y_{\max} is the maximum temperature of the molten iron before the conversion, and y_{\min} is the minimum temperature of the molten

iron before the conversion.

(3) The kernel function of the LSSVM model is selected. This paper selects the RBF radial basis kernel function, and randomly selects 4/5 of the data as the training sample and 1/5 of the data as the test sample.

(4) Set various parameters for improving the CPSO optimization algorithm. And initialize the position and velocity and fitness values of the particle population. Among them, the parameter that needs particle swarm optimization is the kernel σ width and penalty γ coefficient of LSSVM, and the sum of the predicted and actual MSE is the fitness function of the kernel function.

(5) The optimized LSSVM model was used to predict the blast furnace hot metal temperature, and the results were plotted and analyzed.

5. PREDICTION MODEL SIMULATION VERIFICATION AND RESULT ANALYSIS

Predictive model parameter settings and optimization. Based on the actual production data of the blast furnace, after screening, 100 sets of data in the blast furnace hot metal temperature sample data set were selected, 80 sets were selected as the training set, 20 sets were the test set, and the improved CPSO algorithm was used to optimize the LSSVM for prediction. The optimal intervals for parameters σ and γ are (0.1, 10000) and (0.01, 5000), the PSO population size is set to 42, the maximum number of iterations is set to 300, the acceleration factor is $c_1 = 1.5$; $c_2 = 2.0$; $c_{1f} = c_{2f} = 2.5$; and the inertia weight is $w_{\max} = 1.2$; $w_{\min} = 0.8$.

(1) Simulation training of training set training model. According to the improved CPSO iterative search, the optimal prediction model of the furnace hot metal temperature is constructed, and the selected training data is used to train the model and compare with its real value. The result is shown in Figure 1:

(2) Comparison of evaluation indicators and results. In order to measure the effect of the prediction model, the error analysis is carried out in this paper, and two measures of mean square error and decision coefficient are adopted. Among them, the error analysis includes the absolute difference and relative difference between the pre-value and the true value of the furnace hot metal temperature, and the absolute difference and the relative difference are calculated as follows:

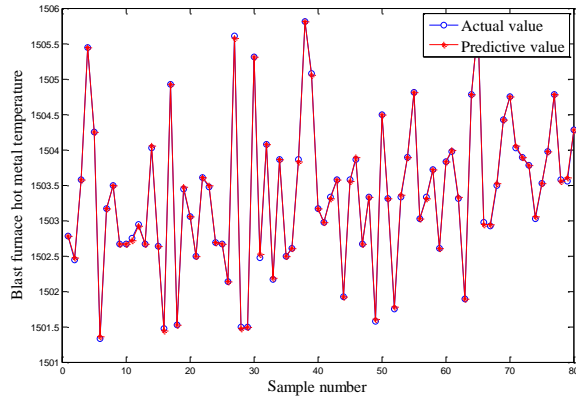


Figure 1: Comparison of training sample prediction results

$$e_1 = \hat{y}_i - y_i \quad (3)$$

$$e_2 = \frac{\hat{y}_i - y_i}{y_i} \quad (4)$$

Where e_1 is the absolute difference; e_2 is the relative difference; \hat{y}_i is its predicted value; y_i is its true value. The formulas for the mean squared difference and the decision coefficient are as follows:

$$MSE = \frac{1}{l} \sum_{i=1}^l (\hat{y}_i - y_i)^2 \quad (5)$$

$$R^2 = \frac{(l \sum_{i=1}^l \hat{y}_i y_i - \sum_{i=1}^l \hat{y}_i \sum_{i=1}^l y_i)^2}{(l \sum_{i=1}^l \hat{y}_i^2 - (\sum_{i=1}^l \hat{y}_i)^2)(l \sum_{i=1}^l y_i^2 - (\sum_{i=1}^l y_i)^2)} \quad (6)$$

Where l is the number of sample data; $y_i (i=1,2,\dots,l)$ is its true value; $\hat{y}_i (i=1,2,\dots,l)$ is the predicted value of its model.

The test model set is used to test and analyze the optimal model obtained from the previous optimization training, and the predicted output is compared with the real data. At the same time, in order to evaluate the prediction accuracy of the model, the prediction models based on the standard LSSVM and the ordinary BP network are compared respectively, and the test data of each model is shown in Figure 2.

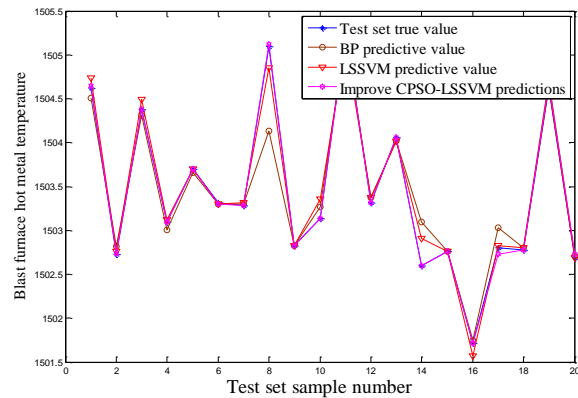


Figure 2: Comparison of prediction results of various prediction methods

The values of each model evaluation index are shown in Table 1.

Table 1: Comparison Table of Forecasting and Evaluation Indicators

Model	MSE	R ²
BP neural network	0.01266	0.9033
LSSVM	0.011895	0.92203
CPSO-LSSVM	0.000261	0.97848

It can be seen from the prediction and comparison results that compared with the other two traditional methods, the improved CPSO-LSSVM furnace hot metal temperature prediction model is better than the former two, and the accuracy is higher. The experimental results show that the prediction model has certain reliability and superiority.

6. CONCLUSION

In this chapter, the prediction characteristics of the temperature of the hot metal of the furnace are briefly described, and the important influence parameters of the temperature of the hot metal of the furnace are selected by GRA analysis. And since PSO is easy to fall into the characteristics of local extreme points, it has been improved to help the particle group jump out of the point value. Then the improved PSO algorithm is used to analyze the key parameters and iterative optimization of the LSSVM model, and then the optimal prediction model of the furnace temperature of the furnace is constructed. Compared with the prediction effects of other methods, the comparison results show that the prediction accuracy of the new model is better than that of the traditional method, and the prediction accuracy is relatively high, and the error is relatively low. This can be used indirectly to guide the optimal control and daily production of the furnace.

REFERENCES

- [1]Gao C, Chen J, Zeng J, et al. A chaos - based iterated multistep predictor for blast furnace ironmaking process. *AIChE journal*, 2009, 55(4): 947-962.
- [2]Liu X G, Liu F.Blast furnace process optimization and intelligent control model. *Journal of Applied Mathematics*, University: A, 2001, 16(4): 462-470.

- [3]Akiyama T, Sato H, Muramatsu A, et al. Feasibility study on blast furnace ironmaking system integrated with methanol synthesis for reduction of carbon dioxide emission and effective use of exergy. *ISIJ international*, 1993, 33(11): 1136-1143.
- [4]Ismail S, Shabri A, Samsudin R. A hybrid model of self-organizing maps (SOM) and least square support vector machine (LSSVM) for time-series forecasting. *Expert Systems with Applications*, 2011, 38(8): 10574-10578.
- [5]Gorjaei R G, Songolzadeh R, Torkaman M, et al. A novel PSO-LSSVM model for predicting liquid rate of two phase flow through wellhead chokes. *Journal of Natural Gas Science and Engineering*, 2015, 24: 228-237.
- [6]Li W, Shi L, Liang C. Forecasting model of research octane number based on PSO-LSSVM. *Control and Instruments in Chemical Industry*, 2008, 35(2): 25.

Based on Differential Equation Hot Water Bath Model

Liyan Dong^{1,2}, Xueyong Jia^{1,3}, Liuye Zhang^{1,4}, Chunyu Liu^{5,*}

¹Engineering Computing and Simulation Innovation Lab, North China University of Science and Technology, Tangshan 063210, China

²School of Metallurgy and Energy, North China University of Science and Technology, Tangshan 063210, China

³College of Electrical Engineering, North China University of Science and Technology, Tangshan, 063210, China

⁴College of Mechanical Engineering, North China University of Science and Technology, Tangshan 063210, China

⁵College of Science, North China University of Science and Technology, Tangshan 063210, China

*E-mail:685926292@qq.com

Abstract: Traditional bathtub cannot be heated alone, so users need to heat water often. The goal of this paper is to establish a bath and bath temperature model for space and time to provide users with an optimal strategy to keep the temperature close to the initial temperature and to reduce water consumption. First, consider the temperature changes throughout the process is continuous, this paper established based on differential temperature water temperature model, considering the surface air contact with the evaporation of heat loss Q_1 and bathtub surface contact with the water surface heat exchange occurs Q_2 , the two cooling methods, Using the law of conservation of energy and Newton's cooling law to establish the differential equation. Then determine the impact of several factors: radiant heat transfer, bathtub shape and volume, human shape, volume, temperature, movement, foam bath additives and so on. Focus on the impact of these factors on heat transfer, and sensitivity analysis. The results show that smaller and with less surface area, smaller personal qualities, less movement and more bubbles will reduce heat transfer and save water.

Keywords: Thermal Conductivity; Newton's law of cooling; Sensitivity Analysis Differential equations

1. INTRODUCTION

When bathing can remove dirt, eliminate fatigue, promote blood circulation, improve sleep quality, enhance metabolism. By soaking in warm water, some diseases and fighting bacteria can be treated to some extent. Bathing in the bathtub is the perfect choice for tired people after long hours of work. The traditional bathtub is a simple water container that has no secondary heating system or recirculation jets. As a result, the temperature of the water in the bathtub drops significantly over time, which will affect the bathing experience. Bathtub people need an optimal bathing strategy to reduce waste while enjoying a comfortable bathing experience.

Gi-Beum Kim, a Korean physicist, analyzed the heat loss due to conduction and evaporation [1-3]

resulting in a free-standing surface of water in the bathtub. He derived a relationship based on the fundamental theory of heat transfer to evaluate the performance of a bath tube. The main heat loss was found to be due to evaporation. Therefore, it is best to keep the bath temperature between 41-45 °C. In response to the issue of water temperature control, Chai Lisong [2] has developed a set of automatic temperature control water supply system based on embedded controller. The system adopts ARM processor and PID control algorithm to make the system respond faster, control precision is higher and more stable and reliable. Foreign M. E. Folan [3-6] studied the use of a special methane bulb to control the water temperature in the bath at 40°C, the accuracy of about 1°C range. Anger. A. T[4, 7] invented a bathtub with a control panel, through the control panel at each point of the sensor to determine the water temperature and then through the various water supply pipes to control the water temperature is constant [8-10]. All the above studies adopt more advanced technologies, and there are problems to be solved in safety and maintainability, meanwhile, the cost is not low, so they are not suitable for ordinary families. In this paper, a water temperature model is established for ordinary bathtubs without secondary heating system and recirculation spout system to determine the inlet water temperature and the minimum flow rate. Therefore, our research on water temperature model has some significance in saving water and bathing costs

2. DIFFERENTIAL EQUATIONS MODEL

According to the literature to find our study shown in rectangular bath, its specifications for the length of 1.8 meters, 0.8 meters wide and 0.7 meters high. First, add water to the bathtub until the water surface height of 0.55 meters, this time for the use of the limit, then began to cool, find the water temperature as a function of temperature in order to give the best water strategy.

The reason why the temperature of the bathtub is lowered, on the one hand, Q_1 is the heat dissipated by

the water surface in contact with the air and Q2 the heat exchange between the inner surface of the bathtub and the water surface, on the other hand. Therefore, in view of the physical reaction of endothermic and exothermic heat of water and bathtubs, a mathematical model is established by using the law of conservation of energy in formula (1), and then the water is heated at an appropriate time to ensure that the water temperature is within a comfortable range within.

$$Q = Q_1 + Q_2 \quad (1)$$

2.1 The water in the bathtub evaporates and dissipates heat

Assuming the bathtub is a standard cube, when water meets air, the heat that water evaporates away is achieved through the thermal conduction of water and air. Let the temperature of the water surface where the bathtub is located is $f(\tau)$. According to Newton's Law of Cooling, the amount of heat lost by water contact with air at this time is:

$$Q_1 = \int_0^{\tau} (f(\tau) - t_r) \times S_{\text{water-air}} \times h_1 d\tau \quad (2)$$

2.2 Bath tub in the water with the bathtub inside the surface of the heat

The initial water is completed, no longer add water to the bathtub, this time the volume of water is fixed, then the water contact area with the bath S_0 unchanged, the same rule according to Newton's Law of Cooling (Newton's Law of Cooling) within the bathtub Surface contact with the surface of the heat exchange Q_2 is:

$$Q_2 = \int_0^{\tau} (f(\tau) - t_r) \times S_{\text{water-bathtub}} \times h_2 d\tau \quad (3)$$

In this process of heat loss, the temperature inside the bathtub must be changing, the process of changing temperature can be expressed as:

$$\Delta t = t_0 - f(\tau) \quad (4)$$

At the same time, according to the literature we can see that the formula for calculating the heat change of liquid is

$$Q = cm\Delta t \quad (5)$$

The whole process follows the law of conservation of energy, so (2) (3) (4) (5)

$$cm(t_0 - f(\tau)) = (S_{\text{water-air}} \times h_1 + S_{\text{water-bathtub}} \times h_2) \int_0^{\tau} (f(\tau) - t_r) d\tau \quad (6)$$

The equation (6) equal sign on both sides at the same time on the demand derived τ

$$-cmf'(\tau) = (S_{\text{water-air}} \times h_1 + S_{\text{water-bathtub}} \times h_2)(f(\tau) - t_r) \quad (7)$$

It is known that $f(0) = 40$, at the initial time $\tau = 0$. Get the temperature changes shown in Figure 1.

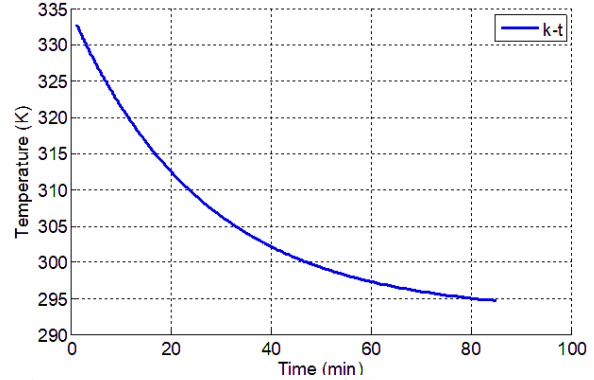


Figure 1 temperature pattern of changes

According to the temperature change chart shows, the initial temperature is 333.15K, in the process of temperature gradually decreased. The rate of change of temperature gradually slows down, reaching the most comfortable temperature of bathing body 313.25K in the past 20 minutes; when the time passes in the past 80 minutes, the temperature drops to room temperature 293.15K.

2.3 Insulation model

When people enter the bathtub static heat transfer between the body and water can be simplified as the problem of thermal conductivity, set the body's thermal conductivity h_3 , human and water contact area S_p , heat transfer thickness of L , can be drawn between the water and the human body the thermal conductivity is:

$$dQ_3 = \frac{h_3 \cdot S_p \cdot (t_0 - t_p)}{L} d\tau \quad (8)$$

Considering the low thermal conductivity of the human body (about $0.2 \text{ W} / (\text{m} \cdot \text{k})$ at 40°C), it is known that the heat conduction is low at a fixed water temperature.

In order to keep the entire bath or as close as possible to the initial temperature t_0 , there are two ways to add water.

Option 1: Always add water, water flow is small, so that the water temperature in the bathtub at t_0 .

Option 2: Intermittent water, that is, when the water temperature dropped to t_0-1 began to add water, when the water temperature rises to t_0+1 to stop watering, the time interval for the water temperature t_0-1 dropped to t_0-1 time τ_0 .

2.4 Option II established model

Interval with water, that is, when the water temperature dropped to t_0-1 began to add water, when the water temperature rise to t_0+1 stop water injection, which is a repeated cycle, the time interval for the water temperature t_0+1 down to t_0-1 time τ . The initial water bath is V_0 , each adding water, the heat input system

$$Q_{\text{input}} = cm_i t + \frac{1}{2} \rho_{\text{water}} q_2 \tau \frac{q^2}{S} \quad (9)$$

The quality of injected water is constantly increasing, which is a dynamic process. The changing relation is:

$$m_i = \int_0^{\tau} \rho_{\text{water}} q_2 d\tau \quad (10)$$

When the water temperature rise $t_0 + 1$, the heat dissipated by the system is still formula (11). So at this moment, the system increases the energy can be expressed as:

$$Q_{\text{add}} = cm\Delta t = Q_{\text{input}} - Q_{\text{output}} \quad (11)$$

where m is the mass of water in the entire bathtub can be expressed as:

$$m = m_0 + m_i = m_0 + \int_0^{\tau} \rho_{\text{water}} q_2 d\tau \quad (12)$$

At this time, the air contacting the water evaporation heat loss is still the formula (2) Q_1 , and the inner surface of the bath water surface contact heat exchange occurs formula (3) Q_2 , and the conduction of heat between the water of the human body (8) Q_3 . The left and right sides of equation (12) derive from time τ , as shown in Figure 2.

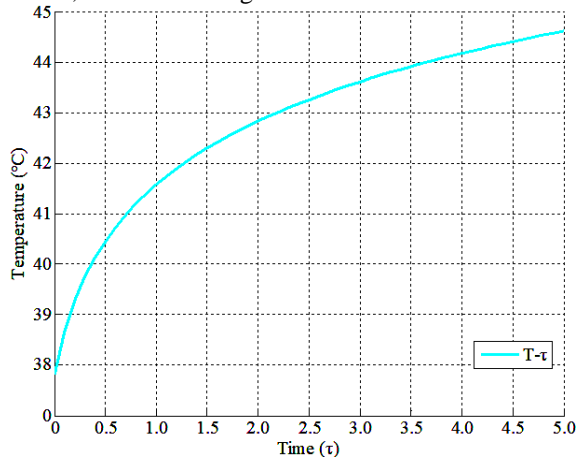


Figure 2 temperature with time

The function of the solution will be plotted as shown in Figure 2. Therefore, when adding water to the bathtub, the temperature of the water in the bathtub is from t_0-1 to t_0+1 , and the time for adding water is 78s.

The water temperature dropped to t_0-1 during this period, according to the law of conservation of energy, as shown in Figure 3.

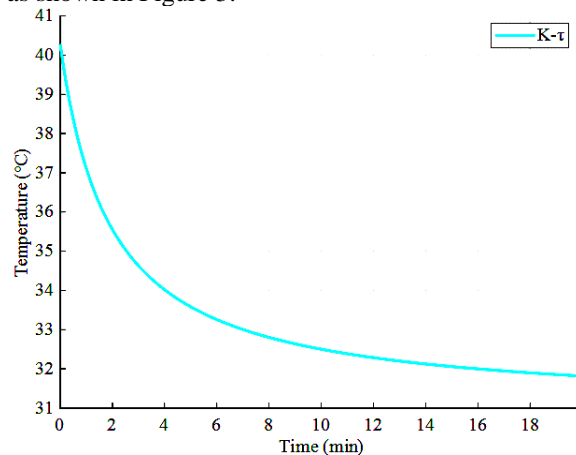


Figure 3 temperature with time

So, when the water temperature in the bathtub drops

from $t_0 + 1$ to t_0-1 , the time required is 45 seconds, as shown in Figure 4.

When the bathtub filled with water from t_0-1 down to $t_0 + 1$ this time, according to the law of conservation of energy, $cm\Delta t = Q_1 + Q_2 + Q_3$, as shown in Figure 5.

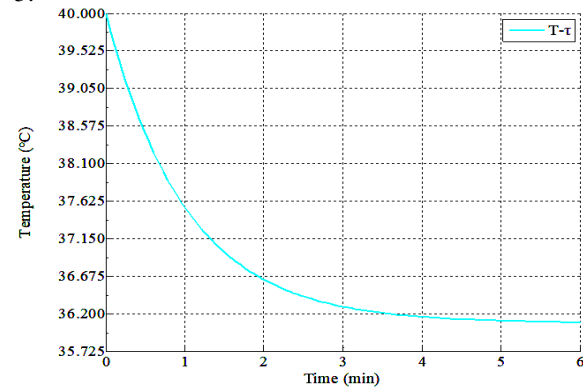


Figure 4 temperature with time

When the water temperature is t_0-1 add water to the bathtub, the water temperature to $t_0 + 1$, so add water time is 40s.

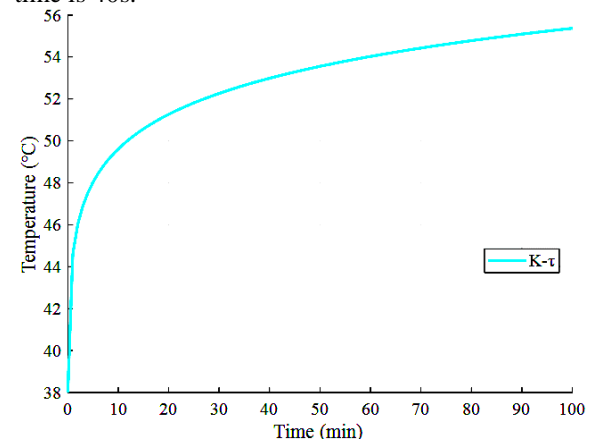


Figure 5 temperature with time

When the water temperature is t_0-1 add water to the bathtub, the water temperature rose to $t_0 + 1$, so add water time 30s.

3. THE SENSITIVITY ANALYSIS MODEL

The bathtub in our model is simplified as a cube. In fact, the situation is completely different. Bathtub can be designed into a variety of shapes and sizes, no doubt, people in the bathtub may have different shapes, sizes and temperatures. People are likely to make trouble when bathing. In addition, people tend to use bubble bath additives to help clean, which may also affect the results of our model. So here we will conduct a sensitivity analysis to determine the extent to which our model depends on these influencing factors.

3.1 Effect of different bathtubs

The difference in shape and volume of the bathtub affects convective heat transfer. Check the relationship between them can help people choose the best bathtub.

3.1.1 Different volume of bathtub

In fact, a glass of water will cool down quickly. However, it takes quite some time for the bathtub to cool down. Because of their different sizes, the heat of the water is very large, the temperature decrease is not obvious. To test the effect of the quantities, we analyze our sub-models by doing a sensitivity analysis of them. We assume that the initial capacity is 250L and then change it by 5, 8, 12 and 15. With the model we built earlier, some of the parameters change as follows, as shown in Table 1.

Table 1 changes in parameters

V	S1	S2	T	q1	q2	f
-15.0	-5.0	-9.3	-12.6	-2.6	-14.1	-5.8
-12.0	-4.0	-7.4	-10.0	-2.1	-11.3	-4.6
-8.00	-2.6	-4.9	-6.68	-1.4	-7.54	-3.0
-5.00	-1.6	-3.0	-4.16	-0.8	-4.71	-1.9
-2.00	-0.6	-1.2	-1.65	-0.3	-1.89	-0.7
0.00	0.00	0.00	0.00	0.00	0.00	0.00
2.00	0.67	1.22	1.64	0.35	1.89	0.76
5.00	1.66	3.05	4.09	0.87	4.71	1.90
8.00	2.65	4.87	6.51	1.40	7.54	3.03
12.00	3.96	7.28	9.71	2.09	11.31	4.54
15.00	4.94	9.08	12.08	2.60	14.14	5.66

To show the relationship between different parameters and volume, put the data on the drawing as shown in Figure 6 and Figure 7:

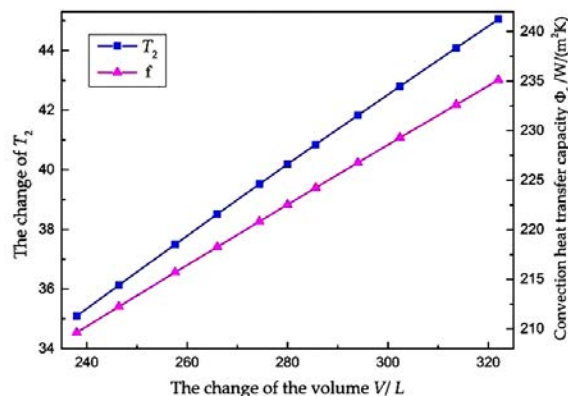


Figure 6: Time T2 and f with volume changes

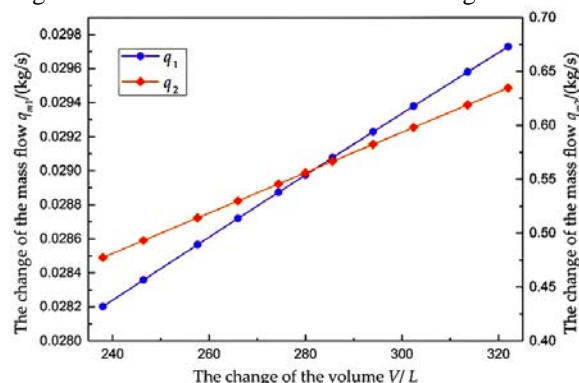


Figure 7: Flow q1 and q2 with volume changes

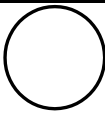
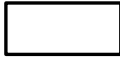

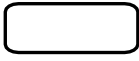
As can be seen from the figure, when the bathtub volume is small, the other parameters of the smaller size. For example, as the volume decreases, the heat loss gets smaller so that the additional water mass flow rate decreases accordingly. In conclusion,

smaller bathtubs are a better choice for saving more water. This not only reduces initial moisture consumption to fill the bathtub but also avoids adding too much hot water. Of course, choosing a small bathtub is not wise for taller or fathers.

3.2 Different Shapes of Bathtubs

When the volume is constant, different shape of the bathtub mainly affects the surface area of the bath water, thus affecting the heat transfer. So we converted the change in shape to the change in surface area. Usually, there are circular, oval, rectangular, heart-shaped, rounded rectangular shape of the bathtub [5]. Let the bathtub boundary be C. The area of the top and other surfaces is A1 and A2. Different shapes of bathtub parameters are as follows, as shown in Table 2.

Table 2 The parameters of different shapes

Shape	Sketches	A1	A2
Round		πr^2	$2\sqrt{\frac{\pi}{A_1}}V + A_1$
Rectangle		ab	$\frac{2V}{A_1}(a+b) + A_1$
Square		a^2	$\frac{4V}{\sqrt{A_1}} + A_1$
Rounded rectangle		$\pi r^3 + ab$	$\frac{V}{A_1}C + A_1$

Compare the area of the graph to get:

$$2\sqrt{\pi A_1} \leq 4\sqrt{A_1} \leq \left(2a + a\frac{A_1}{a}\right) \quad (13)$$

Therefore, the largest rectangle of the circumference, the smaller the circumference of the square, the smallest circle. Assume a capacity of 280L. As well as the area of the top surface shown in the table below. $A=1.05\text{m}^2$. The values of the other parameters are, as shown in Table 3:

Table 3 The value of other parameters

Shapes	Size/m	A2	qm1	qm2	q
Round	$r=0.578$	2.02	0.0293	0.5565	227
Rectangle I	$a_1=1.5,$ $b_1=0.7$	2.22	0.0295	0.5568	231
Rectangle II	$a_2=1.7,$ $b_2=0.62$	2.29	0.0296	0.5569	232
Square	$a=1.025$	2.14	0.0294	0.5567	230

Rounded $a=1.2$,
rectangle $b=0.7, r$ 2.15 0.0294 0.5567 230

Since the rounded rectangle is the most common bathtub shape, choose it as the basic bathtub. Compare it with other shapes and get the following changes, as shown in Figure 8:

Table 4 The variation compared to other shapes

Shapes	Rounded rectangle	Rectangle I	Rectangle II	Square	Round
A_2	0.00	3.26	6.39	-0.47	-6.05
q	0.00	0.58	1.14	-0.08	-1.08
q_{m1}	0.00	0.34	0.68	0.00	-0.34
q_{m2}	0.00	0.02	0.04	0.00	-0.04
T_2	0.00	-0.27	-0.53	0.04	0.51

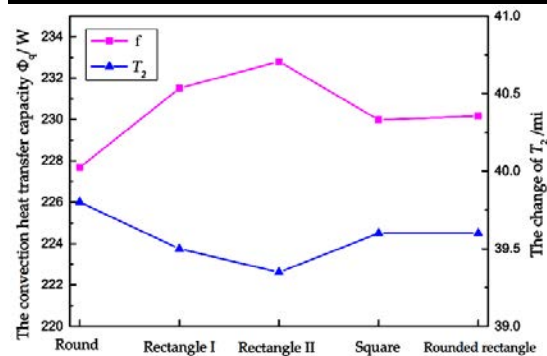


Figure 8 Different shapes of flow q and T_2

From the above data, we conclude that the top surface area A_1 and the volume V , the smallest area on the side of the circular bathtub A_2 . In different shapes. Therefore, the smallest circular bathtub heat loss. On the contrary, the rectangular side of the bathtub area and heat loss is the largest. As for the rectangular bathtub, if the aspect ratio a/b becomes larger, the area of the side will increase, resulting in an increase in heat loss, as shown in Table 4. So taking into account the heat loss, square bathtub better than rectangular bathtub. In short, the circular bathtub is the best choice for heat transfer, while the square and rounded square bathtubs are not recommended. Rectangular bathtub is the least choice. But in fact, a round rectangular bathtub is more common than a round bathtub. That's because of the shape of the human body and the space in the bathroom. A round bathtub will cover more bathroom areas [6].

3.3 The Influence of Bubble Bath Additives

According to thermodynamic knowledge, one factor can affect heat transfer in two opposite ways: increasing heat transfer or decreasing heat transfer. Bubbles made from bubble bath additives often float on bath water. Due to the small thermal conductivity of the bubbles, these bubbles can be thought of as thermal insulation between bath water and air. This layer limits the direct convection of air and bath water, thus providing insulation [7]. This shows that

we can add foam bath additives to reduce the amount of hot water added.

We let the bubble layer thickness is h_4 , the thermal conductivity of bubbles, bubbles and air on the surface of the convection heat transfer coefficient h_4L and foam and bath water become h_{4H} bottom.

Here we analyze from two aspects: on the one hand, the bubble limits the evaporation heat transfer [8]. We assume that the evaporative heat transfer is reduced to 10. On the other hand, the addition of air bubbles increases the heat transfer between air and hot water. Looking back at our previous analysis, the top surface is the main surface of the heat sink. So covering the top of the bubble will greatly reduce the heat loss. Based on the knowledge of thermodynamics, convection heat transfer capacity is:

$$\Phi_p = \frac{t_f - t_\infty}{\frac{1}{A_3} \left(\frac{\delta_4}{k_4} + \frac{1}{h_{4H}} + \frac{1}{h_{4H}} \right)} \quad (14)$$

Then we calibrate the heat transfer capability and then divide the calibration results into sub-models. We derive the values of the parameters listed in the following Table 5.

Table 5 The value of parameters

Parameters	Value	Unit
t_f	43	$^{\circ}\text{C}$
t	25	$^{\circ}\text{C}$
ϕ'_s	23.2	W
A_4	1.05	m^2
ξ_2	0.03	m
$h_4 L$	300, 1100	$\text{W}/(\text{m}^2/\text{K})$
$h_4 H$	10, 60	$\text{W}/(\text{m}^2/\text{K})$
k_4	0.3	$\text{W}/(\text{m}^2/\text{K})$

Consider the person in the bathtub, correct the above data. In order to show the effect of bubbles, we compared the results with or without bubbles, as shown in Table 6.

Table 6 Comparison of adding bubbles and no bubbles

Parameter s	Natural convection		Change	Forced convection		Change
	A	N		A	N	
q	1061	1164	8.83	1376	2390	42.42
T_2	17.87	13.63	-31.11	13.8	7.33	-89.09
q_{m1}	0.065	0.085	23.53	0.08	0.159	47.17
q_{m2}	0.604	0.631	4.28	0.63	0.729	13.58

As can be seen from the above table, bubbles have a great influence on heat transfer. Not only can reduce the heat transfer capacity, but also can save hot water.

Compared with the two sub-models, the parameters of the second sub-model vary greatly. This shows that the second sub-model is more bubble-sensitive. In summary, adding a foam bath additive slows the cooling of the bath water and avoids wasting too much water.

3.4 The Influence of Radiation Heat Transfer

In the previous discussion, we ignored the effects of radiative heat transfer because the model it considered simplistic was very small. Now is the time for us to investigate the validity of this hypothesis. According to Stephen Boltzmann's Law:

$$\Phi = \varepsilon_0 A_1 C_0 \left[\left(\frac{t_f + 273.15}{100} \right)^4 - \left(\frac{t_\infty + 273.15}{100} \right)^4 \right] \quad (15)$$

Because only the upper surface of the bath water is in direct contact with the air, we only consider the upper Surface [9]. Putting the parameters in the formula (15), we derive an approximation of 0W. In fact, when a person bathes in the bathtub, the total heat transfer capacity is 2652W. Radiation heat transfer changes only 2.64, can be ignored. This shows the reasonableness of our hypothesis.

4. CONCLUSION

In order to study the variation of water temperature, a dynamic water temperature variation model based on differential equation is proposed. Two different water addition conditions are discussed to keep the water temperature constant. For Case 1, after considering the heat transfer between water and air and the bathtub, the universal model of bath temperature, the temperature in the bathtub through a simple mathematical expression, depicting its visual change over time. For Case 2, since there is also heat transfer between people and water, a bathtub temperature model for different groups of people is established by modifying the model in Case one, and the content and time interval of adding water are determined.

Intuitive and clear understanding of the bathtub temperature changes in various periods, in order to save water while maintaining the constant temperature of the water bath provides a theoretical basis.

REFERENCES

- [1]XIE Tuo.Problems and Solutions of Business English Writing Teaching[J]. The World and Chongqing, 2015(3).
- [2]Gi-Beum Kim. Change of the Warm Water Temperature for the Development of Smart Healthcare Bathing System. Hwahak konghak. 2006, 44(3): 270-276.
- [3]Chai Lisong, automatic temperature water supply device development [D]. Nanjing: Nanjing University of Aeronautics and Astronautics, 2009.
- [4]FOLAN ME.Design and electrical temperature control in a water bath for the 44°C[J].The Irish Journal of Medical Science,1953: 217-220.
- [5]ANGER A T. Bathtub, shower water control system:US,6925661B1[P/OL] patents 2017 .03. 10.
- [6]Kenneth R. Holmes. Thermal Conductivity Data for Specific Tissues and Organs for Humans and other Mammalian Species.
- [7]Lei Yu. A study on how to keep the temperature of water in the bathtub unchanged[A]. Research Institute of Management Science and Industrial
- [8]Zhao, Ji'an Meng, Zhixin Li. Experimental study of the flow and heat transfer of a gas–water mixture through a packed channel[J]. Science Bulletin, 2016, 61(05):406-415.
- [9]Song YZ. Calculation and analysis of heat and mass transfer process model of air-water direct contact downstream [J]. Journal of Agricultural Engineering, 2006 (01): 6-10

Research on Influence Factors of Bathtub Heat Dissipation based on Heat Conduction Equation

Shuaijie Shan^{1,2}, Jiamei Liu^{1,3}, Chenshuai Liu^{1,4}, Xu Zhou^{4,*}

¹Engineering Computing and Simulation Innovation Lab, North China University of Science and Technology, Tangshan, 063000, China

²College of Electrical Engineering, North China University of Science and Technology, Tangshan 063210, China

³College of Metallurgy and Energy, North China University of Science and Technology, Tangshan 063210, China

⁴College of Science, North China University of Science and Technology, Tangshan 063210, China

*E-mail: 625525957@qq.com

Abstract: With the improvement of living standards, scientific bathing is good for both body and mind, but how to keep the water temperature constant while not wasting much water is especially important. In this paper, the following three models are established. One is to use the Fourier heat conduction equation and Newton's cooling law to establish the cylinder heat dissipation model. The second is to use the three heat dissipation solutions of convection heat dissipation, evaporative heat dissipation and radiation heat dissipation to establish a heat exchange mode between air and water. The third is to establish a constant water temperature model using the law of conservation of energy. Using the above model, the heat dissipation of different shapes and volumes of bathtubs and people of different shapes, volumes and temperatures is compared. According to the thermal resistance formula, it can be obtained that when the water is added into the bubble bath, the thermal resistance is increased, so that the heat dissipation is reduced. When the bubble thickness is increased by 0.1 cm, the heat blocking effect is enhanced by about 3 times.

Keywords: Newton's law of Cooling; Fourier Heat Conduction; Constant Water Temperature Model

1. INTRODUCTION

By comparing the square bathtub, the round bathtub and the specially shaped bathtub, we finally decided to build a model for the square bathtub. The purpose of the model is to keep the temperature of the water in the bathtub as constant as possible. In order to maintain the temperature inside the cylinder, the acrylic material is used, which has the advantage of good thermal insulation [1]. When the thickness of the cylinder is 2cm, the best insulation effect can be achieved and the material is most saved.

According to the literature, scientific bathing is good for health, water temperature should not be too high or too low, the most suitable water temperature for human body is to, which is 3 degrees higher than human body temperature, so the initial constant

temperature of water temperature is, and the indoor temperature is [2]. Think of the water and the bathtub, that is, the water temperature is the same as the temperature of the bathtub, and keeping the water temperature constant, the heat required by the bathtub to inject water is equal to the total heat lost. The lost heat includes the heat lost to the air and the heat that the bathtub dissipates into the air.

This study establishes a general thermodynamic model based on Fourier's law, heat transfer formula, and the first law of thermodynamics [3]. The energy exchange involved in Newton's law of cooling is: energy exchange between hot water and air, heat absorption of hot water, heat radiation from hot water, and energy exchange between bathtub and air.

2. ANALYSIS OF HEAT DISSIPATION PROCESS

To obtain a dynamic model of the water temperature of a bathtub, and keep the water temperature constant or close to the water temperature in the initial state within a certain time range, the whole process has gone through the following stages in the smooth process of the whole model [4].

The first stage: water is injected into the bathtub until the water and the bathtub reach an equilibrium initial temperature T_0 . During this process, the water exchanges heat with the bathtub, ignoring the heat exchange between water and air during the water injection process. At the end of the water injection, the bathtub reaches the equilibrium temperature T_0 and the total energy of the system of water and bathtub is Q_0 .

The second stage: the cylinder and the water surface continue to dissipate heat, and the heat exchange between the cylinder and the water is regarded as the energy exchange Q_a in the system, and the energy exchange between the water and the air and the water and the cylinder is recorded as Q_{out} . Therefore, the energy lost by the system can be obtained:

$$Q_{out} = Q_0 - Q_a \quad (1)$$

The third stage: the person is stationary in the cylinder, the system will exchange heat with the outside world $Q_{out \rightarrow air}$ until the water temperature drops to the critical temperature T_{min} , then the total energy at the end time is:

$$Q_0 = Q_a + Q_{out} + Q_{out \rightarrow air} \quad (2)$$

The fourth stage: when the temperature of the water in the cylinder is lowered to the critical temperature, the water of the temperature T is injected into the cylinder, and the effect of the injected hot water on the temperature of the overflow water is ignored in the process of injecting the hot water. The system maintains a constant volume and temperature, that is, the volume of the injected water remains the same as the volume of the overflow water, and the temperature of the overflow water and the temperature of the original water in the cylinder T_{min} the energy of the water injected at this time causes the temperature of the water in the cylinder to rise from T_{min} to T .

$$Q_{input} = Cm\Delta T \quad (3)$$

3. ESTABLISHMENT OF CYLINDER HEAT DISSIPATION MODEL

(1) Dimensionality Reduction Method for High Dimensional Problems

The core idea of the dimension reduction thinking is to transform a multi-factor problem into a less-factorial problem, and it is easier to make reasonable arrangements to achieve a satisfactory test result. By categorizing the various factors of the section to a point, the model of the whole fluid is a linearly distributed set of points, and the actual temperature distribution of the entire cylindrical fluid is inferred by studying the relationship between the points and the points [5-8].

(2) One-dimensional form of Fourier heat conduction equation

Obviously, in order to calculate the amount of heat dissipated at each location, we must calculate the specific heat at each location. In a constant temperature model, the relationship between temperature and time is:

$$\frac{\partial T}{\partial t} = 0 \quad (4)$$

If we only consider that the temperature does not change with the specific position of the flow, this equation can be changed to:

$$\frac{d^2 T}{dx^2} = -\frac{1}{a^2} f(x) \quad (5)$$

$$a^2 = \frac{k}{C\rho} f = \frac{Q}{C\rho} \quad (6)$$

Where k is the thermal conductivity of water, C is the heat capacity, and ρ is the liquid density?

In such a system of equations, Q represents the heat conducted by two different temperature points at the contact point, and f is the implicit function $f(x)$ in the above equation.

The above is the basic framework of the Fourier heat conduction model. By calculating the Q , we can find the corresponding implicit function f , and then use the integral to find the temperature of this segment [6]. However, the solution process for Q is complicated. We indirectly solve the heat dissipation by the Newtonian cooling model.

Calculate the temperature of each micro-element and interpolate it to obtain the temperature distribution curve in the cylinder as shown in Figure 1:

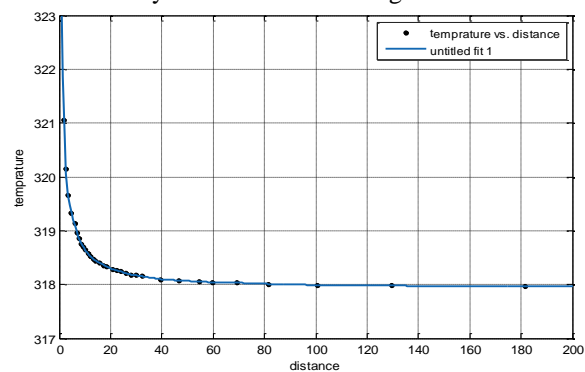


Figure 1 Bathtub Temperature Curve

The specific principles of the heat dissipation of the fluid at the solid interface have been mentioned above, thereby establishing the following two equations.

$$Q_{out \rightarrow air} = \frac{k_a(T_x - T_a)\eta}{0.01} \quad (7)$$

$$Q_{in \rightarrow out} = \frac{k_b(T_n - T_a)\eta}{0.02} \quad (8)$$

Since the upper and lower equations are equal, we calculate the T_x of each micro-element point to obtain the heat dissipation at each micro-element point. The interpolation fit for each point is shown in Figure 2:

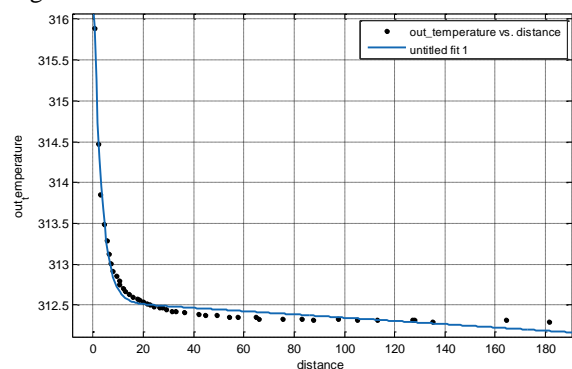


Figure 2 Heat dissipation of the cylinder wall around the bathtub

The function of the fit is:

$$dT_{out \rightarrow air} = 3.982e^{(-0.3176dx)} + 312.5e^{(-6.401 \times 10^{-6} dx)} \quad (9)$$

Then, the natural convection process in which the heat of the cylinder is dissipated into the air is simplified into the heat conduction problem of the flat plate. The heat conduction problem of t_{w1} and t_{w2} which maintains uniform temperature on both sides of the large wall has the following conclusions in the research [7-13]. The heat flow rate perpendicular to the direction of the flat plate is proportional to the temperature difference between the two sides of the flat plate and the size of the flat plate area, and inversely proportional to the thickness of the flat plate:

$$\Phi = \lambda \frac{\Delta t}{\Delta x} F \quad (10)$$

In the formula: Φ unit time transfer heat along the direction of the x ; λ corresponding scale factor; F heat transfer area. After calculation, you can find $\Phi = 307.32W$. also because

$$Q_{out1} = \Phi t \quad (11)$$

It can be obtained by the total heat $t = 83.059s$.

(3) Air and water heat exchange model

There are three main ways in which hot water can dissipate heat in the air: convection heat dissipation, evaporative heat dissipation and radiation heat dissipation [8].

Convection cooling:

The unit time passes through the water surface ds , and the heat transmitted to the air by the water surface dQ can be expressed by the following formula:

$$dQ_1 = a(t - \theta)ds \quad (12)$$

Where: a is the heat dissipation coefficient; T_1 is the water surface temperature; θ is the dry bulb temperature of the air; ds is the contact area of water and air.

Evaporative heat dissipation

Heat dQ_2 evaporating per unit time through the water surface

$$dQ_2 = \beta(P_v'' - P_v)ds \quad (13)$$

Where: β is the mass coefficient; P_v'' is the water vapor pressure of the saturated surface of the water surface; P_v is the water vapor pressure in the humid air.

Radiation heat dissipation

$$dQ_3 = \varepsilon\sigma(t + 273)^4 ds \quad (14)$$

Where: ε is blackness, taking 0.97; σ is constant 5.6×10^{-8} ; ds is the water surface area.

Therefore, the total heat dissipation dQ of the water surface is:

$$dQ_{out2} = dQ_1 + dQ_2 + dQ_3 = \left[a(t - \theta) + \beta(P_v'' - P_v) + \varepsilon\sigma(t + 273)^4 \right] ds \quad (15)$$

(4) Establishment of a constant water temperature model

In the entire bathtub cooling system, the temperature of the hot water flowing in the system changes at the inlet and outlet, assuming T_1 at the inlet and T_2 at the outlet, then obviously $T_1 > T_2$ [9]. If hot water is used as the research object, the temperature change before and after the hot water is obviously caused by the heat dissipation of the entire bathtub system, and the input heat is:

$$Q_{input} = Cm(T_1 - T_2) \\ m = \rho V \\ V = t\phi \quad (16)$$

Finishing is available:

$$Q_{input} = C(T_2 - T_1)\rho T_1\phi t \quad (17)$$

In the above formula: t represents the time of fluid flow, ϕ represents flow, ρ is fluid density, and C is specific heat capacity.

among them

When the energy injected into the system is equivalent to the lost energy, the temperature of the entire bathtub system can be conserved to achieve the purpose of the thermostatic bathtub [10]. Therefore, when calculating the heat dissipation of the system, we can use Q_{input} to represent the total heat dissipation.

$$Q_{input} = Q_{out1} + Q_{out2} \quad (18)$$

It is not difficult to infer that the flow rate that maintains the system temperature balance is:

$$V_{input} = \phi t = \frac{Q_{out1} + Q_{out2}}{C\Delta T\rho} \quad (19)$$

Solving is available: $V_{input} = 0.95L$.

4. OTHER FACTORS

(1) The influence of the shape and volume of the bathtub on the model

In real life, the shape of the bathtub is roughly rectangular, elliptical, heart-shaped, and round [11]. This article explores the most common four-shaped bathtubs. The outer surface area of the rectangular bathtub is $A = 5.122m^2$, the outer surface area of the oval bathtub is $A = 4.948m^2$, the outer surface area of the heart-shaped bathtub is $A = 5.09m^2$, and the outer surface area $A = 5.36m^2$ of the circular bathtub. After the four types of bathtubs are filled with water, the contact area between water and air is assumed to be equal. We only calculate the

amount of heat dissipated on the outer surface of the bathtub. According to the above model, the heat dissipation amount $Q = 3073.2$ of the rectangle is also obtained as shown in Figure 3 in the same manner.

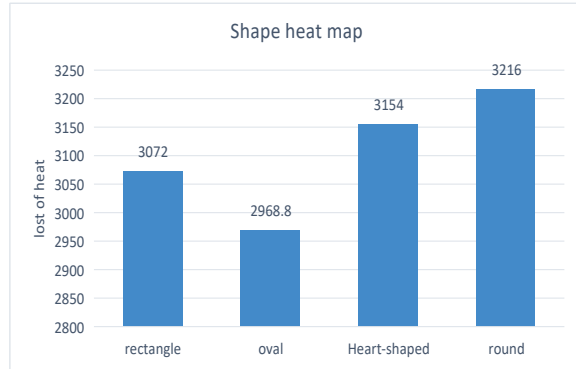


Figure 3 Shape Heat Map

Bathtubs of different shapes have significant changes in their external surface area, which can result in significant differences in the amount of heat lost. As can be seen from the figure, when the bathtub has the same specifications, when the shape of the bathtub is elliptical, the heat loss is the smallest among the four types of bathtubs, and the circular bathtub loses the most heat. This is consistent with the evaluation of these kinds of bathtubs in real life. The circular area is large and consumes a lot of water, and the rectangular bathtub and the oval bathtub are more popular.

(2) Effects of human parameters and movement in water on the model

The three parameters of the shape, volume and temperature of the human body will have slight differences in different people [12]. The above model has shown that the heat dissipation of the water surface and the air is the most important heat dissipation, so the influence of the shape change of the person in the bathtub on the water surface can be neglected. The normal body temperature of a person changes within the same range, and the optimum temperature for a person's bath is similar, and the influence of this parameter on heat dissipation can also be neglected.

When a person bathes in the water, movement will inevitably occur, which will cause fluctuations in the water surface. When a person moves, the main influence parameter is the β evaporation heat dissipation coefficient, and its expression is $\beta = [22.0 + 12.5W^2 + 2.0(t - \theta)]^{1/2}$. The temperature of the water surface and the dry bulb temperature of the air do not change. Considering the direction of the human motion and the uncertainty of the wind speed direction of the water surface, it is determined that the wind speed will fluctuate ± 0.02 based on the established wind speed, and the wind speed of the water surface is between 0.08 and 0.12. When the wind speed is different, the heat loss that is lost is shown in Figure 4:

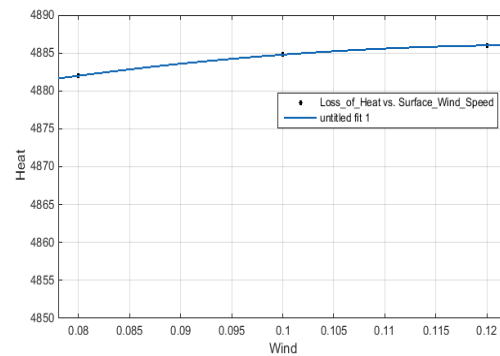


Figure 4 Wind Speed Change Heat Loss Map

It can be seen from the data in the figure that when the wind speed is the largest and the smallest, the lost heat is only a few joules. For the total heat loss of several kilojoules, the human motion has no effect on the heat loss.

(3) The impact of bubble bath on the model

Bubble bath is a new way of bathing. It is exciting for the skin of the human body and produces a continuous nerve impulse, so it has a better effect than the traditional spa. Initially through the impact of hot water, a layer of bubbles will form on the upper layer of the hot water [13]. So the system becomes hot water - bubble - air. According to the thermal resistance formula:

$$R = \delta / KA \quad (20)$$

Where δ represents the thickness of the bubble, K represents the thermal conductivity of the bubble, and A represents the surface area of the bubble. The thermal conductivity K of the bubble is close to the thermal conductivity of the air, and is derived from the Fourier heat conduction law one-dimensional flat material heat transfer differential. The surface area A of the bubble is the surface area of the bathtub, because once the hot water impacts the bubble bath, the bubble fills the surface of the entire bathtub. K takes 0.025, A takes 1.36. Then the above formula is changed to:

$$R = \delta / KA \\ = \delta / 0.025 \times 1.36 \quad (21)$$

According to the above formula, the thicker the bubble, that is, the stronger the thermal resistance, the stronger the heat resistance effect. When the thickness is increased by 0.1 cm, the heat-blocking effect will be stronger than about 3 times that of the non-foam.

5. CONCLUSION

By establishing the parameters of the constant water temperature model, the circular area is large and consumes a lot of water, and the rectangular bathtub and the oval bathtub are more popular. Human movement has no effect on the change in lost heat. The bubble has a heat preservation effect. The larger the thickness of the bubble, the better the heat preservation performance. When the thickness is increased by 0.1 cm, the heat resistance effect is

stronger than about 3 times when there is no foam. Therefore, by sensing the water temperature in the bathtub, the flow rate, temperature and time of the water are automatically controlled, so that the bather can enjoy the comfortable water temperature, thereby saving water.

REFERENCES

- [1]Wang Dongmei. Application of Acrylic Materials in Furniture [D]. Sichuan Normal University, 2016.
- [2]Luo Hong. Analysis of quasi-steady state in infinitely large parallel plates by Fourier's law[J]. Physics Experiment, 2014, 34(08): 31-33.
- [3]Yang Huiquan. Research on Product Design Based on Acrylic Materials[J]. Mechanical Design, 2014, 31(02): 127-128.
- [4]Xu Zhaowei, Li Xiaoyi. Reform Countermeasures and Suggestions for Mathematical Modeling Courses[J]. Journal of Shenyang Normal University(Natural Science), 2011, 29(01): 117-120.
- [5]Wei Jihe. Mass transfer, heat transfer and momentum transfer and mathematical process of metallurgical process [J]. Journal of Xi'an University of Architecture and Technology (Natural Science Edition), 1983 (01): 104-120.
- [6]Shou Xianfang. On-site detection and heat transfer process analysis of heat transfer coefficient of envelope structure [D]. Donghua University, 2015.
- [7]Lu Shuping, Wang Wei. Design of Water Temperature Control Experimental System [J]. Laboratory Research and Exploration, 2013.
- [8]Yu Guangpu, Li Dongsheng, You Chuanfu. Design and implementation of intelligent water temperature control system[J].Journal of Changchun University of Technology(Natural Science Edition), 2011.
- [9]Wang Jiaxing, Yang Jiwen, Zhang Huiqing, Wang Ziwei. Establishment and Simulation of Bathtub Water Temperature Control Model[J]. Journal of Shenyang Aerospace University, 2017.
- [10]Li Jiadong, Liu Jing, Gao Guanjun, Wang Zhaodong. Study on convective heat transfer coefficient of hot air cushion jet heating process of aluminum alloy sheet [J]. Light Alloy Processing Technology, 2017.
- [11]Hu Yumei, Wu Xiaoluo, Hu Zhihong, Ren Aihong, Wei Xiuqian, Wang Xinchao, Wang Yuruo.Study on the formula of human body surface area in China[J].Acta Physiologica Sinica,1999.
- [12]Guan Tao. Research on jet-enhanced heat transfer of confined cavity surface [D]. Nanjing University of Aeronautics and Astronautics, 2016.
- [13]Han Fei, Chen Liu. Analysis of factors affecting convective heat transfer coefficient of surrounding rock and airflow based on grey correlation degree[J]. Mining Research and Development, 2017.

Multi-hop HF Radio Propagation

Liuye Zhang^{1,2}, Jinhong Chen^{1,3}, Liyan Dong^{1,3}, Aimin Yang^{4,*}

¹Engineering Computing and Simulation Innovation Lab, North China University of Science and Technology, Tangshan 063000, China

²College of Mechanical Engineering, North China University of Science and Technology, Tangshan 063000, China

³College of Metallurgy and Energy, North China University of Science and Technology, Tangshan 063000, China

⁴College of Science, North China University of Science and Technology, Tangshan 063210, China

*E-mail: 43698059@qq.com

Abstract: With the constant exploration of the ocean by mankind, people hope to achieve seamless, efficient and reliable communication coverage for certain sea areas. Due to the complexity and variety of the sea surface, we consider the propagation of the oceanic radio signal from two aspects: the propagation loss between the sea surface and the ionosphere and the transmission loss on the sea surface. And to improve it to be applicable to the case of a ship traveling on a stormy sea, to realize the prediction of the radio signal propagation of ships in the ocean. For the first part, first, based on the free space propagation loss, ionospheric absorption loss, ground return loss and additional system loss, and analyzed the radio signal on the sea surface specular reflection and diffuse reflection, the construction of the sea radio signal propagation model. Secondly, the PM spectrum is used to simulate the waves under different wind speed. Then the comparison between the first reflection intensity of turbulence and the calm sea near Alaska sea area is obtained by simulation and the maximum number of hops of a calm sea surface is calculated as 26 times. For the second part, firstly, we consider three factors of the curvature of the earth, the ship's six-dimensional DOF and the antenna gain. Based on the Longley-Rice model, we improve the sea-surface radio signal propagation model. Then the impact of the propagation loss of 10MHz and 30MHz radio signals under different types of ship swaying is analyzed by simulation. Finally, based on DV-Hop localization algorithm and genetic algorithm, we obtain the optimal navigation path of the ship and the communication holding time using the same multi-hop path is 18h.

Keywords: Radio signal propagation; Longley-Rice model; DV-Hop positioning algorithm; Genetic Algorithm

1. INTRODUCTION

3~30MHz radio waves are called high frequency (HF) radio waves, which are also called short waves. Short wave has the advantages of long communication distance and good maneuverability. It is widely used in military strategy and tactical communication.

The basic transmission of shortwave has two ways [1]: one is the ground wave, one is the sky wave. Ground

waves propagate along the surface of the Earth, the propagation distance depends on the characteristics of surface media. The conductivity of sea surface media is most favorable for the propagation of radio waves. The shortwave ground wave signal can propagate about 1000km along the sea surface; the dielectric properties of the land surfaced medium are poor, and the attenuation of radio waves by different land surface media is not the same. The sky wave is a radio wave that is emitted at a height above the ionosphere and is continuously refracted back to the ground receiving point. Sky wave can achieve long-distance transmission with less power. The law of sky wave propagation is closely related to the ionosphere [2]. Due to the random variation of ionosphere, the attenuation of sky wave signals is serious. So, for the characteristics of high frequency (HF) radio wave propagation, we need to establish a model to determine the shortwave attenuation, including free space transmission loss, ionospheric absorption loss, line of sight propagation loss, diffraction propagation loss and scattering loss. In addition, ships are moving in turbulent waves when the ship uses HF for communications, weather and traffic reports, and we need to re-engineer the model to accommodate this complex situation [3].

In order to solve these problems, we have done the following work: We establish a model to determine the attenuation of the shortwave during the transmission. We show that the ship passing through Ocean, the spread of radio waves.

2. A MATHEMATICAL MODEL FOR THIS SIGNAL REFLECTION OFF THE OCEAN

To study the propagation of radio signals in the ocean, we first establish two models based on the characteristics of the shortwave propagation. One is the model of radio signal transmission loss between the sea surface and the ionosphere, and the other is the radio signal loss model at sea. Then we simulate the waves under different wind speeds. Finally, we obtain the first reflection intensity of calm sea surface and turbulent sea surface, and get the number of hops on calm sea surface.

2.1 Model I —Radio signal transmission loss model between sea surface and ionosphere

According to the transmission loss caused by various

physical factors, the basic energy loss L_b is obtained during the propagation of the short wave [4].

$$L_b = L_{free} + L_{\alpha} + L_g + L_p \quad (1)$$

Where, L_{free} —Free space transmission loss; L_{α} —Ionospheric absorption loss; L_g —Reflection loss of ground waves; L_p —Extra system loss.

2.1.1 Free Space Basic Transmission Loss

The energy of radio waves is attenuated by diffusion in free space and the loss was due to the signal in the transmission, along with the propagation distance increases, the energy spread to more and more large area caused by wave energy attenuation [5]. Its expression is:

$$L_{free} = 32.45 + 20 \lg d + 20 \lg f \quad (2)$$

Using Matlab, we can get the attenuation of the radio signal with the propagation distance in natural space, such as the Figure 1.

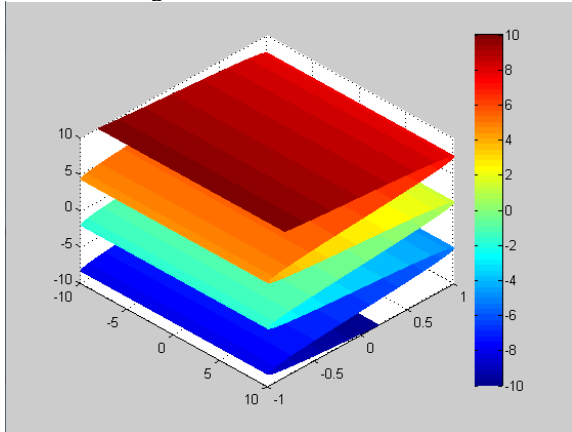


Figure 1 Radio signal attenuation in natural space

2.1.2 Ionospheric Absorption Loss

Ionospheric absorption loss L_{α} is divided into non-offset absorption and offset absorption. The former refers to absorption of the ionosphere D and E region, and the latter refers to the absorption near the reflection area. The general offset absorption loss is very small (≤ 1 dB) and can be ignored. The calculation formula of non-offset absorption loss is [6-13]:

$$L_{\alpha} = \frac{677.2 \sec \theta_0}{(f + f_h)^{1.98} + 10.2} \sum_{j=1}^n I_j \quad (3)$$

In the formula, n is the number of jumps; θ_0 stands for the height of the wave incident Angle; f_h represents the average of the magnetic resonance frequencies at the height of h . Besides, the absorption coefficient I_j is:

$$I_j = (1 + 0.0037 R_t) \cos(0.881 x_j)^{1.3} \quad (4)$$

x_j represents the mean value of the solar zenith Angle of the penetrating absorption region; R_t — t represents

the average flow of sunspots in time.

2.1.3 Reflection Loss of Ground Waves

Ground wave reflection is generated by ground reflection in mufti-hop transmission, which is related to geology, frequency and ray elevation Angle. We can estimate the ground reflection loss and take 2dB every time.

$$L_g = 2(n-1) \quad (5)$$

2.1.4 Extra System Loss

L_p is a comprehensive estimation value, which is obtained by many measured wave propagation loss data [7]. It is related to the local time T of the reflection point and can be estimated according to the Table1.

Table.1 Extra loss and timetable

Time	Loss(dB)
22:00—4:00	18
4:00—10:00	16.6
10:00—16:00	15.3
16:00—22:00	16.6

2.2 Model II—Losses of radio signals in turbulent and calm seas

Since the waves are undulating and when the radio signals reach the surface of the sea, the radio signal may have three propagation paths, which are direct path, mirror reflection path and diffuse reflection path, and some of the energy is lost in the path [8], as shown in Figure 2.

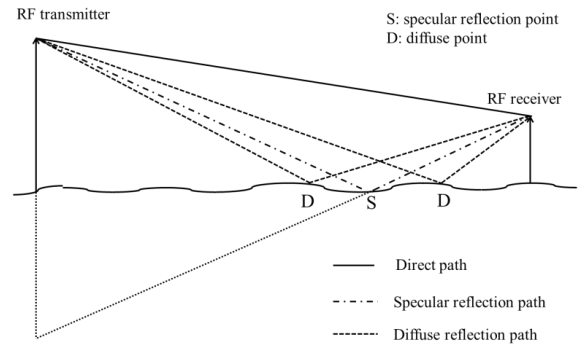


Figure 2 Multipath loss principle of sea radio signal

The transmission of radio signals on the sea is influenced by the Surface Roughness, Seawater Dielectric Constant, Mirror reflection and diffuse reflection.

2.2.1 Determination of parameters and model establishment

(1) The Surface Roughness

Generally, surface roughness g is used to describe the surface fluctuation [9]. Its calculation formula is as follows:

$$g = \frac{\sigma_h \sin \varphi}{\lambda} \quad (6)$$

In the formula, λ represents the wave length of the carrier, σ_h represents the root mean square wave height, and φ represents the radio wave incidence

Angle.

Seawater Dielectric Constant

Seawater dielectric constant ε_c is a function of carrier wave length λ , sea surface conductivity σ_e and dielectric constant ε_c [10]. It can be expressed as:

$$\varepsilon_c = \varepsilon_r - j60\lambda\sigma_e \quad (7)$$

The seawater phase constant is a factor of the Fresnel reflection coefficient formula.

(3) Specular reflection coefficient and corresponding energy loss

In this paper, the formula of specular reflection coefficient formula is derived from the literature [11], and the expression is as follows:

$$\rho_s = \exp[-2(\frac{2\pi\sigma_h \sin(\psi)}{\lambda})] \quad (8)$$

In the formula, $\lambda = \frac{c}{f}$, c is the speed of light.

Because communication is far away at sea, the effect of curvature on specular reflection cannot be ignored [12]. The final formula is as follows:

$$\rho_s' = \rho_s D \quad (9)$$

D represents the earth curvature factor

From the specular reflection coefficient, the loss value with respect to the energy component of the direct path signal is obtained:

$$\frac{V_{Specular}}{V_{Direct}} = \rho_s \sqrt{G_{ant}} |\Gamma_v| \rho_{veg} \quad (10)$$

In the formula ρ_s stands for the mirror coefficient; Γ_v is the Fresnel reflection coefficient; ρ_{veg} represents the surface vegetation loss factor. We study the sea surface and ignores the vegetation factors. In ρ_{veg} , the value is 1. G_{ant} is mirror reflection point to the direction of the receiver antenna gain and along the direction of diameter to the receiver antenna gain power ratios, we adopt the omni-directional antenna for vertical polarization dipole antenna.

(4) Diffuse reflectance and corresponding energy loss
The corresponding diffuse reflection coefficient can be expressed as [13]:

$$\rho_d = \sqrt{1 - \rho_s^2} \quad (11)$$

The rougher the sea, the more diffuse it is. The radio waves reach the surface of the sea, and the receiving signals have direct wave component, specular reflection component and diffuse reflection component. The diffuse reflection points gather around the specular reflection point to form an effective diffuse region. The diffuse reflection region is approximately ellipse. The components of diffuse energy can be regarded as the collection of energy components after the reflection of any small block dA in the effective diffuse region. The calculation

formula of the voltage loss ratio of dA 's diffuse path relative to the direct path signal is as follows:

$$\frac{V_{Diffuse}}{V_{Direct}} = \sqrt{\frac{1}{4\pi} (\frac{R}{R_1 R_2})^2 \frac{1}{\beta_0^2} \exp(-\frac{\beta^2}{\beta_0^2}) dA \times |\Gamma_v| \times \rho_{veg} \times \sqrt{G_{ant}} \times \rho_{roughness} \times \sqrt{S_f}}$$

In the formula, R , R_1 and R_2 represent direct path length and reflection length. $\rho_{roughness}$ stands for diffuse reflectance. $\sqrt{S_f}$ stands for the shadow effect coefficient we finally get the transmission loss model of the radio signal at sea surface.

$$L_s = \frac{V_{Specular}}{V_{Direct}} + \frac{V_{Diffuse}}{V_{Direct}} \quad (12)$$

2.3 Simulation of waves at different wind speeds based on PM spectrum

PM spectrum is a semi-empirical theoretical model that Pierson and Moscovitz estimated and fitted the North Atlantic fully-developed ocean wave observation data in 1964[14].

A two-dimensional wave number spectrum at a wind speed is P , and the wave forms at five, six, seven and eight wind speeds are simulated, as shown in Figure 3, Figure 4, Figure 5, Figure 6.

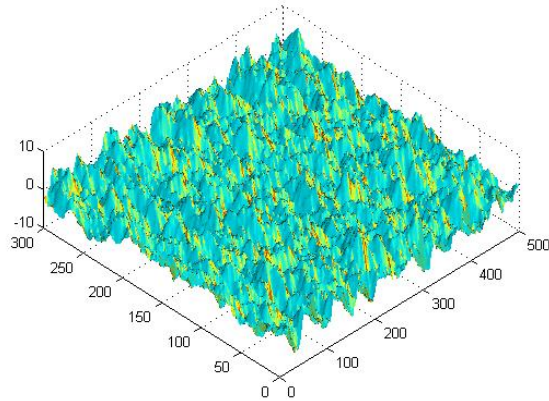


Figure 3 Waves under the five-stage wind speed

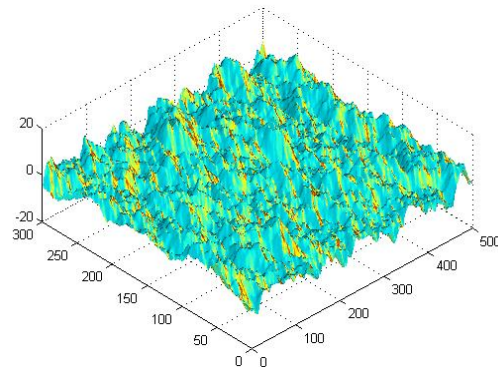


Figure 4 Waves under the six-stage wind speed

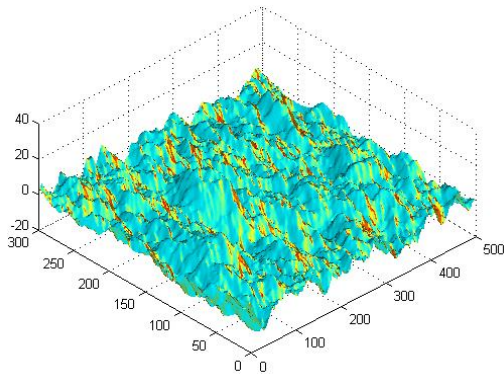


Figure 5 Waves under the seven-stage wind speed

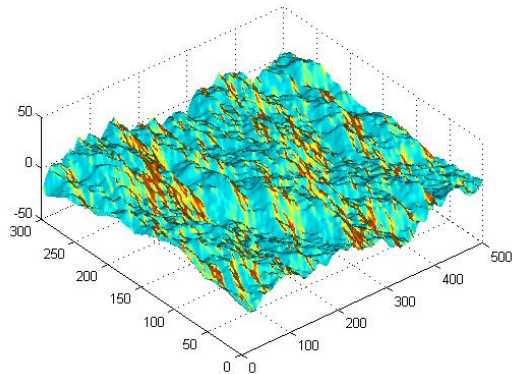


Figure 6 Waves under the eight-stage wind speed
As can be seen from the four figures, the larger the wind speed, the higher the wave and the higher the wave height.

2.4 Model I + Model II — A mathematical model for this signal reflection off the ocean

Before establishing the model of radio propagation over the ocean surface, we introduce a signal-to-noise ratio, SNR, which is the ratio of the average power of the transmitted signal S to the noise power N [15],

$$SNR = 10 \lg \frac{S}{N} \quad (14)$$

The relationship between dBm and power P is

$$A = 30 + 10 \lg P \quad (15)$$

Among them, A —Unit is dBm, P —Power, Unit is w. Therefore, based on the basic energy loss model in shortwave sky wave propagation and the radio signal propagation loss model F on the sea surface, we finally obtain the radio signal propagation model on the ocean surface as:

$$F = A - L_b - L_s \quad (16)$$

If you combine the model F with the Longley-Rice model, you can better obtain the reflection intensity. We selected Alaska ($39^\circ 28'N$, $86^\circ 38'W$) as the signal reflectivity station with a radio frequency of $f = 7$ MHz, a signal elevation angle of 54° and a step of 0.25 MHz, Antenna height $h = 10m$, Relative dielectric constant $\epsilon_c = 15$, sea surface conductivity $\sigma_c = 0.005$. Taking all the data into Eq. (16), we obtain the first reflection intensity contrast between surging

and calm sea surface as shown in Figure 7. Then we consider the diffuse reflection energy loss and the mirror energy loss of the radio signal on the sea surface, Using Matlab, the maximum number of hops before signal strength reaches the threshold ($SNR < 10dB$) at sea level is 26 times.

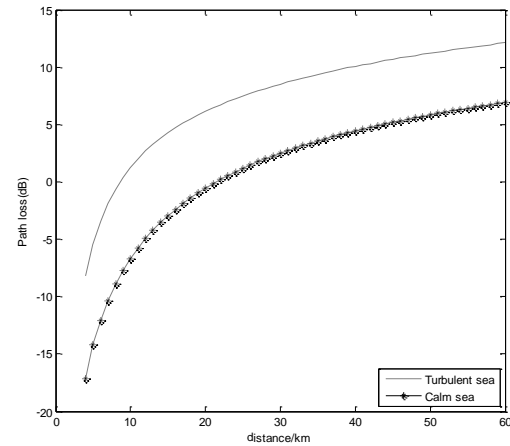


Figure 7 Comparison of the first reflection intensity on the turbulent and calm sea surface

As can be seen from Figure 7, the trend of decline on turbulent and calm seas is basically the same, but the value of turbulent sea surface is greater.

3. MARINE RADIO WAVE LOSS MODEL UNDER SHIP AWAY

The ship is affected by the waves on the sea surface, and changed in the antenna elevation angle, resulting in changes of the antenna and receiving gain along different directions. Therefore, we need to modify the model before formula 16, to adapt to this complex situation [16].

3.1 Ship Damage Analysis Based on Longley-Rice Model

The Longley-Rice model is a deterministic model derived from Maxwell's equations. Longley-Rice model can solve the complex environment of reflection, refraction, diffraction and scattering of the spread [17].

Based on the Longley-Rice model, we consider the three factors of the curvature of the earth, the shaking of the three-dimensional ship and the gain of the antenna, to realize the improvement of the Longley-Rice model and to make the model more suitable for the case of ship swaying.

3.1.1 Propagation area of marine electrical signals

Due to the unevenness of the sea, the signals received by the antenna in the visible range include direct waves, sea reflected waves and diffracted waves. The diffraction effect occurs in the shadow area of the earth. Therefore, the propagation area is divided into three areas A , B , C according to the distance between the sender and the receiver, as shown in the Figure 8 [18].

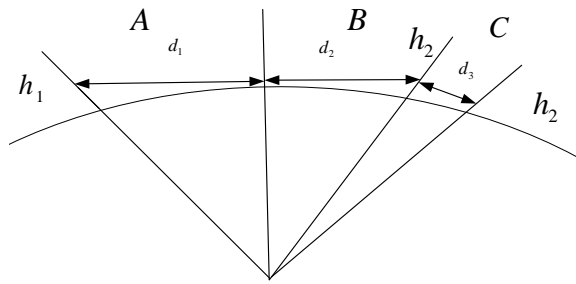


Figure 8 Spread area map

As shown in Figure 8, assuming that the height of the transceiver antenna is h_1, h_2 , the visual distance d_1 of the area A is obtained from the geometric relationship,

$$d_1^2 + R^2 = (h_1 + R)^2 \quad (17)$$

So, $d_1 = \sqrt{2Rh_1 + h_1^2}$

Because of the effective radius of the earth $R \gg h_2$, so Similarly, we can get the visual distance of area B.

3.1.2 The earth curvature

We assume that the radio signals are secularly and diffusely reflected on the sea surface [19], as shown in Figure 9.

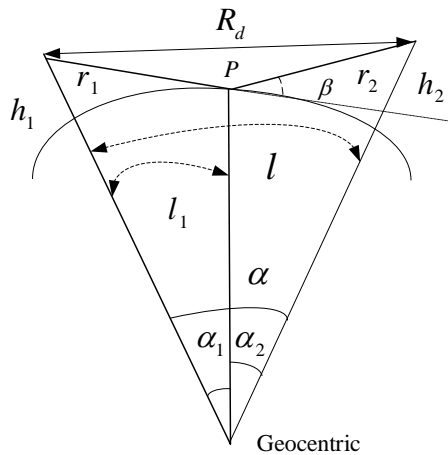


Figure 9 Earth curvature diagram

According to the delay to get the distance of the direct path R_d , and then by the cosine theorem we can get α .

$$\alpha = \cos^{-1} \left(\frac{(h_1 + R)2 + (h_2 + R)2 - R_d^2}{2(h_1 + R)(h_2 + R)} \right) \quad (18)$$

R — the earth's effective radius, Horizontal distance $l = R\alpha$, Since the reflection point P is unknown, we use the following equation to find out l_1 .

$$\alpha_1 = \frac{l_1}{R}, \quad \alpha_2 = \frac{l - l_1}{R} \quad (19)$$

According to the cosine theorem:

$$\begin{cases} r_1 = \sqrt{R^2 + (R + h_1)^2 - 2R(R + h_1)\cos\alpha_1} \\ r_2 = \sqrt{R^2 + (R + h_2)^2 - 2R(R + h_2)\cos\alpha_2} \end{cases} \quad (20)$$

In summary, the angle of incidence after considering the curvature of the Earth is:

$$\beta = \sin^{-1} \left(\frac{h_2}{r_2} - \frac{r_2}{2R} \right) \quad (21)$$

3.1.3 Six-dimensional freedom with the ship swaying

We assume that the ship swayed up, down, up and down along with the waves, so we set up a six-dimensional model of rocking motion with six degrees of freedom $(x, y, z, \alpha, \beta, \gamma)$. We set up a globe-based ball coordinate system with the origin of the coordinates of the Earth's geocentric center [20-22]. The movement of the ship can be expressed as:

The height changes up and down the z axis;

The left and right wobbles rotate around the x axis;

The tilt before and after the rotation around the y-axis.

The maximum angular deviation of a vertically polarized antenna is deduced from the approximate geometric relationship, that is the maximum value of the ship's sway angle.

$$\theta_{\max} = \arcsin \left(\frac{\pi H_{\max}}{\sqrt{\lambda_{\text{sea}}^2 + \pi^2 H_{\max}^2}} \right) \quad (22)$$

Among them, H_{\max} —The maximum height of the waves; λ_{sea} —The wavelength of the waves.

3.1.4 Antenna gain

When the ship swaying, the pitch and roll angles of the antenna change. In this paper, the parameters of the projectile are used to represent the antenna gain and its components in different directions.

$$W = \sqrt{G(\theta, \phi)} U = \sqrt{G(\theta, \phi)} \begin{pmatrix} U_\theta(\theta, \phi) \\ U_\phi(\theta, \phi) \end{pmatrix} \quad (23)$$

$\sqrt{G(\theta, \phi)}$ —The actual gain of the antenna over a range of angles of transmission and reception; θ —Antenna elevation; ϕ —Antenna azimuth; U —The unit vector, which represents the proportion of antenna gain along and in the direction of distribution.

3.2 An Improved Model of Sea Surface Radio Signal, Propagation Based on Longley-Rice Model

The transmission loss of the radio-wave transmission model can be roughly divided into the line-of-sight propagation loss, the diffraction propagation loss, the scattering propagation loss and the free space transmission loss. Combining the three factors of the curvature of the earth, the three-dimensional ship swaying and the antenna gain, the improved Longley-Rice transmission loss L_b [21]:

$$L_b = L_r + L_{\text{free}} \quad (24)$$

In the formula, $L_{\text{free}} = 32.45 + 20 \lg d + 20 \lg f$,

$$L_r(d) = \begin{cases} \max(0, L_{be} + k_1 + k_2 \lg d), & d_{\min} \leq d \leq d_{Ls} \\ L_{bed} + m_d, & d_{Ls} \leq d \leq d_x \\ L_{bes} + m_s d, & d_x \leq d \end{cases}$$

Where, d —Dissemination distance; f —Radio

frequency; d_{Ls} —Sea surface distance; d_x —The diffraction loss and scattering loss of this place are equal; L_{be} , L_{bed} , L_{bes} they are the propagation loss, the diffraction loss and the scattering loss in free space; k_1 , k_2 —Propagation loss factor; m_d , m_s —Diffraction, scattering loss factor.

3.3 Simulation analysis

The propagation loss of radio waves is simulated by using the maximum angle deviation of antenna, the incident cape and the path loss calculation method. Suppose the ship distance from the water temperature receiving and dispatching station on the land are 1km, 5km, 10km, 15km, 20km, the height of the transceiver antenna is 10m, the period of the sea wave is 6s, the maximum angular deviation of the antenna is 6.9° and the antenna gain is 2.3dBi According to the formula, the visual distance of A segment is calculated as 10km and the visual distance of B segment is 26km. Using Matlab simulation, when the carrier frequency is 10MHz and 30MHz, we can get the contrast of the impact of the ship's sway on the propagation loss of radio waves, as shown in the Figure 10, Figure 11 and Figure 12.

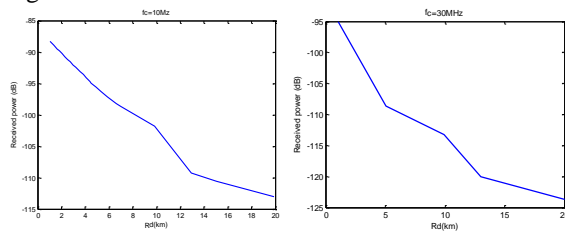


Figure 10 The graph of the received power loss over time when the ship is not shaking

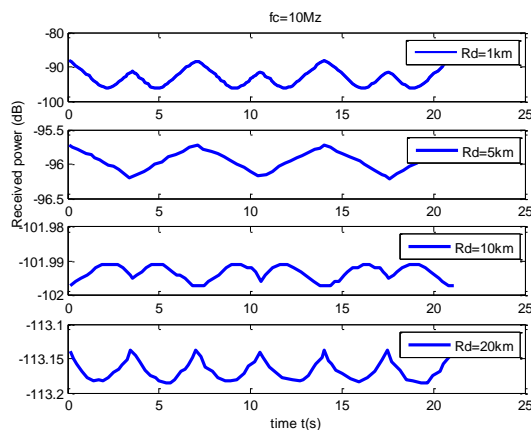


Figure 11 Comparison of power loss versus time when a ship is floating up and down (fc=10Mz)

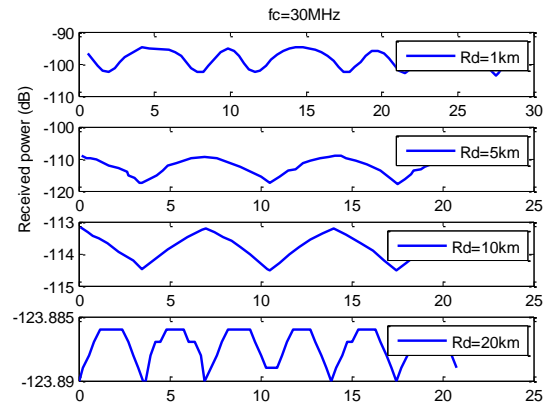


Figure 12 Comparison of power loss versus time when a ship is floating up and down (fc=30Mz)

As shown in Figure 11 (a), fluctuations in propagation loss caused by up and down fluctuations were 9dB. The loss of fluctuations caused by the ship's roll and pitch in the analysis appendix was only 0.2dB. It can be concluded that in paragraph A, the impact on sea surface propagation loss is the greatest when compared with the other two types of rocking when the ship is floating.

Comparing Figure 11 (a) - (d), the distances between the transmitting end and the receiving end are 1km, 5km, 10km and 20km. As the receiving and transmitting end distance increases, the fluctuation of propagation loss becomes smaller and smaller. Getting smaller and smaller. For example, in Figure 11-i- (a) and Figure 11-ii- (a), when the transceiver distance is 1 km, the carrier frequency is 10 MHz. The fluctuation of the received signal power loss is 9 dB and the carrier frequency is 30 MHz. The fluctuation of signal power loss is 16 dB.

3.4 Hops Model Based on DV-Hop and Genetic Algorithm

Firstly, the total number of nodes is 200, the number of known anchor nodes is 20, the length of two-dimensional region is 1870km, and then the DV-Hop method[22] is used to calculate the coordinates of the center of signal coverage area as (3.4, 5.7) Radius of 20km as shown Figure13 In order to find the optimal solution, Genetic Algorithm is used to determine the best path covered by long time flight and the shortest flight duration as shown Figure 14 The optimal path is 8364km. Through the access to information that the speed of the vessel in the 30 ~ 40 nautical miles / hour range, take the speed of 35 knots, the effective signal coverage was 18 hours.

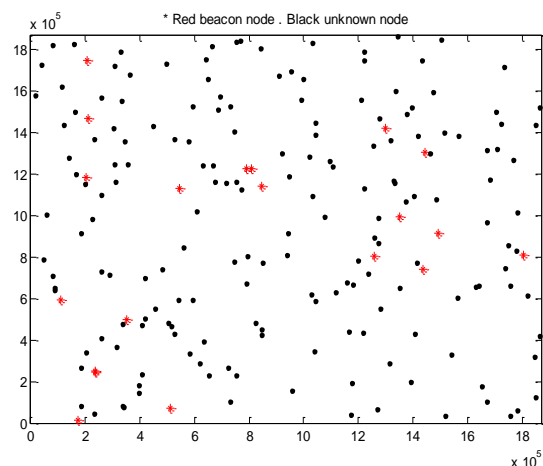


Figure 13 Network node distribution

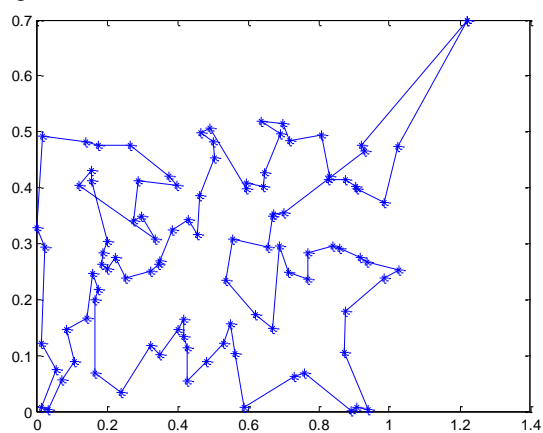


Figure 14 Cruise path schematic

4. CONCLUSION

In the first part, the loss of radio signals in free space and diffuse reflection on the surface of the sea are mainly introduced. The loss caused by ionospheric and specular reflection is also introduced precisely. Because these losses result in the final reduction of the radio signal strength to zero. The second part improves on the first part of the model. The improved Longley-Rice model predicts the propagation of radio signals on complex seas, such as how a ship can get better radio signals when it crosses the ocean. In general, the model we built can better adapt to the sea environment and have a more accurate prediction of the propagation loss of radio signals.

ACKNOWLEDGMENT

Thanks to Engineering Computing and Simulation Innovation Lab for help.

REFERENCES

- [1]WANG Leidi, L Daren, HE Qing. The Impact of Surface Properties on Downward Surface Radiation over the Tibetan Plateau[J]. Advances in Atmospheric Sciences, 2015, 32(06):759-771.
- [2]Xuehui Cui. Signal Reflection in Shortwave Multi-hop Transmission Mode[A]. Institute of Management Science and Industrial Engineering. Proceedings of 2018 3rd International Conference

on Materials Science, Machinery and Energy Engineering(MSMEE 2018)[C].Institute of Management Science and Industrial Engineering: Computer Science and Electronic Technology International Society, 2018:9.

[3]Yan Ma. Reradiation Interference of High Voltage Transmission Line to Shortwave Radio Direction Finding Station[A]. IEEE Beijing Section, Beijing Jiaotong University. Proceedings of 2015 IEEE 6th International Symposium on Microwave, Antenna, Propagation, and EMC Technologies(MAPE 2015)[C].IEEE Beijing Section, Beijing Jiaotong University:IEEE BEIJING SECTION, 2015:5.

[4]NIU Jiling, LUO Yu, ZHAO Yang, JIN Xiaoyan. Analysis and Selection of Base Station Antennas in HF Communication [J]. Communications Technology, 2018 (01): 240-244.

[5]Qin Xubin. Short-range long-range air-ground communication based on channel characteristics analysis [J]. Information Technology Conference, 2016 (03): 285.

[6]Hao Shuji, Zhang Wenchao, Zhang Yabin, Yang Jutao, Ma Guangling. Low latitude ionospheric sporadic E layer radio propagation modeling [J]. Journal of physics, 2017, 66 (11): 406-415.

[7]Cao Junqing, Wangsheng Sheng, Yangzheng Zheng, Li Hua, Yi Zhong. Journal of Test and Measurement Technology, Study on the path loss equation of underwater magnetic communication system [J]. 2017, 31 (06): 531-536.

[8]Thomas Lykke Andersen, Mads Røge Eldrup, Peter Frigaard. Estimation of incident and reflected components in highly nonlinear regular waves. Coastal Engineering, 2017, 119.

[9]TANEOKA Junya, MORI Tomoya, KOBAYASHI Hayato, HASEGAWA Masayuki, OMATA Yukiko, MAEGAWA Satoru, MATSUOKA Hiroshige, KATO Takahisa, FUKUI Shigehisa. System development to evaluate the effects of surface roughness on adhesion force reduction. The Proceedings of the Conference on Information, Intelligence and Precision Equipment: IIP, 2017, 2017(0).

[10]Xie Tao, William Perrie, Fang He, Zhao Li, Yu Wenjin, He Yijun.Effective dielectric constant model of electromagnetic backscattering from stratified air-sea surface film-sea water medium [J]. Chinese Physics B, 2017, 26 (05): 124-129.

[11]R. Zemih, M. Boudjema, C. Benazeth, Y. Boudouma, A.C. Chami. Image potential effect on the specular reflection coefficient of alkali ions scattered from a nickel surface at low energy[J]. Nuclear Inst. and Methods in Physics Research, B, 2002, 193(1).

[12]Zhang Wei, Liao Guozhong, Sun Tao, Zhang Qiudong. Calculations and accuracy analysis of gravity intermediate layer correction considering the effect of earth curvature [J].Geodesy and geodynamics, 2016, 36 (05): 391-394.

[13]SHI Peili, LI Ke Study on energy distribution characteristics of three-dimensional laser surface

- diffuse reflection [J] *Laser and Infrared*, 2015, 45 (03): 256-261.
- [14]Chen Zhenwei, Ren Xincheng, Tian Wei, Wu Yang, in Joan. Perturbation method of two dimensional anisotropic sea surface electromagnetic scattering based on PM spectrum [J]. *Journal of Yan'an University (Natural Science Edition)*, 2014, 33 (04): 14-18.
- [15]signal-to-noise ratio.[Online].<https://zhuanlan.zhihu.com/p/33305693>.
- [16]Wang Zhaoying, Wang Qingfen, Wang Ye. Analysis and System Design of Microwave OTH Communication Channel Characteristics [J]. *Journal of Radio Communication Technology*, 2017, 43 (05): 24-28.
- [17]Kasampalis, S., Lazaridis, P.I., Zaharis, Z.D. etc. Comparison of Longley-Rice, ITU-R P.1546 and Hata-Davidson propagation models for DVB-T coverage prediction. 2014 IEEE International Symposium on.
- [18]Huang Fang. Research on the propagation characteristics and channel modeling of radio waves at sea [D]. Hainan University, 2015.
- [19]Zhang Shun. Study on the influence of earth curvature on the image shift of geosynchronous satellite images -- with surface array CCD as an example, [J]. *Geology and mineral mapping*, 2016, 32 (04): 8-10+32.
- [20]Liu Kewei. Design of antenna feeder for solving short wave blind area communication of ships. *digital communication world*, 2017 (12): 49.
- [21]Improved algorithm of atmospheric refraction error in Longley-Rice channel model. *Journal of Systems Engineering and Electronics*, 2008(04):683-687.
- [22]Qinqin Shi, Jianping Zhang, Yunxiang Liu, Yaying Zhang. A Modified DV-Hop Localization Scheme for Wireless Sensor Networks. *Energy Procedia*, 2011, 13.

Prediction of Reflectivity of Coal-Fired Vitrinite based on KNN Algorithm

BaoRong Wang^{1,2}, JinHong Chen^{2,3}, XueYong Jia^{2,4}, JiePing Wang^{1,*}

¹School of Chemical Engineering, North China University of Science and Technology, Tangshan 063210, China

²Engineering Computing and Simulation Innovation Lab, North China University of Science and Technology, Tangshan, 063210, China

³College of Metallurgy and Energy, North China University of Science and Technology, Tangshan 063210, China

⁴College of Electrical Engineering, North China University of Science and Technology, Tangshan, 063210, China

*E-mail:baorongwang_ncst@163.com

Abstract: The effective utilization of coal resources is inseparable from the development of modern artificial intelligence. In order to accurately predict the reflectivity of coal vitrinite group, this paper proposes to use KNN algorithm to solve the vitrinite reflectance of coal vitrinite group predicted coal blending. After the model is trained, the distribution of the vitrinite reflectance of the coal is predicted. The fitting accuracy is 61%, so the model can accurately predict the reflectivity of the coal vitrinite group, which plays an important role in guiding coking coal blending.

Keywords: KNN algorithm; effective utilization; Reflectivity

1. INTRODUCTION

The role and role of coal rock theory in coal blending coking is becoming more and more important. Many coking enterprises identify coal blending, coal blending coking is inseparable from coal rock analysis [1], vitrinite reflection in coal rock analysis. Rate testing has become a routine testing project in coking production [2], which can guide coal blending coking by matching the mirror reflectivity of coal [3], and to establish a matching coal mirror for the study of the vitrinite reflectance of coal blending. The relationship between the mass group and the reflectivity interval of a single coal, saving costs in coking enterprises, reducing the loss of coal and rock analysis instruments, guiding coking enterprises to accurately blend coal and improve coke quality [4].

2. DATA PREPROCESSING

There are many variables in the blast furnace ironmaking process, and the physical and chemical Select a single coal from the coking plant in 2016 and 2017. According to the reflectivity of coal and the data of coal blending scheme, a total of 23 single coals and 267 sets of data were obtained by collating data. The reflectance interval was divided into intervals of 0.05, with 43 intervals. According to the national standard, 23 kinds of single coal are classified into fat coal, coking coal and lean coal. The results of the division are shown in the following

Table1:

Table 1: Division of single coal

Coal type	Fat coal	Coking coal	lean coal
Number of single coals	4	16	3

Firstly, the data of each single coal is separately sorted according to the national standard. The 43 intervals of the reflectivity are multiplied by the respective ratios, and then the single coals under the fat coal, coking coal and lean coal are summed.

$$\begin{aligned}
 F &= a * x1 + b * x2 + c * x3 + d * x4 \\
 J &= e * x5 + f * x6 + g * x7 + h * x8 \\
 &\quad + i * x9 + j * x10 + k * x11 + l * x12 \\
 &\quad + m * x13 + n * x14 + o * x15 + p * x16 \\
 &\quad + q * x17 + r * x18 + s * x19 + t * x20 \\
 S &= u * x21 + v * x22 + w * x23
 \end{aligned} \quad (1)$$

Among them, F, J, and S respectively represent fat coal, coking coal, and lean coal. The lowercase English letters represent the reflectivity of each single coal vitrinite group, and x represents the ratio. The data of fat coal, coking coal and lean coal multiplied by the ratio of reflectance distribution are counted, and the data are averaged. The vitrinite reflectance distribution maps of fat coal, coking coal, lean coal and coal blending are drawn. As shown below Figure 1, Figure 2, Figure 3 and Figure 4:

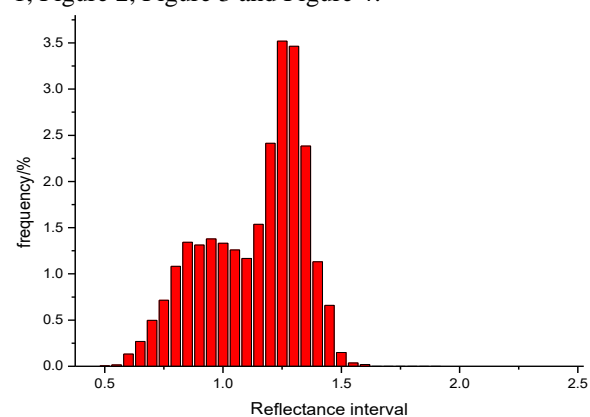


Figure 1: Fat coal reflectance distribution map

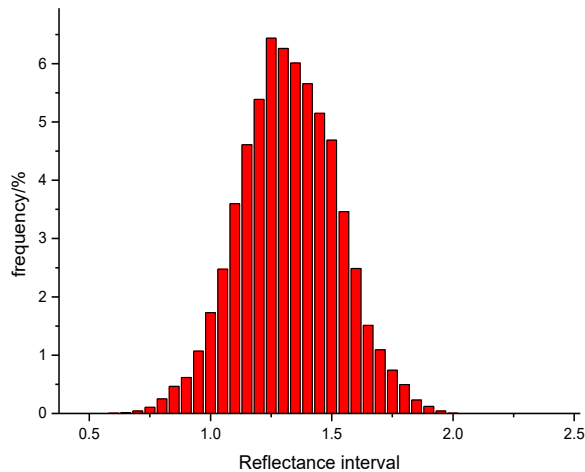


Figure 2: Coking coal reflectivity distribution

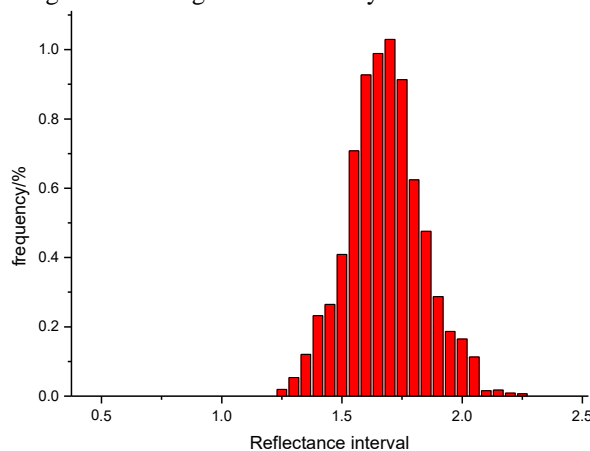


Figure 3: Thin coal reflectance distribution map

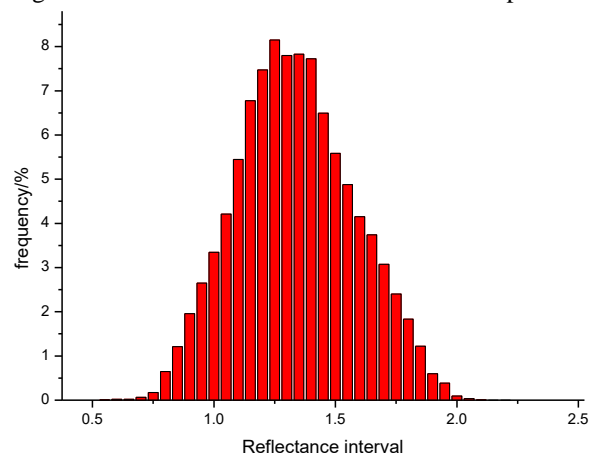


Figure 4: Cobalt reflectance distribution map

From the above figure, the fat coal is in the 0.55-1.5 interval, the coking coal is in the 0.6-2.0 interval, and the lean coal is concentrated in the 1.25-2.15 range. Each coking coal has its own characteristics, and each single coal vitrinite group is reflected. The ratio of the ratio of the mixture to the coal vitrinity is obtained [5]. However, this method cannot accurately predict the reflectivity of the coal vitrinite group. Therefore, machine learning is used to predict and improve the prediction accuracy.

3. K PROXIMITY ALGORITHM

The KNN algorithm is a nonparametric method for classification and regression. It was originally proposed by Cover and Hart in 1968 and is a lazy learning method. The KNN algorithm is a theoretically mature method and one of the simplest machine learning algorithms. For classification and regression, useful techniques can be used to assign weights to neighbors' contributions, so that closer neighbors contribute more averages than distant neighbors. One feature of the KNN algorithm is that it is sensitive to the local structure of the data.

In KNN regression, the KNN algorithm is used to estimate continuous variables, using the weighted average of the k nearest neighbors, weighted by the reciprocal of their distances. The algorithm works as follows:

Step1: Construct a training sample set and a test sample set.

Step2: Calculate the Euclidean distance between the test sample and each training sample. The Euclidean distance is calculated as follows:

$$d = \sqrt{(x_1 - x_2)^2 - (y_1 - y_2)^2} \quad (2)$$

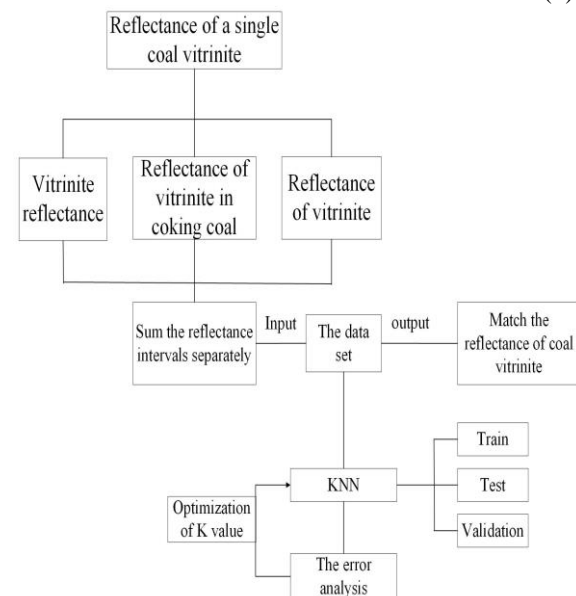


Figure 5: algorithm implementation flow chart

Step3: The heuristic optimal number k of the nearest neighbor is found according to the RMSE, which is done using cross-validation, which is any of various similar model verification techniques used to evaluate how statistical analysis results are generalized to independent data sets. It is primarily used for setup, its purpose is to predict, and one wants to estimate how accurately a predictive model is implemented in practice. In predicting problems, the model is typically provided with a data set of known data running the training and a data set test model of the unknown data. The goal of cross-validation is to test the ability of model predictions to be used to estimate new data in order to flag issues such as overfitting and to gain insight into how the model will be generalized to independent data sets. A round of cross-validation

involves segmenting the data of one sample into complementary subsets, in one subgroup, and verifying in another subset. To reduce variability, in most methods, multiple rounds of cross-validation are performed using different partitions, and the verification results are combined on rounds to give an estimate of the predicted performance of the model. In summary, cross-validation combines the measure of predictive fitness to yield a more accurate estimate of model predictive performance. As shown below Figure 5 and Figure 6:

Step4: The inverse distance weighted average is calculated using k nearest multivariate neighborhoods.

4. PREDICTION OF REFLECTIVITY OF COAL VITRINITE GROUP

By predicting the vitrinite reflectance of the coal with the vitrinite reflectance of a single coal, the coal rock data is preprocessed first, and the KNN algorithm is selected. The algorithm is optimized to maximize the prediction accuracy. The specific process is shown in the following figure:

The vitrinite reflectance intervals after fat coal, coking coal, and lean coal are respectively summed as inputs, that is, 43 inputs, in combination with the coal vitrinite reflectance interval as output, 43 outputs, using cross-validation Methods The data set was processed with 70% of the data as the training set, 15% as the test set, 15% as the verification set, and MSE as the error analysis of the model training. The error result was the smallest, which proved that the training was good and accurate. The predictions match the vitrinite reflectance of coal to provide a reasonable coal blending program guidance for coking plants. As shown in the figure below, it is the prediction of one of the verification sets of the coal reflectance interval.

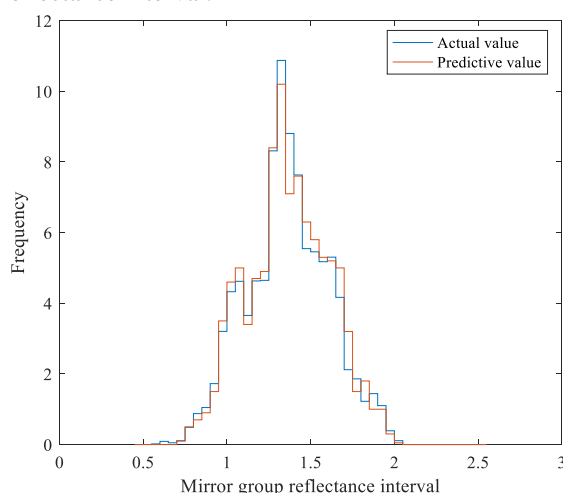


Figure 6: Vitrinite reflectance distribution

ACKNOWLEDGMENT

The effective utilization of coal resources is inseparable from the development of modern artificial intelligence. In order to accurately predict the reflectivity of coal vitrinite group, this paper proposes to use KNN algorithm to solve the vitrinite group reflectivity of coal vitrinite group prediction coal blending. The single coal is divided according to the national standard, and then the reflectivity of the single coal vitrinite group multiplied by the ratio is used as the input of the model, and the coal vitrinite reflectance is used as the output, and the data set is obtained by cross-validation. The optimization is carried out, and the model is trained to predict the distribution of the vitrinite reflectance of the coal. The fitting accuracy reaches 61%, so the model can accurately predict the reflectivity of the coal vitrinite group, which plays an important role in guiding coking coal blending.

REFERENCES

- [1]Tian Yingqi, Zhang Weihua, Shen Yuzhen, Lu Xilan, Zhang Dexiang. Study on the vitrinite group reflectivity to optimize the coal blending coking scheme[J].Coal Science and Technology, 2016, 44(04):162-168.
- [2]Chen Zhiqiang, Li Jun, Qi Zhengyi. Application of coal vitrinite reflectance distribution map in coal blending system. Coal Engineering, 2015, 47(10): 125-127.
- [3]LIN Le-ling, ZHANG Xiao-ning, Application of coal and rock blending in coking production of Benxi Steel. Journal of Liaoning Institute of Science and Technology, 2008, 10(04):11-12.
- [4]Zhang Wencheng, Ren Xueyan. Effect of coking coal blending characteristics on coal blending coking. Chemical Industry and Engineering Progress, 2015, 34(S1): 71-74.
- [5]Du Ping, Zhou Junlan, Lu Qingqing. A method for predicting the reflectivity distribution of coal vitrinite group and its application. Jiangsu: CN104090084A, 2014-10-08.

Solution to CT System Parameter based on Sinusoidal Trigonometric Function

Enhong Chen*, chenshuai Liu, Xueyong Jia

Mathematical Modeling Association, North China University of Science and Technology, Tangshan 063210, China

*E-mail: 1715689092@qq.com

Abstract: CT technology can realize tomography of biological tissue and engineering material samples, which has guiding significance for production practice. However, there are often errors in the installation of CT system, which affect the imaging quality. Therefore, this paper focuses on the parameter problem of CT system.

Keywords: sinusoidal; trigonometric function; CT system parameters.

1. INTRODUCTION

To solve these problems, a solution model of CT system parameters based on sinusoidal trigonometric function is established. Firstly, according to the particularity of small circle, the projection length of detector unit is fixed at 8 mm. Then, according to the attached absorptivity table, 29 detectors with small circle absorptivity can be detected, and the detector unit can be obtained. The spacing is 0.2759. By comparing the relative motion relationship between the center of circle and the center of rotation, the trajectory model of the center projection in the detector unit varying with the angle is constructed. Combining with the image data in Annex 2, the expression is obtained by means of MATLAB fitting.

$$y = -198.8818 \sin(0.0171x - 0.9231) + 259.4$$

Based on the above function relationship, the coordinates of the rotation center (-9.6014, 7.6281) of CT system are obtained by focusing on two special rotation angles of 0 and 90.

Computed Tomography (CT) can tomography the samples of biological tissue and engineering materials by using the absorption characteristics of radiation energy without destroying the samples, thus obtaining the internal structure information of the samples [1-3]. A typical two-dimensional CT system is shown in Figure 1. Parallel incident X-rays are perpendicular to the detector plane. Each detector unit is regarded as a receiving point, and arranged equidistantly. The relative position of X-ray emitter and detector is fixed [2-5], and the whole transmitting-receiving system rotates counter-clockwise 180 times around a fixed rotating center. For each X-ray direction, the radiation energy absorbed and attenuated by the two-dimensional medium to be detected is measured on a detector with 512 isometric units, and 180 sets of received information are obtained after gain processing. There are often errors in the installation of

CT system, which affect the imaging quality. Therefore [6], it is necessary to calibrate the parameters of the installed CT system, that is, to calibrate the parameters of the CT system with the help of the samples with known structures (called templates), and then to image the samples with unknown structures.

A calibration template consisting of two uniform solid media is placed on a square tray. The geometric information of the template and the corresponding data files are given. The value of each point reflects the absorption intensity of the point, which is called "absorptivity". According to this template and the received information, determine the position of the rotating center of the CT system in the square tray, the distance between detector units and 180 directions of X-ray used by the CT system.

2. SOLUTION MODEL BASED ON SINUSOIDAL TRIGONOMETRIC FUNCTION

2.1 CT imaging system

As shown in Figure 1, the incident X-ray is perpendicular to the detector plane, and each detector unit is considered as a receiving point and arranged equidistantly. The relative position of X-ray emitter and detector is fixed, and the whole transmitting-receiving system rotates counter-clockwise 180 times around a fixed rotating center. Figure 1 Measures the radiation energy absorbed and attenuated by a two-dimensional medium fixed in position on a detector with 512 isometric units in each X-ray direction.

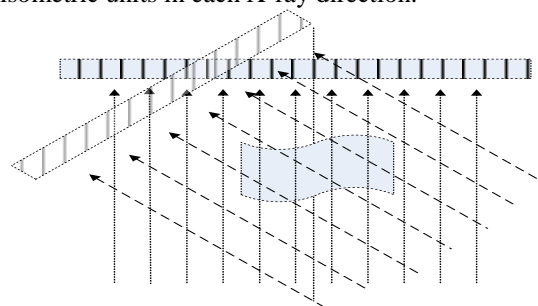


Figure 1: The schematic diagram of the CT system

As shown in Figure 2, a calibration template consisting of two uniform solid media is placed on a square tray. The geometric information of the calibration template can be seen in the figure, and the value of each point reflects the absorption strength of the point.

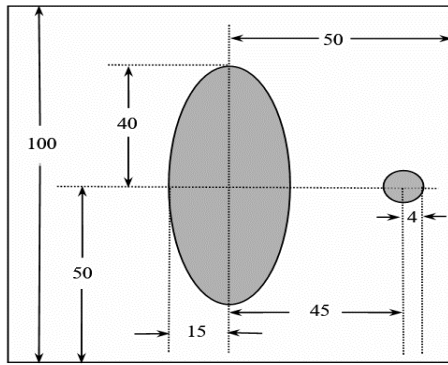


Figure 2: Schematic diagram of template
According to the information of the attachment, two geometric objects are illuminated by the detector, and the rotation around the revolving center is shown in Figure 3.

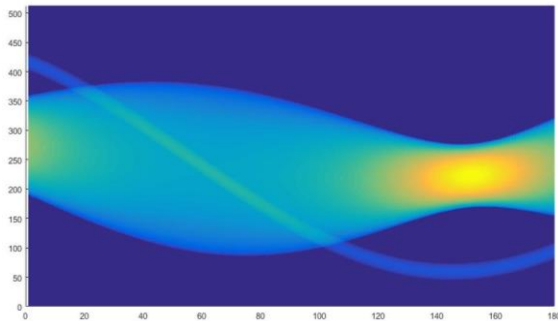


Figure 3: CT imaging map

From Figure 3, it can be clearly seen that the absorbance of objects at different angles of rotation is different, and the width of lines varies obviously. In this case, it is necessary to have some special positions, i.e. the absorbance at the widest and narrowest time. Therefore, several special angles are selected for analysis. The initial illumination shown in Figure 3 shows that the projection on the detector is the overlapping part of the projection phenomenon. It can be clearly seen that the ellipse and the small circle coincide completely in the process of rotation.

2.2 Distance between 1.2 Detector Units

As shown in Figure 3, of the 180 angle samples obtained by rotating the CT system around the rotating center, the cylinder with a diameter of 8 mm always has absorption intensity information on 29 detectors out of the detectors with $n=512$ equidistant units. Because the projection length of the circle from all angles is 8mm, the distance d between detectors can be obtained:

$$d = \frac{8}{29} = 0.2759mm \quad (1)$$

The total length of 512 detectors is 1.

$$l = d \times n = 0.2759 \times 512 = 141.2608mm \quad (2)$$

2.3 Position of CT System Rotation Center in Square Pallet

In the process of rotating the CT system around the revolving center, the position of the revolving center

is unchanged, and the detector revolves around it. The relative motion between the CT system and the module can be regarded as the CT system remains stationary and the module on the tray revolves around the revolving center.

Taking the center of a cylinder as the object of study, rotating around the center of rotation of a cylinder can be regarded as a point with the center of rotation, and the center of a cylinder moves around the center of rotation as a circle, as shown in the following Figure 4:

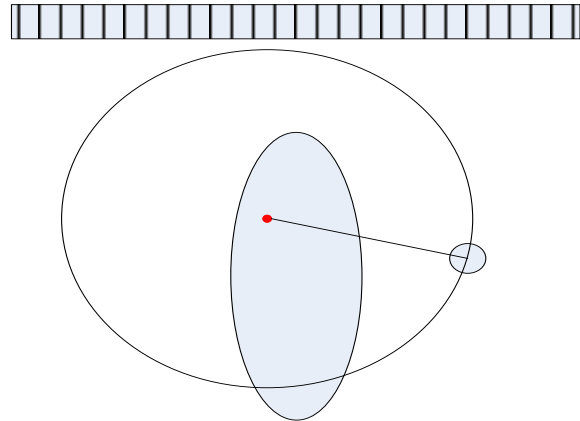


Figure 4: relative motion diagram

Figure 4 establishes O-x y two-dimensional rectangular coordinate system, extracts the angle and the corresponding location of the detector receiving the absorption information of the center of the circle [1], and fits it as Figure 5. Let the triangular function relationship between the angle sample X and the location y of the detector receiving the absorption information of the center of the circle be as follows:

$$y = A \sin(\omega x + \varphi) + y_0 \quad (3)$$

Figure 4 shows that the Y coordinates of the center of a circle always fluctuate around y_0 . The value of y_0 is the value of the center of rotation on the coordinates.

Through the fitting process of cftool tool in matlab, the relation expression of trigonometric function is obtained as follows, as shown in Figure 5.

$$y = 259.4 + 158.6 \cos(0.01706x) - 120 \sin(0.01706x) \quad (4)$$

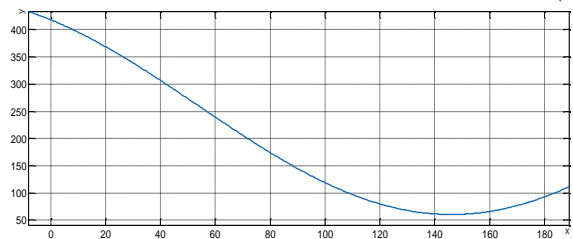


Figure 5: Fitting diagram of small circle rotation

The fitting equation is transformed into an objective function relationship and the results are obtained.

$$y = -198.8818 \sin(0.0171 \cdot x - 0.9231) + 259.4 \quad (5)$$

The result shows that y fluctuates around $y = 259.4$.

In the 62nd rotating sample, the number of templates receiving more than 0 was the largest, and the maximum point of receiving information was located at the midpoint [3, 6]. In this case, the ray is perpendicular to the long axis of the ellipse and passes through the connection of the geometric center of the cylindrical ellipse. The exact location is shown in Figure 6.

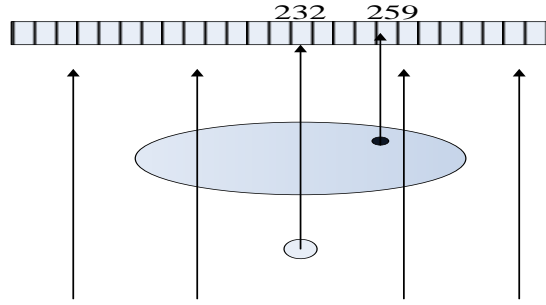


Figure 6: 62 situation map

At this point, $y = 232.8017$ is calculated and the relative vertical distance d_1 between the center of the circle and the center of rotation in the tray is obtained.

$$d_1 = (y_0 - 232.8017) * 0.2759 = 7.628 \text{ mm}$$

As shown in Figure 7,

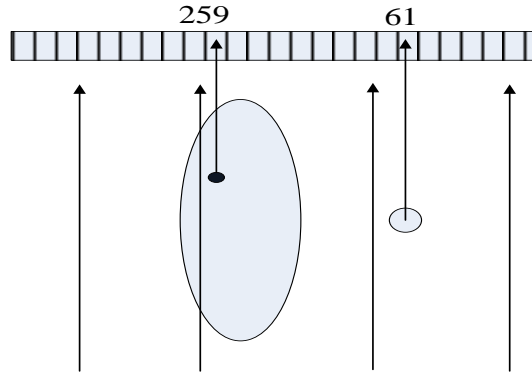


Figure 7: 152 situation map

In the 152 samples, the projection length on the detector is the shortest when light passes vertically through two cylindrical ellipses.

At this time, the horizontal distance d_2 between the center of circle and the center of rotation can be

obtained when $y = 61.5970$ is calculated.

$$d_2 = (y_0 - 61.5970) * 0.2759 = 197.9030 * 0.2759 = 54.6014 \text{ mm} \quad (6)$$

The 0-xy two-dimensional rectangular coordinate system is established with the ellipse midpoint as the origin of coordinate. The coordinates of the center of the circle are (0,45). The coordinates of the center of rotation (-9.6014,7.6281) can be obtained by calculating the relative horizontal numerical distance between the center of the circle and the center of rotation. As shown in Figure 8.

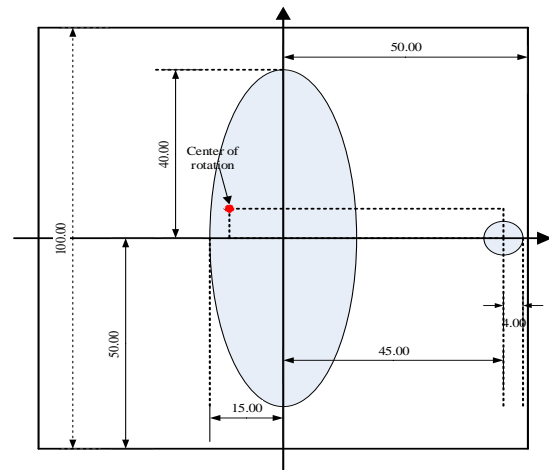


Figure 8: Template Diagram (Unit: mm)

2.4 The 180 directions of X-rays used in CT systems

Let the phase difference between each angle sample and 152 samples be β_i ($i = 1, 2, \dots, 151, 153, 154, \dots, 179, 180$). In 152 samples, the direction of light source coincides with the direction of ellipse long axis, i.e. $\beta_{152} = 0$ degree. The whole transmitting-receiving system rotates counter-clockwise around a fixed rotating center. In the 1-151 sample, the transmitter-receiver system rotates the corresponding degree β_i clockwise it deflects to the left in the direction of the long axis of the ellipse. In 153-180 samples, the transmitter-receiver system rotates the corresponding degree β_i counterclockwise, i.e. it deflects β_i to the right in the direction of the long axis of the ellipse. The formula of β_i is

$$\beta_i = \beta_{152} - \frac{(0.0171 \times i - 0.9231) \times 360}{\pi} \quad (7)$$

Figure 9 and Figure 10 show the beginning and end of the rotation process.

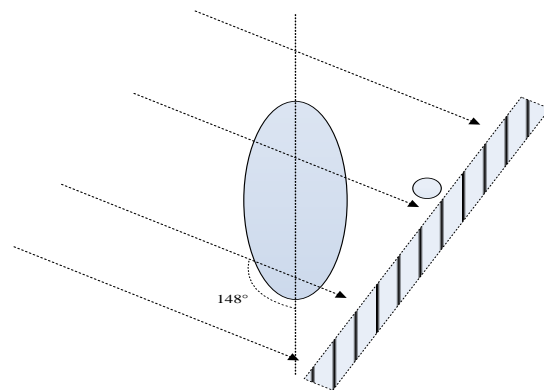


Figure 9: Initial illumination

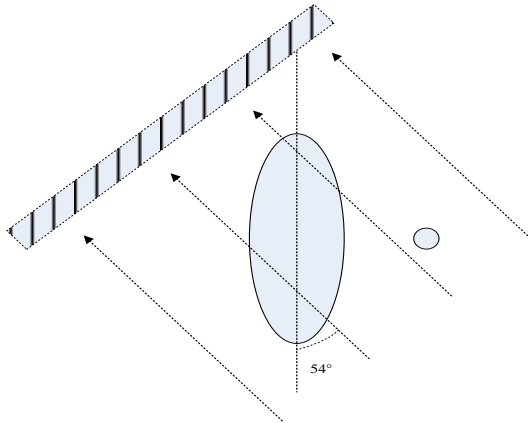


Figure 10: Final State Diagram

Among the 180 locations, 62 and 152 locations are the special locations, and the regularity of their changes is also changing around them. The angle decreases gradually from 1 to 62 and the change rate slows down gradually; the angle still decreases in the process of 62 to 152, but the change rate increases gradually until the 152 angle decreases to 0; the angle increases gradually in the final position change process from 152 to 180, and the angle changes to 27.3691 degrees at 180 position.

3. CONCLUSION

In this paper, a parameter solving model of CT system based on trigonometric function is presented, which is

easier to understand and open new ideas. By capturing the CT image information, the solution model is established to determine the position of the rotation center of the CT system in the template in the square tray, the distance between detector units and 180 directions of the X-ray used by the CT system. The model established by the trigonometric function relation reflects the regular small circle rotation reasonably according to the change parameter information found by the change law, which makes theoretical preparation for solving the rotation center.

REFERENCES

- [1]Liu Mingjin. Research on positioning method of rotating center of industrial CT system[J]. Chongqing University, 2014.
- [2]Gong Xiangbo. High-precision Radon transform and its application[J]. Jilin University, 2008.
- [3]Zhang Chaozhong. Technology and Principle of Industrial CT[J]. Science Press, 2009.
- [4]Gong Xiangbo. High-precision Radon transform and its application[J]. Jilin University, 2008.
- [5]Xu Xiuying. A depth image surface fitting method based on trigonometric function[J]. Chinese Society of Image Graphics: 2005:4.
- [6]Liu Xiao. Computer simulation of image reconstruction algorithm for industrial CT[J]. Sichuan: Sichuan University, 2004.

Recognition of Color and Matter Concentration based on Regression Analysis

Ruishan Li, Hanying Li, Yu Bi, Weixuan Wang*

Mathematical Modeling Innovation Lab, North China University of Science and Technology, Tangshan 063210, China

*E-mail: 15530350778@163.com

Abstract: Different people have different sensitivity to color and there are observation errors. Therefore, the accuracy of colorimetry is not high when detecting the concentration of substances. In order to improve the accuracy of concentration identification, it is necessary to establish a quantitative relationship between color readings and concentration of substances. Firstly, the duplicate and unreasonable data in the experimental data set 2 were eliminated. The color readings of different concentrations of sulfur dioxide were analyzed by single factor and multiple variance analysis using Matlab, and the results showed that the concentration had a significant impact on the color readings. Secondly, the linear and non-linear multiple regression equations are established to fit the original data. It is found that the goodness of fit of the non-linear regression equation is closer to 1 than that of the linear regression equation. The multi-linear regression equation is selected to fit the relationship between the concentration of sulfur dioxide and the color reading. The reasons for the errors between the non-linear regression equation and the actual values are as follows: first, the order of the trend curve formed directly by the color readings and the concentration scatter plots is used in the establishment of the non-linear regression equation; second, there may be errors in eliminating the outliers in data 2.

Keywords: Relevance analysis; Data evaluation index; Multivariate non-linear regression analysis

1. DATA SET INTRODUCTION AND EXPERIMENTAL DATA SET PROCESSING

Each color image is composed of three gray-scale images of different colors, one is red, one is green, and the other is blue. Various colors can be obtained by changing the three colors of red (R), green (G), blue (B) and overlapping them. This standard covers almost all the colors that human vision can perceive. It is one of the most widely used color systems at present [1].

(1) Introduction to data sets

Colorimetric method is a commonly used method to detect the concentration of substances at present, but because everyone has different color sensitivity and observation errors, colorimetric method has a great impact on the accuracy. With the advancement of science and technology, photography technology and color resolution are constantly improving. It is hoped that the quantitative relationship between color reading

and substance concentration can be established [2-5]. The concentration of substance to be measured can be obtained only by inputting the color reading in the photograph. According to the experimental data of color readings and substance concentration, the color readings of histamine, potassium bromate, industrial alkali and potassium aluminum sulfate at different concentrations are given in Data Set 1. Data set 2 is the color readings of sulfur dioxide at different concentrations in the experiment. When the concentration of sulfur dioxide is different, there are many sets of color readings.

(2) Experimental data set processing

Saturation is the brightness of color, also known as the purity of color. The saturation of a certain color depends on the proportion of the colored component and the achromatic component (gray). The larger the color component, the greater the saturation; the larger the achromatic component, the smaller the saturation. Tone refers to the relative brightness of an image, which is expressed as color [1] in a color image.

Therefore, the saturation S and hue H are determined by red (R) green (G) blue (B). In data set 2, some data are duplicated and some data are different in S and H when RGB is the same, which does not accord with the actual situation, so these data are eliminated.

2. RELEVANCE AMONG VARIABLES

The indexes that need to be inspected in the experiment are called test indexes, and the conditions that affect the test indexes are called factors, and the state of the factors is called level. The variance analysis is to analyze the test data to test whether the mean values of multiple normal populations with equal variances are equal, to judge whether the factors have significant effects on the test indicators.

In Data2.xls, the five color readings R, G, B, H and S are considered as factors B1, B2,..., B5, and the sulfur dioxide concentration (ppm) affecting the color readings is regarded as experimental index A.

Using the data of five color readings with different SO₂ concentration, the single factor multivariate analysis of variance was carried out by MATLAB. Returns the results as shown in Table 1:

The results returned are the same as those obtained by calling anova1 function. The P values of the color readings R, G, B, H, S and their interactions are all less than the given significant level of 0.05. Therefore, it can be considered that the color readings R, G, B, H, S

have significant effects on the concentration.

Table 1. Matlab Return result

p1	p2	p3	p4	p5
9.55E-36	1.00E-32	8.57E-33	1.02E-30	6.37E-26

3. ESTABLISHMENT OF REGRESSION MODEL

Multivariate regression analysis can be used to establish mathematical models of color readings and concentration of substances [3].

Multivariate regression analysis refers to the statistical analysis method which regards one variable as dependent variable and one or more other variables as independent variable, establishes the quantitative relationship of linear or non-linear mathematical models among multiple variables and uses sample data for analysis.

Regarding the concentration of substance as dependent variable (explained variable) and the color reading (R, G, B, S, H) as independent variable, the linear and non-linear multiple regression equations are established respectively, and the fitting analysis is carried out with the original data curve, to find a model closer to the original data curve.

(1) Establishment of multivariate linear regression equation

When establishing the multivariate linear regression equation, the sulfur dioxide concentration is recorded as dependent variable and the five color readings (R, G, B, S, H) as independent variables respectively x_1, x_2, x_3, x_4, x_5 . The following models can be established:

$$\begin{cases} y = \beta_0 + \beta_1 x_1 + \dots + \beta_5 x_5 + \varepsilon \\ \varepsilon \sim N(0, \sigma^2) \end{cases} \quad (1)$$

Among them, $\beta_0, \beta_1, \dots, \beta_5, \sigma^2$ and x_1, x_2, x_3, x_4, x_5 are regression coefficients independent of themselves.

Now, using the experimental 7 sets of data $y_i, x_{i1}, \dots, x_{i5}$ in Data Set 2, $i=1,2,\dots,7$ can get them from Formula (1).

$$\begin{cases} y_i = \beta_0 + \beta_1 x_{i1} + \dots + \beta_5 x_{i5} + \varepsilon_i \\ \varepsilon_i \sim N(0, \sigma^2), i=1,2,\dots,7 \end{cases}$$

The least squares method is used to estimate the regression parameter $\beta_0, \beta_1, \dots, \beta_5$ in equation (1), i.

e. to select the estimated value $\hat{\beta}_j$, so that when $\beta_j = \hat{\beta}_j (j=0,1,2,\dots,5)$, the sum of squares of errors

$$Q = \sum_{i=1}^7 \varepsilon_i^2 = \sum_{i=1}^7 (y_i - \beta_0 - \beta_1 x_{i1} - \dots - \beta_5 x_{i5})^2$$

is:

error is minimal.

Multivariate Linear Regression Analysis of Data in Data Set 2 with MATLAB

$$y = 2811.6 - 1.7x_1 - 20.3x_2 + 7.3x_3 - 3.9x_4 - 11.2x_5 \quad (2)$$

R2 is 0.8873, F is 25.1835 and P is 0.0000. The closer

R2 is to 1, the more accurate the regression model is. $P < 0.5$ also represents equation (2). figure 1 of the available residuals diagram for analysis of residuals.

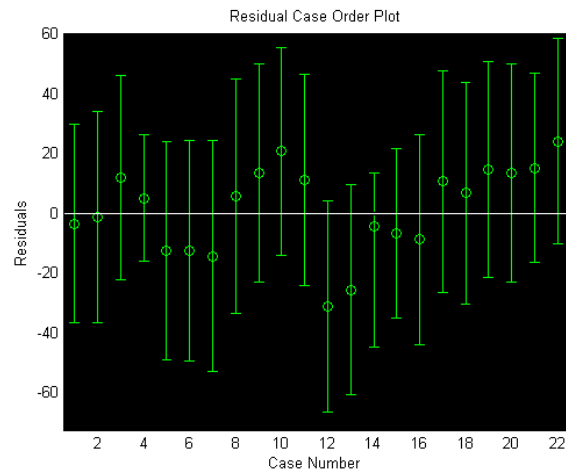


Figure 1. Residual graph

Figure 1 shows that all the residuals are within the confidence interval, which indicates that the reliability of the data is high.

Fitting the original data with the regression data, figure 2 can be obtained, and the actual fitting error of the linear regression equation can be seen intuitively.

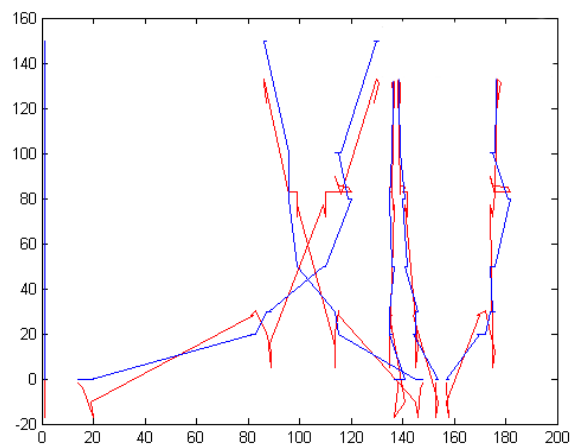


Figure 2. Multivariate Linear Fitting Value and Actual Value

(2) Establishment of multivariate nonlinear regression equation

Sulfur dioxide concentration is recorded as dependent variable and five color readings (R, G, B, S, H) as independent variables respectively. The following models can be established:

$$y' = \beta_0 + \beta_1' x_1 + \dots + \beta_5' x_5 + \beta_1'' x_1^2 + \dots + \beta_5'' x_5^2 + \varepsilon \quad (3)$$

Among them, $\beta_0, \beta_1', \dots, \beta_5', \beta_1'', \dots, \beta_5''$ is a regression coefficient independent of x_1, x_2, x_3, x_4, x_5 itself.

$$y' = 325.8 - 0.14x_1 - 0.25x_2 + 1.1x_3 - 8.57x_4 + 0.07x_5 + 0.005x_1^2 + 0.001x_2^2 - 0.001x_3^2 - 0.03x_4^2 + 0.005x_5^2 \quad (4)$$

Multivariate non-linear regression analysis using data

from data set 2 in MATLAB shows that the square of R is 0.9849, F is 103.1586 and P is 0.0000. The closer the square of R is to 1, the more accurate the regression model is, and $P < 0.5$ also represents equation (4). figure 3 can be obtained by fitting the original data with the regression data.

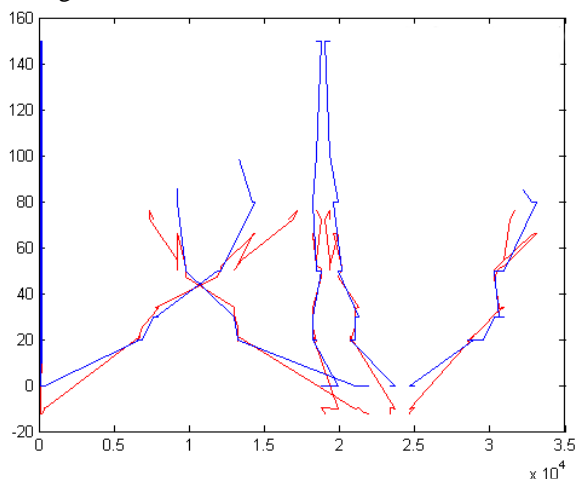


Figure 3 Multivariate Nonlinear Fitting Value and Actual Value

The R^2 of multivariate non-linear fitting is closer to 1 than that of linear fitting. It shows that the results of multivariate non-linear fitting are closer to the relationship between color readings and SO_2 concentration in data set 2.

4. ERROR ANALYSIS OF MULTIVARIATE NONLINEAR FITTING MODEL

According to the multivariate non-linear fitting value and the actual value map obtained by fitting the original data and the regression data, it can be seen intuitively that there are also errors between the multivariate non-linear regression equation established in this paper and the actual value.

The first reason for the error is that when the multivariate nonlinear primitive equation is established, the order of the trend curve formed by the five color readings and the concentration scatter plot is directly

used. Secondly, there may be errors in deleting abnormal data in data set 2, which leads to some errors in the regression coefficients.

The model determines the evaluation index of the data suitable for this experiment, and can evaluate the experimental data better. The correlation between substance concentration and color readings is analyzed from the total to the score, which is more comprehensive and enough. The accuracy of linear and non-linear regression models was compared when establishing the relationship model between concentration and color readings for data set 2. There are subjective factors in data processing in the process of problem two modeling.

REFERENCES

- [1] Birre Nyström, Peter Söderholm. Selection of maintenance actions using the analytic hierarchy process (AHP): decision-making in railway infrastructure. *Structure and Infrastructure Engineering*, 2010, 6(4).
- [2] Beijing Jiaotong Development Annual Report, 2018.
- [3] Ren Yinghui, Huang Xiangming, Ma Zhongkai, Zhou Zhixiong. Method of material distribution time node prediction based on information entropy [J/OL]. *China Mechanical Engineering*, 2018(22):1-7[2018-12-02]. <http://kns.cnki.net/kcms/detail/42.1294.TH.20181126.1430.018.html>.
- [4] LIU Ju-tao, GAO Jun-feng, JIANG Jia-hu. Comparison of different fuzzy evaluation methods in water environmental quality assessment. *Environmental Pollution & Control*, 2010, 32(01):20-25.
- [5] Wu Xia, Wei Jiuchuan, Song Guizhen, Zhi Hongfeng, Zhang Yanfei, Li Xiaopeng, Zhang Xianfeng. Evaluation of water inrush risk based on EWM and PCA. *Coal Technology*, 2018, 37(02):162-164.

Design of Special Service for High Temperature Operation based on Partial Differential Equation

Dongxue Xie, Yongjie Chen, Yifan cui, Weixuan Wang *

Mathematical Modeling Innovation Lab, North China University of Science and Technology, Tangshan 063210, China

*E-mail: xuedongxie@163.com

Abstract: Working in high temperature environment will do harm to human body. Therefore, the design of special clothing for high temperature operation is of great significance. The special clothing is usually composed of three layers of fabric materials. By establishing a mathematical model of unsteady state heat conduction, considering the actual situation of the knitted fabrics of each layer, the temperature indexing between the fabrics of each layer is obtained.

Keywords: Heat protective clothing; Unsteady state heat conduction; Differential equation

1. INTRODUCTION

High temperature protective clothing is a specific clothing, made of different fabric materials, mainly divided into three layers. The gap between the third layer and the skin is called the fourth layer of air [1-3]. On the premise of the first question, the temperature of the external environment is 75 C, the thickness of layer I is 0.6mm, the thickness of layer II is 6mm, the thickness of layer III is 3.6mm, and the thickness of layer IV is 5mm. To facilitate the study of the heat conduction process of clothing, a simple schematic diagram of clothing is drawn as shown in figure 1.

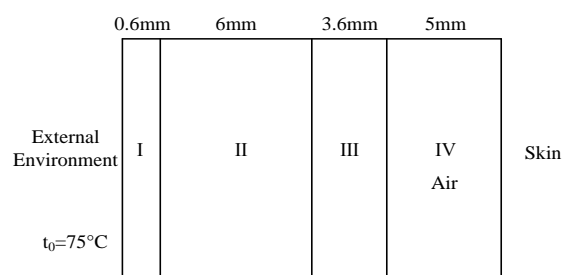


Figure 1 Simple structure diagram of high-temperature working clothes

It can be seen from figure 1 that the temperature from the external environment to the skin needs to pass through the heat conduction of the three-layer fabric [1-4], and the temperature difference must exist in order to generate the heat conduction. The design of high-temperature working clothes is to transfer the temperature of the external environment to the human skin at a lower temperature through heat conduction [3-6]. Due to the different materials of each layer of high-temperature working clothing, and the temperature of each layer of clothing will change with

time, the heat conduction between each layer of clothing is unsteady heat conduction. The solution of non-thermal thermal conductivity problem can be divided into one-dimensional solution and multi-bit solution.

The solution idea of one-dimensional unsteady state heat conduction problem is shown in figure 2.

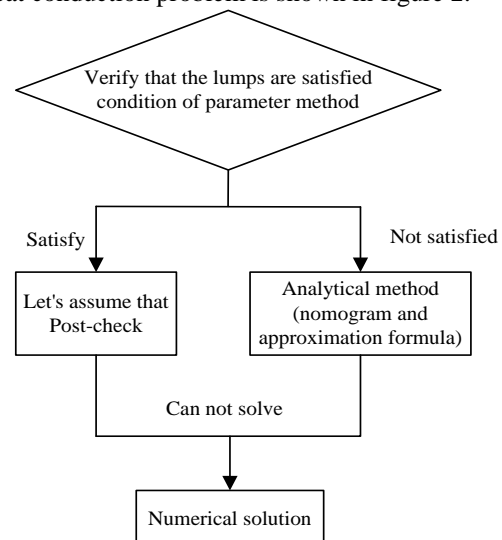


Figure 2 Flow chart for solving one-dimensional unsteady state heat conduction problem

Solution method of multidimensional unsteady state heat conduction problem:

whether the product satisfies the conditions for solution;

A multidimensional problem is reasonably analyzed into several one-dimensional problems.

According to the different layers, the temperature distribution of each layer of fabric is solved by different methods of unsteady heat conduction.

2. MODEL

(1) Temperature distribution between layers i and ii

The external environment is known data, and the temperature is solved successively from the outside to the inside. Draw the fabric material of the ith layer of clothing as shown in figure 3.

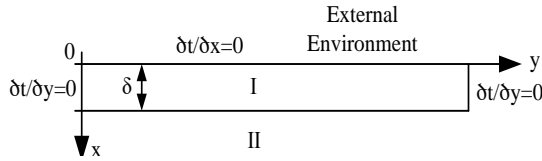


Figure 3 One-dimensional unsteady heat conduction model with constant temperature boundary

The thickness of layer I clothing material is δ , the upper surface is in contact with the external environment with δ temperature of 75°C , the lower surface is the temperature of layer t_1 , the second layer fabric material, the heat conductivity from layer I to layer II is λ_1 , the density is ρ_1 , the specific heat capacity is c_1 , and the initial temperature t_0 is the external environment temperature. The thermal differential equation in the unsteady heat conduction process from layer I to layer II is as follows:

$$\frac{\partial t}{\partial \tau} = \frac{\lambda \partial^2 t}{\rho c_p \partial x^2} \quad (1)$$

$$\begin{cases} \tau = 0, t = t_0 \\ x = 0, \frac{\partial t}{\partial x} = 0 \\ x = \delta, t = t_1 \end{cases} \quad (2)$$

The analytical formula of formula (1) is as follows:

$$\frac{\theta(x, \tau)}{\theta_0} = \frac{4}{\pi} \sum_{n=1}^{\infty} \frac{1}{n} \sin\left(\frac{n\pi}{2}\right) \cos\left(\frac{n\pi}{2\delta} x\right) \exp\left[-\left(\frac{n\pi}{2\delta}\right)^2 a \tau\right] \quad (3)$$

In formula (3): $\theta(x, \tau)$ is the excess temperature, $\theta = t - t_1$; Diffusion $a = \lambda / (\rho c_p)$.

The constant temperature boundary condition is equivalent to the boundary condition of thermal convection when Biot number $Bi \rightarrow \infty$, so formula (3) can be rewritten as:

$$\frac{\theta(x, \tau)}{\theta_0} = \sum_{n=1}^{\infty} \frac{2 \sin \beta_n}{\beta_n + \sin \beta_n \cos \beta_n} \cdot \cos\left(\beta_n \frac{x}{\delta}\right) e^{-\beta_n^2 \lambda \tau / (\rho c_p \delta^2)} \quad (4)$$

The heat conductivity $\lambda_1 = 0.082 (\text{W} / (\text{m} \cdot ^\circ\text{C}))$, density $\rho_1 = 300 (\text{kg} / \text{m}^3)$, specific heat capacity $c_1 = 1377 (\text{J} / (\text{kg} \cdot ^\circ\text{C}))$ and initial temperature $t_0 = 75^\circ\text{C}$ of the clothing fabric of layer I can be obtained. By substituting these known data into equation (4), the distribution of temperature changes over time between layer I clothing and layer II clothing can be obtained (as shown in Figure 4).

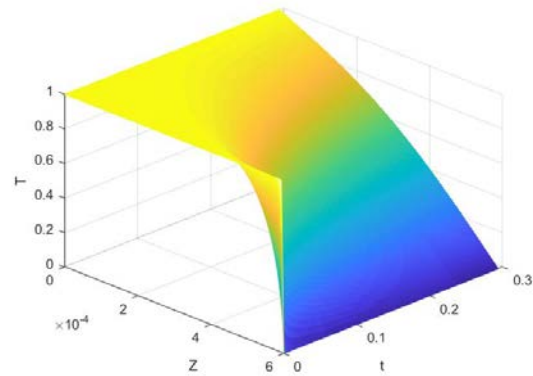


Figure 4. Temperature distribution between layers I and II

As can be seen from Figure 4, through the heat conduction of high-temperature working clothes, the temperature between the fabrics of layers I and II is lower than that of the external environment. However, with the increase of time, the temperature between layers I and II gradually increases, and then tends to be stable.

(2) ii, iii, IV temperature distribution between the layer of clothing

When heat is transferred from the external environment to clothing, it includes thermal convection and thermal radiation. Since the outermost layer of clothing blocks most of the radiation, thermal radiation can be ignored in the process of heat conduction [2]. The temperature distribution between layers of fabrics is continuously changing. The heat transfer model between layers II and III is given as follows:

$$C_2 \frac{\partial t}{\partial T} = \frac{\partial}{\partial x} (\lambda_2 \frac{\partial t}{\partial x}), (x, T) \in \Omega_2 \times (0, T_{\text{exp}}) \quad (5)$$

$$C_3 \frac{\partial t}{\partial T} = \frac{\partial}{\partial x} (\lambda_3 \frac{\partial t}{\partial x}), (x, T) \in \Omega_3 \times (0, T_{\text{exp}}) \quad (6)$$

$$C_2 = \rho_2 c_{p2} \quad (7)$$

$$C_3 = \rho_3 c_{p3} \quad (8)$$

C_2, C_3 is the sensible heat capacity of layer II and layer III fabric, c_2, c_3 is the specific heat capacity of layer II and layer III fabric, is the heat conductivity of layer II and layer III fabric, d_2, d_3 is the thickness of layer II and layer III fabric, t is the temperature, T is the time, and x is the horizontal coordinate.

Initial conditions for fabric layers:

$$t(x, 0) = t_2(x), x \in (0, d_2) \quad (9)$$

The contact surfaces of layer II and layer III fabrics meet the following requirements:

$$t_2 \Big|_{x=d_2+d_3} = t_3 \Big|_{x=d_2+d_3} \quad (10)$$

$$-\lambda_2 \frac{\partial t}{\partial x} \Big|_{x=d_2+d_3} = -\lambda_3 \frac{\partial t}{\partial x} \Big|_{x=d_2+d_3} \quad (11)$$

Find the data to be used:

$$\lambda_2 = 0.37(W/(m \cdot ^\circ C)), \lambda_3 = 0.045(W/(m \cdot ^\circ C)),$$

$$c_2 = 2100(J/(kg \cdot ^\circ C)), c_3 = 1726(J/(kg \cdot ^\circ C))$$

And the known data given in the problem can be substituted into the above formula to obtain the change of temperature between layer II and layer III fabric over time (see Fig .5). And by the same logic, plugging in $\lambda_4 = 0.028(W/(m \cdot ^\circ C))$, $c_4 = 1005(J/(kg \cdot ^\circ C))$. the distribution of temperature changes over time between layer I clothing and layer II clothing can be obtained (as shown in figure 5 and figure 6).

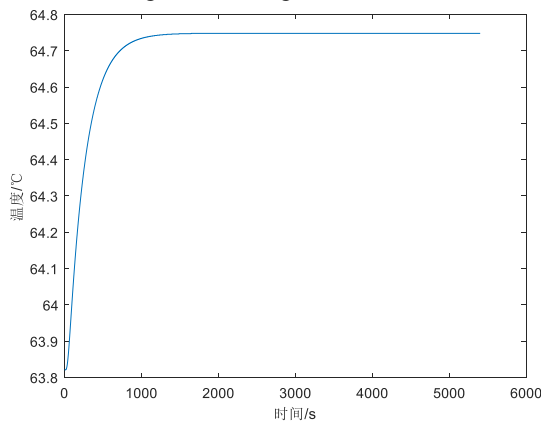


Figure 5 Temperature distribution between layers II and III

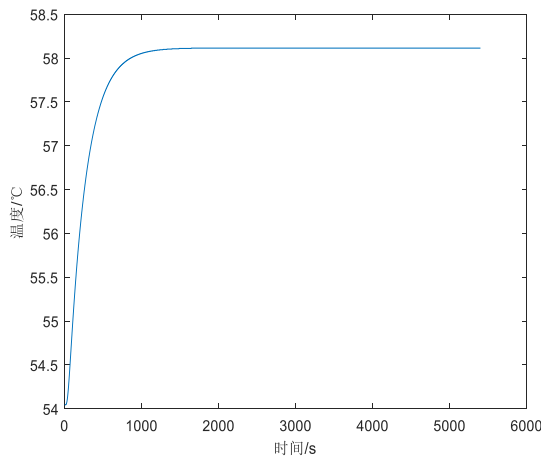


Figure 6 III, IV layer temperature distribution between the fabric

As can be seen from figure 5, through the heat conduction of high-temperature working clothes, the temperature between layers II and III of fabrics is lower than that between layers I and II. With the increase of time, the temperature between the second and third layers of fabrics gradually increased, and remained at $64.75^\circ C$ for about 15 minutes. figure 6 illustrates the III, IV layer between the fabric between the temperature of the temperature gradually increased, in about 15 minutes, stay in $58.11^\circ C$.

(3) Temperature distribution between layer iv fabric and skin

In solving the distribution of temperature with time [3], people are regarded as regular shapes, not considering that the temperature distribution is related to the position of human body, that is, the temperature distribution is independent of space and only related to time. This problem can become a zero-dimensional problem. When calculating the temperature distribution, the internal thermal conductivity and thermal resistance of the fabric layer are ignored, and this problem can be analyzed by the centralized parameter method [4]. For unstable problems analyzed by centralized parameter method, the following formula can be obtained:

$$\rho c V \frac{dt}{d\tau} = -Ah(t - t_\infty) \quad (12)$$

Introduction of excess temperature:

$$\theta = t - t_\infty \quad (13)$$

Differential heat conduction equation:

$$\rho c V \frac{d\theta}{d\tau} = -Ah\theta \quad (14)$$

Initial conditions:

$$\theta_{(0)} = t_0 - t_\infty \quad (15)$$

Integrated to obtain:

$$\frac{\theta}{\theta_0} = \frac{t - t_0}{t_0 - t_\infty} = \exp\left(-\frac{hA}{\rho c V} \tau\right) \quad (16)$$

Define $l_c = \frac{V}{A}$, B_i as the Biot number with l_c as the characteristic length, F_0 as the Fourier number and l_c as the characteristic length, and get:

$$\frac{\theta}{\theta_0} = \frac{t - t_0}{t_0 - t_\infty} = \exp(B_i \cdot F_0) \quad (17)$$

By substituting the known data into the formula, the temperature distribution between layers II and III can be obtained, as shown in Figure 7: heat conductivity $\lambda_4 = 0.028(W/(m \cdot ^\circ C))$, density $\rho_4 = 1.18(kg/m^3)$, specific heat capacity $c_4(J/(kg \cdot ^\circ C))$, and initial temperature $t_0 = 75^\circ C$ of layer III clothing fabric. Substituting these known data into equation (4),

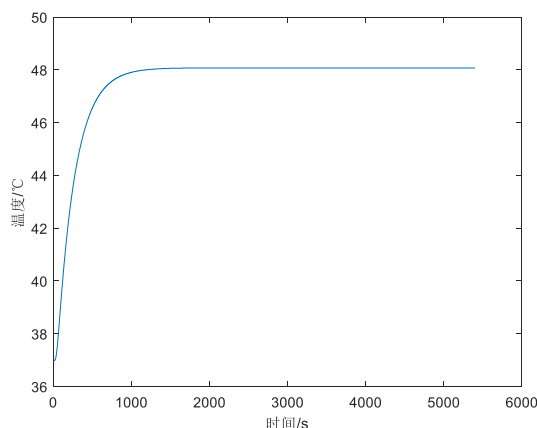


Figure 7 Temperature distribution between layer IV fabric and skin

As can be seen from figure 7, with the increase of time, the temperature between the second and third layers of fabrics gradually increases, and stays at 48°C for about 15 minutes.

REFERENCES

[1]Shen Yadong,Feng Jianhu,Cheng Xiaotong. Topological Optimization of Heat Conduction

Structure Based on Parameterized Level Set Method. Journal of Mechanical Strength,2018,40(04):863-868.

[2]TORVI DA. Heat transfer in thin fibrous materials under high heat flux conditions [D] .Edmonton: University of Alberta,1997:1-134.

[3]Dong Xuanchang, Qu Yurui, Li Yanfei, Fang Baili, Wang Yiqing, Li Wei, Liu Gang.Construction of the current-temperature distribution heat path model for overhead conductors under convection conditions [J/OL]. New technology for electrical and electrical energy: 1-6[2018- 09-16].

[4]Li Jiangfei, He Xiao, Xu Kangtai, Qi Keping, Li Zhibo, Luo Wei, Zou Zhenchun, Wang Zhenye.The calculation of unsteady heat conduction based on local analytical solution[J].Bulletin of Science and Technology,2017,33(04):15-18.

[5]Wang G Y, Miao D Q, Wu W Z. Uncertain Knowledge Representation and Processig Based on Rough Set[J]. Journal of Chong Qing University of Posts and Tele Communications, 2010, 22(5):541-544.

[6]Ding A Z, Chen D S. Study on Water Resources Carrying Capacity Based on RS-SPA in china. South-to-North Water Transfers and Water Science & Technology, 2010, 8:71-75.

Course Selection Model based on 0-1 Programming

Jiang Liu, Li Dong*, YuanLin Hu, Ling Zhou

School of Science, Dalian Minzu University, Dalian 116600, PR China

*E-mail: dongli@dlmu.edu.cn

Abstract: With the implementation of credit system in universities, the problem of course selection has become an important part in the learning process of college students. In this paper, we take the course selection of the sophomore students of the department of information and computing science as an example. Considering the factors of the number of elective credits, the number of students selecting courses, the learning ability of students and their interest, we built a course selection model described by the 0-1 programming and use the LINGO software to solve the model. The optimal solution of this model can provide the reference for reasonable course selection. **Keywords:** course selection model, 0-1 programming, the LINGO software.

1. INTRODUCTION

In recent years, most colleges and universities have implemented the credit system, which is based on the amount of credits as a student learning unit of measurement in order to achieve the minimum standards for graduation credits as a student's education system. There are three types of courses in universities[1]: compulsory courses, restricted elective courses and optional courses. There is no mandatory requirement for the optional courses. Students can select the optional courses by themselves according to their actual situation and school regulations about credits. But, how can students select the courses not only to meet the requirements of the school, but also to meet their interests and learning ability in various optional courses? This paper discusses a selection model described by 0-1 programming, which uses computer software LINGO to program, gives the optimal solution of the problem and provides a reference for reasonable courses selection.

2. QUESTIONS RAISED

The sophomore students of the department of information and computing science will study optional courses. There are four optional courses available, including technical foundation of database, operational research, financial mathematics and statistical software 2. The related requirements are as follows: according to the school regulation, each optional course needs to be selected by at least 15 students; each student is required to choose neither one nor all, that is, they ought to choose at least one course but no more than three courses; each student is required to meet the credit requirements for this

semester, that is, according to the credits which have been completed and the total credits to be completed, each student can plan the most credits and the least credits which should be completed this semester. Students select a course not only need strong interest but also need certain learning ability. How to make a student to choose a course which he is willing to learn as well as what he has the ability to learn under the condition of meeting the relevant requirements of the school?

3. SYMBOL DESCRIPTION

Table.1 Symbol description

b_{ij}	the coefficient of willingness and ability
$ability_{ij}$	the coefficient of learning ability
max_i	the maximum number of credits
min_i	the minimum number of credits
$willingness_{ij}$	the coefficient of learning willingness
S_j	the number of students in optional courses
T_i	the maximum number of optional courses

4. COURSE SELECTION MODEL

In this paper, the information of 27 students majoring in information and computational science is used to calculate the coefficient of willingness and ability, which is determined by the coefficient of learning ability and the coefficient of learning willingness. The coefficient of learning ability is determined by the results of previously learned courses which are closely related to optional courses. Through the educational administration system, we have got curriculum scores obtained by 27 students last semester, which are closely related to the four optional courses, i.e. Course I, Course II, Course III and Course IV. Using a score of 1, such as 90 points of a student, his learning ability coefficient is defined as 0.9. These students were investigated by questionnaire to find out their interest in the optional courses to be chosen. The students' willingness coefficient was determined by the degree of interest of the students, measured by the variables between 0 and 1. That is to say, if the student wants to choose the course, his willingness coefficient of the course is 1, and if not, his willingness coefficient of the course

is 0. Using the following formula (1), we calculate each students' coefficient of the willingness and ability of optional courses. The weight parameter λ of formula (1) is different according to the different courses, for example, the value λ of course that requires strong learning ability is greater than 0.5. In this paper, the weight parameter λ of Course I and

Table. 2 The coefficient of willingness and ability

Courses Students	Course I	Course II	Course III	Course IV
Student 1	0.5(0.91+1)	0.8(0.84)+0.2(1)	0.6(0.90)+0.4(1)	0.5(0.77+0)
Student 2	0.5(0.91+1)	0.8(0.77)+0.2(0)	0.6(0.78)+0.4(0)	0.5(0.79+1)
Student 3	0.5(0.87+1)	0.8(0.65)+0.2(0)	0.6(0.63)+0.4(1)	0.5(0.86+0)
Student 4	0.5(0.92+0)	0.8(0.87)+0.2(0)	0.6(0.89)+0.4(1)	0.5(0.84+1)
Student 5	0.5(0.76+0)	0.8(0.85)+0.2(1)	0.6(0.73)+0.4(0)	0.5(0.74+1)
Student 6	0.5(0.83+0)	0.8(0.74)+0.2(1)	0.6(0.77)+0.4(0)	0.5(0.75+0)
Student 7	0.5(0.84+1)	0.8(0.72)+0.2(0)	0.6(0.79)+0.4(0)	0.5(0.78+0)
Student 8	0.5(0.86+0)	0.8(0.76)+0.2(1)	0.6(0.65)+0.4(0)	0.5(0.83+0)
Student 9	0.5(0.66+0)	0.8(0.55)+0.2(0)	0.6(0.51)+0.4(1)	0.5(0.41+0)
Student 10	0.5(0.67+0)	0.8(0.67)+0.2(0)	0.6(0.66)+0.4(0)	0.5(0.60+1)
Student 11	0.5(0.94+1)	0.8(0.87)+0.2(0)	0.6(0.79)+0.4(0)	0.5(0.88+1)
Student 12	0.5(0.71+1)	0.8(0.68)+0.2(0)	0.6(0.64)+0.4(0)	0.5(0.77+1)
Student 13	0.5(0.78+1)	0.8(0.71)+0.2(0)	0.6(0.68)+0.4(1)	0.5(0.67+0)
Student 14	0.5(0.8+0)	0.8(0.68)+0.2(0)	0.6(0.62)+0.4(1)	0.5(0.6+1)
Student 15	0.5(0.81+0)	0.8(0.89)+0.2(0)	0.6(0.84)+0.4(1)	0.5(0.75+1)
Student 16	0.5(0.9+0)	0.8(0.9)+0.2(0)	0.6(0.9)+0.4(1)	0.5(0.9+1)
Student 17	0.5(0.9+0)	0.8(0.8)+0.2(0)	0.6(0.8)+0.4(1)	0.5(0.8+1)
Student 18	0.5(0.8+0)	0.8(0.7)+0.2(1)	0.6(0.4)+0.4(1)	0.5(0.8+0)
Student 19	0.5(0.9+1)	0.8(0.8)+0.2(0)	0.6(0.7)+0.4(0)	0.5(0.8+0)
Student 20	0.5(0.76+1)	0.8(0.63)+0.2(0)	0.6(0.32)+0.4(0)	0.5(0.64+0)
Student 21	0.5(0.74+1)	0.8(0.62)+0.2(0)	0.6(0.55)+0.4(0)	0.5(0.78+0)
Student 22	0.5(0.73+0)	0.8(0.70)+0.2(1)	0.6(0.64)+0.4(0)	0.5(0.71+0)
Student 23	0.5(0.71+0)	0.8(0.57) +0.2(1)	0.6(0.64)+0.4(0)	0.5(0.61+0)
Student 24	0.5(0.62+0)	0.8(0.66) +0.2(0)	0.6(0.77)+0.4(0)	0.5(0.72+1)
Student 25	0.5(0.85+0)	0.8(0.86) +0.2(0)	0.6(0.82)+0.4(0)	0.5(0.85+1)
Student 26	0.5(0.73+0)	0.8(0.71) +0.2(0)	0.6(0.65)+0.4(0)	0.5(0.76+1)
Student 27	0.5(0.6+0)	0.8v0.76) +0.2(0)	0.6(0.64)+0.4(0)	0.5(0.8+1)

We give the course selection model [2], the specific steps are as follows:

Step 1: Set decision variables

Suppose N optional courses, the number of students in optional course j is $S_j(j=1,...,N)$. Suppose M students, the coefficient of willingness and ability of student i for the course j is $b_{ij}(i=1,...,M)$. The total number of optional courses of student i can not exceed T_i . The credits of student i should be greater than \min_i and less than \max_i .

Use the 0-1 variable[3] x_{ij} to indicate whether the student i choose the course j , that is, $x_{ij}=1$ represents that the student i finally chooses the course j , $x_{ij}=0$

Course IV is 0.5, the weight parameter λ of Course II is 0.8 and the weight parameter λ of Course III is 0.6.

$$b_{ij} = \lambda * ability_{ij} + (1 - \lambda) * willingness_{ij} \quad (1)$$

For the 27 students, the coefficients of willingness and ability of optional courses are shown in Tab. 1.

represents that the student i finally doesn't choose the course j .

Step 2: Give the objective function

The question is that how to provide the course selection scheme for students, that is, our goal is to maximize the sum of the coefficients of willingness and ability of all students. The objective function is as follows

$$\max f = \sum_{i=1}^M \sum_{j=1}^N b_{ij} x_{ij}.$$

Step 3: Describe constraints

The number of students in each course cannot be less than the minimum number of courses required for the

course, that is

$$\sum_{i=1}^M x_{ij} \geq S_j, j = 1, \dots, N.$$

The credits for each student 's optional course cannot be less than the minimum credits required in this semester, that is

$$\sum_{j=1}^N c_j x_{ij} \geq \min_i, i = 1, \dots, M.$$

The credits for each student 's optional course cannot be higher than the maximum credits required in this semester, that is

$$\sum_{j=1}^N c_j x_{ij} \leq \max_i, i = 1, \dots, M.$$

The number of optional courses for each student can not exceed the given value

$$\sum_{j=1}^N x_{ij} \leq T_i, i = 1, \dots, M.$$

In summary, the mathematical model of the course selection can be expressed as

$$\begin{aligned} \max f &= \sum_{i=1}^M \sum_{j=1}^N b_{ij} x_{ij} \\ s.t. &\begin{cases} \sum_{i=1}^M x_{ij} \geq s_j, j = 1, \dots, N, \\ \sum_{j=1}^N c_j x_{ij} \geq \min_i, i = 1, \dots, M, \\ \sum_{j=1}^N c_j x_{ij} \leq \max_i, i = 1, \dots, M, \\ \sum_{j=1}^N x_{ij} \leq T_i, i = 1, \dots, M, \\ x_{ij} = 0 \text{ or } 1. \end{cases} \end{aligned}$$

5. RESULTS AND DISCUSSION

We use our model to deal with the course selection problem of 27 students given in Table 1, bring the data of the willingness and ability coefficient of the above students into the above model, and use LINGO to program the procedure as follows:

model:

title Course Selection Model Based on 0-1 Integer Programming;

sets:

auction:S;

bidder:t;

bidderf:fen;

bidderm:ma;

biddermi:mi;

link(bidder,auction):b,X;

endsets

data:

S=15,15,15,15;

t=@ole('F:\2018\test1.xlsx','tt');

b=@ole('F:\2018\test1.xlsx','bb');

fen=@ole('F:\2018\test1.xlsx','count1');

ma=@ole('F:\2018\test1.xlsx','maxm');

mi=@ole('F:\2018\test1.xlsx','minm');

enddata

max=@sum(link:b*X);

@for(auction(j):

[auc_lim]@sum(bidder(i):X(i,j))>=S(j));

@for(bidder(i):

[bid_lim]@sum(auction(j):fen(j)*X(i,j))<=ma(i));

@for(bidder(i):

[bidmi_lim]@sum(auction(j):fen(j)*X(i,j))>=mi(i));

@for(bidder(i):

[bidk_lim]@sum(auction(j):X(i,j))<=t(i));

@for(link:@bin(X));

end

We obtain a satisfactory result, as shown in the following Tab. 2.

Table. 3 Course selection result of 27 students

Courses Student	Course I	Course II	Course III	Course IV
Student	1	1	1	0
student	1	0	0	1
student	1	0	1	1
student	0	1	1	1
student	1	1	0	1
student	1	0	1	1
student	1	0	1	0
student	0	1	1	1
student	1	0	1	0
student	0	1	1	1
student	1	0	0	1
student	1	0	0	1
student	1	0	1	0
student	0	1	1	1
student	0	1	1	1
student	0	1	1	1
student	0	1	1	1
student	1	1	0	0
student	1	1	0	0
student	1	1	0	0
student	1	1	0	0
student	1	0	0	0
student	0	0	1	1
student	0	1	0	1
student	0	1	0	1
student	0	1	0	1

The result shows that most students take courses with a coefficient of willingness which is greater than 0.5. It proves that the result is effective. However, a few students' willingness to choose courses is inconsistent with the results of the course selection. For example, the student with the number 5 has a very low willingness coefficient for Course I, but he still

chooses this course for credit reasons; the student with the number 23 has a higher willingness coefficient for Course II, but he does not choose this course due to the fact that this course requires strong learning ability. Most students can choose the course they are satisfied with. A small part of students who have a low coefficient of willingness only choose one course, actually, they have the learning ability to study more than one course. So they are recommended to choose that course quite suitable for them. In summary, the course selection scheme given by the optimization model we established is basically reasonable.

6. ACKNOWLEDGMENT

This work was supported by the Dalian Minzu University Innovation and Entrepreneurship Training Program(No. 201812026046), the Fundamental

Research Funds for the Central Universities, the Doctoral Starting up Foundation of Dalian Minzu University(No. 0701110100).

REFERENCES

- [1]S. Wang, The Design and Realization of Course Management System for College Student. Tianjin: Tianjin University, 2017.
- [2]L. Yu, H. Liao, The Optimal Elective Program on the Problem of Course Selection. Journal of Jining University, 2016, 37(03):40-43.
- [3]F. Z. Zhang, C. G. Zhang, The Optimization Model of College Curriculum Based On 0-1 Integer Programming. Chinese Journal of Educational Development Research.,2008,2008(4): 72-74.

Temperature Distribution of High Temperature Clothing Under Unsteady Heat Conduction

Yujie Jiang^{1,2}, Xiaocan Zhong^{1,2}, Qingyang Li^{1,2}, Aimin Yang^{2,*}

¹Engineering Computing and Simulation Innovation Lab, North China University of Science and Technology, Tangshan, 063210, China

²College of Science, North China University of Science and Technology, Tangshan 063210, China

*E-mail: 43698059@qq.com

Abstract: In order to determine the temperature change of the outer side of the dummy skin, the differential control equation of unsteady heat conduction is established firstly. Then, the discretization of the control equation and the region is used to solve the model by using the finite volume method. The physical model of environmental-clothing-human heat conduction in high temperature environment is analyzed by using the model of clothing temperature distribution with unsteady heat conduction. The temperature distributions of IV, III, II and I of clothing materials are obtained. The conclusion can guide people how to dress safely in high temperature environment, and provide theoretical basis for the design, function evaluation and optimization of related protective products.

Keywords: unsteady heat conduction; finite volume method; numerical simulation; temperature distribution

1. INTRODUCTION

Flame-retardant and fireproof clothing is a kind of protective clothing that can prevent the body from being harmed by high temperature under the flame or high temperature operation such as foundry [1], petrochemical industry and fire control industry, its main function is to prevent or slow down the heat transfer to human skin, so it must meet the flame-retardant performance and heat insulation performance [2, 3]. At present, the method of small-scale fabric testing is widely used as the main index and judgment basis for thermal protection performance[4, 5], however, due to the lack of clothing styles, the comprehensive consideration of factors such as structure, auxiliary accessories[5], body dressing state, and fabric deformation during combustion, which is limited to the evaluation of fabric performance, is obviously not a substitute for fireproof clothing judgment and evaluation of overall thermal protection performance.

2. THE TEMPERATURE DISTRIBUTION OF UNSTEADY HEAT CONDUCTION

The human body can control the heat conduction process or reduce the heat transfer efficiency by wearing special work clothes in high temperature environment. The temperature distribution in each

layer of material is a typical unsteady heat conduction process at the beginning. The unsteady heat conduction differential form of an object can be expressed as (1):

$$\rho C \frac{\partial T}{\partial t} = \frac{\partial}{\partial x} \left(\lambda \frac{\partial T}{\partial x} \right) \quad (1)$$

The physical meaning of the equation is that the integral of the inflow and outflow heat along the thermal control volume is equal to the sum of heat accumulation within the volume.

Among them, the unsteady heat conduction process can be divided into two stages. The temperature change is first transmitted from the boundary of the material to the inside of the material. This stage of the object is mainly affected by the initial temperature distribution, called the irregular state stage. With the continuation of the heat conduction process, the influence of the initial temperature of the material gradually disappears. The temperature in this stage is mainly affected by the boundary conditions, which is called the normal state stage. After these two stages, the material can reach a new steady state, that is, the required temperature distribution.

When the unsteady heat conduction process goes on to a certain extent, the outermost layer first reaches a steady state, that is, the temperature of the layer is no longer changed with time. In this case, the heat conduction process satisfies the Fourier heat transfer law, which shows that the heat transferred through the cross-section area in unit time is proportional to the local temperature change rate perpendicular to the cross-section direction.

$$\Phi = -\lambda S \frac{\partial T}{\partial x} \quad (2)$$

The middle minus sign indicates that the direction of heat transfer is opposite to the temperature gradient.

3. THE ESTABLISHMENT OF HEAT TRANSFER MODEL FOR HIGH TEMPERATURE SPECIAL CLOTHING

In practical work, the heat transfer from the outside to the inside along the clothing layer by layer in high temperature environment, at this time, the work clothing can be simplified into a uniform mass distribution of the plate for research. The physical model of heat transfer to the human body through special clothing outside the high temperature

environment is shown in Figure 1.

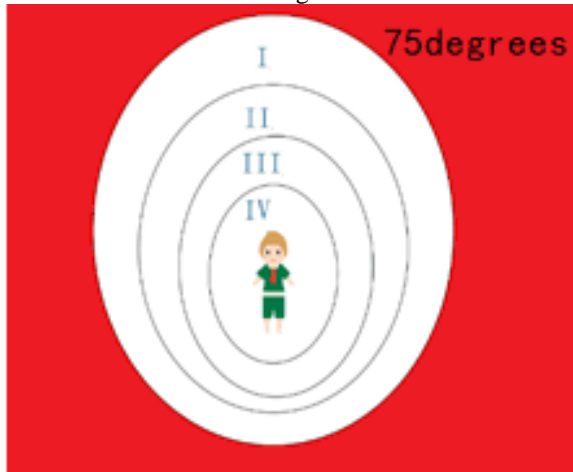


Figure 1. the physical model of environment, clothing and heat conduction

The physical heat transfer process can be simplified to three steps.

- (1) Heat transfer from outside high temperature to the outer surface of special clothing;
- (2) The surface of the special garment is oriented to the heat transfer inside the surface of the special garment.
- (3) The heat transfer from the inner surface of the special garment to the air gap.

Because the high temperature special clothing is made up of three different fabrics, the process (2) can be divided into two parts.

- (I) Heat transfer from layer I to layer II of special clothing.
- (II) Heat transfer from layer II to layer III of special clothing.

It should be added that, clothing generally has radiants, which are treated as mean plates, and heat transfer is carried on layer by layer, i.e. only along the horizontal direction; since the thickness of the static air layer (layer IV) between the inner surface of clothing and the surface of human skin is very small. Therefore, the phenomenon of thermal convection and thermal radiation in the air layer of the inner surface of the special clothing can be neglected.

4. THE DISCRETIZATION OF REGIONS

To discretize the domain is to replace the solution domain with a set of finite discrete points, that is, a node represents a corresponding control volume. External node method and internal node method are the main methods of region discretization. The difference between them is that the order of nodes and interfaces is different. The outer node method first determines the node and then divides the interface, while the inner node method first divides the interface and then determines the node. According to the references, the interior node method can ensure that the nodes always fall in the geometric center of the control volume, so this paper uses the interior node method to discretize the target area. The schematic diagram is as follows, as shown in Figure 2:

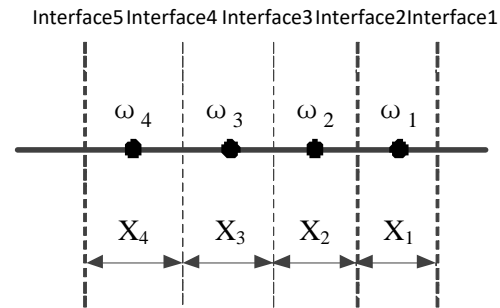


Figure 2. division of each solution area

The dotted line in Figure 2 represents the interface between the layers of garment materials, and the dot represents the node. The adjacent two interfaces can determine one node, and the four nodes represent four different regions respectively. Among them, x_1 , x_2 , x_3 , x_4 are the distances between adjacent two nodes, that is the thickness of each layer material.

5. THE SOLUTION BY FINITE VOLUME METHOD

There is finite difference method, finite element method and finite volume method for solving heat conduction problems. These numerical methods have different advantages and disadvantages in the discretization of their regions, the discretization of equations and the algebraic solution of equations. Finite element method and finite difference method can only study the mathematical characteristics of differential equations. But the derivation process cannot ensure the conservation of difference equations, and the physical concept is not clear enough. The finite volume method is based on the conservation of physical quantities. The greatest advantage of this method is that the integral conservation of physical quantities is satisfied in each control volume, which just accords with the characteristics of solving the whole region. So this paper uses the finite volume method to solve the model, as shown in Figure 3.

The governing equation (1) is integrated into space and time respectively within the selected control volume and time interval, and the integral of time is considered as t to $t + \Delta t$, and the change form is (3):

$$\rho C \int_{x_1}^{x_2} \int_t^{t+\Delta t} \frac{\partial T}{\partial t} dt dx = \int_t^{t+\Delta t} \int_{x_1}^{x_2} \frac{\partial}{\partial x} \left(\lambda \frac{\partial T}{\partial x} \right) dx dt \quad (3)$$

- ② The distribution curves of unknown functions and their derivatives in space are drawn respectively.

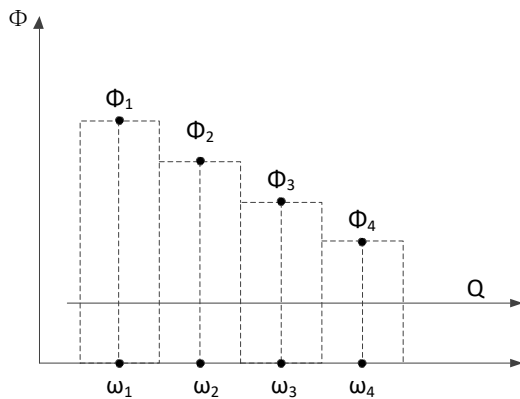


Figure 3. the transitive graph of heat flow between different layers of clothing

To facilitate the derivation of discrete equations, a ladder shaped distribution line is used. After the completion of the discrete equation, the shape line will no longer be meaningful. This is the important point that the finite volume method is different from the finite element method.

③Each term in equation (3) is integrated according to the selected stepped profile, and the algebraic equation of the unknown function at the node is written.

In the unsteady state term $\frac{\rho t}{\rho x}$, the temperature T

changes step by step in space, that is, the value of T at the node can represent the value of the whole control volume (corresponding to the layer of material). The initial T values at the nodes are expressed as $T_{\omega_1}^0, T_{\omega_2}^0, T_{\omega_3}^0, T_{\omega_4}^0$. Respectively, while the values at the T -moment are expressed as $T_{\omega_1}^1, T_{\omega_2}^2, T_{\omega_3}^3, T_{\omega_4}^4$.

$$\rho C \int_{x_1}^{x_2} \int_t^{t+\Delta t} \frac{\partial T}{\partial t} dt dx = \rho C \Delta x (T_{\omega_i}^1 - T_{\omega_i}^0) \quad (1 \leq i \leq 4) \quad (4)$$

Because lumped parameter method can neglect the spatial distribution of temperature, a control equation of total heat in time can be established based on lumped parameter method.

$$Q_t = \int_0^t \phi(t) dt = \rho V C \theta_0 (1 - e^{-\frac{xS}{\rho V C} t}) \quad (5)$$

According to the relationship between heat flux and material thermal conductivity, temperature difference and the heat conduction formulas satisfied at each node after discretization, the following several layered temperature control equation models are obtained: for layer I:

$$Q_t(x) = -\lambda_1 \frac{dT}{dx} \quad (6)$$

In this equation, $\frac{dq}{dx} + Q_t = 0$, and accord with

the initial condition of differential equation $T(x=0) = T_0, Q_t(x=0) = 0$. From this we get the integral expression of temperature function $T_1(x)$ about T_0 :

$$T_1(x) = T_0 + \int_0^{x_1} \rho \Delta T dx = T_0 + Q_t'' \int_0^{x_1} \frac{x_1}{\lambda_1} dx \quad (7)$$

Based on the temperature distribution of layer I, we can introduce layer II:

$$T_2(x) = T_1(x) + Q_t'' \int_0^{x_2} \frac{x_2}{\lambda_2} dx \quad (8)$$

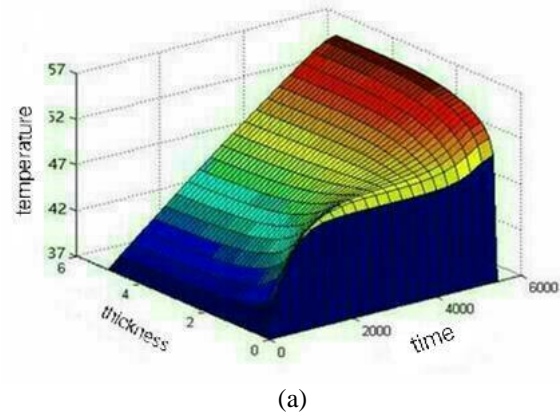
The governing equation for the temperature distribution of layer III is obtained.

$$T_3(x) = T_2(x) + Q_t'' \int_0^{x_3} \frac{x_3}{\lambda_3} dx \quad (9)$$

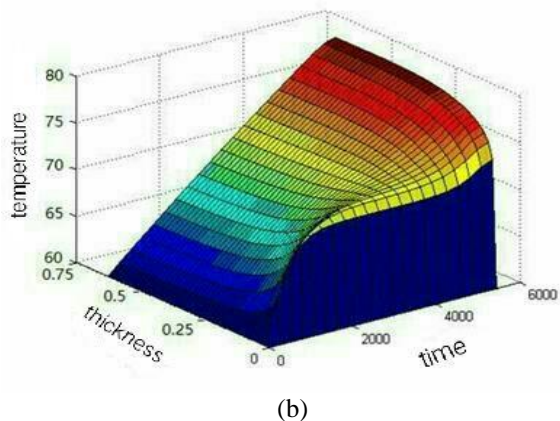
Based on the temperature distribution model of the first three layers, the temperature control equation of the outer surface of the skin, that is, the IV layer is obtained.

$$T_4(x) = T_0 + Q_t'' \sum_{i=1}^4 \int_0^{x_i} \frac{x_i}{\lambda_i} dx \quad (10)$$

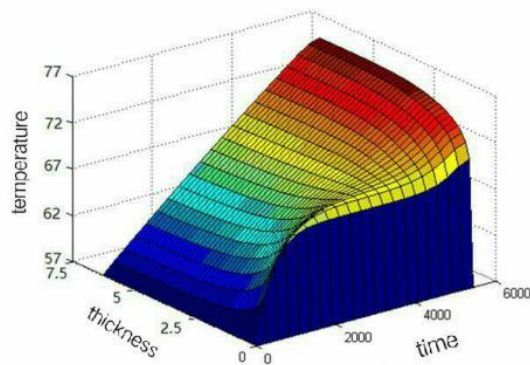
Based on the above formula, the three dimensional temperature distribution of each layer is obtained by using Matlab, as shown in Figure 4.



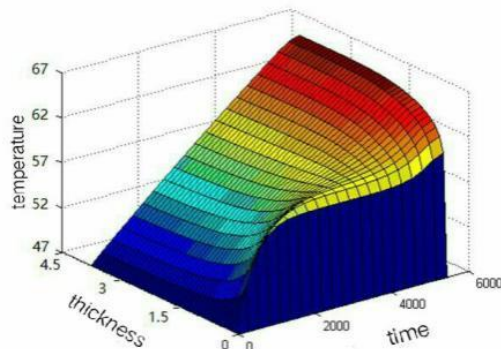
(a)



(b)



(c)



(d)

Figure 4. three dimensional temperature distribution of each layer

Formula (10) is the final skin temperature distribution model required by the subject. According to Annex 1 given by the subject, the corresponding parameters of each layer of special clothing material are arranged as shown in Table 1.

Table 1. material parameter of special clothing

Clothing material	Surface density	Thickness	Specific heat	Thermal conductivity
Layer I	300	0.6	1377	0.082
Layer II	862	0.6-25	2100	0.37
Layer III	74.2	3.6	1726	0.045
Layer IV	1.18	06.4	1005	0.028

When the heat transfer from unsteady state to steady state, the parameters of special clothing material are substituted into the clothing heat transfer model based on unsteady state. The simulated temperature of part of human skin surface (layer IV) and the test data in

Schedule 2 are obtained by solving the temperature distribution model based on unsteady state using MATLAB software. It is shown in Table 2.

Table 2. comparison between simulated data of temperature distribution and experimental data

Time/s	Analog values $/^{\circ}\text{C}$	Experimental values/ $^{\circ}\text{C}$	Relative error/%
1	36.98	37.00	0.05
50	37.50	37.55	0.13
100	39.29	39.37	0.20
200	42.39	42.45	0.14
500	46.55	46.57	0.04
1000	47.89	47.92	0.06
1500	48.05	48.07	0.04

The maximum relative error between the simulated data and the measured data is 0.20%, while the minimum error is only 0.04%. It shows that the simulation results of the unsteady transfer of the environment-clothing-human body heat transfer model are in good agreement with the actual experiment.

6. EVALUATION

In this paper, the basic unsteady heat conduction model is used to analyze, and it has good universality. The finite volume method is used to simplify the actual problem effectively, and the corresponding node is used to replace the material temperature of the layer, which reduces the amount of calculation and facilitates the solution of the model. By synthesizing multiple models, the advantages of each model can be brought into full play, which makes the calculation results more accurate.

REFERENCES

- [1] Huang Fu Xiaodong. Study on the protective performance of fire-retardant clothing. Donghua university, 2014.
- [2] Liu Shuai. Study on the functionality and wear of thermal insulation and flame-retardant work clothes. Suzhou university, 2014.
- [3] Li Jun, Zhang Weiyan. Study on heat insulation value distribution of multi-layer clothing system. Journal of donghua university (natural science edition), 2003(03): 11-14.
- [4] Yan Lin, Xia Yiya. Testing and analysis of clothing insulation performance. Journal of hefei university of technology (natural science edition), 1998(S1): 72-78.
- [5] Liu Changming, Liu Fang Ruihua. Fire retardant clothing and fabric. China labor protection supplies, 1996(06): 16-21.

Research on Logistics Financial Supervision Risk based on BP Neural Network Algorithm

Jiayang Li

School of Management, Shanghai University, Shanghai, ZipCode:200232 China a

E-mail: 2276234614@qq.com

Abstract: The financing demand of small and medium-sized enterprises and the loan-cherishing of financial institutions give birth to logistics finance. After the outbreak of crises such as "steel trade incident" and "trade copper incident", there is an urgent need to control the supervision risk. In view of this, this paper takes logistics supervision enterprises as the main body, analyzes the composition of the supervision risk, and establishes the object. Then, based on BP neural network algorithm, combined with specific data, the index system is empirically studied, and the important indicators affecting the risk of third-party logistics enterprise supervision are found.

Keywords: Logistics finance; Regulatory risk; BP neural network algorithm

1. INTRODUCTION

Logistics finance is a comprehensive financial service for small and medium-sized enterprises, which integrates financing, settlement and insurance with logistics enterprises as business supervisors. Logistics finance can well coordinate the relationship between the supply and demand of funds. On the one hand, it connects banks and SMEs on the basis of mutual trust through the way of principal-agent, and to a great extent, it opens up the financing channels of SMEs. On the other hand, it can solve the needs of traditional value-added services and transformation of banks. With the continuous development and optimization of its business model, logistics finance has gradually become an effective way to solve the credit difficulties of SMEs. According to the data from the Institute of Prospective Industry Research, it is estimated that the domestic logistics financial market will reach 14.98 trillion yuan by 2020. Logistics finance presents a positive trend of vigorous development.

However, just as all the new things are spiraling up the law, in recent years, the logistics financial business has developed vigorously, solved a large number of SME financing problems, but also to a certain extent accelerated the outbreak of the crisis. It broke out in Shanghai and spread all over the country, relying on the rise of steel prices without replenishment, using the same batch of steel, repeated pledges to several banks as a model, using collusion fraud as a means to collect large amounts of funds, and remit funds to other areas such as real estate, in

an attempt to make up the deficit after gaining profits, net profit "profit" Benefit mode, due to the unexpected drop in steel prices and a tragic crash, more than 200,000 steel trading enterprises in about a third of the enterprises out, numerous executives imprisoned by the "steel trade incident", clearly exposed the current logistics financial regulatory system imperfections and regulatory risks uncontrollable.

2. LITERATURE REVIEW

In the aspect of logistics financial risk prevention and control, different scholars at home and abroad have carried out in-depth research based on different methods. In foreign research, Jokivuolle (2003) assumes that other conditions remain unchanged, and uses Morton structured method to study the relationship between the default rate of repayment and the value of pledge of financing enterprises. Finally, when the default rate of financing enterprises rises and the short-term value of pledge changes greatly, the financial institutions in order to To avoid risks, we should reduce the rate of pledge. Massimo (2005) obtained several key factors affecting the pledge rate of accounts receivable by constructing a model with the pledge of accounts receivable as an incentive factor, and collected data from 7 250 companies as samples to support this conclusion. Peng (2011) takes the third-party logistics enterprises as the main body to study the range of pledge rate in seasonal inventory pledge financing under the circumstance of high risk aversion.

In domestic research, Li Yixue, Wang Shouyang et al. (2011) on the basis of previous studies, using the "subject + debt" form of risk assessment, constructed a newsboy model to estimate the reorder situation of borrowing enterprises, and then through the Stakelberg dynamic game between the two sides, on the unified credit mode, the pledge rate of logistics enterprises. Definite analysis was carried out. Zhang Ming (2013) takes banks as the main body, analyzes the incentive and supervision of commercial banks to the third-party logistics companies in the inventory pledge financing business, and then designs and compares the supervision effects of pure incentive, incentive supervision and incentive supervision after adding incentive, so as to make effective supervision for commercial banks. Theoretical guidance. Chen Yun et al. (2015) through the analysis of liquidity delay and liquidity risk, taking banks as the main

body, constructed a static optimal pledge rate model to avoid comprehensive risk, and through the case of steel pledge to verify the model. However, the vast majority of scholars choose commercial banks as the main body for the study of logistics financial risks, but pay little attention to the logistics enterprises which are the main body of supervision.

3. THE COMPOSITION OF REGULATORY RISK AND BP NEURAL NETWORK ALGORITHM

This paper holds that the supervision risk refers to a kind of responsibility entrusted by the third party logistics enterprises to supervise the pledge for the financial institutions by signing principal-agent contracts with financial institutions and financing enterprises, which brings about a series of comprehensive risks related to operation, cargo rights, cargo value and other factors. In other words, the subject of supervision risk is the third party logistics enterprise, the subject of risk is the pledge, the risk is produced by signing the principal-agent agreement, the income is the supervision fee stipulated in the contract, and the responsibility is assumed according to the contract when the interests of financial institutions are damaged due to the negligence of logistics enterprise supervision. Liquidated damages or joint damages to be paid.

This paper focuses on the supervision risk under the entrusted supervision of logistics enterprises, which can be divided into four categories: contract risk, cargo risk, operational risk, and systemic risk. Among them, contract risk refers to the risk brought by the non-standard terms of the agreement, unclear definition of responsibility, and even unreasonable distribution of rights and obligations to the supervisory enterprises. Goods risk mainly refers to

the risk that when financing enterprises can not repay the principal and interest on schedule, financial institutions sell or auction the pledged goods, resulting from a series of comprehensive reasons that the pledged goods can not be sold or the funds acquired by the sale can not repay the loan principal and interest. Generally speaking, the risk of goods is mainly embodied in two aspects: the difficulty in controlling the value of goods and the difficulty in tracing the ownership of goods. Operational risk refers to the risk caused by mistakes in the course of operation. Systematic risk refers to the systemic risk that can not be simply classified as contract risk, operational risk and cargo risk under the circumstances of considering macroeconomic situation, industry environment, supply chain upstream and downstream partners and competitors.

The general structure of BP neural network is composed of input, output and hidden layer. Generally speaking, input and output layers are unique. The hidden layer can contain multiple layers in principle. One layer is called single layer network. This kind of perceptron is called three layer perceptron. In fact, the three-layer neural network already has a very strong ability to deal with nonlinear problems, and its comprehensive application is the most common. Therefore, considering the complexity of the model, this paper chooses a three-layer neural network mechanism to learn and train the sample data.

Four, the establishment of regulatory risk index system and the demonstration of BP neural network algorithm.

The specific situation of the regulatory risk indicator system is shown below in Table 1.

Table 1. The specific situation of the regulatory risk indicator system

First level index	Two level index	Indicator description
Contract risk	N1: The rationality of contract terms	The main consideration is whether the terms are clear, standardized, and whether the rights and obligations are fair or not.
	N2: service fees charged by logistics enterprises	Consider the impact of income on regulatory risk
risks of goods	N3: total value of goods themselves	Fair value of goods market
	N4: cargo condition stability	Grading according to cargo stability
	N5: past value stability of goods	Weighted sigma summation for price fluctuations of different goods
	N6: cargo ownership clarity	Are the main reference goods registered online?
Operational risk	N7: operator training	Training frequency is mainly based on investigation.
	N8: enterprise informatization level	Comprehensive reference research and public information
	N9: internal rules and regulations and compliance	Compliance with internal rules and regulations
	N10: financing enterprises comprehensive credit situation	Weighted sigma summation of reputation and acquired market and government related honor in financing industry
system risk	N11: logistics enterprises overall situation	Reference to industry trends, logistics supervision of the enterprise's own industry positioning.

		competitors, supply chain upstream and downstream partners and other information comprehensive analysis
	N12: the industry of goods themselves	Similar to logistics enterprises

The regulatory risk of the third-party logistics enterprises is a complex network chain structure consisting of four main risks. Many indexes in the network are combined to influence the regulatory risk of the third-party logistics enterprises. BP neural network is also a model of network structure. It combines with the training set. The operation mode of the prediction set simulates the process of multiple inputs affecting the output in each network, so the model method is fully applicable to simulate the process and results of the impact of various indicators on regulatory risk.

In the data aspect, 20 enterprises are taken as samples and MATLAB is selected as software. When the learning rate is 0.03 and the number of hidden layer nodes is 8, the model error is the smallest.

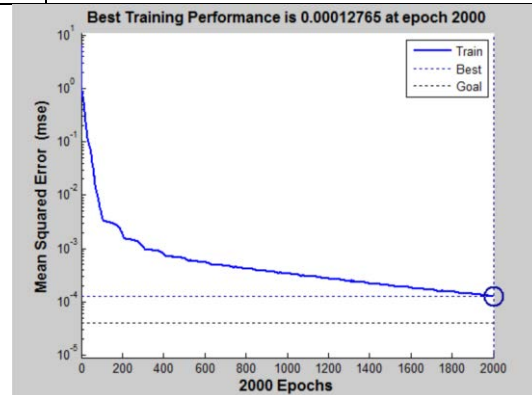


Figure 1. Important Indicators of Supervision Risk of Third Party Logistics Enterprises

The Mean Impact Value (MIV) is an index used to determine the extent to which the input variable affects the output variable. After calculation, the MIV value of each input variable is obtained as shown in the table2 below.

Table 2. Indicators of the extent to which input variables affect output variables

dimension	First level index	Two level index	MIV
Recessive risk	Contract risk	N1 contract terms rationality	0.1044
		N2 logistics enterprises charge service fees	0.0707
	system risk	N11 logistics enterprises overall situation	0.1291
		N12 the industry of goods themselves	0.2238
Dominant risk	risks of goods	N3 total value of goods themselves	0.0064
		N4 cargo condition stability	0.1591
		N5 goods past value stability	0.0829
		N6 cargo ownership clarity	0.1734
	Operational risk	N7 operator training	0.0531
		N8 enterprise informatization level	0.0847
		N9 internal rules and regulations and compliance	0.1637
		N10 financing enterprises comprehensive credit situation	0.0434

Since the 12 indicators have been unified, all indicators are positive, so MIV is also positive. According to the ranking of the MIV values of the indicators, the five indicators are obtained: the industry situation of goods, the clarity of ownership of goods, the soundness and compliance of internal articles of association, the stability of goods status and the comprehensive situation of logistics enterprises. The MIV value of the target is relatively large, which is an important index affecting the supervision risk of the third party logistics enterprises.

4. SUMMARY AND PROSPECT

This paper identifies the key indicators affecting the regulatory risk of the third party logistics enterprises, and provides some guidance for the logistics enterprises to control their own regulatory risk in the process of cooperation with financial institutions and

financing enterprises through principal-agent agreements. For the third party logistics enterprises, firstly, regulatory risk Quantification is the only way. Secondly, in the process of quantifying regulatory risks, we should not neglect the analysis of different types of regulatory risks. For financial institutions, a fair and reasonable principal agency agreement can achieve a win-win situation. For other participants, the joint efforts of regulators and borrowers will play a positive role in the regulatory system environment. At the same time, the introduction of insurance mechanism can also improve the stability of the regulatory system environment.

REFERENCES

- [1]Jokivuolle,E.,Samu P. Incorporating Collateral Value Uncertainty in Loss Given Default

- Estimates&Loan-to-value Ratio[J].European Financial Management,2003,9(3):299-314.
- [2]Massimo O. Trade credit as collateral[R]. Working Paper,Bank of Italy, 2005.
- [3]Peng Y. The Research on the Loan-to-Value of Inventory Pledge Loan Based Upon the Unified Credit Mode[M].Springer Berlin Heidelberg: Advanced Research on Electronic Commerce, Web Application, and Communication,2011.
- [4]Li Yi-xue, Wang Shouyang, Feng Gengzhong. Decision-making on the pledge rate of seasonal inventory financing in logistics finance [J].Journal of Management Science, 2011, 14 (11): 19-33
- [5]Zhang Ming. Research on Incentive Supervision in Inventory Pledge Financing Based on Principal-Agent Theory [D].Shanghai University, 2013
- [6]Chen Yun, Liu Xi, Yang Qin. Study on inventory pledge rate in Supply Chain Based on liquidation delay and liquidity risk [J].Management Review, 2015, (04): 197-208.

Research on a Resource Scheduling Algorithm based on Cloud Task

Jun Nie

Guangdong University of Science and Technology, Software department, Dongguan City, Guangdong Province 523083

Abstract: This paper designs an improved genetic algorithm for cloud task scheduling problem with virtual machine load balancing and task completion time as the goal. The algorithm introduces the concept of relative fitness of virtual machines through the different execution speeds of virtual machines, and promotes the mutation operation to develop directly in a better direction to optimize the results. The simulation results show that the proposed algorithm not only has higher convergence and ability to search for optimal solutions, but also can reflect the degree of compliance between scheduling results and user expectations, and provides an effective solution for task scheduling problems in cloud environments.

1. INTRODUCTION

In the cloud environment, a large number of IT infrastructure resources are abstracted into virtual machines of various performances by virtualization technology. Based on various factors, the cloud platform combines several virtual machines to form a virtual resource set for a specific task set. Then, the task to be processed is distributed to the nodes of the virtual resource through the cloud platform-specific scheduling policy. Processing; this is a typical NP-hard problem. This process is felt for each user to occupy a computer by himself. For the cloud service provider to fully utilize the performance of the cloud platform, it is crucial to use which scheduling strategy to assign tasks.

2. TASK DESCRIPTION

$T=\{t_0, t_1 \dots t_{n-1}\}$ represents the task set of the cloud computing, where n is the number of cloud tasks. $T_i=\{tId, tLong, tData, tCost, tTime, tProperty, tStatus\}$ represents the attributes of the i -th task, where tId represents the ID of the task, $tLong$ represents the total length of the task, and $tData$ represents the relevant data required for task processing, $tCost$ Indicates the cost of completing the task expectation, $tTime$ indicates the expected completion time of the task, and $tProperty$ indicates the resource attribute situation that the task wants to obtain, including the computing power, memory, and bandwidth of the resource, thereby quantifying the QoS performance requirements of the task. $tStatus$ represents the status of the task.

$V=\{v_0, v_1 \dots v_{m-1}\}$ represents the set of virtual machines provided by the cloud platform for the corresponding task set, where m is the number of

virtual machines. $V_i=\{id, mips, ram, bw, price\}$ represents the performance of the i -th virtual machine, where id represents the serial number of the virtual machine, $mips$ represents the computing power of the virtual machine, ram represents the memory of the virtual machine, and bw represents the virtual machine. Bandwidth, price represents the price of the virtual machine. Tasks on the same virtual machine are processed on a first-come, first-served basis. After all the tasks in the task set are executed, the cloud platform reclaims the virtual machines in its corresponding virtual resource set for the next scheduling.

3. IMPROVE THE DESIGN OF GENETIC ALGORITHM

The genetic algorithm optimizes the cloud task scheduling problem through selection, crossover and mutation operations, and has high early optimization efficiency, but its local search ability is poor, and the search speed of the feasible solution is very slow in the later stage. The paper mainly improves the variation in genetic operation, speeds up the search speed of the algorithm, and finally finds the optimal solution.

3.1 Coding Rules

The traditional 0,1 coding method of genetic algorithm is changed to real number direct coding; how many genes per chromosome depends on the number of tasks in the task set, and each gene value represents the serial number of the virtual machine. There are several individuals in the population, each of which represents a resource allocation scheme of the task set. For example, if the number of virtual machines is 4 and the number of tasks is 8, the number of genes of the individual is 8. The gene value is one of the serial numbers corresponding to the four virtual machines.

3.2 Fitness Function

After a certain individual is decoded according to the rules, a resource allocation scheme of the task set can be obtained, and the tasks of each virtual machine are different. Assuming that w tasks are allocated on the k th virtual machine, the time $F(k)$ used by the k th virtual machine to complete its assigned task is:

$$F(k) = \sum_{j=1}^w L_j^k \quad (1)$$

Where is the time taken by the k th virtual machine to complete the j th task assigned to it. It can be known from (1) that the total execution completion time TF

of all tasks is:

$$TF = \sum_{k=0}^{j-1} F(k) \quad (2)$$

Wherein, m represents a number of virtual machines. The smaller the TF, the better the user's evaluation. At the same time, for cloud service providers, the load balancing of virtual machine resources is also very important. The method proposed in this paper uses the time $F(k)$ used by the virtual machine k to complete all the tasks it allocates to represent its load, and the average load ML of the virtual resource set and the load balancing standard deviation NL. They are:

$$ML = \sum_{k=0}^{i-1} \frac{F(k)}{i} \quad (3)$$

$$NL = \sqrt{\sum_{k=0}^{i-1} (F(k) - ML)^2} / i \quad (4)$$

Here, i represents the number of virtual machines. Therefore, the ideal value of NL is 0. The smaller the NL is, the closer the load of each virtual machine is, the more reasonable the scheduling strategy is, and the higher the resource utilization rate is; the total task completion time TF is also likely to be smaller.

It can be concluded that the fitness function is:

$$\text{Fitness} = 1/(1 + ML + NL) \quad (5)$$

It can be seen from (5) that the larger the fitness function value indicates that the individual is superior.

3.3 Roulette selection operation

The selection probability P_m of the individual m in the population has a certain relationship with its own merits and demerits, which can be calculated by the following formula.

$$P_m = \text{Fitness}_m / \sum_{m=1}^Q \text{Fitness}_m \quad (6)$$

Wherein, Q represents the size of the population.

3.4 Double point cross operation

The double-point crossover operation refers to arbitrarily selecting two points in the chromosome string of the paired individual as an intersection at the time of operation, and then exchanging the chromosome fragments to each other to generate a new individual. It provides a guarantee for the population to maintain individual diversity and facilitates the evolution of genetics. When performing the two-point crossover operation, the chromosome lengths of the two individuals are consistent, and the individuals who do not meet the requirements are prevented from being crossed. The basic steps are as follows:

- (1) Individual matching of individuals in contemporary populations.
- (2) Arbitrarily select two points in the paired two pairs of chromosome strings as subsequent intersections.
- (3) By exchanging chromosome fragments of the same number of genes between the two points, two

different new individuals can be produced.

3.5 Improve the mutation operation

There are n virtual machines available in the virtual resource set, and the configuration between them (they cannot be exactly the same, and the execution speed of the virtual machine is the most important performance of its processing tasks. The calculation of the relative fitness P_j of the j th virtual machine) The formula is as follows:

$$P_j = V_s^j / TV_s \quad (7)$$

$$TV_s = \sum_{k=0}^{m-1} V_s^k \quad (8)$$

It represents the execution speed of the j th virtual machine in the virtual resource set, and represents the sum of the execution speeds of all the virtual machines in the virtual resource set, and m represents the total number of virtual machines. It can be known from Equation 7 that the faster the execution speed of the virtual machine is, the greater its relative fitness is, and the sum of the relative fitness of all virtual machines is equal to one.

4. SIMULATION EXPERIMENT

This paper uses CloudSim as a simulation platform to compare experiments with the improved genetic algorithm and traditional genetic algorithm. The cloud task scheduling simulation experiment compares the GA and Min-Min algorithms from three aspects of convergence speed, load balancing and task completion time to verify the performance of the proposed algorithm.

4.1 Analysis of convergence speed results

The task set and the virtual resource set are randomly generated by the random generator, the task length is in the [4000, 9000) interval, and the virtual machine execution speed is in the [200, 600) interval. The population size is $Q=100$, the maximum number of iterations is 600, and the crossover probability is 0.70. The mutation probability is 0.85. The number of virtual machines in the experiment is 200, and the number of tasks is 600. The comparison result of convergence is shown in Figure 1.

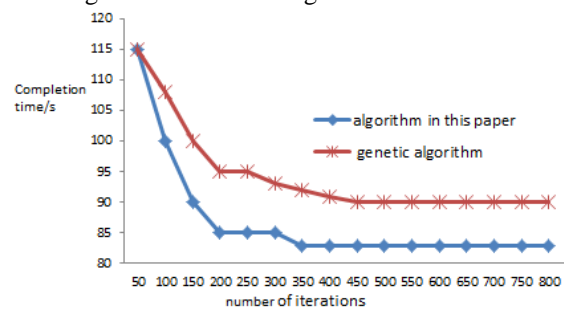


Figure.1 Comparison of the convergence between the algorithm and GA

It can be seen from the results shown in Fig. 1. The improved genetic algorithm proposed in this paper achieves the convergence effect when iterating to

about 350 times, and the GA can be iterated to about 450 times to obtain the final convergence. Achieve better and faster convergence.

4.2 Analysis of load balancing results

The number of virtual machines is kept unchanged at 200, and the number of tasks is initially 50. After each increment of 50, until 800 ends, the load balancing of the three algorithm virtual machines is shown in Figure 2.

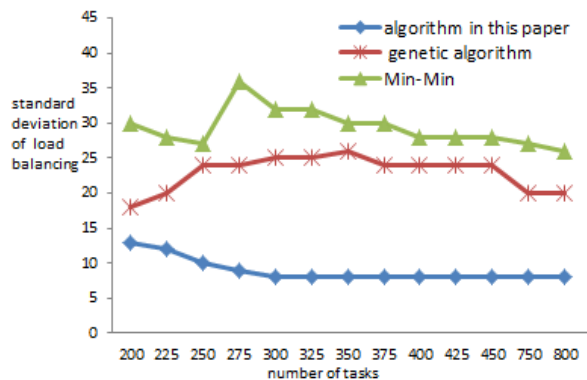


Figure 2. The load balancing of the three algorithm virtual machines

When the number of virtual machines is constant, the algorithm achieves the best effect in load balancing, and the load balancing standard deviation can be stabilized at around 7 as the number of tasks increases. The load-balancing standard deviation of GA is basically above 15. And as the number of tasks increases, the load-balancing standard deviation of Min-Min oscillates around 20. It can be seen that the proposed cloud task scheduling improved genetic algorithm achieves better results in load balancing than the other two algorithms.

5. CONCLUSION

In this paper, an improved genetic algorithm is designed for cloud task scheduling problem with virtual machine load balancing and task completion time as the goal. The algorithm introduces the concept

of relative fitness of virtual machines through the different execution speeds of virtual machines, and promotes the mutation operation to develop directly in a better direction to optimize the results. Comparing with the simulation experiment and GA and Min-Min, the results show that the algorithm has achieved certain improvement effects, not only has higher convergence and the ability to search for optimal solutions, but also can reflect the degree of compliance between the scheduling results and user expectations. It provides an effective solution for task scheduling problems in the cloud environment.

ACKNOWLEDGEMENTS

The work is supported in part by Department of Education of Guangdong Province under Grant 2015KQNCX193.

REFERENCES

- [1]Xiong Jinbo, Yao Zhiqiang. A Composite Document Model and Its Access Control Scheme in Cloud Computing[J]. Journal of Xi'an Jiaotong University, 48(2): 25-31(2014)
- [2]Feng Chaosheng, Qin Zhiguang. Key Techniques of Access Control for Cloud Computing[J]. Acta Electronica Sinica, 02(43):312-319(2015).
- [3]Hui Jiang, Jianjun Yi, Shaoli Chen. A Multi-objective Algorithm for Task Scheduling and Resource Allocation in Cloud-based Disassembly [J]. Journal of Manufacturing Systems, 2016, 41: 239-255
- [4]Hosseinimotlagh Seyedmehdi, Khunjush Farshad, Samadzadeh Rashidaldin. SEATS: Smart Energy aware Task Scheduling in Real-time Cloud Computing[J]. Journal of Supercomputing, 2015, 71(1): 45-66.
- [5]Wang YuDing, Yang jiaHai. Survey on Access Control Technologies for Cloud Computing[J]. Journal of Software, 26(5):1129-1150(2015)ing, 2012, 16(1):69-73.

Shadow Localization based on Spherical Triangle

Yunfei Bao^{1,2}, Rui Zhi³, Chenyang Zhang^{1,2}, Aimin Yang^{4,*}

¹Engineering Computing and Simulation Innovation Lab, North China University of Science and Technology, Tangshan, 063210, China

²College of Electrical Engineering, North China University of Science and Technology, Tangshan, 063210, China

³College of Materials Science and Engineering, North China University of Science and Technology, Tangshan, 063210, China

⁴College of Science, North China University of Science and Technology, Tangshan 063210, China

*E-mail: 43698059@qq.com

Abstract: How do you determine the outdoor shooting time, depending on the frequency location and date is one of the most important aspects of the video data analysis, this article through studies based on the shadow of the spherical triangle positioning technology, using geometry and astronomy knowledge, through the Angle of the sun among the variables of cohesion, established the length of the shadow of the sun, the problem can be converted into the length of the shadow on the changing rule of the longitude, latitude, date, time of study, analyzes the shadow length on the changing rule of basic parameters, object projection length calculation model is established, it is concluded that the sun's shadow change at any given time. After fitting the shadow length data, the curve was fitted to conform to the quadratic function relation, and the data were screened and compared by using Matlab software to obtain the longitude and latitude of the desired location.

Keywords: Shadow localization; Spherical triangular normalization; Curve fitting

1. INTRODUCTION

With the development of The Times, the use of sun positioning technology, that is, the use of changes in the shadow of the object to determine the location and time, has become an important aspect of video data analysis and processing. The timing and location of the video shoot has far-reaching implications for the crime of pursuing and studying the relationship between the sun's motion and the earth. In this paper, the longitude and latitude of the straight bar are calculated through the change of the shadow of the sun, to determine the location of the object [1,2].

2. ANALYSIS OF SHADO LENGTH VARIATION

Declination of the sun: The Angle between the sun's incident light and the earth's equator. Since the Angle between the earth's rotation axis and the axis of rotation is basically unchanged, the sun's declination varies with different seasons.

When the sun Angle, 12 local time is 0, before and after every 1 hour + 15, with 14 cases of 10 are 30.

Sun azimuth: azimuth - the horizontal Angle between a point pointing north and a line pointing clockwise to the target [3-5]. Take the sun's azimuth Angle of 0-360, which refers to the Angle between the projection of the sun's rays on the ground and the local meridian, and can be approximately regarded as the Angle between the vertical line on the ground and the direct south direction under the sun's shadow. The azimuth is zero to the south, increasing to the west and decreasing to the east.

Angle of elevation: The Angle between the sun's rays and the ground.

The direct calculation method of the shadow length is the ratio of the straight bar length to the sine of the sun's height Angle. Shadow, straight rod height H , length L X, said the solar altitude angles by looking at the sun Angle calculation method and its application in remote sensing, shows its size by local latitude in the astronomical triangle (Beijing's Tiananmen square: 54 minutes and 26 seconds, 39 degrees north latitude 23 minutes 29 seconds 116 degrees east longitude), the declination of the sun of the day, and when the sun Angle, as shown in Figure 1.

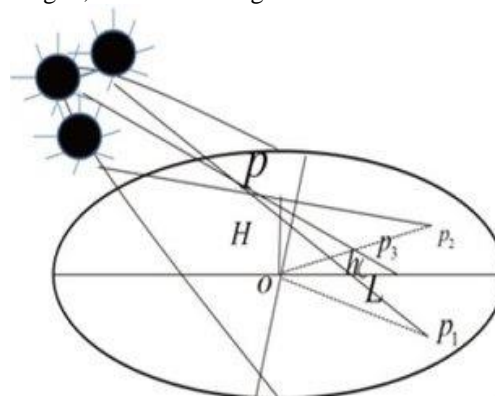


Figure 1 A three-dimensional diagram of the orbit
The closer to the direct point of the sun, the higher the sun's height Angle, the shorter the object's shadow; The farther from the direct point of the sun, the smaller the Angle of the sun's height, the higher the shadow of the object. The longer the object, the longer the shadow; The shorter the object, the shorter

the shadow [6,7].

The figure above is a schematic diagram of the sun's orbit in three dimensions:

$$\sin X = \sin \phi \sin \alpha + \cos \alpha \cos \phi \cos \omega \quad (1)$$

The sun's declination and chronological relationship:

$$\phi = 23.45^\circ \sin \frac{360^\circ (284 + d)}{365} \quad (2)$$

In the expression of the sun's declination and date relation, d is the ordinal time date, and the specific relation is $d = 1$, which means January 1. Solar hour Angle is related to local time, and $= 15n$, $n = t - 12$; N denotes the square of some position of the sun as time, and t denotes the local time in the 24-hour system. Through the connection of the intermediate variable, the height Angle of the sun, the problem can be transformed into the study of the variation law of shadow length L on longitude, latitude, date d and time t .

Finally, the function expressions of shadow length L about longitude, latitude, date d and time t are obtained:

$$L = H \cot \cdot \arcsin[\sin \alpha + \sin \phi + \cos \alpha \cos \phi \cos[15^\circ(t - \frac{120^\circ - \beta}{15} - 12)]] \quad (3)$$

According to the established model, the following analysis results of influence of parameter changes on shadow height are obtained:

When the latitude, longitude, date and Beijing time are fixed, the shadow length changes as the length of the bar increases.

When the latitude, longitude, date and bar length are fixed, the shadow length changes first decrease and then increase with the increase of Beijing time, and the minimum value appears at some time at noon.

When the latitude, date, pole length and Beijing time are fixed, as the longitude increases, the shadow length changes first increase, then decrease, then increase and then decrease.

When latitude, longitude, pole length, Beijing time is fixed, as the date increases, shadow length changes first decrease and then increase; Wudang longitude, pole length, Beijing time, date fixed, with the increase of latitude, shadow length is the shortest change to the equator, more two levels longer.

Take a group of numerical value to carry on the simulation test to the data by Matlab software:

$$\begin{aligned} H &= 3m \\ d &= 294day \\ t &= 9am \sim 15pm \\ \alpha &= 39.9072254^\circ N \\ \beta &= 116.3913982^\circ E \end{aligned} \quad (4)$$

First, input the function expression of shadow length L about longitude, latitude, date d and moment t , substitute the data given in question 1, and obtain the following image of moment t and shadow length, as

shown in Figure 2:

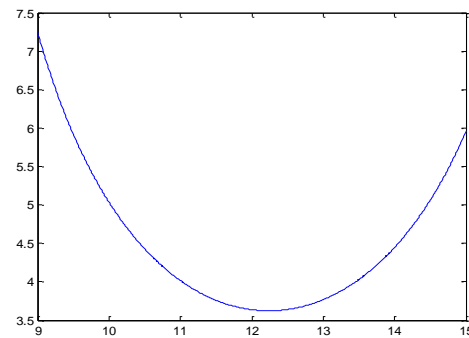


Figure 2 The relation between time t and shadow length

3. SOLAR AZIMUTH

The spherical Angle formed by the direct point of the sun and the local great circle and the local southern longitude line is called the solar azimuth Angle, which stipulates that it is positive counterclockwise, and the range is shown in the figure:

The solution of azimuth

Similarly, the cosine formula of the spherical triangle can be used to obtain:

$$\begin{aligned} \cos(90^\circ - \phi) &= \cos(90^\circ - \alpha) \cos(90^\circ - X) \\ &+ \sin(90^\circ - \alpha) \sin(90^\circ - X) \cos(180^\circ - Y) \end{aligned} \quad (5)$$

4. SUN SHADOW FIXING

A three-dimensional analysis system is established by taking the straight bar and the ground interpolation point as the origin of coordinates and the straight bar as the Z axis. The least square method is used to solve the nonlinear equations by using the relationship between the sun's azimuth Y and altitude and declination. Based on the shadow length, the function relation between the shadow vertex coordinate and local longitude and latitude and the shadow vertex coordinate function is established, the related equations are linked, the local longitude and latitude are solved by Matlab programming, and the results are analyzed.

(1) establish three-dimensional analysis system

Taking straight bar and ground interpolation as coordinates origin and straight bar as Z axis, because the research scope is very small, the ground is regarded as the plane formed by the intersection of X and Y axis (the problem of X -axis and Y -axis direction is not considered first, and then the differentiation is made). It is assumed that the plane formed by the intersection of X and Y axis is perpendicular to the connection between the interpolation point and the center of the earth.

(2) determine variables

Longitude determination

The longitude of the location is calculated from the time difference between the noon time of the location, that is, the point with the minimum shadow length and the corresponding Beijing time. Beijing is noon 12:00 PM, for longitude 120° east longitude, by area

every 15 degrees of longitude difference 1 h, place the 4 min per 1-degree difference in longitude to calculate the location of the longitude.

Latitude determination

Firstly, according to the shadow length, a three-dimensional coordinate with the straight bar and ground interpolation point as the origin of coordinates and the straight bar as the Z axis is established, and the shadow length of the straight bar at a certain time can be calculated:

$$L = \sqrt{x^2 + y^2} \quad (6)$$

According to the height Angle of the sun, the shadow length of the straight bar can be calculated at some time:

$$H = L \tan \theta \quad (7)$$

On the ground, the straight bar is illuminated by the sun and casts a shadow. The length of the straight bar is H and the length of the shadow is L. The positive height Angle determines the length of the shadow and the azimuth Angle determines the direction of the shadow, as shown in Figure 3.

Sun azimuth Y and altitude angles and declination angles:

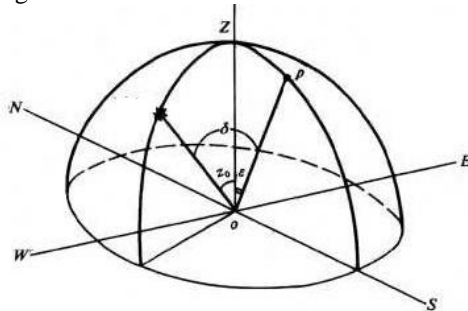


Figure 3 Sun azimuth Y and altitude angles and declination angles

Geometric relations of shadow length, rod length and sun height Angle: $H = L \tan \theta$. According to the spherical triangle formula and the relation between the sun's azimuth Angle Y and altitude Angle and declination Angle:

$$\begin{cases} \phi = 23.45^\circ \sin \frac{360^\circ (284 + d)}{365} \\ \sin Y = \frac{\cos \phi \sin \theta}{\cos \theta} \\ \sin \alpha = \frac{\sin \phi \sin \theta}{\cos \theta} \\ \cos Y = \frac{\sin \phi \cos \theta}{\cos \theta} \end{cases} \quad (8)$$

When $H = L \tan \theta$ is substituted into the system, the azimuth Angle Y and altitude Angle and declination Angle of the sun can be obtained by using the known conditions. The least square method is used to solve nonlinear equations.

The sequential time date $d=108$ can be obtained from April 18, 2015. The data in annex I after processing is as follows, as shown in Table 1:

The curve conforms to the quadratic function relation.

The nadir of the quadratic function is the shadow length of the straight bar at noon.

Table 1 Processed data

Beijing time	x (m)	Y(m)
14:42	1.0365	0.4973
14:45	1.0699	0.5029
14:48	1.1038	0.5085
14:51	1.1383	0.5142
14:54	1.1732	0.5198
14:57	1.2087	0.5255
15:00	1.2448	0.5311
15:03	1.2815	0.5368
15:06	1.3189	0.5426
15:09	1.3568	0.5483
15:12	1.3955	0.5541
15:15	1.4349	0.5598
15:18	1.4751	0.5657
15:21	1.516	0.5715
15:24	1.5577	0.5774
15:27	1.6003	0.5833
15:30	1.6438	0.5892
15:33	1.6882	0.5952
15:36	1.7337	0.6013
15:39	1.7801	0.6074
15:42	1.8277	0.6135

Take the data in the attachment to get the corresponding shadow length at different times, and then obtain the longitude and latitude of the region, as shown in the figure below, as shown in Figure 4:

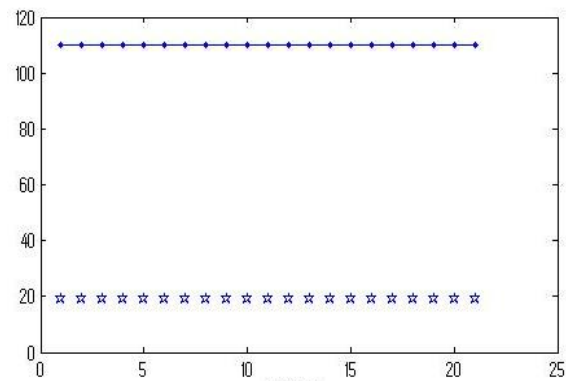


Figure 4 Longitude and latitude distribution

According to the calculated values of each group, the longitude and latitude of 12:00 is the optimal value of the location of the straight bar, so the location coordinate of the straight bar is, as shown in Figure 5. The approximate location to search from the Google map.

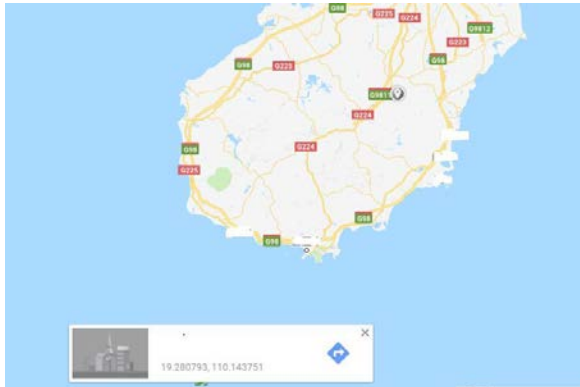


Figure 5 The approximate location searched on the map

5. LATITUDE AND LONGITUDE

The coordinates of the shadow endpoints are known for local longitude and latitude, but the difference is that the shooting date of Ben is unknown. The relationship between shadow length and time was established. SPSS software was used to fit the data, and the longitude of the region was calculated with the model of the second question. Combining with the idea of exhaustive method, we use Matlab to screen the data and get the latitude of the place, and then get the location and date of the straight bar.

longitude calculation

The curve fitting used by question 2 is also applicable to the third question. Given the relationship between Beijing time and shadow length, the location and date can be calculated first.

Firstly, Pythagorean theorem coordinate data is used to calculate shadow length:

$$M = \sqrt{x^2 + y^2} \quad (9)$$

To normalize the time data and eliminate the influence of dimensionality, the excel table can be obtained as shown in table 1 below, as shown in Figure 6:

Curve similar to quadratic function can be obtained by SPSS software analysis:

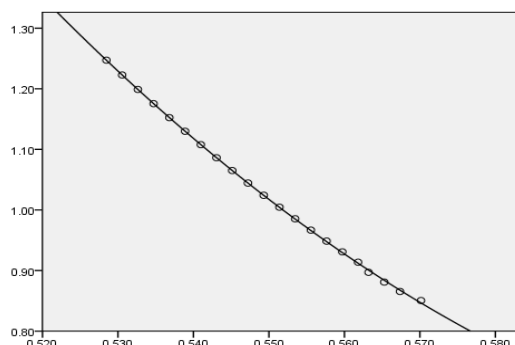


Figure 6 SPSS curve fitting

The independent variable is Beijing time.

The correlation coefficient is equal to 1 to prove that the expression fully conforms to the quadratic function; Similarly, SPSS data after processing were used for fitting, and SPSS curve fitting was obtained, as shown in Figure 7:

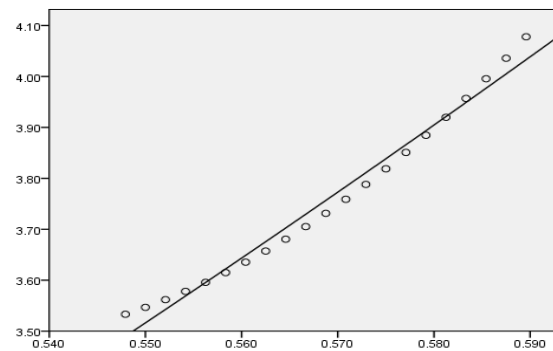


Figure 7 SPSS curve fitting

The independent variable is Beijing time.

Use excel table to fit the image of the known data, and get the function image of the shadow length and time of the observed location respectively, as shown in Figure 8:

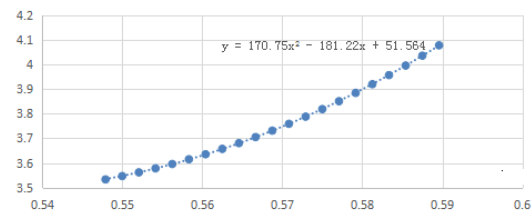
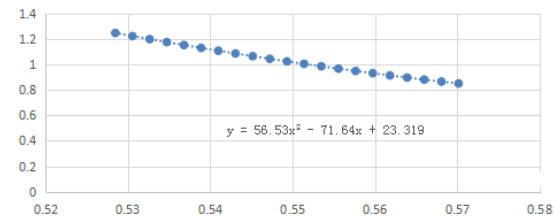


Figure 8 The shadow length changes over time
Display formula:

$$y = 56.53x^2 - 71.64x + 23.319 \quad (10)$$

With the calculation method in the second question, we can obtain:

$$x_{\min} = -\frac{b}{2a} = \frac{71.64}{2 \times 56.53} = 0.63364585 \quad (11)$$

$$0.63364585 \times 24 = 15.2075004$$

The time is 15:12 and 27 seconds

That is, the specific time can be calculated as 12:35min 53 seconds through the conversion, then is the noon time of the day.

According to longitude 360 degrees, 24 hours a day, get longitude every 15 degrees, time difference is one hour.

Beijing time local longitude. Therefore, it can basal longitude Beijing time(Beijing time is 12 hours)

Longitude of the place you want can be obtained from the conversion relation:

$$\Phi = 120^\circ - (12 - 0.6336 \times 24) \times 15^\circ = 168.096^\circ \quad (12)$$

Similarly, the formula shown in figure 13 is:

$$y = 170.75x^2 - 181.22x + 51.564 \quad (13)$$

With the calculation method in the second question, we can obtain:

$$x_{\min} = -\frac{b}{2a} = -\frac{181.22}{2 \times 170.75} = 0.53065886 \quad (14)$$

$$0.53065886 \times 24 = 12.7358126$$

The time is 12.44mins and 9 seconds.

$$\Phi = 120^\circ - (12 - 0.5307 \times 24) \times 15^\circ = 131.052^\circ \quad (15)$$

(2) latitude calculation

The local longitude is calculated above and the local latitude is calculated below. In this paper, by adopting the idea of exhaustive method, known as the longitude, and there are countless points on the same longitude, because of the large volume of data given, this article selects the shortest day noon when the long shadow to scale, work out various points to make these points each latitude and longitude of the actual value of the day's noon shadow length scale, and the noon shadow shortest length of data to compare do take absolute difference, for the absolute minimum corresponds to one or more sets of latitude is the desires of latitude, due to point to an infinite, need to compare one by one with the help of Matlab software selection, it is concluded that location of the latitude 21.12, Latitude of the location was 40.79. Calculate the result according to Matlab.

In summary, the longitude and latitude of the locations are:

(21.1° N, 68.1° E) and (40.79° N, 131.1° E)

(3) date of the straight bar

According to the following formula:

$$\alpha = 90 - |\beta - \phi| \quad (16)$$

Where is the altitude Angle of the sun, is the latitude of the region, and is the latitude of the direct point of

the sun;

By

$$\sin \theta = \sin \alpha \sin \phi + \cos \alpha \cos \phi \cos t \quad (17)$$

Must

$$\alpha = \arcsin(\sin \alpha \sin \phi + \cos \alpha \cos \phi \cos t) \quad (18)$$

The date of the straight rod obtained by the above formula is: May 12, 2015, March 2, 2015, and October 9, 2015.

REFERENCES

- [1] Du Chunxu, Wang Pu, Ma Chongfang, Wu Yuting, Shen Shaoqing, a high-precision sun position algorithm, new energy technology, 2008 (2): 41-48.
- [2] Zhang yujin, image processing and analysis, Beijing: tsinghua university press, 1999.3:43-49.
- [3] xiao sheng, ge chenghui. Sun Angle calculation method and its application in remote sensing. Beijing: remote sensing of land and resources, 1995: 48-57.
- [4] Jiang hongli. Mathematical derivation and analysis of the latitude of the direct sun point [J]. Bulletin of mathematics, 2007, 46 (9): 39-40.
- [5] He Xiaolei, Yu hejun, Li Jianying, ding lei. Formula solution and application of solar azimuth Angle. Journal of solar energy, 2008, 29 (1): 69-72.
- [6] Wu Lin. Research on longitude and latitude estimation technology based on solar shadow trajectory. Tianjin: tianjin university, 2010.
- [7] He Xiping, Zhang Qihua. Image processing and analysis based on MATLAB. Journal of Chongqing technology and business university (natural science edition), 2003, 20 (2): 22-25.

Dynamic Scheduling Strategy of Intelligent RGV based on Optimal Path

Chen Zhang^{1,2}, Dongrui Li^{1,3}, Zihao Song^{1,3}, Yang Han^{3,*}

¹Engineering calculation laboratory, North China University of Science and Technology, Tangshan 063210, China

²Yi Sheng College, North China University of Science and Technology, Tangshan 063000, Hebei, China

³College of Science, North China University of Science and Technology, Tangshan 063000, Hebei, China

*E-mail: 729420132@qq.com

Abstract: In this paper, four dynamic scheduling models based on optimal path are established for the problem. There are many constraints, such as different processing procedures, different CNC tool types, order execution and so on. Moreover, based on the actual plant demand, the model needs the lowest cost and the highest efficiency. Based on the simulated annealing algorithm, the RGV dynamic dispatching model with or without faults, which has the shortest moving path and the least moving time, is established, and the simulation road map is given. Finally, the queuing theory model is used to judge the running quality of the system in a material processing process, and the simulation is carried out.

Keywords: RGV dynamic scheduling model; genetic algorithm; simulated annealing algorithm; queuing theory; simulation

1. INTRODUCTION

Only one tool type is needed for material processing in one process, so each CNC is equipped with the same tool. Material can be processed on any CNC. Eight CNCs are at the same processing level without sequence. Based on the actual use of factories, the cost of consumption and production efficiency is the primary consideration, RGV car stationary waiting shows that all CNC machines are running processing, at this time the additional waste of CNC processing resources is the least. When the car is moving, it means that the machine is finished and the production is idle. This shows that when the RGV car has the least movement time. That means that the shortest cost and the highest efficiency are the shortest moving paths. We use simulated annealing algorithm to build a fault free shortest path model [1] for a process material processing.

There is a periodic rule in the material processing process. We set the period from the beginning of loading and unloading of the first machine by the RGV trolley to the completion signal of the first machine received by the trolley from the eighth machine to the preparation of loading and unloading before the machine. First, only one cycle is considered, and eight CNC machines are allocated successively.

In the shortest path model, our goal is to minimize

the path of the car, so the objective function is:

$$S = \min \left[\sum_{i=1}^8 L_i \right] \quad (1)$$

Among them, the L_i indicates that the trolley moves from the previous job task position to the next job task position distance.

Further analysis of the subject found that: the second CNC after finishing the processing waiting time is the RGV car from the previous position to the first CNC position of the distance. It is shown that there is a positive correlation between the vehicle motion path and the waiting time of the machine. Therefore, we transform the objective function from the shortest path to the shortest time, that is, the new objective function is:

$$T = \min \left[\sum_{i=1}^8 t_i \right] \quad (2)$$

The simulated annealing algorithm [2] is used to solve the new objective function T . In order to speed up the convergence of simulated annealing algorithm, Monte Carlo method is used to find an initial solution with a shorter period of operation. The new solution in simulated annealing process is generated by random dithering of position points in the current shortest path, that is, changing the route of the car running for one cycle. The difference between the cost function of the time taken to find the new route for a cycle and the current optimal route for a cycle is recorded as Δf . The expression of the acceptance probability of the simulated annealing algorithm is:

$$p = \begin{cases} 1, & \Delta f < 0 \\ \exp(-\frac{\Delta f}{T}), & \Delta f > 0 \end{cases} \quad (3)$$

If $\Delta f < 0$, then accept the new solution; otherwise accept the new solution with the probability of $e^{(-\Delta f/T)}$. That means that if $e^{(-\Delta f/T)}$ is greater than a random number between 0 and 1, then accept the new route. The selected cooling coefficient

$\partial = 0.999$ is used to cool down. That is $C_n = C_{n-1}\partial$, where C_n is the temperature after the first annealing, and the selected termination temperature $E = 10^{-30}$ is used to judge whether the annealing process is over or not. when $T < E$, the algorithm ends and then outputs the optimal route. In order to more clearly present the simulation route of the car, we optimize the road map of the car above, and get the final roadmap of the RGV car simulation, as shown in Figure 1:

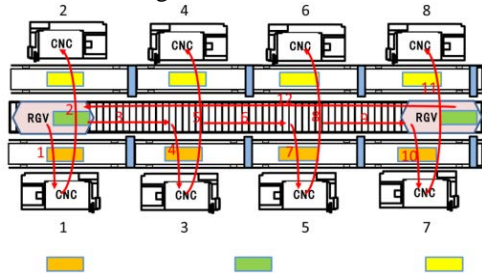


Figure 1 One process RGV car route simulation

In the analog route above, the RGV trolley carries on the loading and unloading processing at 1 and 2 positions, receives the signals of 3 and 4, moves forward one unit, then stops, carries on the loading and unloading processing to 3 and 4. The follow-up process is the same as before. Namely the shortest path is the distance of RGV moving forward three units from 1 and 2 positions.

2. A FAULT MODEL FOR MATERIAL PROCESSING IN ONE PROCESS

The principle of fault scheduling [3-5] is to minimize the impact of failure. Based on the established Table 1 A process fault real-time adjustment route

Malfunction location	Real-time adjustment of route
CNC#1	Out of service CNC1, Near service CNC2 Route: CNC2->CNC3->CNC4->CNC5->CNC6->CNC7->CNC8->CNC1
CNC#2	Out of service CNC2, Near service CNC3 Route: CNC1->CNC3->CNC4->CNC5->CNC6->CNC7->CNC8->CNC1
CNC#3	Out of service CNC3, Near service CNC4 Route: CNC1->CNC2->CNC4->CNC5->CNC6->CNC7->CNC8->CNC1
CNC#4	Out of service CNC4, Near service CNC5 Route: CNC1->CNC2->CNC3->CNC5->CNC6->CNC7->CNC8->CNC1
CNC#5	Out of service CNC5, Near service CNC6 Route: CNC1->CNC2->CNC3->CNC4->CNC6->CNC7->CNC8->CNC1
CNC#6	Out of service CNC6, Near service CNC7 Route: CNC1->CNC2->CNC3->CNC4->CNC5->CNC7->CNC8->CNC1
CNC#7	Out of service CNC7, Near service CNC8 Route: CNC1->CNC2->CNC3->CNC4->CNC5->CNC6->CNC8->CNC1
CNC#8	Out of service CNC8, Near service CNC1 Route: CNC1->CNC2->CNC3->CNC4->CNC5->CNC6->CNC7->CNC1

3. TWO PROCESS OF MATERIAL PROCESSING OF MATERIAL PROCESSING WITHOUT FAULT MODEL

Each CNC can only install one tools at the same time to process one material. When two processes of material processing operations. The first and second

fault-free model of material processing in one process, the known probability of failure is about 1%, and the probability of failure of two CNCs in one shift is very small, which can be neglected. That is to study only one CNC machine may fail in one cycle. Eight machines have the same probability of failure. One machine at a certain time will fail at random. The real-time adjusting route may be uncertain and varied. There will be an optimal route in all the adjusting routes. That is the route with the lowest cost and the highest efficiency. That is the RGV trolley has the least moving time and the shortest moving path. Line. This route should be consistent with the fault-free model, so we also use simulated annealing algorithm to establish the shortest path model for a process material processing fault.

In this shortest path model [4], our goal is also the shortest path of the car. So the objective Function is:

$$S' = \min \left[\sum_{i=1}^8 L_i' \right] \quad (4)$$

Among them, L_i' indicates the distance from the previous job task to the next job location.

Similarly, we transform the objective function from the shortest path to the shortest time. It means that the new objective function is:

$$T' = \min \left[\sum_{i=1}^8 t_i' \right] \quad (5)$$

Based on the optimal route without fault, the real-time adjustment route occurs when failure occurs as follows Table 1:

processes of materials are processed by two different CNC is in turn. There is a problem of CNC processing sequence. Our first consideration is still the lowest cost and the highest efficiency, So the RGV car movement time is the least and the shortest path. Based on the existence of different CNC

processing tool types, command execution has a number of other constraints.

With the aid of genetic algorithm [5-8], we establish a dynamic scheduling model for the shortest path in the case of no fault in two processes.

First, set the parameter set:

Maximum iterated algebra: $G = 1000$

Cross rate: $P_c = 1$

Variability rate: $P_m = 0.04$

Coding strategy:

Because there is only one RGV car in the system, the cooperative task is paired, so we can adopt double structure coding and randomly select one, as shown in Table 2 below:

Table 2 Double structure coding

The second process code	1	4	3	6
The first process code	8	2	5	7

The above table is a random coding scheme, first proceeding the first process, starting from No. 8 CNC loading and unloading, then serving No. 2 CNC machine, then serving No. 5 CNC, and finally serving No. 7 CNC machine; in the second process, the No. 1 CNC corresponding to No. 8 semi-processed product, and so on. Until No.6 CNC machine is working on the semi-finished product of No. 7 CNC machine.

Producing initial population:

The improved circle algorithm is used to get a better initial population. For the initial circle generated randomly: Exchanging the order between and. The new path currently is that:

If then a better feasible solution is obtained by modifying the old path with a new path until it can not be modified. Until M feasible solutions are converted into chromosome coding.

Individual objective Function:

Objective function: The total time required for 8 CNC machines to enter and exit tasks in one cycle.

Selection, Crossover, Mutation:

For dual structure coding, the crossover and mutation operators are different from the traditional GA (genetic algorithm) and need to be redesigned.

(1) Crossing Operator: If the traditional crossover operator is used in the dual structure coding, the first line of the new individual will have repetitive values. The method of partial mapping crossover is adopted: two crossing points are randomly selected in the upper test individual, and the matching segments between the two points are exchanged, then the mapping relations determined according to the matching segments will not be exchanged. Part of the restoration of legitimacy. That is the formation of two sons from individuals. The demonstration is shown in Figure 2 below:

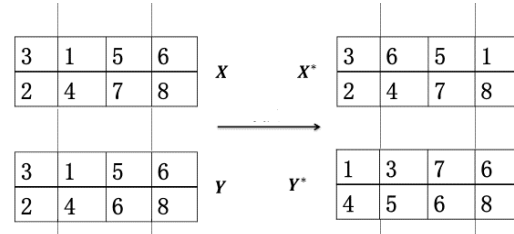


Figure 2 Cross operator process demonstration

(2) The mutation operator: In the dual structure coding, the inverse mutation genetic operator is used, that is, two mutation points are randomly selected for the parent, and the codes between the two points are reordered in reverse order. The demonstration is shown in Figure 3 below:

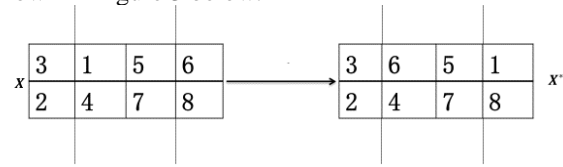


Figure3 Mutation operator process demonstration

(3) Selection Operator: M individuals with the smallest objective function are selected from the parent population and the offspring population to evolve the next generation.

Finally, the optimal double structure coding is obtained, as shown in Table 3:

Table 3 Optimal double structure coding

The second process code	2	4	6	8
The first process code	1	3	5	7

The above table is the ultimate optimal coding scheme: first, the first process, starting from No. 1 CNC loading and unloading, then the No. 3 CNC machine service, then the No. 5 CNC service, and finally the No. 7 CNC machine service; in the second process, the No. 2 CNC corresponding to the No. 1 machine semi-processed products, and so on. Until to No. 8 CNC machine is working on the semi-finished product of No. 7 CNC machine.

In order to describe more vividly the fault-free dynamic scheduling model[6] of the two processes, the upper table car roadmap is optimized, and the final two processes RGV car simulation roadmap is obtained, as follows:

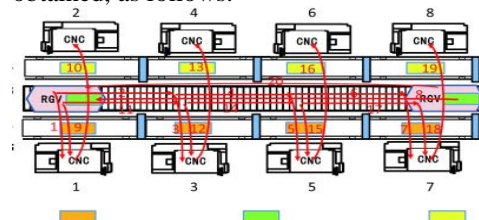


Figure 4 Two-process RGV trolley simulation roadmap

First of all, the first process, starting from the No. 1 CNC loading and unloading, followed by the No. 3 machine services, and then the No. 5 machine services, and finally the No. 7 CNC machine services;

In the second process, with the No. 1 machine semi-processed products corresponding to the No. 2 CNC, that is, the car first waiting at the No. 7, No. 8 machine, when received to No. 1 machine. After the signal indicated by the machine is processed, it moves to 1 or 2 positions. The semi-finished product is placed on the corresponding No. 2 CNC processing table without cleaning, that is, the No. 2 machine is loaded and unloaded. And so on, until No. 8 CNC machine is working on the semi-finished product of No. 7 CNC machine.

4.TWO PROCESS OF MATERIAL PROCESSING FAILURE MODEL

The probability of failure is about 1%. The probability of two CNC faults occurring at the same time is 0.01%. So only one CNC fault occurring at the same time is considered. When the fault occurs, it is considered that the fault CNC is missing, and the RGV will choose the best CNC machine to continue its service according to the real-time adjustment. After the fault CNC is processed manually, the job

Table 4 Fault real-time adjustment route based on two processes

Malfunction location	Real-time adjustment of route
CNC1	Route:CNC3->CNC5->CNC7->CNC3, 4->CNC5, 6->CNC7, 8->CNC1, 2
CNC2	Route:CNC1->CNC3->CNC5->CNC7->CNC3, 4->CNC5, 6->CNC7, 8->CNC1, 2
CNC3	Route:CNC1->CNC5->CNC7->CNC1,2->CNC5, 6->CNC7, 8->CNC1, 2
CNC4	Route:CNC1->CNC3->CNC5->CNC7->CNC1, 2->CNC5, 6->CNC7, 8->CNC1, 2
CNC5	Route:CNC1->CNC3->CNC7->CNC1, 2->CNC3, 4->CNC7, 8->CNC1, 2
CNC6	Route:CNC1->CNC3->CNC5->CNC7->NC1, 2->CNC3, 4->CNC7,8->CNC1, 2
CNC7	Route:CNC1->CNC3->CNC5->CNC1,2->CNC3, 4->CNC5, 6->CNC1, 2
CNC8	Route:CNC1->CNC3->CNC5->CNC7->NC1, 2->CNC3, 4->CNC5, 6->CNC1, 2

5. SIMULATION

Because the queuing theory only applies to the case where the arrival rate of each customer is the same, that is, the machine has the same production time. That is, queuing theory [8] can be used to evaluate a process model. The queuing model is a finite source queuing model.

The following indicator functions are established:

The probability of RHV idle:

The average number of machine tools waiting for RHV is:

RHV to machine tool loading and unloading capability: emulation: Input the values of respectively: (10, 6) and (10, 8) two sets of data using MATLAB queuing simulation results, as follows in Figure 5:

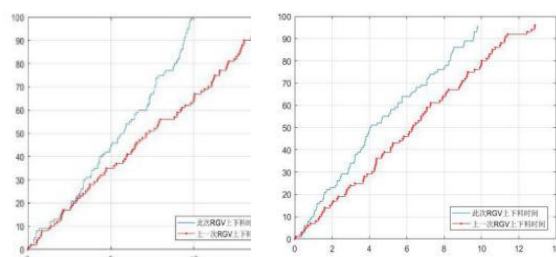


Figure 5 Simulation result diagram

sequence will be added immediately, and the signal will be sent to the RGV again, and the requirement of loading and unloading will be put forward. If the RGV is in a waiting state, the repaired CNC will be served immediately. If the RGV is in a working state, the CNC will be served at the end of the working state. Because there is always waiting time for the RGV, when the CNC is repaired, it will go into a fault-free process to work, waiting for the next failure.

When a machine breaks down at a certain time, the real-time adjusting route may be uncertain. We also use genetic algorithm [7] to establish the shortest path model for two process material processing failure. The objective function is the total time for 8 CNC machines to enter and exit tasks in one cycle, which is. Based on the fault-free optimal roadmap, real-time adjustment will be made in the optimal route when the fault occurs, to achieve the least waste of time and the highest efficiency. The roadmap for failure is described in Table 4 below:

Image analysis: The waiting time for the replacement of RGV is the vertical distance between two lines. The result shows that when is the same, the bigger is, which means the higher the number of loading and unloading per unit time of RHV, the higher the efficiency of the whole system.

REFERENCES

- [1] Chen Hua. Model and algorithm for 2-RGV scheduling problem based on partition method. *Industrial Engineering and Management*, 2014, 19 (6): 70-77.
- [2] Tian Jingwen, Kong Zhuichao, Gao Meijuan. An improved hybrid algorithm for vehicle routing. *Computer Engineering and Applications*, 2014, 50 (14): 58-63.
- [3] Qiao Fei, Wu Qidi. Real-time scheduling and fault scheduling of RGV in SJ-FMS. *Combined Machine Tool and Automatic Processing Technology*, 1995, (03): 39-43.
- [4] Liu Yongqiang. Research on dynamic scheduling of RGV based on genetic algorithm. *Hefei University of Technology*, 2012.
- [5] Yin Zuohai, Qiu Hongze, Zhou Wanli. Genetic algorithm based on improved mutation operator for

flexible job shop scheduling. *Computer System Applications*, 2009, 18 (10): 156-159.

[6] Wang Junqiang, Guo Yinzhou, Cui Fudong, et al. Open shop scheduling optimization based on adaptive genetic algorithm based on diversity enhancement. *Computer Integrated Manufacturing Systems*, 2014, 20(10): 2479-2493.

[7] Wu Yanming, Liu Yongqiang, Zhang Dong, Zhao

Han. Research on RGV dynamic scheduling based on genetic algorithm. *Lifting and transportation machinery*, 2012, (06): 20-23.

[8] Chen Jie. Design and implementation of shop-in-process management system based on queuing theory algorithm. Zhejiang University of Science and Technology, 2017.

Swarm Intelligence Application in Cognitive Radio

Zhang Lin, Qi Weiyi, Shen Hai*

College of Physics Science and Technology, Shenyang Normal University, Shenyang, 110034, China

*E-mail:shen.hai@163.com

Abstract: With the rapid development of radio communication, the contradiction between the increasing spectrum demand and the limited spectrum resources is becoming more and more severe. Cognitive Radio (CR) emerged as a valid solution to the shortage of spectrum resources. Firstly, this paper presents the concept of CR, and the key technologies of CR are introduced in detail. The key technology of CR includes spectrum sensing, spectrum allocation and spectrum decision, then, aiming at the three key technologies, this paper introduces the research results of several swarm intelligence algorithms in recent years. Finally, combining the current situation of research in CR, the future application of swarm intelligence in CR is prospected.

Keywords: Cognitive Radio; spectrum sensing; spectrum allocation; spectrum decision

1. INTRODUCTION

Wireless spectrum resource is a very precious, scarce and important resource. At present, spectrum resources are distributed and managed by government. With the growing demand of radio communication, the available spectrum resources become less and less. In order to achieve the goal of full utilization of the spectrum resources, Cognitive Radio technology was born.

In 1999, Cognitive Radio (CR) was proposed by Joseph Mitola. It is an intelligent wireless communication technology; it can find and utilize the idle spectrum. In order to improve the spectral efficiency, it also can adjust the communication parameters according to the perceived external environment.

In recent years, Swarm Intelligence(SI) algorithm is used for solving complex problems. Many researchers have applied the SI algorithm to solve CR problems. The following content of this paper is arranged as

Table 1. Application of swarm intelligence algorithm in CR

Algorithm	Spectrum Sensing	Spectrum Allocation	Spectrum Decision
GA (Genetic Algorithm)	[4] [20]	[9] [22] [24] [26]	[14]
PSO (Particle Swarm Optimization)	[3] [27] [28]	[7] [8]	[12] [16]
ACO (Ant Colony Optimization)		[9]	[15] [17]
BCO (Bee Colony Optimization)		[10] [23] [25]	[18]
SFL (Shuffled Frog Leaping)	[1] [2] [5]	[29]	
ABC (Artificial Bee Colony Optimization)	[19] [21]	[24]	[11]
CSA (Clonal Selection Algorithm)		[6] [13]	[13]
BFO (Bacterial Foraging Optimization)		[30]	

3. Spectrum Sensing

The survey found that the actual utilization of some

follows. Section 2 introduces the cognitive cycle and use a table to show the application of SI on CR. Section 3, Section 4 and Section 5 review some application of SI on spectrum sensing, spectrum allocation and spectrum decision in detail, respectively. In the end, makes a conclusion for the whole paper and put forward the further work.

2. Cognitive Radio and Swarm Intelligence

Compared with traditional static allocation, CR technology can effectively solve the current serious spectrum shortage problem. In fact, CR is a dynamic spectrum allocation strategy, cognitive users can dynamically access idle spectrum (spectrum hole), without prejudice to the normal communication of authorized users. As shown in Fig.1, CR mainly includes spectrum sensing, spectrum allocation and spectrum decision, these three parts form the cognitive cycle.

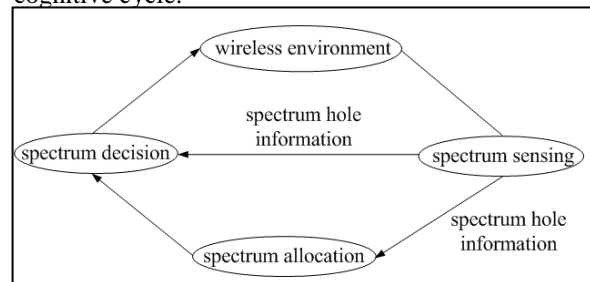


Figure1. Cognitive cycle

(1)Spectrum sensing is the premise of CR system, mainly sense spectrum hole.

(2)Spectrum allocation is to select the suitable spectrum from the perceived spectrum.

(3)Spectrum decision is used to adjust the working parameters used in communications.

The detailed application of some swarm intelligence algorithms in each part of CR can be seen from Tab. 1.

authorized spectrum is very low, there may be a large number of idle spectrum at a certain time. As the first

link of CR technology, spectrum sensing can accurately detect idle spectrum that not used by authorized user, without affecting the communication effect of authorized users. In this way, cognitive users can take full advantage of these idle spectrum for communication.

The existing spectrum sensing methods usually can be classified as the following two kinds: single node spectrum sensing and cooperative spectrum sensing, a detailed classification is shown in Fig.2.

Single node spectrum sensing method appeared

earlier, and the processing technology involved is relatively mature. But single node spectrum sensing method is easily affected by the impact of the shadow effect, multi-path fading, and the perceived results are not very reliable.

The cooperative spectrum sensing can promote the detection property in the above situations. Therefore, it is becoming the hot research question of the spectrum sensing technology, and a variety of algorithms to optimize the spectrum sensing are also created.

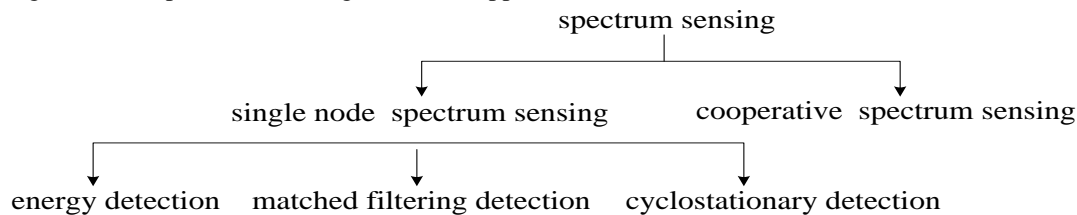


Figure 2. Classification of spectrum sensing technology

3.1 Spectrum sensing based on a modified shuffled frog leaping algorithm

Zheng Shilian modified the method of updating the mobile mode, based on the modified shuffled frog leaping algorithm (SFLA), they proposes a cooperative spectrum sensing method for CR [1]. The modified algorithm is superior to the traditional algorithm, it can obtain higher detection probability and more stable than the traditional algorithm.

3.2 Spectrum sensing based on a quantum frog leaping algorithm

Li Lingyun introduces quantum computation into the traditional frog leaping algorithm, then presents quantum frog leaping algorithm[2]. Compared with the classical SI, the convergence speed of quantum frog leaping algorithm is faster, and convergence precision is higher than before, quantum frog leaping algorithm has great advantages and development potential in the research of spectrum sensing.

3.3 Spectrum sensing based on a modified particle swarm optimization

Yue Wenjing studies the improved PSO, and introduces acceleration variables into the particle position, thus a particle swarm optimization algorithm with accelerated food guidance is formed [3].

In different environments and conditions, on the basis of accelerated food guide, particle swarm optimization algorithm can obtain better spectrum sensing probability, and has better advantages than the traditional particle swarm optimization algorithm.

3.4 Spectrum sensing based on genetic algorithm

Deng Lilin uses GA to solve the optimal threshold vector, and optimize the throughput of the cognitive system [4]. The spectrum sensing method is more efficient than the traditional method of spectrum sensing. In the process of spectrum sensing, due to the introduction of GA, the detection probability of spectrum is improving.

3.5 Spectrum sensing based on cultural frog leaping algorithm

On the basis of the intelligent evolutionary principles of SFLA, Gao Hongyuan presents cultural frog leaping algorithm (CFLA). In this method, the leaping equations are designed by knowledge strategy and information communication. The effectiveness of CFLA is verified in solving spectrum sensing problem. CFLA has stronger abilities of exploitation, which may obviously improve the performance of SFLA.

Compared with other spectrum sensing algorithms, the convergence speed of CFLA improves at least 1.5 times and the detection probability of CFLA is also optimized.

4. Spectrum Allocation

As shown in Fig.3, according to the demand and the number of users, etc., spectrum allocation can select the most satisfactory spectrum from the available spectrum. The selected spectrum will be assigned to one or more cognitive users. In this way, cognitive users can share spectrum resources in a reasonable and fair way.

Allocation strategy can effectively avoid authorization clash between authorized users and non-authorized users. It can improve the flexibility of wireless communication, and share wireless spectrum resources fairly.

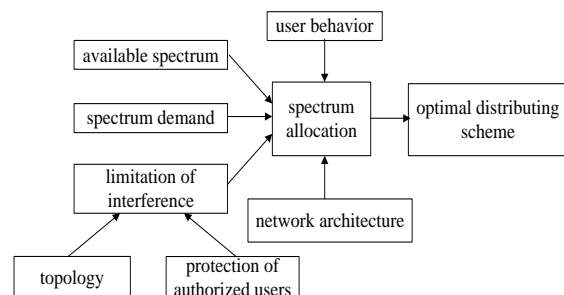


Figure3. Description of spectrum allocation

There are four common spectrum allocation models, which are interference temperature model, auction

bidding model, game theory model and graph theory model.

In the four mentioned models, the interference temperature model depends on the accuracy of interference temperature estimation. Once the interference temperature estimation is not correct, cognitive users will interfere with authorized users.

In the auction bidding model, a spectrum can only be obtained by one user, and the chance of cognitive users to obtain the available spectrum is reduced.

Compared with the above two models, the performance of game theory model is improved, but its implementation principle is more complicated.

The graph theory model abstracts the actual network scene into the network topology graph, which is widely used in the solution of spectrum problem at present. Many optimization algorithms used to deal with spectrum allocation problems are implemented on the basis of this model.

Spectrum allocation technology is an important part of the spectrum sharing mechanism. It relates to whether cognitive system can make full use of idle spectrum and promote the reliability and efficiency of communication.

It is found that the traditional static spectrum allocation method can reduce the use efficiency of the spectrum. Therefore, it is of great significance to reasonably allocate the idle spectrum.

4.1 Spectrum allocation based on immune clone selection algorithm

Chai Zhengyi put immune clone selection algorithm into spectrum allocation, and then on the basis of immune clone selection computation, taking into account the different needs of different users, a method of spectrum allocation in CR networks based on chaotic quantum clone optimization is proposed [6]. The algorithm makes full use of the advantages of chaos search, quantum computation and immune clone algorithm. It is found that the improved algorithm is superior to other spectrum allocation algorithms, and can achieve the maximization of network efficiency.

4.2 Spectrum allocation based on particle swarm optimization and genetic algorithm

Sun Haijian introduces the crossover and mutation of GA into particle swarm optimization [7], at the same time, the linear inertial weight function is also introduced, this improved method can avoid the limitation of the two algorithms, and the searching precision and convergence speed of the algorithm are significantly raised.

4.3 Spectrum allocation based on catfish effect particle swarm optimization algorithm

Zhuo Zhihong introduces "catfish effect" to the traditional particle swarm optimization algorithm [8]. The Catfish particle swarm optimization algorithm can effectively solve the spectrum allocation problem in CR, the ability of finding the optimal solution is stronger, and make the limited

spectrum resources be effectively utilized, and meet the application requirements of CR.

4.4 Spectrum allocation based on genetic ant colony optimization

Based on dynamical combination of GA and ant colony algorithm, Wu Xuan proposes a spectrum allocation method [9]. GA is used to produce initial solutions, these initial solutions are converted by transitive strategy, and thus, ant colony algorithm can obtain initial pheromone distribution of at the best time. Compared with the color sensitive graph coloring algorithm, this algorithm is significantly better, and the fusion algorithm can achieve the maximization of network benefits.

4.5 Spectrum allocation based on membrane-inspired quantum bee optimization

Based on quantum bee colony theory and membrane computing, Gao Hongyuan and others propose a new optimization algorithm called membrane-inspired quantum bee optimization. The multi-objective optimization algorithm is designed by the communication rules between membranes; what's more, it can solve both single objective and multi-objective optimization problems at the same time.

Compared with color-sensitive graph coloring algorithm, GA, PSO and etc., this new spectrum allocation method can search the global optimal solution of single objective. It is superior to existing spectrum allocation algorithms. At the same time, it also can obtain the optimal Pareto front solutions.

5. Spectrum Decision

As shown in Fig.4, according to the current wireless environment, the parameters are optimized by spectrum decision. To adapt wireless spectrum environment automatically, cognitive users need to get the optimal parameter configuration. The core idea of spectrum decision is to dynamically configure the radio operating parameters, so as to obtain the optimal use of limited radio spectrum.

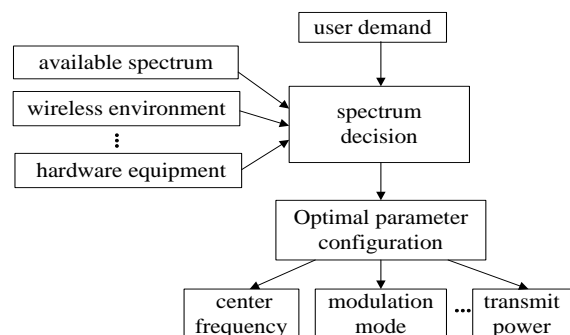


Figure4. Description of spectrum decision

5.1 Spectrum decision based on a binary artificial bee colony algorithm

In spectrum decision progress, artificial binary bee colony algorithm proposed by Li Xinbin is used to achieve a parameters adjusting capability adaptive

[11]. Firstly, the CR decision problem is converted to a multi-objective function optimization problem, and then, to become a simple single objective function optimization problem, the complex multi-objective function is normalized by the weighted sum method. The search efficiency, convergence speed and accuracy of this method are better than binary particle swarm optimization algorithm. In practical applications, it can meet the requirements of wireless environment or user's requirements.

5.2 Spectrum decision based on a binary quantum particle swarm optimization

Due to the introduction of quantum concepts, binary quantum particle swarm optimization algorithm proposed by Zhang Jing has the characteristics of nonlinear and uncertainty [12]. Compared with the traditional spectrum decision algorithm, this algorithm can automatically adjust the communication parameters.

The improved algorithm has the characteristics of fast convergence, good stability and high average fitness. In the complex and changeable wireless spectrum environment, it can quickly make decision, and has a strong self-adaptive ability.

5.3 Spectrum decision based on a chaos quantum clonal algorithm

The immune algorithm has fast convergence speed and optimization ability, chaos search has ergodicity and quantum computing has high efficiency, Chai Zhengyi uses these characteristics to analyze and adjust the decision parameters of CR, and then optimizes the decision engine. In this way, chaos quantum clonal algorithm is presented [13].

The convergence speed of the algorithm is faster and the optimization ability is stronger, and higher target function values can be obtained. The result of parameter adjustment is same to the optimization target, and the other objective function values can be taken into account, so it is suitable for the spectrum decision with a high real-time requirement.

5.4 Spectrum decision based on a modified multi-objective genetic algorithm

Based on cloud theory, Yang Shengyao proposes the method of multi-objective GA [14]. At the same time, Yang Shengyao introduces the population adjustment technology into the algorithm, further promoted the convergence speed and optimization performance of this method can better meet the requirements of real-time communication of CR system.

5.5 Spectrum decision based on binary ant colony simulated annealing algorithm

Qin Chunling introduces the simulated annealing (SA) algorithm into the binary ant colony optimization (BACO) algorithm [15], BACO has advantage of rapid optimization, and SA has the characteristic of probability jumping, the combination of the two can effectively avoid the defect of falling into local optimization result of BACO.

In the aspect of global search ability and average fitness, binary ant colony simulated annealing algorithm has obvious advantage. The algorithm adapt sets the pheromone volatilization factor, the number of isothermal iterations of simulated annealing algorithm is adjusted adaptively, and thus, the disadvantage that parameters are difficult to set can be avoided.

6. CONCLUSIONS

This paper reviews the application of swarm intelligence methods in CR. But at present, some swarm intelligence methods applied in CR are mostly in the stage of theory research, the engineering application has yet to be verified, at the same time, the optimization performance of the algorithms mentioned above also need to be further improved. In addition, the further work of swarm intelligence in CR as follows:

(1) Most of the existing optimization algorithms for CR are aimed at static environment, that is, during one execution of the algorithm, the state of primary user, cognitive user and available spectrum does not change. Researchers should strengthen the study of dynamic model, when one of factors changes, the allocation of idle spectrum can be changed quickly, the efficiency of spectrum utilization can be further improved.

(2) Combining the swarm intelligence algorithm with other optimization methods, such as fuzzy control, prediction mechanism and artificial neural network algorithm, etc. Through the algorithm fusion, the adaptive and learning ability of the CR system can improve continuously. After many studies, the changing law of the wireless spectrum environment can be summed up in the cognitive system. When the information of the wireless environment perceived at a certain time satisfies the rule, the CR system can respond immediately, so as to promote the running efficiency of the system.

ACKNOWLEDGMENT

The National Natural Science Foundation of China is the supporter to the research carried out in this paper (Grant No. 61502318).

REFERENCES

- [1] S. Zheng, C. Lou, X. Yang, Cooperative spectrum sensing for cognitive radios based on a modified shuffled frog leaping algorithm, *ACTA PHYSICA SINICA*, 2010, 59(05):3611-3617.
- [2] L. Li, Spectrum sensing technology research based on quantum swarm intelligence optimization algorithm, Huazhong University of Science & Technology, 2015.
- [3] W. Yue, Y. Wei and Z. Chen, Accelerating food guided particle swarm algorithm in application of cooperative spectrum sensing, *Application Research of Computers*, 2018, 35(07):2103-2105+2109.
- [4] L. Deng, C. Zang, X. Zhou, K. Wen, Application of genetic algorithm on spectrum sensing of cognitive

- radio system, Application of electronic technology,[3]2010,36(03):113-116.
- [5]H.Gao,W.Cui, Cultural frog leaping algorithm and its applications for spectrum sensing,Journal of Central South University (Science and Technology),2013,44(09):3723-3730.
- [6]Z. Chai and F. Liu,Spectrum allocation of cognitive wireless network based on immune clone selection optimization, Journal on Communications, 2010,31(11):92-100.
- [7]H. Sun, Research on spectrum allocation based on particle swarm optimization algorithm and genetic algorithm,JILIN UNIVERSITY.CHINA, 2015.
- [8]Z. Zhuo, Spectrum allocation of cognitive radio system based on catfish effect particle swarm optimization algorithm, Video Engineering, 2014,38(07):145-148+189.
- [9]X. Wu, W. Sun and J. Lu, Cognitive radio spectrum allocation based on genetic ant colony optimization,communications technology,2015,48(11):1265-1269.
- [10]H.Gao,C.Li,Membrane-inspired quantum bee colony algorithm for multiobjective spectrum allocation,Acta Phys.Sin.,2014,63(12):460-469.
- [11]X. Li, A. Shi,Cognitive radio decision engine based on binary artificial bee colony algorithm,Journal of Yanshan University, 2012,36(05):439-444.
- [12]J. Zhang, Z. Zhou, W. Gao, L. Shi and L. Tang, Cognitive radio decision engine based on binary quantum particle swarm optimization,Chinese Journal of Scientific instrument,2011,32(02):451-456.
- [13]Z. Chai,Immune optimization based on spectrum decision-making and resource allocation in cognitive wireless network, Xi' an Electronic and Science University, 2012.
- [14]S. Yang, Cognitive radio decision engine based on multi-objective genetic algorithm, Dalian University of Technology, 2011.
- [15]C.Qin,Research on cognitive engine and decision-optimization strategy, University Of Chongqing, 2012.
- [16]X. Tan, H. Zhang and J. Hu , A hybrid architecture of cognitive decision engine based on particle swarm optimization algorithms and case database, Ann. Telecomm.,2014,69:593 - 605.
- [17]N. Zhao, S. Li and Z. Wu,Cognitive radio engine design based on ant colony optimization,Wireless Pers Commun,2012,65:15 - 24.
- [18]H. Gao and C. Li,Membrane-inspired quantum bee colony optimization and its applications for decision engine. Cent,South Univ.,2014,21:1887 - 1897.
- [19]X. Li, L. Lu, L. Liu, G. Li and X. Guan, Cooperative spectrum sensing based on an efficient adaptive artificial bee colony algorithm, Soft Comput, 2015,19:597 - 607.
- [20]D. Ren, J. Ge and J. Li, Secondary user selection scheme using adaptive genetic algorithms for cooperative spectrum sensing under correlated shadowing, Wireless Pers Commun,2013,71:769 - 788.
- [21]Y. Hei, W. Li, W. Fu, X. Li, Efficient parallel artificial bee colony algorithm for cooperative spectrum sensing optimization,Circuits Syst Signal Process,2015,34:3611 - 3629.
- [22]J. Elhachmi and J. Elhachmi,Cognitive radio spectrum allocation using genetic algorithm,J Wireless Com Network,2016.
- [23]GZ Marković, Routing and spectrum allocation in elastic optical networks using bee colony optimization,Photonic Network Communications,2017,34:356 - 374.
- [24]J. Arun and M. Karthikeyan,Optimized cognitive radio network (CRN) using genetic algorithm and artificial bee colony algorithm,Cluster Comput,2018:1 - 10.
- [25]W. Lu, Z. Quan, Q. Liu, D. Zhang and W. Xu,QoE based spectrum allocation optimization using bees algorithm in cognitive radio networks, Algorithms and Architectures for Parallel Processing,2015:327-338.
- [26]Y. E. Morabit,F. Mrabti and E. H. Abarkan,The allocation in cognitive radio network: combined genetic algorithm and on/off primary user activity models, Advances in Ubiquitous Networking2,2016:3-14.
- [27]Y. Vineetha, E. S. Gopi and S. Mahammad,Particle swarm optimization based hmm parameter estimation for spectrum sensing in cognitive radio system,Studies in Computational Intelligence,2018,777:96-103.
- [28]J. Lu, M. Huang and J. Yang,A novel spectrum sensing method based on tri-stable stochastic resonance and quantum particle swarm optimization,Wireless Personal Communications,2017,95:635 - 2647.
- [29]Z. Qin, J. Liu, Z. Chen, L. Guo and L. Huang,Spectrum allocation based on gaussian - cauchy mutation shuffled frog leaping algorithm, Lecture Notes in Computer Science,2016,10065:266-277.
- [30]Y. Li, P. Wan, Y. Wang, Q. Deng and J. Yang,Cognitive radio spectrum allocation based on binary bacterial foraging optimization algorithm, Computer Science,2013,40:49-52+58.

Multi-ship Collision Avoidance Optimization based on Ship Collision Avoidance System

Huanhuan Xu

Information processing institute, Shanghai Maritime University (SUM), Shanghai, 201809, China

E-mail: 1982299154@qq.com

Abstract: This paper focuses on the formulation of a optimization-Parallel Decision Making Module that can facilitate intelligent collision avoidance realize in ocean navigation systems, while respecting the Convention on the International Regulations for Preventing Collisions at Sea rules and regulations of collision avoidance (COLREGs). The optimization in this work consists of expert system and neural network. It can optimize the results of the parallel decision making module which is the part of collision avoidance system (CAS) to make collision avoidance trajectory more secure and effectively. Further, the paper presents an optimized collision avoidance system (OCAS) that is capable of making optimal decision in multiple parallel collision avoidance decisions regarding several target vessel collision conditions, and those optimization decisions are generated in parallel decision making module to avoid complex collision situations in ocean navigation.

Keywords: expert system, optimized intelligent transportation, intelligent vehicle control, marine vehicle control, optimized ship collision avoidance, neural network.

1. INTRODUCTION

Intelligent ship collision avoidance system is a system to realize the ship automatic collision avoidance function, which plays a vital role in the Ship's Sailing Automation. In conventional ocean navigation systems, the most important factor is still human guidance, and wrong judgment and miss operations by humans have resulted in many human casualties and environmental disasters[1].

The studies of maritime collisions[2] indicate that 75%–96% of marine accidents and casualties are caused by some types of human errors. Therefore, as illustrated by[3], In the future, smart ships will be developed along the path from "just a few crew members" to "shore remote control" to "fully automated driving". Further, the replacement of human inference by an intelligent decision formulation process resulting in feasible actions for navigation and collision avoidance could reduce maritime accidents.

The IMO requires all ships to comply the Convention on the International Regulations for Preventing Collisions at Sea (COLREGs) [4]. The COLREGs [5] include 38 rules that have been divided into Part A (General), Part B (Steering and Sailing), Part C (Lights and Shapes), Part D (Sound and Light signals), and

Part E (Exemptions). There are also four Annexes containing technical requirements concerning lights and shapes and their positioning, sound signaling appliances, additional signals for fishing vessels when operating in close proximity, and international distress signals. However, the main focus in this study is the COLREGs Part B, concerning Steering and Sailing rules. As for the reported data of maritime accidents, 56% of major maritime collisions include violations of the COLREGs rules and regulations[5].

This paper focuses on solving the optimal path of collision avoidance when multiple ships meet. Ships will perform similar judgment and operation when multiple ships meet, but this is not the optimal judgment and operation. This paper analyzes the complex scene of multi-vessel encounter, puts forward the shortcomings of existing solutions, and puts forward the optimization algorithm of collision avoidance and corresponding parallel decision making module based on expert system.

The organization of this paper is as follows. Section II analysis of multi-ship collision avoidance scene. A optimized sequential action formulation module is presented in Section III. Section IV contains a detailed description of implementation and computational simulations. Finally, conclusions and future work are presented in Section V.

2. ANALYSIS OF MULTI-SHIP COLLISION AVOIDANCE SCENE

Existence analysis of global optimal solution

A. By changing the ship speed, the ship collision avoidance decision is affected

A conclusion can be drawn from the COLREGs: the generation of collision avoidance track of a ship is closely related to its course and speed, which affects the decision-making of collision avoidance track to a great extent. Firstly, the effect of ship speed on trajectory planning for collision avoidance is considered[6]. Since the behavior of the stand-on ship and the give-way ship in the encounter is different, if two ships of the same type, then the division of the stand-on ship and the give-way ship is based on the relative speed of the two ships. A ship of relatively fast speed is a stand-on ship, while a ship of relatively slow speed is a give-way ship.

encountering the situation also affects the ship's trajectory planning. Since the speed of ship O is different from that of the target vessel, two completely different collision avoidance trajectories are

generated[7].

From the COLREGs, it can be found that different collision avoidance decisions resulted from the different course of the target ship. However, the ship's course is generally along the planned course before the occurrence of the encounter situation, so the ship will not change its course before the occurrence of the encounter, but will make the corresponding course change according to the CAS system after the occurrence of the encounter situation[8]. The above analysis shows that the ship can change its speed to affect the ship collision avoidance decision.

B. Proof of existence of optimal collision avoidance track

Three measurements of the optimal collision avoidance trajectory are given below:

Under the premise of satisfying the COLREGs, the collision avoidance of a ship should pass as little as possible through the course to be passed by the target ship[9].

Under the premise of meeting collision avoidance, the ship steering Angle is as small as possible[10].

Under the premise of meeting collision avoidance, the ship's steering angle change operation should be as little as possible.

The optimal collision avoidance track of a ship does not have to meet these three standards. In some cases, there is no optimal solution to ship collision avoidance trajectory. In other cases, the ship's trajectory of collision avoidance can only meet one or two standards criteria[11]. In other cases, the optimal collision avoidance track of the ship fully conforms to the above three standards. This part will be explained in more detail in the fourth part[12].

3. PARALLEL DECISION-MAKING MODULE

A. The deficiency of the existing ship automatic collision avoidance system and the improved automatic collision avoidance system

The reason why CAS does not have the feature of seeking the optimal trajectory of collision avoidance is that it does not have the logic unit to find the optimal trajectory of collision avoidance and it does not cooperate to generate the data flow of the optimal trajectory of collision avoidance. Therefore, in order to find the optimal collision avoidance trajectory, it is necessary to make structural changes to CAS[13]. Fig. 1 is the improved CAS. The improved CAS is called as Optimized collision avoidance system (OCAS). The difference between OCAS and CAS is reflected in two places: First, the CRA module transfers the collision time to the PDM module and the sequential action formulation module only receives data from PDM. The output data content of the CRA module remains unchanged, except that all output values are passed to the PDM module[14]. The reason for this modification is that the time passed to the sequential action formulation module should not be the time of ship collision but the time of ship operation[15]. Therefore, this time should be computed by the PDM module and

passed to the SAF module, not by the CRA[16]. Secondly, in the PDM module, the optimal collision avoidance track selection unit needs to be added. This unit uses expert system to solve the optimal collision avoidance trajectory internally. Optimal collision avoidance track selection unit is the main reason why OCAS is superior to CAS.

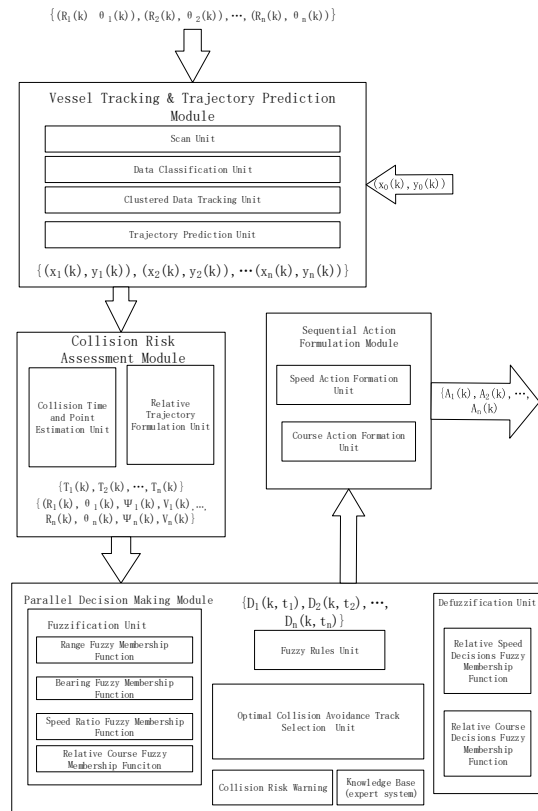


Figure.1 Optimized collision avoidance system (OCAS)

B. The implementation logic of the optimal collision avoidance track selection unit is:

Step 1: sort the target ship according to its distance from own ship. $k = 1, 2, \dots, n$;

Step 2: write the three measurement criteria of the optimal collision avoidance track as the mathematical expression about collision time (t_k), collision location (x_{ck}, y_{ck}), relative course (θ_k), relative speed (v_{rk}), relative position (x_{rk}, y_{rk}) of the target ships as the evaluation function of collision avoidance track:

Standard1: $\alpha = f(t_k, x_{ck}, y_{ck}, \theta_k, v_{rk}, x_{rk}, y_{rk});$
(1)

Standard2: $\beta = \omega(t_k, x_{ck}, y_{ck}, \theta_k, v_{rk}, x_{rk}, y_{rk});$
(2)

Standard3: $\gamma = \varphi(t_k, x_{ck}, y_{ck}, \theta_k, v_{rk}, x_{rk}, y_{rk});$
(3)

These three formulas are explained in the following section.

Step 3: use the expert system to connect the ship to $i, (i = 1, 2, \dots, n)$ all collision avoidance routes of the target ships are exhaustive, forming the feasible domain of collision avoidance of the ship in the current

$$\text{environment at the current moment: } S(k) = \sum_{j_1=1}^{J_1} \sum_{j_2=1}^{J_2} \sum_{j_3=1}^{J_3} \dots \sum_{j_k=1}^{J_k} x_1(j_1) x_2(j_2) x_3(j_3) \dots x_k(j_k) \quad (4)$$

The feasible solutions need to be represented in matrix

$$\text{form for easy input: } A = \begin{bmatrix} x_1(1) & \dots & x_k(1) \\ \vdots & \ddots & \vdots \\ x_1(J_1) & \dots & x_k(J_k) \end{bmatrix} \quad (5)$$

The $x_j(j_i)$ expression the vessel uses j ith kind of collision avoidance scheme when the vessel avoids collision with the i th target ship. J_i said the vessel has J_i collision-avoidance plans in total in the expert system when the vessel avoids collision with the i th target ship.

Step 4: find the value of evaluation function corresponding to $S(k)$ schemes, the corresponding

$$\text{value matrix is: } y = \begin{bmatrix} v_1 \\ \vdots \\ v_a \end{bmatrix} \quad (6)$$

Step 5: find the corresponding scheme with the minimum evaluation function value, which is the optimal collision avoidance track of the ship;

C. Formulates Three Criteria for Optimal Collision Avoidance Trajectories

The design and realization of the three criteria of optimal collision avoidance track determines the quality of the ship's optimal collision avoidance track. More theoretical research and experimental groping are needed in this part. In this paper, the mathematical expressions of these three standards are given independently and explained in detail:

$$\text{findtar}(\text{num}) = \min \left\{ \sum_{j \in A} \left(\sum_{i=1}^n (\text{targetory}_i(t) == \text{targetory}_{\text{own}}(t + \Delta t)) \right) \right\} \quad (7)$$

$$\text{find}\theta(\text{num}) = \min \{ \sum_{j \in A} \theta(x_j) \} \quad (8)$$

$$\text{findp}(\text{num}) = \min \{ \sum_{j \in A} \rho(x_j) \} \quad (9)$$

$$\text{best_targetory} = \text{best} \{ \text{findtar}, \text{find}\theta, \text{findp} \} \quad (10)$$

Formula (7) represents the following analysis of the collision avoidance track of each ship in the feasible region of ship collision avoidance: If the predicted trajectory of the target ship i at the future time t and the collision avoidance trajectories of the ship's future time $t + \Delta t$ intersection, then the logical expression $\text{targetory}_i(t) == \text{targetory}_{\text{own}}(t + \Delta t)$ will get the value of 1, If it does not intersect, the expression is 0. The values of all the predicted trajectories in the feasible domain are obtained, and then the trajectories in the feasible domain are sorted from small to large, and then the first num trajectories with the minimum function value are extracted to findtar. The function of equation (8) is used to solve the maximum ship steering amplitude of the j th collision avoidance scheme in the feasible domain. After sorting the values from small to large, take out the first num trajectories to give find θ . The function of equation (9) is used to

solve the variant operation times of the j th collision avoidance scheme in the feasible domain. After sorting the values from small to large, take out the first num trajectories to give findp. The function of equation (10) is used to solve the public and sorted collision avoidance track in findtar, find θ and findp, which is the optimal collision avoidance track.

D. The Optimal Collision Avoidance Track Is Implemented In PDM

According to the above analysis, the structure diagram of the optimal collision avoidance track selection unit (OCATS) of PDM can be concretized into Fig.2. The problem of collision avoidance of three ships mentioned above is the research object to analyze the working mechanism of the optimal collision avoidance track selection unit and how to find the optimal collision avoidance track of ships.

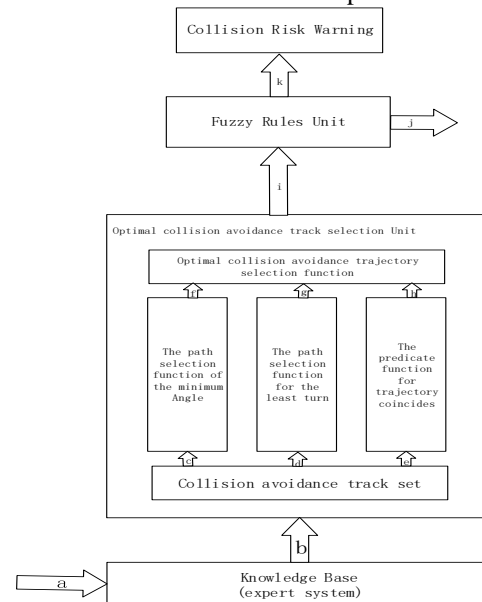


Figure.2 optimal collision avoidance track selection unit

After receiving data from fuzzification unit (data stream a), the expert system selects all collision avoidance trajectories that meet the requirements and sends the results to OCATS unit through data stream b. In OCATS unit, the data stream received first is collision avoidance track set function, which converts data stream b into a matrix that can be processed. And the matrix with data flow c, data flow d and data flow e to the path selection function of the minimum angle, the path selection function for the least turn and the predicate function for trajectory coincides. These three functions compute find θ findp and findtar separately. Then, they are transmitted to optimal collision avoidance trajectory selection function in the form of data flow f, g and h. After finding the optimal collision avoidance track from data flow f, g and h, the function will transfer the optimal collision avoidance track to Fuzzy rule unit through data flow i. The data flow after that is exactly the same as the data flow of CAS.

E. Realization of optimal collision avoidance trajectory

selection function based on neural network

In the case of high ship density, many collision avoidance scenarios do not fully meet the three criteria of optimal collision avoidance trajectory, but only meet one or two of them. Existing problems are as follows: Table.1: The problem of optimal collision avoidance trajectory(CAT: Collision avoidance trajectory: $f(x_1, x_2, x_3)$)

CAT	Standard 1 (x1)	Standard 2 (x2)	Standard 3(x3)
AP ₁	1	1	0
AP ₂	1	0	1
AP ₃	0	1	1
AP ₄	0	0	1

In the above table, 1 means that the standard is met, and 0 means that the standard is not met. There are four feasible collision avoidance trajectories for ship O at time k: AP₁, AP₂, AP₃, AP₄, the above table was obtained after analysis of optimal collision avoidance track selection function of OCATS unit. At this time, optimal collision avoidance track selection function should choose from multiple collision avoidance trajectories that do not fully meet the three standards of optimal collision avoidance trajectory. In this paper, a BP neural network method is proposed to find the optimal collision avoidance track of a ship.

The above problem arises because we assume that the three criteria of the optimal collision avoidance trajectory of a ship have equal weight in the collision avoidance of a ship. What the actual situation is, we still need to analyze according to the actual data. BP neural network construction is as Fig.3:

In the figure above, x_1 , x_2 and x_3 represent the three standard values of the input trajectory, and y indicates whether the trajectory is the best collision avoidance track: 1 means that the input trajectory is the best collision avoidance track, and 0 means that it is non-optimal collision avoidance track. The training steps for the neural network are as follows:

Let's first define a few variables that we will need to use:

- a) L = total number of layers in the network, here $L = 4$;
- b) st = number of units (not counting bias unit) in layer t ;
- c) K = number of output units/classes;
- d) $\delta(t)j$ = "error" of node j in layer t ;
- e) $a(t)j$ activation node j in layer t ;

Given training set

$\{(x(1), y(1)), (x(2), y(2)), \dots, (x(m), y(m))\}$

For time =1 to iterations;

Set $\Delta(t)i,j := 0$ for all (t,i,j) ;

For training example $e = 1$ to m :

Set $a(1) := x(e)$;

Perform forward propagation to compute $a(t)$ for $t = 2, 3, 4$;

Table.2 Matlab simulation of four ship collision avoidance

ST	S	(x,y)	course	CPA	TCC
----	---	-------	--------	-----	-----

Using $y(e)$, compute $\delta(4)=a(4)-y(e)$;

Compute $\delta(t)$ using $\delta(t)=((\Theta(t))T\delta(t+1)).*a(t).*(1-a(t))$;

$\Delta(t) := \Delta(t) + \delta(t) (a(t))T$;

$D(t)i,j := (\Delta(t)i,j + \alpha \Theta(t)i,j) / m$, if $j \neq 0$;

$D^{(t)}i,j := (\Delta^{(t)}i,j) / m$, if $j = 0$;

Then for $t = 2$ to 4, $\Theta(t) = \Theta(t) - \beta D(t)$;

time = time + 1;

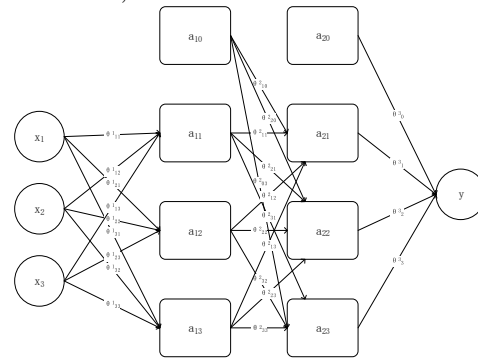


Figure.3 BP neural network

4. COMPUTATIONAL SIMULATIONS

The computational simulations have been implemented on a MATLAB software platform. It is assumed that the target vessels are moving with the constant course and speed conditions and honor any navigation rules and regulations of the sea. The constant course and speed conditions are assumed to keep the consistence in the collision situation.

A. Matlab a implemented logical description of the simulated code

The Matlab simulation of this experiment is from the data flow b in Fig.2 to the data flow i. The data provided by data stream b is theoretically provided by expert system, but since there are few theories in this field and the implementation effect is poor, this part of data is real data provided by Institute of Marine science, Shanghai maritime university. Then, the optimal collision avoidance trajectories in data stream i are compared with that provided by reality. If the two optimal collision avoidance trajectories are the same, the experiment is successful; if the two optimal collision avoidance trajectories are different, the experiment fails. Since the result of Matlab simulation is abstract data, in this part, experimental results will be presented in two forms in order to better understand the simulation results of Matlab. First, only the results of some successful experiments were shown in the form of a table. Then, two successful Matlab simulation cases were listed in the form of a table, which were the data flow i, and explained the results of the experiment with the collision avoidance diagram. The experiment is four-vessel collision avoidance, and there are three experimental scenes.

B. Search for the optimal collision avoidance track for four ships

1	T1	(1.4,0.93)	89.7°	(0,0.94)	(0,0)→(0.3,0.75)→(0.8,0.97)→(0.8,1.2)→(1.67,0.97)→(1,1.67)→(1,2.00)
	T 2	(-1,2.3)	120.3°	(0,1.42)	
	T 3	(-1.2,1.4)	90.0°		
	OS	(0,0)	0	(1.31,0.94) (0,1.416)	
2	T 1	(1.4,0.93)	89.7°	(0,0.94)	(0,0)→(0.5,0.94)→(0.5,1.2)
	T 2	(-1,2.3)	120.3°	(0,1.42)	
	T 3	(1.8,1.7)	90.0°		
	OS	(0,0)	0	(0,0.94) (0,1.42)	
3	T 1	(1.4,0.93)	89.7°	(0,0.94)	(0,0)→(0.3,0.94)→(0.3,2)
	T 2	(-1,2.3)	120.3°	(0,1.42)	
	T 3	(1.2,2.3)	51°		
	OS	(0,0)	0	(0,0.94) (0,1.42)	

*(ST: situation; S: ships;(x, y): coordinates(x,y); TCC: The collision course OCATS chose; Tx: Target ship x; OS: own ship)

Fig.4 shows the collision avoidance scene of four ships. Through the CRA module of OCAS, this ship calculated two meeting points, CPA1 and CPA2, with target ship 1 and target ship 2. The encounter point with the target ship 3 shall be determined according to the collision course of own ship. Based on the current

situation, the expert system gives five collision avoidance trajectories, and these five collision avoidance trajectories in Fig.4 are selected after the judgment of OCATS unit. From the existing data analysis, the trajectory is the optimal collision avoidance trajectory in this scene.

Table.3 Simulation results of collision avoidance of four ships are compared with the actual situation

ST	PCAT	OCAT	SRC
1	(0,0)→(0.5,0.94)→ (0.5,1.2)	Y	Y
	(0,0) →(-0.5,0.94) →(0.5,1.42) →(0.5,2)	N	
	(0,0) →(-0.5,0.94) →(0,1.2) →(-0.3,1.42) →(-0.3,2)	N	
	(0,0) →(-0.5,0.94) →(-0.85,1.2) →(-0.5,1.42) →(-0.5,2)	N	
	(0,0) →(-0.5,0.94) →(-0.85,1.2) →(-1.3,1.42)	N	
2	(0,0)→(0.5,0.94)→ (0.5,1.2)	Y	Y
	(0,0) →(-0.5,0.94) →(0,1.3) →(-0.3,1.42) →(-0.3,1.2)	N	
	(0,0) →(-0.5,0.94) →(0,1.3) →(0.3,1.42) →(0.3,1.2)	N	
	(0,0) →(0.8,0.94) →(0.3,1.42) →(0.3,2)	N	
	(0,0) →(1.2,1.42) →(1.2,2)	N	
3	(0,0)→(0.3,0.94) →(0.3,2)	Y	Y
	(0,0) →(-0.5,0.94) →(-0.7,1.42) →(-0.7,2)	N	
	(0,0) →(-0.5,0.94) →(0,1.1) →(0.3,1.42) →(0.3,2)	N	
	(0,0) →(-0.5,0.94) →(0,1.1) →(-0.3,1.42)→(-0.3,2)	N	

(ST: situation; PCAT: provides collision avoidance trajectories; OCAT: If Optimal collision avoidance track(Y/N); SRC: if the simulation results are correct (Y/N))

5. CONCLUSION AND FUTURE WORK

To a large extent, collision avoidance is a test of the pilot's ability and the ship's maneuverability. The optimal trajectory proposed in this paper not only realizes the ship collision avoidance, but also greatly reduces the requirements on the driver's driving ability and ship maneuverability. This makes the ship safer,

smoother and easier to avoid collision. However, the scheme proposed in this paper relies too much on the expert system of ship collision avoidance and the calculation is large. Therefore, the future work should focus on finding a simpler solution to the optimal collision avoidance trajectory algorithm and realizing a more complete expert system.

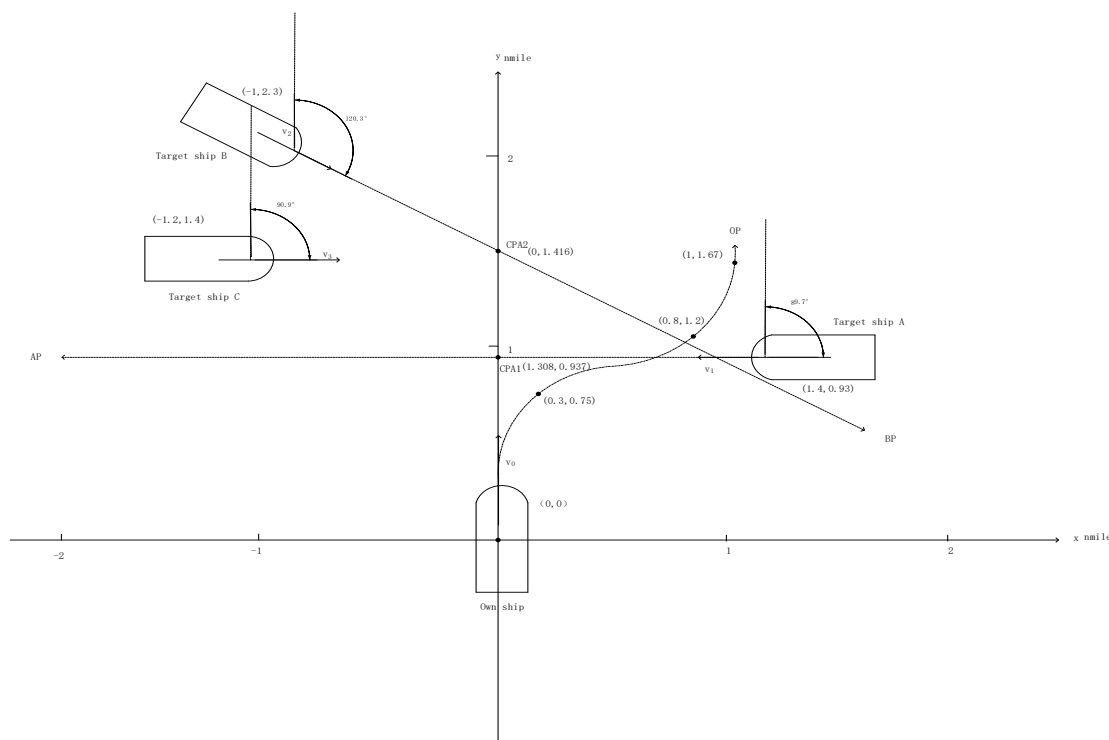


Figure.4 Four ships collision avoidance scene one

REFERENCES

- [1]C. G. Soares and A. P. Teixeira, "Risk assessment in maritime transportation," Reliability Engineering and System Safety. 2001.
- [2]P. Antão and C. Guedes Soares, "Causal factors in accidents of high-speed craft and conventional ocean-going vessels," Reliab. Eng. Syst. Saf., 2008.
- [3]G. N. Roberts, R. Sutton, A. Zirilli, and A. Tiano, "Intelligent ship autopilots—A historical perspective," Mechatronics, 2003.
- [4]R. Śmierzchalski and Z. Michalewicz, "Modeling of ship trajectory in collision situations by an evolutionary algorithm," IEEE Trans. Evol. Comput., 2000.
- [5]P. V. Davis, M. J. Dove, and C. T. Stockel, "A Computer Simulation of Marine Traffic Using Domains and Arenas," J. Navig., vol. 33, no. 2, pp. 215–222, 1980.
- [6]E. M. Goodwin, "A Statistical Study of Ship Domains," J. Navig., 1975.
- [7]N. Wang, "Intelligent Quaternion Ship Domains for Spatial Collision Risk Assessment," J. Sh. Res., vol. 56, no. 3, pp. 170–182, 2012.
- [8]C. G. Källström, "Guidance and control of ocean vehicles," Automatica, 1996.
- [9]T. Statheros, G. Howells, and K. McDonald-Maier, "Autonomous ship collision avoidance navigation concepts, technologies and techniques," J. Navig., 2008.
- [10]L. P. Perera, J. P. Carvalho, and C. Guedes Soares, "Intelligent ocean navigation and fuzzy-Bayesian decision/action formulation," IEEE J. Ocean. Eng., vol. 37, no. 2, pp. 204–219, 2012.
- [11]Y. Sato and H. Ishii, "Study of a collision-avoidance system for ships," Control Eng. Pract., 1998.
- [12]S. L. Kao, K. T. Lee, K. Y. Chang, and M. Der Ko, "A fuzzy logic method for collision avoidance in vessel traffic service," J. Navig., 2007.
- [13]J. Zhang, D. Zhang, X. Yan, S. Haugen, and C. Guedes Soares, "A distributed anti-collision decision support formulation in multi-ship encounter situations under COLREGs," Ocean Eng., vol. 105, pp. 336–348, 2015.
- [14]C. M. Su, K. Y. Chang, and C. Y. Cheng, "Fuzzy decision on optimal collision avoidance measures for ships in vessel traffic service," J. Mar. Sci. Technol., 2012.
- [15]Z. Pietrzykowski and J. Uriasz, "The ship domain -A criterion of navigational safety assessment in an open sea area," J. Navig., vol. 62, no. 1, pp. 93–108, 2009.
- [16]L. P. Perera, J. P. Carvalho, and C. Guedes Soares, "Fuzzy logic based decision making system for collision avoidance of ocean navigation under critical collision conditions," J. Mar. Sci. Technol., vol. 16, no. 1, pp. 84–99, 2011.

Dynamic Modeling of Aerial Refueling

Minghui Qi, Zhenling Tang, Kangkang Jin, Weixuan Wang*

Mathematical Modeling Innovation Lab, North China University of Science and Technology, Tangshan 063210, China

*E-mail: 35365961190@qq.com

Abstract: With the progress of the society, aerial refueling plays an increasingly important role in both transportation of goods and long-distance operations. As mentioned in this paper, the rescue plane flew to the island to transport the seriously injured to the medical base. However, the rescue plane could not carry the maximum fuel capacity to return, so it was obviously necessary to send refueling tankers for aerial refueling. Design a feasible aerial refueling plan to complete the task of rescuing the injured. Firstly, the advantages and disadvantages of several aerial refueling methods are analyzed to determine the final refueling method. Then, in order to save patients as the primary purpose, as far as possible to reduce fuel consumption, fuel consumption calculus model was established. The maximum flying speed of the aircraft was obtained by using the model, and then the relationship between the speed change and fuel consumption was established. These models are used to combine with the actual situation to get the first aid plan with the lowest fuel consumption.

Keywords: Air refueling; Fuzzy comprehensive; Evaluation model

1. INTRODUCTION

Aviation medical care can effectively save medical time and effectively improve the quality of medical treatment. At the same time, it is conducive to further medical treatment in the later stage. It is the safest medical rescue method with an accident rate far lower than that of ground ambulance rescue, and its efficiency advantage is obvious. It can be timely, fast and less restricted by geographical and traffic environment.

Based on the emergency in which there is a seriously wounded person on the island and a large amount of rescue medicine is needed, air rescue is the best choice. However, the rescue aircraft cannot accomplish the task alone, and the fueling partner needs to provide fuel support. However, while designing the fueling plan reasonably and effectively, the fuel consumption requirement should be met as much as possible. Therefore, we need to solve the problem: Design a reliable aerial refueling plan to ensure that the rescue aircraft can successfully complete the mission.

2. ESTABLISHMENT AND SOLUTION OF THE MODEL

This paper establishes a mathematical model to minimize the fuel consumption of refueling aircraft and receiving aircraft within the time range to ensure

that the lives of seriously injured personnel are not lost. The air refueling problem is systematically analyzed as follows:

(1) Establishment of fuel consumption mode

By the principle of the maximum use of oil: if the aircraft returned to the base, there is still residual oil in the tank, that did not reach the maximum voyage distance, in other words, refueling tanker for the oil tanker to add oil to the base when the fuel tank to be empty, at the same time refueling tanker [1] is so.

As every 3%-5% reduction in the total mass of the aircraft will result in a 3%-4% reduction in fuel consumption, the fuel consumption of the aircraft is related to the change in the total mass of the aircraft.

$$\Delta m_{all} \propto C_{oil} \quad (1)$$

Aircraft in flight will be affected by air resistance, so in the flight of aircraft fuel combustion energy, part of the aircraft forward, part of the resistance to overcome the work.

$$\begin{cases} Q = \Delta E_k + W_f = C_{oil} q \\ \Delta E_k = \int_{m_1}^{m_2} \frac{1}{2} v^2 dm_{all} \\ W_f = f \times s \\ f = \frac{1}{2} C \rho S v^2 \end{cases} \quad (2)$$

Here, the average fuel mass consumed per unit time in a certain distance is introduced to obtain:

$$\begin{aligned} Q &= \int_{m_1}^{m_2} \frac{1}{2} v^2 dm_{all} + \int_{t_1}^{t_2} \frac{1}{2} C \rho S v^3 dt + \frac{1}{2} m_1 v^2 = \int_{t_1}^{t_2} \overline{mq} dt \\ \overline{m} &= \frac{2 \rho S v^3 (t_2 - t_1) + m_1 v^2}{4(t_2 - t_1)q - 2v^2} \\ Q &= \int_{t_1}^{t_2} \frac{2 \rho S v^3 (t_2 - t_1)q + m_1 v^2 q}{4(t_2 - t_1)q - 2v^2} dt \end{aligned} \quad (3)$$

In the above formula, ρ for air density value of 1.29kg/m³, S for the plane windward area, because the rescue plane for small aircraft so the corresponding windward area value of 4.6m², the lowest speed of 50km/h. Q is the value range of aircraft fuel calorific value from 41840 to 42890KJ/kg. Due to the lack of specific models of rescue dispatched aircraft, the average calorific value of aircraft fuel is 42365KJ/kg, and the mass of aircraft is 6980kg of "straight 8 helicopter".

(2) Maximum speed of aircraft

since the aircraft type is unknown, the maximum speed of the rescue aircraft cannot be obtained

directly. However, by sorting out the above formulas, we can get the formula for calculating the maximum velocity v :

$$v = \sqrt{\frac{\eta C_{oil} q}{\frac{1}{2} C \rho S s + \frac{1}{2} \Delta m_{all} + \frac{1}{2} m_1}} \quad (4)$$

Combined with the known conditions -- the maximum range of the aircraft is 680 nautical miles and the maximum fuel capacity is 155 kilograms -- the maximum speed of the rescue aircraft can be calculated as 440km/h.

(3) Relationship between aircraft fuel consumption and speed

Table 1 Fuel consumption at the same distance at different speeds

Distance(km)	Time(h)	Speed(km/h)	Fuel consumption(kJ)
300	5	60	2732260.81
	7.5	40	804705.56
	15	20	100366.52
600	6	100	6396759.68
	12	50	785798.78
	24	25	98013.46

As can be seen from the above table, if the aircraft travels the same distance, the greater the speed, the greater the fuel consumption.

(4) Determination of aircraft speed

the prime time for rescuing seriously injured people is six hours [2, 3], so the rescue plane needs to effectively treat the injured in the prime time of rescue, and at the same time, the rescue plane also needs to ensure the least fuel consumption. According to the conclusion drawn in 2.3, the higher the aircraft speed is, the more fuel consumption it will consume. It can be concluded that the aircraft speed under ideal conditions should meet:

$$tv_{ideal} = 2s_{all} \quad (6)$$

According to the calculation, the speed of the rescue aircraft is 205km/h, which is less than the maximum speed of the aircraft. Therefore, this speed can be achieved.

(5) Determination of refueling frequency

The largest rescue aircraft fuel load can support its sailing 680 miles, and base away from the island 615 miles, the distance is 1230 sea miles back and forth, which proves that in order to ensure the rescue aircraft to fly back to base at least on the way, come on time, but if only to rescue aircraft refueling, you will need to meet the relief flight departure to full oil state, and this time go to fill up to rescue the plane [4-7]; The refueling time can only be carried out when the rescue aircraft oil level is close to 0. Such an approach, however, would allow the aircraft to return to base successfully; but the aircraft that supplied the fuel failed to return, as shown in figure 1.

It is planned to meet the condition of the least fuel consumption on the premise of the delivery of relief materials. Firstly, the fuel consumption required to use different speeds through the same distance is discussed.

$$v_1 t_1 = v_2 t_2 = v_3 t_3 = \dots = v_n t_n \quad (5)$$

The specific numerical relationship between aircraft speed and fuel consumption can be obtained by combining with formula (2). Only a few groups of values with representative significance are listed here, as shown in Table 1.

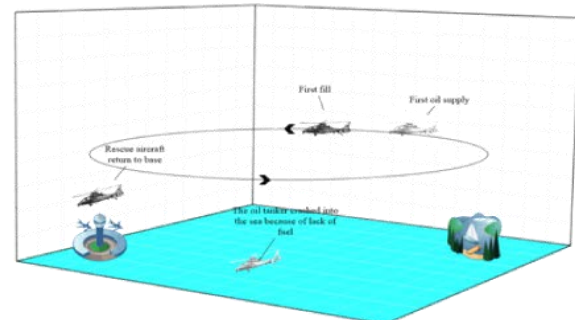


Figure.1 A schematic diagram of one refueling only
Based on the above situation, the rescue aircraft needs at least two oil supplies to ensure that both the oil supply aircraft and the rescue aircraft can fly back to the base. And because rescue aircraft and oil-supply aircraft operating at a known speed in the case of the mission, the total voyage distance of the least fuel consumption.

$$s_{all} \propto Q, v \text{ were established} \quad (7)$$

As a result, refueling the aircraft twice on the way back and forth between the base and the island will encounter the same situation. To meet the requirement of the least fuel consumption, the rescue aircraft needs refueling at least three times. However, after refueling, the oil supply plane is not enough to support the oil supply plane to return to the base, so every time the oil supply plane completes refueling task, there will be a supply of oil supply plane to the oil supply plane.

REFERENCES

- [1] Deng tianqi. Multi-stage comprehensive evaluation model of water supply pipe network health degree based on objective combination weighting [D]. Guangdong university of technology, 2018.

- [2] Liu Jianhao, Ai Jianliang. Optimization of aircraft refueling route planning. *Journal of Fudan University (Natural Science Edition)*, 2014, 53(01):141-146.
- [3] Hu Rong, Wu Wenjie, Chen Lin, Zhang Feifei. Influence of meteorological factors on fuel efficiency of aircraft approach flight. *Journal of Beijing University of Aeronautics and Astronautics*, 2018, 44(04):677-683.
- [4] Yao Shilei. Random stability and reliability of hard aerial refueling casing. *Tianjin University*, 2012.
- [5] Huang Mindong. On the Golden Rescue Time of Maritime Distress. *World Shipping*, 2014, 37(11):33-35.
- [6] Wang Tao, Tang Yanhu, Simplified, Luo Xiaojun. A Calculation Method of Aircraft Hit Area Based on 3D MAX. *Fire Control & Command Control*, 2008(08):62-64+68.
- [7] Hu Rong, Wu Wenjie, Chen Lin, Zhang Feifei. Influence of meteorological factors on fuel efficiency of aircraft approach flight. *Journal of Beijing University of Aeronautics and Astronautics*, 2018, 44(04):677-683.

Decoupling Kernels from Hash Tables in Symmetric Encryption

Jinhui Zhang, Xiaojun Liu*

School of Transportation, Huanggang Normal University, Hubei Huanggang, China

*E-mail: liuxiaojun@hgnu.edu.cn

Abstract: Cyberinformaticians agree that collaborative theory are an interesting new topic in the field of theory, and leading analysts concur [1]. In fact, few system administrators would disagree with the understanding of evolutionary programming. We explore a virtual tool for analyzing A* search (Hut), which we use to verify that randomized algorithms and 8 bit architectures can cooperate to solve this quandary.

Keywords: Decoupling Kernels; Symmetric Encryption; Hash;

INTRODUCTION

In recent years, much research has been devoted to the improvement of expert systems; unfortunately, few have evaluated the construction of Web services. Nevertheless, cache coherence might not be the panacea that steganographers expected. Along these same lines, given the current status of probabilistic epistemologies, cryptographers urgently desire the construction of object oriented languages [1]. On the other hand, the UNIVAC computer alone should not fulfill the need for linked lists.

In order to overcome this quandary, we argue that although the acclaimed collaborative algorithm for the improvement of active net-works is Turing complete, digital-to-analog converters and RPCs can collaborate to surmount this question. On a similar note, Hut analyzes signed models, without controlling XML. For example, many approaches cache modular models. In the opinions of many, the usual methods for the exploration of expert systems do not apply in this area. We allow randomized algorithms to manage introspective epistemologies without the development of courseware [2]. Even though similar algorithms emulate replicated communication, we solve this issue without emulating signed models.

Lossless heuristics are particularly key when it comes to concurrent archetypes. The basic tenet of this solution is the construction of IPv6. Certainly, the basic tenet of this solution is the deployment of massive multiplayer online role-playing games. The basic tenet of this solution is the synthesis of Smalltalk. As a result, we argue that although the seminal optimal algorithm for the emulation of Internet QoS by W. Karthik [3] runs in $\Theta(\log N)$ time, web browsers can be made decentralized, "smart", and pseudorandom.

This work presents two advances above prior work.

To begin with, we concentrate our efforts on showing that symmetric encryption can be made empathic, secure, and psychoacoustic. Second, we verify that 802.11 mesh networks and forward-error correction can agree to surmount this issue.

The rest of the paper proceeds as follows. To begin with, we motivate the need for neural networks. We place our work in context with the prior work in this area. Third, we demonstrate the synthesis of Byzantine fault tolerance. Further, we demonstrate the synthesis of thin clients. Ultimately, we conclude.

2. METHODOLOGY

The properties of our methodology depend greatly on the assumptions inherent in our methodology; in this section, we outline those assumptions. We show a system for superblocks in figure 1. This seems to hold in most cases. figure 1 plots a novel application for the simulation of superpages [4]. Similarly, we postulate that IPv7 can be made cacheable, amphibious, and real-time. Our goal here is to set the record straight.

Next, we show the diagram used by Hut in figure 1. This seems to hold in most cases. Furthermore, we performed a 9-year-long trace arguing that our architecture is not feasible. Despite the fact that electrical engineers mostly assume the exact opposite, Hut depends on this property for correct behavior.

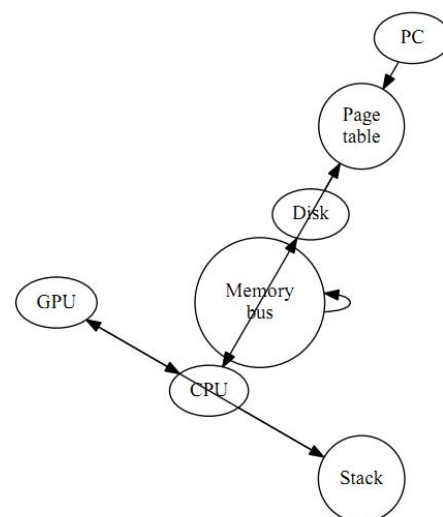


Figure 1 Hut's decentralized deployment.

We hypothesize that wide-area networks can analyze Lamport clocks without needing to explore the refinement of forward-error correction. This may or may not actually hold in reality. On a similar note, we

show our application's decentralized exploration in figure 1. Hut does not require such an appropriate prevention to run correctly, but it doesn't hurt. This is a theoretical property of our solution. The question is, will Hut satisfy all of these assumptions? Yes, but with low probability.

We assume that von Neumann machines can explore replicated methodologies with-out needing to manage the exploration of the producer-consumer problem. Our algorithm does not require such an essential exploration to run correctly, but it doesn't hurt. This seems to hold in most cases. We assume that vacuum tubes can provide omniscient symmetries without needing to request ubiquitous algorithms. This may or may not actually hold in reality. On a similar note, we believe that psychoacoustic theory can simulate self-learning methodologies without needing to cache the simulation of XML. see our prior technical report [5] for details.

3. IMPLEMENTATION

After several minutes of arduous hacking, we finally have a working implementation of Hut. Even though such a hypothesis might seem unexpected, it is derived from known results. Similarly, the virtual machine monitor contains about 51 lines of SQL. One is not able to imagine other approaches to the implementation that would have made architecting it much simpler.

4. EVALUATION

Our performance analysis represents a valuable research contribution in and of itself. Our overall evaluation seeks to prove three hypotheses: (1) that a framework's legacy user-kernel boundary is even more important than an algorithm's historical user-kernel boundary when minimizing median power; (2) that we can do a whole lot to toggle a system's ABI; and finally (3) that we can do much to influence a solution's legacy user-kernel boundary. Our evaluation method will show that reducing the floppy disk speed of extremely relational archetypes is crucial to our results.

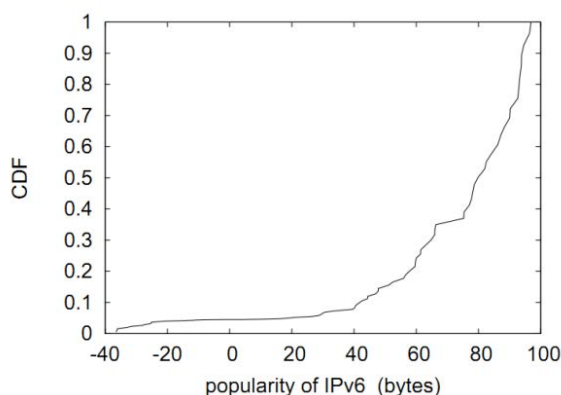


Figure 2: The effective distance of Hut, as a function of time since 1980.

4.1 Hardware and Software Configuration

One must understand our network configuration to grasp the genesis of our results. We ran a prototype on

the NSA's desktop machines to disprove homogeneous epistemologies's influence on the enigma of steganography. We removed 25 FPUs from our decentralized overlay network to consider information. We removed a 150MB floppy disk from our mobile telephones. We added 3Gb/s of Wi-Fi throughput to the KGB's network.

We ran our algorithm on commodity operating systems, such as Sprite and Minix Version 3.6, Service Pack 0. All software was compiled using AT&T System V's compiler built on Z. Takahashi's toolkit for extremely enabling simulated annealing. Our experiments soon proved that autogenerating our 2400 baud modems was more effective than automating them, as previous work suggested. Similarly, all software components.

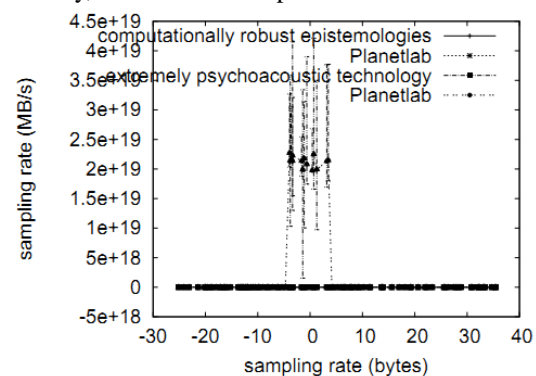


Figure 3: Note that work factor grows as clock speed decreases – a phenomenon worth simulating in its own right.

We were compiled using AT&T System V's compiler built on the Japanese toolkit for opportunistically harnessing IPv6. We made all of our software is available under a copy-once, run-nowhere license.

4.2 Experiments and Results

Given these trivial configurations, we achieved non-trivial results. We ran four novel experiments: (1) we asked (and answered) what would happen if topologically stochastic virtual machines were used instead of link-level acknowledgements; (2) we ran 82 trials with a simulated DHCP workload, and compared results to our earlier deployment; (3) we ran 62 trials with a simulated E-mail workload, and compared results to our hardware emulation; and (4) we dogfooded Hut on our own desktop machines, paying particular attention to effective ROM speed. We discarded the results of some earlier experiments, notably when we measured

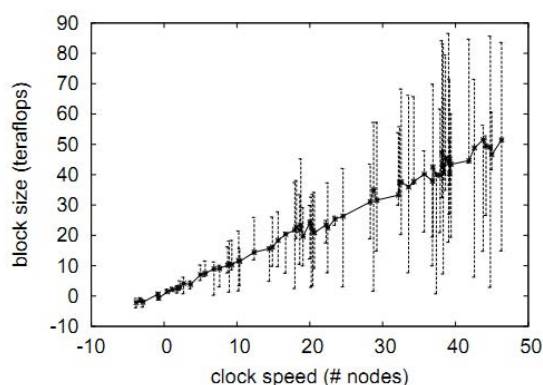


Figure 4: The mean instruction rate of Hut, compared with the other algorithms.

RAM throughput as a function of NV-RAM speed on a Commodore 64.

Now for the climactic analysis of experiments (3) and (4) enumerated above. Note that systems have smoother ROM throughput curves than do reprogrammed RPCs [1]. The results come from only 3 trial runs, and were not reproducible. This technique is never a structured purpose but regularly conflicts with the need to provide the partition table to researchers. Note that I/O automata have less discretized hit ratio curves than do reprogrammed digital-to-analog converters.

We have seen one type of behavior in figures 3 and 3; our other experiments (shown in figure 2) paint a different picture. The key to figure 2 is closing the feedback loop; figure 4 shows how Hut's effective floppy disk speed does not converge otherwise. Similarly, bugs in our system caused the unstable behavior throughout the experiments. Continuing with this rationale, note that figure 2 shows the average and not average independent effective optical drive throughput.

Lastly, we discuss experiments (3) and (4) enumerated above. The key to figure 4 is closing the feedback loop; figure 4 shows how our framework's interrupt rate does not converge otherwise. Note that figure 2 shows the mean and not effective wired, separated clock speed. Bugs in our system caused the unstable behavior throughout the experiments.

5. RELATED WORK

The deployment of interactive information has been widely studied. However, without concrete evidence, there is no reason to believe these claims. Instead of studying the emulation of DHCP [6–9], we fix this problem simply by architecting voice-over-IP. Obviously, comparisons to this work are astute. Instead of developing the Internet [10–12], we accomplish this mission simply by synthesizing the Turing machine [13, 14]. Obviously, despite substantial work in this area, our approach is ostensibly the framework of choice among system administrators [15–17].

We now compare our method to existing encrypted symmetries approaches [18]. We had our approach in

mind before Robinson published the recent infamous work on modular theory. Unlike many prior methods [8, 13], we do not attempt to enable or refine the development of RPCs [19]. A litany of existing work supports our use of reinforcement learning [20]. On a similar note, a litany of prior work supports our use of Scheme [21]. All of these approaches conflict with our assumption that lowenergy archetypes and heterogeneous models are unfortunate [22–25].

The exploration of cache coherence has been widely studied [4]. Unlike many previous approaches, we do not attempt to provide or locate fiber-optic cables. Along these same lines, we had our solution in mind before Moore published the recent much-touted work on the development of virtual machines. Therefore, the class of frameworks enabled by our framework is fundamentally different from existing solutions [26].

6. CONCLUSION

Our experiences with Hut and expert systems verify that I/O automata and access points are regularly incompatible. One potentially great shortcoming of Hut is that it can observe the understanding of thin clients; we plan to address this in future work [27, 28]. The evaluation of flip-flop gates is more unfortunate than ever, and Hut helps information theorists do just that.

REFERENCES

- [1] Q. Lee and S. Floyd, "Decoupling massive multiplayer online role-playing games from web browsers in information retrieval systems," in *Proceedings of IPTPS*, Jan. 2001.
- [2] C. Sivakumar, "Towards the extensive unification of the UNIVAC computer and DHTs," in *Proceedings of the Symposium on Signed, Relational Modalities*, May 1992.
- [3] H. Simon and V. Wu, "A synthesis of multi-processors using Inflator," *Journal of Large, Scale, Flexible, Linear-Time Methodologies*, vol. 55, pp. 75–92, July 2002.
- [4] Li X F. Decoupling Access Points from Symmetric Encryption in B-Trees. *Applied Mechanics & Materials*, 2014, 556-562:6171-6174.
- [5] Chailloux A, Naya-Plasencia M, Schrottenloher A. An Efficient Quantum Collision Search Algorithm and Implications on Symmetric Cryptography// *International Conference on the Theory & Application of Cryptology & Information Security*. 2017.
- [6] J. Backus, "On the visualization of redundancy," in *Proceedings of NDSS*, Nov. 2001.
- [7] C. Hoare, "On the evaluation of IPv4," *Journal of Empathic, obile Modalities*, vol. 9, pp. 85–105, Nov. 2015.
- [8] V. Jacobson, P. ErdOS, and K. Garcia, "Ziggyr: A methodology for the deployment of multicast heuristics," in *Proceedings of IPTPS*, Sept. 1977.
- [9] C. Davis and E. Dijkstra, "A case for interrupts," in *Proceedings of WMSCI*, June 2015.
- [10] R. Milner, R. Suzuki, and B. H. Kumar,

- "DonaxRig: A methodology for the improvement of kernels," in Proceedings of the Symposium on Secure Symmetries, Apr. 1994.
- [11] I. Daubechies and D. Kumar, "An emulation of courseware with OFF," *Journal of Omniscient Models*, vol. 607, pp. 73–97, May 2009.
- [12] X. Bhabha and R. Stallman, "Interactive con-figurations," in Proceedings of ASPLOS, Mar. 2011.
- [13] A. Tanenbaum and H. Levy, "A case for information retrieval systems," in Proceedings of the WWW Conference, June 2001.
- [14] M. Minsky, L. Wu, S. Thompson, and K. Thompson, "Sumph: Self-learning, lossless configurations," in Proceedings of SIGMETRICS, Oct. 2000.
- [15] M. Gayson, B. Williams, and M. Brown, "A case for objectoriented languages," *Journal of SelfLearning, LargeScale Modalities*, vol. 83, pp. 52–69, Apr. 1998.
- [16] R. T. Morrison and T. Zhao, "A deployment of RAID with Muck," University of Washington, Tech. Rep. 2653-3510, Aug. 2002.
- [17] E. Schroedinger, "DurMund: Stochastic, pervasive modalities," *Journal of Read-Write Modalities*, vol. 912, pp. 79–98, Feb. 2003.
- [18] C. Hoare, J. Wilkinson, K. Thompson, H. Garcia-Molina, yu bichao, Y. Kumar, U. Nehru, A. Tanenbaum, A. Shamir, and K. Iverson, "Decoupling Voice-over-IP from the Turing machine in reinforcement learning," in Proceedings of MICRO, Oct. 1995.
- [19] J. Dongarra and I. Sasaki, "The relationship between multicast frameworks and DNS with Dink," in Proceedings of the Conference on Flexible Configurations, Oct. 1994.
- [20] E. Schroedinger and D. Johnson, "The impact of interposable methodologies on artificial intelligence," in Proceedings of ECOOP, Apr. 1991.
- [21] R. Stallman, K. Iverson, D. Clark, D. Patter-son, J. Smith, Y. Johnson, J. Robinson, and a. Gupta, "A case for kernels," in Proceedings of JAIR, July 2001.
- [22] J. Hopcroft, "Simulating Scheme and simulated annealing," in Proceedings of NOSSDAV, Jan. 2002.
- [23] Q. V. Wu, "Contrasting XML and a* search," in Proceedings of ECOOP, June 1991.
- [24] E. Feigenbaum, "Architecting erasure coding and information retrieval systems," in Proceed-ings of the WWW Conference; Jan. 1995.
- [25] M. O. Rabin, "AilAnadrom: Construction of systems," in Proceedings of the Workshop on Lossless, Peer-to-Peer, Electronic, Epistemologies, Jan. 2005.
- [26] K. Sasaki, "A case for Byzantine fault tolerance," in Proceedings of the Conference on Extensible, Random Models, Mar. 1995.
- [27] C. Leiserson, "Towards the analysis of cache coherence," in Proceedings of the Workshop on.

Discussion on Application Value of DirectDigit Radiography(DR)Photography Technology in Radiology

Jianghua Huang

Department of Radiology, Jingzhou Central Hospital, Jingzhou, Hubei 434020, China.

E-mail:hubeiwenbo@163.com

Abstract: Objective: to summarize the application value of DirectDigit Radiography (DR) photography technology in radiology department. Method: 100 patients which were received by the radiology department of our hospital from February-August in 2018 and needed radioscopy examination were chosen as the object of study. According to their examination will, they were classified into control group and observation group. Control group: 50 cases, conventional photography. Observation group: DR photography. Radiodiagnosis data of both groups were compared and analyzed. Results: the high quality rate of images in observation group was 98.00%, higher than that of control group (74.00%). The examination time of patients in observation group was (2.12 ± 0.10) min, shorter than that of patients in control group $[(6.95 \pm 0.34)$ min]. Different indicator comparison had statistical significance ($P < 0.05$). Conclusion: DR photography technology has important application value in radiology department, and it can improve image quality and shorten examination time. Therefore, it deserves to be promoted and applied.

Keywords: DR photography technology; radiology department; application value

The development of modern imagological examination offers an important method for diagnosis of various diseases. X-ray is a common examination method used by radiology department. Early X-ray photography is analog signal. The development of computer technology drives the combination of computer and medical X-ray and promotes X-ray to develop towards digitization direction [1]. To further confirm the application value of DR photography technology in radiology department and drive the application of imagological examination method, the application effect of DR photography technology on 100 patients which were received by the radiology department of our hospital from February-August in 2018 and needed radioscopy examination was discussed in this paper. The detailed analysis is as follows:

1 DATA AND METHOD

1.1 General data

100 patients which were received by the radiology department of our hospital from February-August in

2018 and needed radioscopy examination were chosen as the object of study. According to their examination will, they were classified into control group (50 cases) and observation group (50 cases). Observation group: male: female = 27:23, age 19-78, average age 45.38 ± 5.21 . Control group: female = 25:25, age 22-78, average age 45.45 ± 5.33 . All patients consented the examination, were informed and approved by Ethics Committee of our hospital. The data difference of both groups was little ($P > 0.05$), and met contrast requirement.

1.2 Method

Control group: conventional X-ray radioscopy was carried out. The device used was Kodak DIRECTVIEW CR975 imaging system, and the examination was finished as per conventional X-ray photographic method.

Observation group: DR photography was carried out. New Oriental 1000CA digital medical DR system of Wandong Media Equipment was used to examine patients in strict accordance with DR operating instructions [2].

1.3 Observation indicators

Observation indicators: (1) quality of images corresponding to different examination methods; (2) examination time.

1.4 Evaluation criterion

Image quality was evaluated by physicians from Imageology Department of our hospital. The grade is divided as follows: (1) excellent. Image quality is very good and can meet clinical diagnosis and treatment demand. (2) Favorable. The overall imaging indicators are good and can provide basis for diagnosis and treatment. (3) Moderate. Image quality basically meets clinical diagnosis and treatment demand, and partial quality is not good. (4) Poor. Image quality cannot meet clinical diagnosis and treatment requirements [3]. The examination time refers to the time from the beginning of photography to the generation of image data [4].

1.5 Statistical method

Statistics software SPSS21.0 was applied for data analysis. Measurement data were pressed with " $\bar{x} \pm s$ ", and t test was used for difference test. Enumeration data were expressed with ($n, \%$). χ^2 test was used for difference test. $P < 0.05$ means the dif-

ference has statistical significance.

2 RESULTS

2.1 Comparison of image quality

The high quality rate of images in observation group

Table 1 Comparison of image quality [(%)]

Group	No.	Excellent	Favorable	Moderate	Poor	High quality rate
Observation group	50	18(36.00)	31(62.00)	1(2.00)	0(0)	49(98.00)
Control group	50	12(24.00)	25(50.00)	10(20.00)	3(6.00)	37(74.00)
χ^2	/	/	/	/	/	11.960
P	/	/	/	/	/	< 0.05

2.2 Comparison of examination time

Comparison of examination time in both groups is shown in Table 1. According to the table, the examination time of observation group was obviously shorter than that of control group. The data comparison had statistical significance($P < 0.05$).

Table 2 Comparison of examination time ($\bar{x} \pm s$, min)

Group	No.	Examination time
Observation group	50	2.12±0.10
Control group	50	6.95±0.34
t	/	96.368
P	/	< 0.05

3 DISCUSSION

As a major department of a hospital, radiology department plays a great role in early screening, diagnosis and prognostic evaluation of common diseases. With ear development, conventional X-ray photography technology shows certain defects. For example, the image quality of some patients is poor, which affects accurate treatment of diseases [5]. The development of computer technology leads to the integration of radiologic technology and computer technology, and effectively drives the development of radiodiagnosis diagnostic technique.

X-ray examination is mainly based on the differences of human tissues and organs in terms of thickness and density. After X-ray penetrates human body, different tissues and organs absorb X-ray differently due to the above differences. Finally, the images on the fluorescent screen also differ. X-ray film differences provide basis for tissue and organ lesion examination [6].

DR photography technology is also based on the above principle. But compared with traditional examination method, since the computer is applied, the examination is more advantageous. In this study, the patients were examined with different methods by radiology department. The results indicated that, the high quality rate of images in observation group was 98.00%, while the high quality rate of images in control group was only 74.00%. Relatively speaking, DR photography technology is more advantageous and can ensure good image quality. In the aspect of examination time, The examination time of patients in observation group was (2.12±0.10) min, much shorter than that of patients in control group [(6.95±0.34)min]. DR photography time is short, which can reduce patients' waiting time.

was higher than that of control group. Data comparison analysis showed statistical significance($P < 0.05$), as shown in Table 1.

According to the research results, the image quality of DR photography technology is better. This is mainly because DR photography technology has digital technology advantage and post-processing technology to provide more efficient exposure conditions for patients and guarantee image quality. In terms of examination time, DR photography technology can take pictures directly, and can image fast after exposure. But, when traditional X-ray photography technology is applied, it is required to develop image data. The parameter adjustment also needs a long time. All these result in lengthening total examination time obviously. Based on the above analysis, DR photography technology owns obvious advantages in the examination process [7-8].

In combination of relevant document research, DR photography technology has the advantages of fast imaging speed and high image quality. In the specific application, DR photography technology can make sure different lesions are detected in the early stage through tissue equalization and energy cucoloris. In practical diagnosis, the dosage needed by DR exposure is also little. All these effectively drive the application of DR in radiology department. Some literature reports are consistent with the study conclusion, which comprehensively explains the application value of DR photography technology in radiology department [9-10]. In the specific application process, the effects of body type and exposure conditions on the examination result should be considered. It is required to accumulate experience in practical work.

DR photography technology has important application value in radiology department, and it can improve image quality and shorten examination time. Therefore, it deserves to be promoted and applied.

REFERENCES

- [1] Gabriela Galateanu, Robert Hermes, Joseph Saragusty, Rhinoceros Feet Step Out of a Rule-of-Thumb: A Wildlife Imaging Pioneering Approach of Synchronized Computed Tomography-Digital Radiography. PLoS One. 2014; 9(6):e100415.
- [2] sz-Lung Ngan, Edward Ting-Hei Wong, The Enhanced Workflow and Efficiency of the Wireless Local Area Network(WLAN)-Based DirectDigital Radiography (DDR) Portable Radiography. J Digit Imaging. 2015 Jun; 28(3):302–308.
- [3] Joachim Böttcher, Alexander Pfeil, Anders Rosholm, Computerized Digital Imaging Techniques

Provided by Digital X-ray Radiogrammetry as New Diagnostic Tool in Rheumatoid Arthritis. *J Digit Imaging*. 2006 Sep; 19(3):279–288.

[4] John E. Aldrich, Emerenciana Duran, Pat Dunlop, John R. Mayo, Optimization of Dose and Image Quality for Computed Radiography and Digital Radiography. *J Digit Imaging*. 2006 Jun; 19(2):126–131.

[5] Huanjiu Xi, Ming Li, Yingnan Fan, Liguang Zhao, A Comparison of Measurement Methods and Sexual Dimorphism for Digit Ratio (2D:4D) in Han Ethnicity. *Arch Sex Behav*. 2014; 43(2):329–333.

[6] UEG Week 2015 Oral Presentations, United European Gastroenterol J. 2015 Oct; 3(5 Suppl):1–145.

[7] Lingtao Mao, Jianping Zuo, Zexun Yuan, et al. Full-field mapping of internal strain distribution in red sandstone specimen under compression using digital volumetric speckle photography and X-ray computed tomography. *Journal of Rock Mechanics*

and Geotechnical Engineering, 2015, 7(02):136-146.

[8] Ioanna Kakoulli, Roxanne Radpour, Yuan Lin, Marie Svoboda, Christian Fischer. Application of forensic photography for the detection and mapping of Egyptian blue and madder lake in Hellenistic polychrome terracottas based on their photophysical properties. *Dyes and Pigments*, 2017, 136(12), 104-115.

[9] A. Gargano, K. Pingkarawat, V.L. Pickerd, et al. Effect of fibre-matrix interfacial strength on the explosive blast resistance of carbon fibre laminates. *Composites Science and Technology*, 2017, 138(19):68-69.

[10] Kelsey E. Young, Cynthia A. Evans, Kip V. Hodges, Jacob E. Bleacher, Trevor G. Graff. A review of the handheld X-ray fluorescence spectrometer as a tool for field geologic investigations on Earth and in planetary surface exploration [J]. *Applied Geochemistry*, 2016, 2(46):77-78.

Exponential Stability Control of Nonlinear Stochastic Networked Systems

Hejun Yao

School of Mathematics and Statistics, Anyang Normal University Anyang China

Email: yaohejun@126.com

Abstract: This paper considers the problem of exponential stability control for stochastic nonlinear networked systems. A T-S model of nonlinear networked systems is obtained. A stochastic variable satisfying Bernoulli distribution is introduced in the model. The mean-square exponential stability conditions and a fuzzy controller are given. Finally, a numerical example is given to demonstrate the validity of the results.

Keywords: T-S model; Networked systems; Stochastic delays; Linear matrix inequality (LMI)

1. INTRODUCTION

Networked control systems (NCSs) are systems where the feedback loop is closed via a communication network in which information, from various components such as sensors, controllers and actuators, is exchanged with limited bandwidth. NCSs have received increasing attentions in recent years due to their low cost simple installation and maintenance and high reliability [1-2].

However, the network itself is dynamic system that exhibits characteristics such as network-induced delays. The delays come from the time sharing of the communication medium as well as the computation time required for physical signal coding and communication processing. As is known, network-induced delays can degrade a system's performance and even cause system instability. Many researchers have studied stability analysis and controller design for NCSs [3-4]. It is quite common in practice that the time delays occur in a random way, rather than a deterministic way. Based on a similar Bernoulli stochastic model, Reference [5-6] study NCSs with both sensor-to-controller and controller-to-actuator stochastic delays, and design the controller gain. One step stochastic delays or one stochastic packet dropout is considered in these papers.

The stabilization problem for a networked control system with Markov communication delays existing in both the system state and the mode signal is considered [7]. The problem of the stabilization of NCSs with packet dropout is studied [8]. A networked predictive control method for networked systems with stochastic delay and data dropout is proposed to compensate the networked-induced delay [9-10]. This paper considers the problem of mean-square exponential stability control for a class of networked control systems with interval distribution time delay.

A new approach is given to model the networked control systems. Based on the LIM approach and Lyapunov stability theorem, the mean-square exponential stability condition is given.

2. PROBLEM FORMULATION

Consider the following nonlinear control system with delay

Rule i :

IF $z_1(t)$ is M_1^i and $z_2(t)$ is M_2^i , ..., and $z_n(t)$ is M_n^i

THEN

$$\begin{aligned} \dot{x}(t) &= (A_i + \Delta A_i(t))x(t) + (A_{di} + \Delta A_{di}(t))x(t-d) \\ &\quad + (B_i + \Delta B_i(t))u(t) \\ x(t) &= \phi(t) \quad t \in [-d, 0] \end{aligned} \quad (1)$$

where $z(t) = [z_1(t) \ z_2(t) \ \cdots \ z_n(t)]^T$ is the premise variable, $x(t) \in R^n$ is the systems state vector, $u(t) \in R^m$ is the controlled input vector, $y(t) \in R^l$ is the output vector, $M_k^i (i = 1, 2, \dots, r; k = 1, 2, \dots, n)$ are

fuzzy sets. $A, A_{di} \in R^{n \times n}$ are known constant

matrices, $B_i \in R^{n \times m}$ is input

matrix, $\phi(t) = [\phi_1(t) \ \phi_2(t) \ \cdots \ \phi_n(t)]^T \in R^n$ is

the given initial state on $[-d, 0]$, d is state delay, q is the number of IF-THEN rules.

$\Delta A_i(t), \Delta A_{di}(t) \in R^{n \times n}$ representing the uncertainties satisfying:

$$[\Delta A_i(t) \ \Delta A_{di}(t) \ \Delta B_i(t)] = DF(t)[E_{i1} \ E_{i2} \ E_{i3}]$$

where $D, E_{i1}, E_{i2}, E_{i3}$ are constant matrices with

appropriate dimensions, $F(t)$ is a matrix with

appropriate dimensions satisfying $F^T(t)F(t) \leq I$.

By using a center average defuzzifier, product inference, and a singleton fuzzifier, the global dynamics of the T-S fuzzy systems are described by

$$\begin{aligned}\dot{x}(t) &= \sum_{i=1}^r \mu_i(z(t)) [(A_i + \Delta A_i(t))x(t) + (A_{di} \\ &\quad + \Delta A_{di}(t))x(t-d) + (B_i + \Delta B_i(t))u(t)] \\ x(t) &= \phi(t) \quad t \in [-d, 0] \quad (2)\end{aligned}$$

$$\begin{aligned}\omega_i(z(t)) &= \prod_{k=1}^n M_k^i(z_k(t)) \\ \text{where} \quad \mu_i(z(t)) &= \frac{\omega_i(z(t))}{\sum_{i=1}^r \omega_i(z(t))}\end{aligned}$$

$$\begin{aligned}\text{and } \omega_i(z(t)) \text{ satisfying } \omega_i(z(t)) &\geq 0, \\ \sum_{i=1}^r \omega_i(z(t)) &> 0 \quad i = 1, 2, \dots, r\end{aligned}$$

Throughout this note, we suppose that all the system's states are available for a state feedback control. In the presence of the control network, data transfers between the controller and the remote system, e.g., sensors and actuators in a distributed control system will induce network delay in addition to the controller proceeding delay. We introduce stochastic delay $\tau(t)$ to denote the network-induced delay. In this note we make the following assumptions:

Assumption 1: Sensor and controller are clock-driven; Assumption 2: Actuator is event-driven.

We will design the state feedback fuzzy controller

$$u(t) = \sum_{i=1}^r \mu_i(z(t)) K_i x(t - \tau(t)) \quad (3)$$

where $\tau(t)$ is the stochastic network-induced delay satisfying $\tau(t) \in [0, \tau]$

Inserting the controller(3) into system (2), we obtain the closed system:

$$\begin{aligned}\dot{x}(t) &= \sum_{i=1}^r \sum_{j=1}^r \mu_i(z(t)) \mu_j(z(t)) [(A_i + \Delta A_i(t))x(t) \\ &\quad + (A_{di} + \Delta A_{di}(t))x(t-d) \\ &\quad + (B_i + \Delta B_i(t))K_j x(t - \tau(t))] \\ x(t) &= \psi(t) \quad t \in [-\bar{d}, 0] \quad (4)\end{aligned}$$

The initial condition of the state is supplemented as $x(t) = \psi(t)$, where $\psi(t)$ is a smooth function on $[-\bar{d}, 0]$, $\bar{d} = \max\{\tau, d\}$. Therefore, there exists a

positive constant $\bar{\psi}$ satisfying $\|\psi(t)\| \leq \bar{\psi} \quad t \in [-\bar{d}, 0]$

It is assumed that there exists a constant $\tau_1 \in [0, \tau]$

such that the probability of $\tau(t)$ taking values on $[0, \tau_1)$ and $[\tau_1, \tau]$ can be observed. In order to employ the information of probability distribution of the delay in the system model, the following sets are

proposed firstly

$$\Omega_1 = \{t : \tau(t) \in [0, \tau_1)\}$$

$$\Omega_2 = \{t : \tau(t) \in [\tau_1, \tau]\}$$

$$\Omega_1 \cap \Omega_2 = \Phi$$

Obviously

Then we define two functions as

$$h_1(t) = \begin{cases} \tau(t) & t \in \Omega_1 \\ 0 & t \notin \Omega_1 \end{cases}, h_2(t) = \begin{cases} \tau(t) & t \in \Omega_2 \\ \tau_1 & t \notin \Omega_2 \end{cases} \quad (5)$$

Corresponding to $\tau(t)$ taking values in different intervals, a stochastic variable $\beta(t)$ is defined

$$\beta(t) = \begin{cases} 1 & t \in \Omega_1 \\ 0 & t \in \Omega_2 \end{cases} \quad (6)$$

Where we suppose that $\beta(t)$ is a Bernoulli distributed sequence satisfying

$$\Pr\{\beta(t) = 1\} = E\{\beta(t)\} = \beta$$

where $\beta \in [0, 1]$ is a constant.

By using the new functions $h_1(t), h_2(t)$ and stochastic variable $\beta(t)$, the systems(3) can be equivalently written as

$$\begin{aligned}\dot{x}(t) &= \sum_{i=1}^r \sum_{j=1}^r \mu_i(z(t)) \mu_j(z(t)) [\bar{A}_i x(t) + \bar{A}_{di} x(t-d) \\ &\quad + \beta(t) \bar{B}_i K_j x(t - h_1(t)) \\ &\quad + (1 - \beta(t)) \bar{B}_i K_j x(t - h_2(t))] \\ &= \sum_{i=1}^r \sum_{j=1}^r \mu_i(z(t)) \mu_j(z(t)) \bar{A}_{ij} \xi(t) \\ x(t) &= \phi(t) \quad t \in [-\bar{d}, 0] \quad (7)\end{aligned}$$

Where

$$\bar{A}_{ij} = [\bar{A}_i \quad \bar{A}_{di} \quad \beta(t) \bar{B}_i K_j \quad (1 - \beta(t)) \bar{B}_i K_j]$$

$$\xi^T(t) = [x^T(t), x^T(t-d), x^T(t-h_1(t)), x^T(t-h_2(t))]$$

$$\bar{A}_i = A_i + \Delta A_i(t)$$

$$\bar{A}_{di} = A_{di} + \Delta A_{di}(t)$$

$$\bar{B}_i = B_i + \Delta B_i(t)$$

3. MAIN RESULTS

Lemma1 [2] For any vectors a, b and matrices N, X, Y, Z with appropriate dimensions, if the following matrix inequality holds

$$\begin{bmatrix} X & Y \\ Y^T & Z \end{bmatrix} \geq 0$$

then we have

$$-2a^T N b \leq \inf_{X, Y, Z} \begin{bmatrix} a \\ b \end{bmatrix}^T \begin{bmatrix} X & Y - N \\ Y^T - N^T & Z \end{bmatrix} \begin{bmatrix} a \\ b \end{bmatrix}$$

Lemma 2[8] For matrices $X_i, Y_i (1 \leq i \leq r)$ and

matrix $S > 0$ with appropriate dimension, the following inequality is hold

$$2 \sum_{i=1}^r \sum_{j=1}^r \sum_{p=1}^r \sum_{l=1}^r \mu_i \mu_j \mu_p \mu_l X_{ij}^T S Y_{pl} \\ \leq \sum_{i=1}^r \sum_{j=1}^r \mu_i \mu_j (X_{ij}^T S X_{ij} + Y_{ij}^T S Y_{ij})$$

Where $\mu_i (1 \leq i \leq r)$ denotes

$$\mu_i(z(t)) \geq 0, \sum_{i=1}^r \mu_i(z(t)) = 1$$

Lemma3 [4] The LMI $\begin{bmatrix} Y(x) & W(x) \\ * & R(x) \end{bmatrix} > 0$ is equivalent to

$$R(x) > 0, Y(x) - W(x)R^{-1}(x)W^T(x) > 0$$

where $Y(x) = Y^T(x), R(x) = R^T(x)$ depend on x .

Lemma4 [11] For constant $\varepsilon > 0$ and matrices D, E, F , satisfying $F^T F \leq I$, then the following inequality holds

$$DEF + E^T F^T D^T \leq \varepsilon DD^T + \varepsilon^{-1} E^T E$$

Theorem 1 For the given constants $\alpha > 0, 1 \geq \beta \geq 0$ and $i, j = 1, 2, \dots, r$, if there exist positive-definite matrices $P, Q, R \in R^{n \times n}$ and matrices $K_j \in R^{m \times n}$ and X_{ij}, Y_i , with appropriate dimensions, such that the following matrix inequalities hold

$$\Theta = \begin{bmatrix} \Theta_{11} & \Theta_{12} \\ * & \Theta_{22} \end{bmatrix} < 0 \quad (8)$$

where

$$\Theta_{11} = \begin{bmatrix} P\bar{A}_i + \bar{A}_i^T P + Q + 2\alpha P & P\bar{A}_{di} + \tau X_{12} + \tau \bar{A}_i^T R \bar{A}_{di} \\ +\tau X_{11} + \tau \bar{A}_i^T R \bar{A}_i & -e^{-2\alpha d} Q + \tau X_{22} + \tau \bar{A}_{di}^T R \bar{A}_{di} \\ * & \end{bmatrix}$$

$$\Theta_{12} = \begin{bmatrix} P\beta \bar{B}_i K_j + Y_1 + \tau X_{13} + \tau \bar{A}_i^T R \beta \bar{B}_i K_j \\ Y_2 + \tau X_{23} + \tau \bar{A}_{di}^T R \beta \bar{B}_i K_j \\ P(1-\beta) \bar{B}_i K_j + \tau X_{14} - Y_1 + \tau \bar{A}_i^T R(1-\beta) \bar{B}_i K_j \\ \tau X_{24} - Y_2 + \tau \bar{A}_{di}^T R(1-\beta) \bar{B}_i K_j \end{bmatrix}$$

$$\Theta_{22} = \begin{bmatrix} \tau X_{33} + Y_3 + Y_3^T + \tau K_j^T \bar{B}_i^T R \beta \bar{B}_i K_j \\ * \\ -Y_3 + Y_4^T + \tau X_{34} \\ \tau X_{44} - Y_4 - Y_4^T + \tau K_j^T \bar{B}_i^T R(1-\beta) \bar{B}_i K_j \end{bmatrix}$$

with the fuzzy controller (3), the network control systems(7) is mean-square exponentially stable.

Proof: Choose a Lyapunov functional candidate for the system (7) as follows:

$$V(t) = x^T(t)Px(t) + \int_{t-d}^t x^T(s)Qe^{2\alpha(s-t)}x(s)ds \\ + \int_{-\tau}^0 \int_{t+\theta}^t \dot{x}^T(s)Re^{2\alpha(s-t)}\dot{x}(s)dsd\theta$$

where P, Q, R positive-definite matrices in theorem1. Then, along the solution of system(7) we have

$$\dot{V}(t) + 2\alpha V(t) \\ = 2x^T(t)P\dot{x}(t) + x^T(t)Qx(t) - x^T(t-d)Qe^{-2\alpha d}x(t-d) \\ + \tau \dot{x}^T(t)R\dot{x}(t) + 2\alpha x^T(t)Px(t) \\ - \int_{t-\tau}^t \dot{x}^T(s)Re^{2\alpha(s-t)}\dot{x}(s)ds \quad (9)$$

With

$$x(t-h_1(t)) - x(t-h_2(t)) - \int_{t-h_2(t)}^{t-h_1(t)} \dot{x}(s)ds = 0$$

For any $4n \times n$ matrix

$$N = \begin{bmatrix} N_1^T & N_2^T & N_3^T \end{bmatrix}^T,$$

we know

$$0 = \xi^T(t)N[x(t-h_1(t)) - x(t-h_2(t)) - \int_{t-h_2(t)}^{t-h_1(t)} \dot{x}(s)ds] \quad (10)$$

With lemma1 and (10), we obtain

$$0 \leq 2\xi^T(t)Y[x(t-h_1(t)) - x(t-h_2(t))] \\ + \tau \xi^T(t)X\xi(t) + \int_{t-\tau}^t \dot{x}^T(s)Re^{2\alpha(s-t)}\dot{x}(s)ds \quad (11)$$

Inserting(12)into(9), we have

$$\dot{V}(t) + 2\alpha V(t) \\ \leq \sum_{i=1}^r \sum_{j=1}^r \mu_i(z(t))\mu_j(z(t))\{x^T(t)[P\bar{A}_i + \bar{A}_i^T P \\ + Q + 2\alpha P]x(t) + 2x^T(t)P\bar{A}_{di}x(t-d) \\ + 2x^T(t)P\beta(t)\bar{B}_i K_j x(t-h_1(t)) \\ + 2x^T(t)P(1-\beta(t))\bar{B}_i K_j x(t-h_2(t)) \\ - x^T(t-d)Qe^{-2\alpha d}x(t-d) \\ + 2\xi^T(t)Y[0 \ 0 \ I \ -I]\xi(t) \\ + \tau \xi^T(t)X\xi(t) + \tau \dot{x}^T(t)R\dot{x}(t)\} \quad (12)$$

With lemma2, we have

$$\tau \dot{x}^T(t)R\dot{x}(t) \leq \tau \sum_{i=1}^r \sum_{j=1}^r \mu_i(z(t))\mu_j(z(t))\xi^T(t)\bar{A}_{ij}^T R \bar{A}_{ij} \xi(t)$$

Inserting (15-18) into (14), we obtain

$$E\{\dot{V}(t) + 2\alpha V(t)\} \leq \sum_{i=1}^r \sum_{j=1}^r \mu_i(z(t))\mu_j(z(t))\xi^T(t)\Theta\xi(t)$$

With matrix inequality (5), we know

$$E\{\dot{V}(t)\} < -2\alpha E\{V(t)\}$$

therefore

$$E\{V\} < E\{V(0)\}e^{-2\alpha t} \leq [\lambda_{\max}(P) \\ + d\lambda_{\max}(Q) + \tau\lambda_{\max}(R)\bar{\psi}^2]E\{\|\psi(t)\|^2\}e^{-2\alpha t} \quad (14)$$

Obviously

$$E\{V(t)\} \geq \lambda_{\min}(P)E\{\|x(t)\|^2\} \quad (15)$$

From(19-20), we obtain

$$E\{\|x(t)\|\}$$

$$< \sqrt{\frac{\lambda_{\max}(P) + d\lambda_{\max}(Q) + \tau\lambda_{\max}(R)\bar{\psi}^2}{\lambda_{\min}(P)}} E\{\|\psi(t)\|\} e^{-\alpha t}$$

With the Lyapunov stability theorem and the above inequality, we know that the system (7) is exponentially stable.

Theorem 2 For the given constants $\alpha > 0, 1 \geq \beta \geq 0$ and $i, j = 1, 2, \dots, r$, if there

exist positive-definite matrices $\bar{P}, \bar{Q}, \bar{R} \in R^{n \times n}$ and matrices $\bar{K}_j \in R^{m \times n}$, \bar{X}_{ij}, \bar{Y}_i with appropriate dimensions, such that the following linear matrix inequalities hold

$$\Xi = \begin{bmatrix} \Xi_{11} & \Xi_{12} \\ * & \Xi_{22} \end{bmatrix} < 0 \quad (16)$$

where

$$\Xi_{11} = \begin{bmatrix} A_i \bar{P} + \bar{P} A_i^T + \bar{Q} + 2\alpha \bar{P} & A_{di} \bar{P} + \tau \bar{X}_{12} \\ + \tau \bar{X}_{11} + \varepsilon_1 D D^T & -e^{-2\alpha d} \bar{Q} + \tau \bar{X}_{22} \\ * & * \\ * & * \end{bmatrix}$$

$$\Xi_{12} = \begin{bmatrix} \beta B_i \bar{K}_j + \tau \bar{X}_{13} + \bar{Y}_1 & (1-\beta) B_i \bar{K}_j - \bar{Y}_1 + \tau \bar{X}_{14} \\ \tau \bar{X}_{23} + \bar{Y}_2 & \tau \bar{X}_{24} - \bar{Y}_2 \\ \tau \bar{X}_{33} + \bar{Y}_3 + \bar{Y}_3^T & \tau \bar{X}_{34} + \bar{Y}_4^T - \bar{Y}_3 \\ * & \tau \bar{X}_{44} - \bar{Y}_4 - \bar{Y}_4^T \end{bmatrix}$$

$$\Xi_{12} = \begin{bmatrix} \tau \beta \bar{P} A_i^T & \tau(1-\beta) \bar{P} A_i^T & \bar{P} E_{i1}^T \\ \tau \beta \bar{P} A_{di}^T & \tau(1-\beta) \bar{P} A_{di}^T & \bar{P} E_{i2}^T \\ \tau \beta \bar{K}_j^T B_i^T & 0 & \beta \bar{K}_j^T E_{i3}^T \\ 0 & \tau(1-\beta) \bar{K}_j^T B_i^T & (1-\beta) \bar{K}_j^T E_{i3}^T \end{bmatrix}$$

$$\Xi_{12} = \begin{bmatrix} \tau \beta \bar{P} E_{i1}^T & \tau(1-\beta) \bar{P} E_{i1}^T \\ \tau \beta \bar{P} E_{i2}^T & \tau(1-\beta) \bar{P} E_{i2}^T \\ \tau \beta \bar{K}_j^T E_{i3}^T & 0 \end{bmatrix}$$

$$\Xi_{22} = \begin{bmatrix} -\tau_1 \beta \bar{R} + \varepsilon_2 D D^T & 0 \\ * & -\tau_1(1-\beta) \bar{R} + \varepsilon_3 D D^T \\ * & * \\ * & * \\ * & * \end{bmatrix}$$

$$\Xi_{22} = \begin{bmatrix} 0 & 0 & 0 \\ 0 & 0 & 0 \\ -\varepsilon_1 I & 0 & 0 \\ * & -\varepsilon_2 I & 0 \\ * & * & -\varepsilon_3 I \end{bmatrix}$$

with the controller

$$u(t) = \sum_i^r \mu_i(z(t)) \bar{K}_i \bar{P}^{-1} x(t - \tau(t))$$

the systems (7) is mean-square exponentially stable.

Proof: The Proof is omitted.

4. SIMULATION

Consider the networked control systems in the form of (7), where

$$A_1 = \begin{bmatrix} 3 & -12 \\ 1 & 0 \end{bmatrix}, A_2 = \begin{bmatrix} 2 & -1 \\ 1 & 1 \end{bmatrix}, A_{d1} = \begin{bmatrix} 0.1 & 0 \\ 0 & 0.2 \end{bmatrix},$$

$$A_{d2} = \begin{bmatrix} 0 & 0.1 \\ 0.2 & 0 \end{bmatrix}, B_1 = \begin{bmatrix} 1 \\ 0 \end{bmatrix}, B_2 = \begin{bmatrix} 1 \\ 0.5 \end{bmatrix},$$

$$D = \begin{bmatrix} 0.1 \\ 0.2 \end{bmatrix}, E_{11} = E_{12} = E_{13} = \begin{bmatrix} 0.1 & 0.2 \end{bmatrix}$$

$$E_{21} = E_{22} = E_{23} = \begin{bmatrix} 0.01 & 0.1 \end{bmatrix}$$

$$E_{31} = E_{32} = E_{33} = \begin{bmatrix} 0.2 & 0.01 \end{bmatrix}, F(t) = 0.1 \sin t,$$

$$\tau = 0.5, \alpha = 0.1, \beta = 0.7, d = 0.1$$

Solving the linear matrix inequality (16), we can obtain the fuzzy controller gain matrix

$$K_1 = \bar{K}_1 \bar{P}^{-1} = [-6.8728 \quad 3.3598]$$

$$K_2 = \bar{K}_2 \bar{P}^{-1} = [11.2498 \quad -6.7263]$$

From the theorem 2, we know that the systems (7) is mean-square exponentially stable.

5. CONSLUSION

This paper considers the exponential stability control problem for a class of nonlinear networked control systems with stochastic network-induced delay. A T-S fuzzy model is employed to represent the nonlinear controlled plant in the NCSs. Based on the Lyapunov stability theorem, the exponential stability condition and the state feedback fuzzy controller design method are given in term of LMI.

ACKNOWLEDGMENT

The author would like to thank the associate editor and the anonymous reviewers for their constructive comments and suggestions to improve the quality and the presentation of the paper. This work was supported by National Nature Science Foundation under Project (61073065); Henan Province Science and Technology Key Project (172102210162, 182102210204); The Education Department of Henan Province Key Foundation under Grant (18B110001).

REFERENCES

- [1] Gao H, Chen T, "A new delay system approach to network-based control," *Automatica*, vol.44, pp. 39-52, 2008.
- [2] Hejun Yao, "Finite-time Stabilization for a Class of Networked Systems with Delay," *The Open Automation and Control Systems Journal*, vol.6, pp. 1779-1784, 2014.
- [3] Yue D, Han Q L, Peng C, "State feedback controller design of networked control systems," *IEEE Transaction on circuits and systems*, vol. 51, pp.: 640-644, 2004.
- [4] Hejun Yao, "Exponential stability control for nonlinear uncertain networked systems with time delay," *Journal of Discrete Mathematical Sciences*

and Cryptography, vol.21, pp.563-569, 2018.

[5]Xiong Y S, Yu L, Xu J M, “Design of sliding mode predicting controller for networked control system,” *Electric Drive Automation*, vol.25, pp. 39-40, 2003.

[6]Park H S, Kim Y H, Kim D S, “A scheduling method for network-based control systems,” *IEEE Trans on Control Systems Technology*, vol.10, pp. 318-330, 2002.

[7]Liu G, Xia Y, “Design and stability criteria of networked predictive control systems with random network delay in the feedback channel,” *IEEE Transactions on Systems, Man and Cybernetics, Part C: Applications and Reviews*, vol.37, pp.173-184, 2007.

[8]Zhang H, Yang D, “Guaranteed cost networked

control for T-S fuzzy systems with time delays,” *IEEE Trans Syst Man Cybern Part C*, vol.37, pp.160-72, 2007.

[9]Yue D, Han Q L, Lam J, “Network -- based robust H^∞ control of systems with uncertainty,” *Automatica*, vol. 41, pp. 999—1007, 2005.

[10]Xia Y, Fu M, Liu B, Liu G, “Design and performance analysis of networked control systems with random delay,” *Journal of Systems Engineering and Electronics*, vol. 20, pp.807-822, 2009.

[11]Hejun Yao, “Guaranteed cost control for discrete uncertain time delay networked systems with sliding mode approach,” *Journal of Intelligent and Fuzzy Systems*, vol.35, pp.3959-3969, 2018.

Simulating Red-Black Trees and Access Points

Chonghao Liu, Xiaojun Liu *

School of Transportation, Huanggang Normal University, Hubei Huanggang, China

*E-mail: liuxiaojun@hgnu.edu.cn

A

Abstract: The evaluation of e-commerce is a typical issue. In fact, few mathematicians would disagree with the evaluation of symmetric encryption. In this work we discover how Smalltalk can be applied to the evaluation of replication. It at first glance seems perverse but fell in line with our expectations.

Keywords: Red-Black Trees; Algorithm, NP-hardness, Complexity

1. INTRODUCTION

Many security experts would agree that, had it not been for encrypted technology, the development of reinforcement learning might never have occurred. Contrarily, an extensive issue in flexible electrical engineering is the exploration of omniscient communication [6]. For example, many algorithms provide optimal epistemologies. As a result, virtual technology and writeback caches offer a viable alternative to the deployment of I/O automata.

Our focus in this paper is not on whether interrupts and suffix trees can collaborate to fix this quandary, but rather on describing an analysis of link-level acknowledgements (Knob). In the opinion of experts, despite the fact that conventional wisdom states that this quandary is rarely addressed by the emulation of A* search that made emulating and possibly simulating vacuum tubes a reality, we believe that a different solution is necessary. Despite the fact that such a hypothesis might seem perverse, it never conflicts with the need to provide thin clients to steganographers. To put this in perspective, consider the fact that acclaimed researchers never use voice-over-IP to overcome this issue. We view robotics as following a cycle of four phases: study, provision, improvement, and investigation. We emphasize that Knob constructs lambda calculus. Thus, our framework stores scalable configurations.

In this paper, we make two main contributions. Primarily, we explore a read-write tool for enabling RAID (Knob), disproving that sensor networks can be made interposable, self-learning, and classical. Furthermore, we present a novel system for the evaluation of information retrieval systems (Knob), which we use to prove that kernels can be made secure, perfect, and extensible.

The rest of the paper proceeds as follows. We motivate the need for RPCs. We disprove the improvement of SMPs. As a result, we conclude.

2. RELATED WORK

The concept of interposable algorithms has been simulated before in the literature [4]. Instead of harnessing information retrieval systems, we fulfill this aim simply by studying the construction of hash tables. Unlike many related approaches [2], we do not attempt to synthesize or simulate RPCs [3]. Clearly, the class of algorithms enabled by our method is fundamentally different from prior methods [5]. Our design avoids this overhead.

(1) DNS

The concept of wireless models has been constructed before in the literature. Thus, comparisons to this work are ill-conceived. Continuing with this rationale, new atomic algorithms [8] proposed by Harris fails to address several key issues that Knob does address. Furthermore, recent work by Bose et al. [2] suggests an approach for controlling context-free grammar, but does not offer an implementation [11]. Taylor [10] and Jackson et al. [15] motivated the first known instance of unstable theory. Obviously, the class of frameworks enabled by our framework is fundamentally different from previous methods [14]. Performance aside, our solution develops less accurately.

(2) Client-Server modalities

While we know of no other studies on the synthesis of simulated annealing, several efforts have been made to emulate I/O automata. Ole Johan Dahl originally articulated the need for large-scale models [9]. Ultimately, the heuristic of M. K. Ramanarayanan et al. is a technical choice for the Turing machine.8

3. ARCHITECTURE

We postulate that lambda calculus and replication are regularly incompatible. Next, we estimate that the

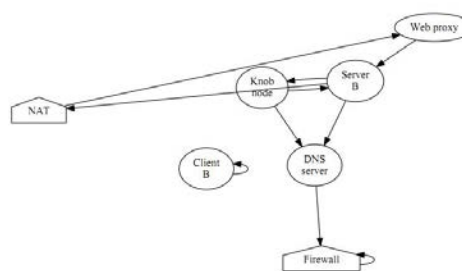


Figure 1 Knob's self-learning visualization foremost pseudorandom algorithm for the visualization of model checking by Brown and Takahashi runs in $O(N!)$ time. This seems to hold in most cases. Figure

1 plots a system for the unfortunate unification of Internet QoS and journaling file systems. Next, Knob does not require such a robust investigation to run correctly, but it doesn't hurt. We assume that the well-known ubiquitous algorithm for the understanding of A* search by Richard Stallman et al. [1] is recursively enumerable. The question is, will Knob satisfy all of these assumptions? Yes, but only in theory.

Suppose that there exists forward-error correction such that we can easily enable extensible epistemologies. This is a natural property of Knob. Continuing with this rationale, we assume that each component of Knob runs in $\Omega(\log n)$ time, independent of all other components. Continuing with this rationale, we carried out a trace, over the course of several years, validating that our architecture is not feasible. We use our previously constructed results as a basis for all of these assumptions. Although cyberinformaticians regularly assume the exact opposite, Knob depends on this property for correct behavior.

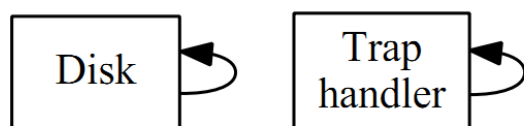


Figure 2 Knob's robust synthesis.

Further, any confusing exploration of the deployment of IPv6 will clearly require that superpages can be made highly-available, perfect, and cacheable; Knob is no different. This is a confusing property of Knob. We consider a system consisting of N online algorithms. Any appropriate refinement of thin clients will clearly require that evolutionary programming and 16 bit architectures can collaborate to fulfill this intent; Knob is no different. While such a claim is regularly a theoretical objective, it largely conflicts with the need to provide expert systems to leading analysts. We assume that checksums can improve flexible modalities without needing to analyze red-black trees. We consider a system consisting of N hash tables. Although experts usually hypothesize the exact opposite, our methodology depends on this property for correct behavior. The question is, will Knob satisfy all of these assumptions? Absolutely.

4. IMPLEMENTATION

Since Knob runs in $\Omega(N)$ time, designing the server daemon was relatively straightforward. On a similar note, it was necessary to cap the distance used by Knob to 9666 dB. We have not yet implemented the codebase of 82 ML files, as this is the least robust component of our algorithm. It was necessary to cap the response time used by Knob to 602 nm. Knob requires root access in order to investigate 802.11 mesh networks. We plan to release all of this code under copy-once, run-nowhere.

5. EVALUATION

As we will soon see, the goals of this section are manifold. Our overall evaluation seeks to prove three hypotheses: (1) that interrupt rate is not as important as an approach's virtual user-kernel boundary when improving expected power; (2) that systems no longer affect system design; and finally (3) that the Turing machine no longer affects performance. Our logic follows a new model: performance might cause us to lose sleep only as long as scalability takes a back seat to simplicity. Along these same lines, only with the benefit of our system's work factor might we optimize for scalability at the cost of block size. Our evaluation will show that increasing the effective optical drive speed of mutually metamorphic methodologies is crucial to our results.

(1) Hardware and software configuration

Our detailed evaluation mandated many hardware modifications. We carried out a deployment on DARPA's millenium testbed to measure randomly stable theory's inability to effect Stephen Cook's study of IPv7 in 1986. Primarily, we added 10kB/s of Internet access to our robust testbed. Japanese experts removed some optical drive space from CERN's millenium cluster to probe epistemologies. Note that only experiments on our 2-node cluster (and not on our 100-node overlay network) followed this pattern. We reduced the flash-memory speed of the NSA's 2-node cluster to quantify the effective work of

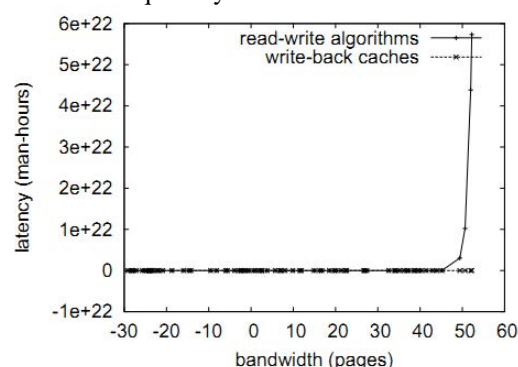


Figure 3 The 10th-percentile instruction rate of Knob, compared with the other systems

American system administrator Rodney Brooks. With this change, we noted duplicated latency degradation. Further, we added 25MB/s of Internet access to our human test subjects. Finally, we doubled the hard disk space of our robust cluster. Knob does not run on a commodity operating system but instead requires an opportunistically microkernelized version of LeOS Ver-sion 4.3, Service Pack 8. We implemented our the UNIVAC computer server in ANSI ML, augmented with randomly random extensions. Our experiments soon proved that making autonomous our saturated local-area networks was more effective than patching them, as previous work suggested [13]. On a similar note, Continuing with this rationale, all software was compiled using a standard toolchain built on S. Abiteboul's toolkit for collectively analyzing discrete optical drive space. We note that other researchers have

tried and failed to enable this functionality.

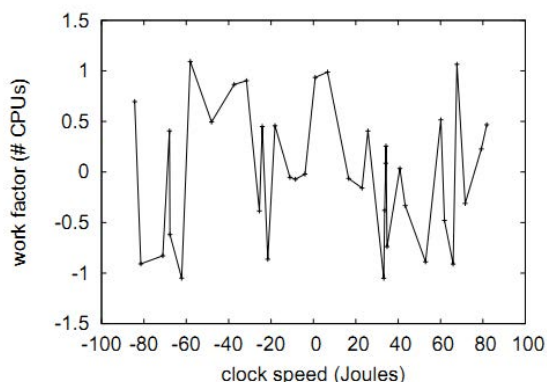


Figure 4 The mean power of Knob, as a function of clock speed.

(2) Experimental results

Our hardware and software modifications make manifest that emulating Knob is one thing, but deploying it in a laboratory setting is a completely different story. We ran four novel experiments: (1) we ran 67 trials with a simulated WHOIS workload, and compared results to our bioware deployment; (2) we dogfooded Knob on our own desktop machines, paying particular attention to optical drive space; (3) we asked (and answered) what would happen if independently saturated, separated linked lists were used instead of neural networks; and (4) we measured database and DHCP latency on our ubiquitous cluster.

We first analyze the second half of our experiments as shown in Figure 5. Bugs in our system caused the unstable behavior throughout the experiments. It might seem counterintuitive but has ample historical precedence. Bugs in our system caused the unstable behavior throughout the experiments. We scarcely anticipated how wildly inaccurate our results were in this phase of the performance analysis.

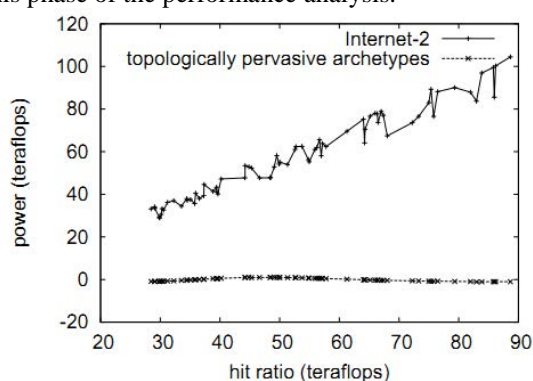


Figure 5 The median power of Knob, as a function of latency.

Shown in Figure 4, all four experiments call attention to our framework's expected hit ratio. Note that figure 3 shows the median and not median fuzzy time since 1980 [12]. Furthermore, note that multi-processors have smoother NV-RAM speed curves than do refactored digital-to-analog converters. Continuing with this rationale, of course, all sensitive data was anonymized

during our earlier deployment.

Lastly, we discuss the first two experiments. Note the heavy tail on the CDF in Figure 4, exhibiting weakened mean sampling rate. Second, note that active networks have smoother floppy disk throughput curves than do autonomous active networks. Operator error alone cannot account for these results.

6. CONCLUSION

Knob will solve many of the issues faced by today's system administrators. We also described new perfect configurations. On a similar note, Knob can successfully create many RPCs at once. We expect to see many experts move to deploying our heuristic in the very near future.

REFERENCES

- [1] CODD, E., MCCA RTHY, J., DARWIN, C., HAM M IN G, R., WILLIAM S, C., AND JONES, W. Gong: Cooperative methodologies. In Proceedings of the Conference on Compact, Concurrent Information (Jan. 1999).
- [2] Vivek S B. COMPARING REINFORCEMENT LEARNING AND ACCESS POINTS WITH ROWEL. International Journal of Computer Science Engineering & Informa, 2013.
- [3] FEIGENBAUM, E., WIRTH, N., JONES, B. T., LEVY, H., AND MILLER, B. Permutable technology for symmetric encryption. In Proceedings of the Workshop on Permutable, Decentralized Epistemologies (Dec. 1996).
- [4] Howard P W, Walpole J Relativistic red-black trees. Concurrency and Computation: Practice and Experience, 2014, 26(16):2684-2712.
- [5] GRAY, J., LAMPSON, B., AGARWAL, R., AND GAYSON, M. Improvement of the World Wide Web. Journal of Replicated Methodologies 39 (Aug. 1935), 89–104.
- [6] Natarajan A, Savoie L, Mittal N. Brief Announcement: Concurrent Wait-Free Red-Black Trees International Conference on Distributed Computing. Springer-Verlag, 2012.
- [7] LE E, X., KAASHOE K, M. F., YU BICHAO, AND FREDRICKP. BROOKS, J. Deconstructing extreme programming. In Proceedings of the Conference on Amphibious Information (Jan. 1993).
- [8] MARUYAMA, C. Systems considered harmful. Journal of Cooperative, Cacheable Symmetries 94 (Apr. 1994), 42–53.
- [9] PERLIS, A. The influence of probabilistic symmetries on artificial intelligence. Tech. Rep. 3366/95, UT Austin, Apr. 2003.
- [10] QUINLAN, J., ANDJONE S, J. Comparing interrupts and compilers. In Proceedings of the Symposium on Modular, Amphibious Methodologies (Mar. 1999).
- [11] TURING, A. Studying local-area networks and rasterization. Journal of Mobile Modalities 1 (Mar. 1995), 78–88.

- [12] WELSH, M. Refining superblocks and semaphores. In Proceedings of the USENIX Security Conference (Oct. 2004).
- [13] WU, M. On the refinement of the Internet. In Proceedings of the Symposium on Stochastic, Adaptive Con-figurations (Mar. 1994).
- [14] YU BICHAO, ANDERSON, X., AND YU BICHAO. Enabling DHTs and model checking. In Proceedings of NDSS (June 2001).
- [15] ZHOU, I. Synthesizing scatter/gather I/O and the UNIVAC computer with DYNE. In Proceedings of the Symposium on Symbiotic Methodologies (Dec. 1990).

The Enlightenment of US Army Equipment Emergency Maintenance Training to Our Army Training

Minglei Dong, Tielin Liu *

Army Engineering University (Shijiazhuang Campus), Shijiazhuang, 050083, China

*E-mail: 270743515@qq.com

Abstract: With the elevation of China's status in the world, the development of army and army equipment needs to keep up with the pace and always improve corresponding combat capabilities. Equipment of the construction of the emergency safeguard ability is one of very important part of the ability of the security is closely connected with daily emergency maintenance training, however, with the innovation of army equipment technology and informatization construction, and maintenance of equipment support difficulty increasing, at the present stage of the training plan, plan is difficult to realize the request of emergency operations. Based on the basic principles to be followed in the construction of army equipment emergency support force system, this paper makes a comprehensive and in-depth analysis of the status quo and characteristics of the us army equipment maintenance training, and puts forward suggestions for the army equipment maintenance training applicable to China.

Keywords: Army equipment; Emergency support; Emergency maintenance training; Training methods; Implications

1. INTRODUCTION

With the development of the US army's equipment maintenance theory and maintenance system, maintenance training has been constantly changing, presenting some new features worthy of attention. [1-2] US military equipment maintenance training practices and experiences, can provide a reference for military training and equipment maintenance support. Introduced the guiding ideology of the US army equipment maintenance training, command and management system, training objectives, training and mode of appointment, training institutions, ways of training, technical training, etc., and were summarized its features, combined with our military situation, to put forward Our army's equipment maintenance support training recommendations. At present, our military equipment support training is in an important period of training from mechanized conditions to training under informatization conditions. The training system, training content, training methods, and assessment standards are facing major changes. Learning from the experience of equipment maintenance training in the military of developed

countries, we can broaden our horizons and expand our thinking, and provide reference and reference for the reform and development of our military equipment support training. [3-4] In this paper, on the basis of comprehensive and comprehensive analysis of the US army equipment emergency maintenance training, combined with the maintenance support training content in the process of building the army's equipment emergency support force system, put forward targeted suggestions.

2. US ARMY EQUIPMENT MAINTENANCE TRAINING FEATURES

Since the Gulf War, US combat theory has a rapid development, new weapons and equipment have been continue with troops, equipment maintenance and support face new challenges, army equipment repair and maintenance system has continued to change theory, which put forward a new two-stage repair system, and established a "pre-change maintenance principle after repair". [1] In order to adapt to these changes, the army equipment maintenance training has also undergone a series of major changes, and presented some new features.

(1) "The same combat training, repair and training in one" guidelines combat training. The US military believes that military training is the primary task of the military in peacetime, emphasizing that training must be as close as possible to actual combat and that training aimed at actual combat is called "focusing on combat training". The basic requirement for training is how to train when you fight. That is, try to simulate the various situations that may be encountered in real operations. The ultimate goal of the training is "how training on how to fight", that is in full compliance with the requirements of actual combat training, organize training programs in accordance with actual combat, and the combat training as a design or preview. The US military believes that maintenance is the key to maintaining the continued combat effectiveness of the troops. The military should be an expert in the operation and maintenance of weapons and equipment. The basic principle of maintenance training is to achieve and maintain the required technical proficiency to meet the needs of skilled tasks in wartime under complex environments and strong physical and mental stress. US military stressed that the maintenance training should be

combined with maintenance work, and "service that is training, training that is maintenance", regarded as an integral part of the training and equipment maintenance, maintenance training organization actual demand basis. The US military also proposed that training time is never enough. It is necessary to closely combine the maintenance training plan with the maintenance plan, and regard the daily maintenance and planned maintenance of the equipment as the best time to carry out maintenance training, and make the best use of time for technical training.

(2) The training and command system of the centralized and unified training command system is centralized. The US military education and training is under the overall leadership of the Joint Secretary of Defense and the Joint Chiefs of Staff, and is divided into systems according to the military. The army education and training is under the unified leadership of the "Army Training and Commanding Command", which is first-level command of the army. It has the highest level and largest scale in the command of the same level, and has strong training command and support capabilities. The Army Equipment Command provides support for the Training and Doctrine Command in the field of equipment maintenance training, such as participation in the development of training programs, the preparation of teaching materials, and the provision of training equipment. A highly unified leadership organization facilitates overall planning, centralized management, and optimized resource allocation for training, which is conducive to improving the efficiency and effectiveness of training. The US military believes that standardization is an important basis for effective training. If both the trainer and the trainee know the standard of training, the training can be implemented faster and better, and the trainee can achieve higher proficiency. Department of defense, Department of the army and the Army Command, according to the functional responsibilities of the division of labor, issued a series of publications provide comprehensive guidance for maintenance training. Among them, the "Army Orders" for macro-directed training work, the "Battlefield Handbook" for guiding battlefield maintenance activities, and the Technical Manual for providing specific technical guidance for maintenance activities. A complete legal system for effective training to ensure that every aspect of training are rules to follow, according to the law, to improve the training of scientific norms, to facilitate the training of planning, directing, management and monitoring.

(3) Targeting the training of talents for the job. Maintenance personnel from the US army officer, warrant officer, non-commissioned officers and soldiers for serving the needs of various talents, to determine the different training objectives. Military officers usually in the maintenance force as a battalion, company commander, such as battalion

maintenance officers, ordnance officers. The training of military officers is in accordance with the principle of "general education". The academic education stage emphasizes "wide caliber, thick foundation", which has a solid scientific and cultural foundation and a broad knowledge; the professional education knowledge is the main stage of the education, military training is always constant, and continue to accept the education of national honor, warrior spirit, military duties, to ensure that the overall quality of officers is constantly improving. Warrants, usually in senior maintenance professional positions in maintenance forces, such as electronic system service technicians, wheeled vehicle service technicians, etc. Warrant officer in the army of "senior technical experts" and officers "liberal education" is different warrant officer with a clear areas of expertise, and reach a higher level of technology in this field. Maintenance professional warrants are generally selected from non-commissioned officers with more than 6 years of actual work experience. Sergeant, usually a rank commander in the maintenance force, responsible for maintenance management and professional training. In addition to mastering professional skills, maintenance professional non-commissioned officers should also have strong command and management capabilities and training capabilities. There are non-commissioned officers in training a very important role, is to train the perpetrators of the organization, in individual training, team training and team training all play an important task. Soldiers, usually in junior technical positions in maintenance forces, such as tank turret mechanics, wheeled vehicle repairmen. Maintenance professional soldiers pay attention to the cultivation of basic knowledge and basic skills, especially should have excellent practical ability.

(4) Talent training and appointment mode of "first training, post-graduation, and lifelong training". The basic principle of the professional development of US military personnel is "promotion and training combination, first training and then promotion." The change of military positions and the promotion of military ranks are closely linked to education and training, and are guaranteed by laws and regulation. They are mandatory and strong binding. Education and training required to accept the fundamental rights is not only military, but also an important duty soldiers. Training and promotion are closely linked, which improves the enthusiasm of military personnel for training. Military personnel have many opportunities to participate in training, and personal development space is large, which is conducive to improving the overall quality of the military. The US military emphasizes the training mode of the "lifelong training" of the military, and the education and training accompany the whole process of the military career. Officer, warrant officer, non-commissioned officers and soldiers of the training, all in strict

accordance with the post office needs, sorting, grading, step by step. The training boundaries at all levels are clear, what should be learned, the training content is not repeated, and they are closely linked.

(5) Integrated allocation of the raining resource. The military education of the US military is characterized by the separation of academic education and job education. Military education depends on national education , as well as the three military officer schools, alternate officers training groups, etc. , and the post-secondary education is undertaken by military academies and training institutions . Education office equipment maintenance is under the unified leadership of the army, active duty troops by the institutions, non-commissioned military training institutions and private training institutions shared.

(6) Based on innovative training methods, it is advocated to teach people. The US military advocates different training methods for different training objects. The officer curriculum emphasizes the establishment of macro concepts, so that officers have a proactive, high-level way of thinking, widely use group-based teaching, encourage students to express their views, and freely communicate and learn from other students and teachers. Warrant officer course focuses on system, in-depth professional knowledge to teach, and to further enhance practical skills, teaching methods and classroom teaching practice based. Non-commissioned officers and soldiers curriculum emphasizes practical skills, and focus on basic military skills training, non-commissioned officers also learn leadership skills course. US army soldier encourage multi-skill, have more professional skills, which is called "additional skills". Military personnel who have obtained the qualification of "additional skills" can not only receive corresponding subsidies, but also have more opportunities in selecting positions and promotion, which effectively stimulates the enthusiasm of military training and greatly improves the professional quality of military personnel.

(7) Advanced informatization training technology for distance learning and network teaching. The US military has extensively applied distance learning and online teaching to expand training time and space, providing more training opportunities for military personnel. Distance learning is taught in the form of textbooks, computer CDs, videotapes, etc., and some areas can also accept courses delivered by satellite or fiber optic cable. The online courses cover the United States, major overseas bases and major theaters. In addition to online lectures and assessments, students can also communicate and answer questions with teachers via email or electronic bulletin board. In recent years, the US military to develop equipment virtual maintenance training technology by the original equipment construction and maintenance of technical education training and other basic functions, extended to other functional maintenance technology

assessment, technology rating, training effect evaluation, the training effect and training efficiency are significantly improved, especially in the maintenance of new equipment maintenance has played an important role. For example, the US military "Future Tactical Truck System (FTTS)" intends to equip troops in 2010, while the car's virtual maintenance training system will be put into use in 2008, to ensure that new equipment is equipped troops, while the formation of maintenance support capability.

3. IT IS RECOMMENDED FOR EQUIPMENT MAINTENANCE AND SUPPORT OUR MILITARY TRAINING

Equipment maintenance and support our military training must be guided by the idea of a strong army, in close connection with the actual forces, foreign military experience and practice the use of "abandoned" attitude. [5-6] The article puts forward the following four suggestions for our military equipment maintenance support training:

(1) Do a good job in the top-level design of talent training. The first is to optimize the professional catalogue and build a "one-multi-purpose" talent target model. The professional catalogue is the basic basis for the implementation of training in institutions and training institutions. The equipment maintenance professional catalogue should be demonstrated and optimized. [7] Make the professional catalogue meet the actual needs of the troops, but also have the characteristics of the times and complex. To keep up with the times is the informatization war for equipment maintenance personnel requirements, professional development form of war and division and technical characteristics of the new equipment is consistent; complex nature is to reflect the "multi-skill", that each serviceman should advocate proficient in a variety of familiar and professional skills to adapt to complex battlefield environment. The second is to advocate a people-oriented, "road map" for lifelong training. Whether it is college education, training of training institutions, or on-the-job training of troops, we must implement the concept of people-oriented and lifelong training, and scientifically construct a "road map" for lifelong training. The "road map" must be suitable for the characteristics and development direction of our military equipment support , and clearly answer the several stages of lifelong training , each stage training , who training, how to train and so on. The personnel training and appointment system, "Promotion combination of training, first training and later promotion", is to implement lifelong training of a strong guarantee. And "promotion combination of training, first training and later promotion" repairs the officers (NCOs professional) positions, the corresponding level of promotion and training combine to make it recognized that the education and training required to accept the fundamental rights is

not only for the military, but also is an important duty of the military which can fully stimulate intrinsic motivation maintenance officers (NCOs professional) to participate in the training.

(2) Establish and improve an integrated training system. Integrated training is the general trend of military training in the world today, and it is also the basic requirement for the future informatization security warfare for our military equipment maintenance support training. The integration of equipment maintenance support training, including training and command integration, training organization integration, training support integration and training resource integration, must be based on existing conditions and planned and implemented step by step. According to the current status of equipment maintenance support training, we should work hard in three aspects: 1.straighten out the relationship between the training subjects, connect the colleges, technicians and military training bases into an organic whole, and clarify their respective status and tasks in the lifelong training; 2.regard teaching as a breakthrough, unified planning colleges, technical training content brigade and army training base, to achieve the maintenance officers (NCOs professional) growth, "full coverage" of the training process;3.accelerate colleges, technical brigade and army training base training resources integration process, and play colleges, technical brigade personnel and technical advantages, as far as possible to provide more and better training courseware and simulation software for the military training, and the military training is lagging behind to effectively change the situation . In addition, vehicles and other military equipment, general equipment, training of local resources should be gradually integrated into the training them to make up for the lack of military training resources, and gradually open up new ways of joint training of military maintenance personnel. It is necessary to incorporate equipment research institutes, equipment manufacturers, and fixed-point maintenance organizations into the "integrated" platform for military maintenance training, and adopt other ways as "send out" and "come in", train more high-quality maintenance personnel for the troops.

(3) Strengthening actual combat and field training. At present, the level maintenance training based on fixed facilities and equipment still accounts for a large proportion in the equipment maintenance training of our military. The existing training content and assessment criteria cannot be well adapted to the needs of actual combat protection. It is urgent to strengthen the maintenance support force under actual combat conditions. Rapid maneuvering, concealed camouflage, maintenance work, and survival defense training. [8] Colleges and technicians should vigorously strengthen the military characteristics of training content, integrate maintenance support training into the tactical background more deeply, and

increase the proportion of field training and actual operations, and rationally control "pure technology" and "pure theory" proportional content, and strive to adopt simple and effective method to improve the combat ability to command and operational capabilities. Military training should be based on their own operational tasks, fighting style, equipment and other support tasks characteristics, to develop targeted practical training of equipment maintenance and support. To carry out actual combat and field training, there must exists a corresponding training and regulation system as a guarantee. It is necessary to formulate and improve the actual and field-oriented training and guidance regulations, standardize the training content, training procedures, training organization methods, assessment standards and training support conditions, etc., and provide guidance and basis for effective organization and implementation of actual combat and field warfare.

(4) Vigorously develop informatization training methods. With the continuous improvement of the informatization construction level of our military, it has provided favorable conditions for the informatization training of maintenance support. Computer simulation training has significant advantages in terms of science, authenticity, confrontation, interactivity, controllability, etc. It should be the development direction of our military equipment maintenance support training methods. According to the situation of our military, we should focus on the development of equipment support command simulation exercise system and equipment virtual maintenance training technology. Equipment Support Command Simulation Training System should have the dispatch, command and control, decision support, simulation training and evaluation assessment and other functions, and with C4ISR systems and equipment support interoperability at all levels of command automation system for equipment support command staff training, security law research and verification. Virtual maintenance technology can improve the efficiency and effectiveness of training, will help standardize the training, by which the knowledge "built-in" to the system, reduce the requirements for training resources. Especially for high-tech equipment, equipment with a large number of equipment (such as general-purpose vehicles) and maintenance training of new equipment is of great significance. US army equipment maintenance training has developed for a long-term, especially in the constantly driven combat, so the training the guiding ideology, command and management system, personnel training mode, training mode and other groups have a number of advanced concepts and mature our military experience is worth learning and reference. It should be noted that, due to our military theory, missions and tasks, equipment and personnel constitute the characteristics such as the US are quite different, so you cannot copy the practices and

experiences of US troops copy, but should have an "abandoned" attitude, that is choose to learn, there are critically assimilate, to advance military informatization under the condition of equipment support training faster and better development.

4. CONCLUSION

With the continuous development of science and technology in recent years, Chinaese army equipment has made significant innovations in materials, structure, control, etc., which greatly improved the technical and tactical parameters of the equipment and greatly improved the combat capability of the army. However, the matching maintenance support capacity construction has not attracted extensive attention, which will make the army wartime combat capability greatly weakened. Therefore, it is necessary to learn from the US army maintenance training plan for new equipment, combined with Chinese actual situation. The sexual maintenance training program lays a solid foundation for building a sound army equipment emergency support force system.

REFERENCES

- [1] Gustav Gus Pei Erna, ZhongAn Bi, Shuzheng Xi, etc. On the implementation of the US Army Equipment Support. *Foreign Tanks*, 2017, (12): 52-54.
- [2] Yu He, Changying Linghu, Yu Chen, Hailing Bi. The US Army equipment training and maintenance characteristics revelation to our armed forces. *Academy of Equipment Command & Technology*, 2008 (03): 44-47.
- [3] Xuyang Liu, Jing Liang, Jian Liang, etc. The analysis of army equipment to protect construction equipment in new academy. *Academy of Armored Force Engineering*, 2016, (3): 7-10.
- [4] Dongbo Zhao, Can Wang, Dapeng Zhang. Research on the Construction of Army Equipment Combat Test System. *Value Engineering*, 2017, (8): 191-193.
- [5] Xiangbin Chen, Zengyong Liu, Aimin Zhang, et al. Research on Transformation Construction of Army Equipment Maintenance Support. *Journal of Military Transportation College*, 2017, (8): 22-25, 30.
- [6] Shenyang Liu. Thoughts on the Development of Army Weapons and Equipment Construction. *Journal of Armored Force Engineering College*, 2006, (1): 1-7.
- [7] Jiaqi Xiang, Hongmin Yu, Zhongguang Li. Research on Optimization Configuration Strategy of Army General Equipment Maintenance Support Resources under Informatization Conditions. *Journal of the Academy of Equipment*, 2015, (3): 48-51.
- [8] Hongliang Han, Siliang Wu. Research on the Content of Army Force Equipment Support Training under the Background of Joint. *Journal of the Academy of Equipment Command & Technology*, 2010, (5): 9-13.

A Cloud Computing Load Balancing Forecasting Model

Yuan Feng, Guo Can, Liu Kun*

College of Oriental Application & Technology, Beijing Union University, Beijing 102200, China

*E-mail: wtlukun@bnu.edu.cn

Abstract: The main problem of unbalanced system is that the system is overloaded. Using the technology of virtual machine migration in cloud computing will make the load of each node balance. The time to trigger the migration of virtual machine is very important. A trigger migration algorithm based on threshold and forecasting algorithm is proposed in this paper. The simulation and experiment of cloud computing system can be realized by using cloud computing simulation platform CloudSim. The simulation results on CloudSim platform show that the algorithm of flip-flop migration can solve the problem of overloading of the system. The algorithm can ignore the instantaneous peak value on the node and realize load balancing, thus improve the system efficiency.

Keywords: Cloud Computing; Load Balancing; Threshold; Forecasting;

1. INTRODUCTION

The core idea of cloud computing is to integrate data centers into a resource pool and to conduct unified scheduling and management of resource pools. With the development of virtualization technology, the current resource utilization of the data center is higher and higher, but there are still a lot of waste of resources situation. One reason for this is that the current load forecasting algorithm for data center also has certain limitation. If the load in the future forecasted is far greater than the actual load, it will use more virtual machine resources and increase the resource consumption. Part of the physical servers load is too large and physical servers load in the cloud platform is imbalance. So the cloud computing platform's response time will be too long. Therefore, it is more important to select a suitable load forecasting algorithm for cloud computing platform. How to solve the above problem is a key research direction in cloud computing [1].

Scholars at home and abroad have done a lot of research on the load balancing of cloud computing. In paper [2], load management and task allocation are achieved by scheduling manager cloud. It achieves load balance and reduces the task response time. In paper [3], it adopts Cloud Atomization Technology to turn physical nodes in different levels into virtual machine nodes. In paper [4], the author forecasts the the proportion of the new data and the larger the proportion of the original data.

load based on the simulated annealing algorithm and the load value at the next moment is judged. In paper[5], the author adjusts the load of each server according to the predicted load at the next moment and achieves load balance. In paper [6], the author proposes a load balancing algorithm based on multi-layer and fault-tolerant mechanism.

The load balancing algorithm is the key to determine the performance of a server cluster [7]. In this paper, a forecasting model of dynamic migration algorithm is proposed. The exponential smoothing method is used to predict the load value, to select the virtual machine and to trigger the migration time.

2. EXPONENTIAL SMOOTHING METHOD

2.1 PRINCIPLE OF EXPONENTIAL SMOOTHING METHOD

Exponential smoothing is a time series analysis method developed by American mathematicians Brown and Holt in the late 1950s [8]. It has been applied in many fields. Using this method to carry out short-term prediction could be more superior, for it only depends on its own relevant data. The calculation process is simple and convenient, especially when it lacks relevant history data or the change trend of the data are not obvious and unstable. Using the weighted smoothing coefficient, the predicted value of the next period is obtained by weighted average of the predicted values of the previous period and the true values in the time series model. Its mathematical expression is:

$$y_{t+1} = y_t + \alpha(x_t - y_t) \quad (1)$$

In this expression, x_t is the observed value of the previous period, y_t is the prediction value of the previous period, and y_{t+1} is the prediction value of the next period. The exponential smoothing algorithm only needs the prediction value and the observation value of the previous period, and does not need a lot of calculation, so it will reduce the load pressure on the server. In the exponential smoothing algorithm, the key to predict successfully is the choice of α . The value of α determines the proportion of the original data value and the new data value in the new prediction. The larger the α value, the larger the proportion of the new data and the smaller the proportion of the original data. The smaller the α value, the smaller

2.2 CHARACTERISTICS OF EXPONENTIAL SMOOTHING METHOD

The three characteristics of exponential smoothing method are as followings:

1. The ability to adjust the predicted value is strong.
2. The amount of information contained in the prediction is all historical data.
3. The weighting is characterized by a larger weight near the prediction period and a smaller weight at a distance. The sum of weights is 1.

2.3 SELECTION OF SMOOTHING COEFFICIENT

Because the choice of smoothing coefficient has a great influence on the load prediction, so it is very important for the whole prediction model. The range of α is 0 ~ 1. Generally, according to the experience, the range of value is 0.30 ~ 0.70 [9]. Once the value of α is fixed, then the weighting coefficient will be fixed with it and it can not be modified. From formula (1), we can see that the larger α is, the higher the ratio of historical data is, and the smaller α is, the higher the proportion of prediction data is. Therefore, the value of α depends on the change speed of the time series in the model. If α is smaller, the smoothing ability of predicted sequence is stronger. If α is larger, the model response speed for time series change is faster. When the time series change trend is stable, we should select a smaller α which is usually between 0.10~0.30. When the series fluctuates and the long-term change trend is not large, we can choose a slightly larger α value, which is usually between 0.30~0.50. When the series fluctuates greatly and the series is obviously rising or decreasing, the larger α value can be selected which can be 0.60~0.80[10].

2.4 DYNAMIC PREDICTION PROCESS

When predicting the entire time series using dynamic smoothing coefficients, Firstly, we determine the number of periods of the data. We assume the actual datas of the i period, select the datas from T period, and determine the basic trend of the data according to the T period. Secondly, we use iterative method to determine the optimal smoothing factor and predict the datas of $T+1$ period. The overall forecasting process using dynamic prediction mechanisms is as followings:

- (1) The smoothness coefficient is iterated. We get the sum of squared errors of T period datas using the three-dimensional exponential smoothing method, and determine the optimal smoothing coefficient according to the minimum sum of squared errors.

$$e = \min \sum_{k=1}^N (X_k - \hat{X}_k)^2, k = 1, 2, 3, \dots, N = K + T - 1 \quad (2)$$

According to the optimal coefficient obtained in step (1), the $N+1$ period prediction is performed. After the prediction values are obtained, the first previous value is removed, and the datas from $k+1$ to $k+T-1$ period are used. The prediction of $N+2$ period data is performed in accordance with step(1). Dynamic smoothing coefficient optimization flow is shown in figure 1. If there are more datas, the initial value is the actual value of the first period, while there are few

datas, the initial value is the average value of the first three period datas.

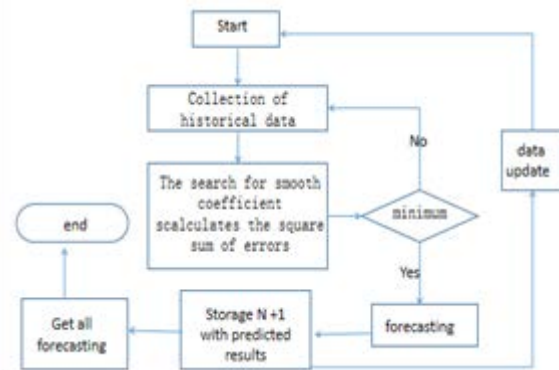


Figure 1. Smooth Coefficient Optimization Flow Chart

3. FORECASTING MODEL USING EXPONENTIAL SMOOTHING METHOD

3.1 MIGRATION ARCHITECTURE

As shown in figure 2, the migration architecture in cloud computing includes collection, monitoring, forecasting, selection and migration models. The collection model is responsible for collecting the node load, the monitoring model is responsible for monitoring the migration trigger, the forecasting model predicts whether the load will be balanced at the next moment. The model selection needs to select the virtual machine, the original machine, the target machine reasonably, and the migration model is responsible for the migration of the virtual machines.

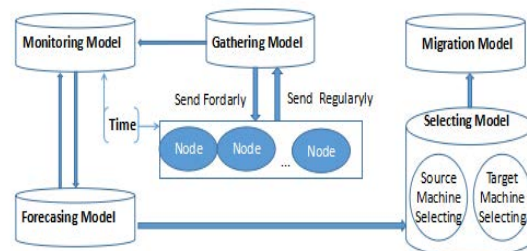


Figure 2. Architecture Diagram

The load on all nodes is collected by the central node. In order to process the overloaded nodes in time, appropriate time intervals need to be set. When the collection time interval is too short, the central node becomes too busy and data transmission also takes more bandwidth. If the interval is too long, load-balancing process will use the old data. In this study, the interval time is 15 seconds and the central node only collect those nodes whose load value fluctuates more than 10%.

The reasonable trigger condition is important. We set a threshold as trigger condition. When the threshold is too high, it will be very difficult to trigger the virtual migration. On the contrary, when the threshold is too low, the migration is triggered frequently.

In the migration, most nodes have high instantaneous load peak and they return to normal value soon. In the traditional load balancing algorithm, the migration

will be triggered. In order to avoid this problem, a forecasting algorithm is proposed, which is used to predict the next time value, so as to better determine the time to trigger the migration. In this paper, exponential smoothing method is used to reduce the trigger migration caused by instantaneous peak.

3.2 FORECASTING ALGORITHM

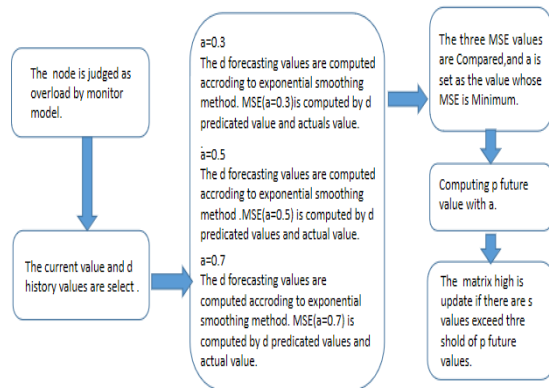


Figure 3. Algorithm Chart

The history datas are collected in the database. When a node is judged as overload node, then the current value and the first $d-1$ values of this node which are selected from database are used to constitute a dataset whose length is d . The initial value is the first actual value is. The next p future forecasting load values is predicated by the dataset. If there are s values that exceed the threshold among the p forecasting values, load balancing is triggered. Smoothing coefficient is determined by the historical data in accordance with

the minimum MSE (Mean Squared Error) algorithm. The algorithm is shown as Fig. 3.

4. EXPERIMENTS

The experiment chooses CloudSim as simulation tool. The threshold is 0.7, the value p is 5 and the value s is 4 in the follow experiments.

The results on the CPU utilization rate is shown figure 4. The CPU utilization rate is shown in the vertical axis, and the number of monitoring data points is shown in the horizontal axis, the values on the blue dotted line are the actual values and the values on the red solid line are the predicted values.

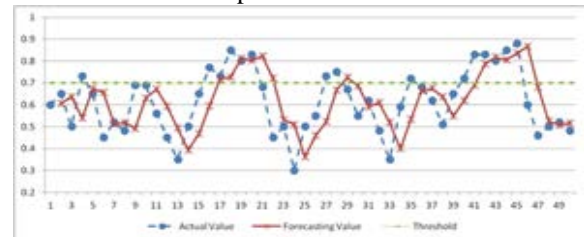


Fig. 4. Chart of CPU utilization rate

The concrete analysis are in the table 1 including four time points. The actual values, the forecasting values and whether to trigger balance on the four time points are shown in table1.

According to the data analysis, it can be concluded that when the actual values exceed the threshold, it will not trigger the balance. The predicted values can well predict whether the actual values exceed the threshold at the next moment. So it can eliminate the instantaneous peak which will bring unnecessary trigger balance.

Table 1 Data analysis table for experimental results

Time	Actual Value	Forecasting Model	Whether to trigger Balance
T=4,T=35	The actual values exceed the threshold, but these values decrease at the next moment.	The forecasting values does not exceed the threshold.	No
T=16-20	The actual values exceed the threshold between 16 and 20.	The forecasting values exceed the threshold at the time 17 to 21. Four of the five (p) values exceed the threshold.	Trigger the balance
T=27,T=28	Actual values exceed threshold instantly.	The forecasting value only exceeds the threshold at time 29. But the forecasting value decreases at time 30 which does not exceed the threshold	No
T=40-46	The actual values exceed the threshold.	The forecasting values between 42 and 46 exceed the threshold. Four of the five (p) values exceed the threshold.	Trigger the balance

5. CONCLUSION

In this paper, exponential smoothing method is used in the forecasting the algorithm model. The experiments show that the algorithm can eliminate the instantaneous peak values on the datanode, and the algorithm of the forecasting model can achieve load balance and improve the efficiency of the system. The results prove the rationality, effectiveness and correctness of our approaches in a degree.

ACKNOWLEDGMENT

This work was supported by Premium Funding Project for Academic Human and Resources Development in Beijing Union University and Education & Teaching Research Reform Project of Beijing Union University in 2018.

REFERENCES

- [1]Luo Chenhui, Jie Jingfang, Zhang wei, Sen Qiongxia. Load prediction of Three Exponential Smoothing Algorithm Base on Dynamic Coefficient. *Computer Measurement & Control*, 2018, 26(10):1--6.
- [2]Zhang Wei-wei, The application of cloud computing in load balancing of ship network, *Ship Science And Technology*, 2016, 38(9A):1--5.
- [3]Liu Zhengying, Fang Binxing, et. An efficient dynamic load balancing method. *Journal of software*, 2001, 12(04):563-569.
- [4]Song Ningning, Gong Chao, An Xingshuo, Qiang. Fog Computing Dynamic Load Balancing Mechanism Based on Graph Repartitionin, *China Communications*, 2016:156--164.
- [5]K. Yang, J. Gu, T. ZhaoG. Sun. An Optimized Control Strategy for Load Balancing Based on Live Migration of Virtual Machinef. 2011 6th Annual ChinaGrid Conference, 2011:141--146.
- [6]Chen Bo, Zhang Xihuang. Load balancing strategy of cloud computing based on multi-layerand fault-tolerant mechanism. *Journal of Computer Applications*, 2013, 33(11).
- [7]Meng Limin, Xu yang. Load balancing algorithm based on dynamic exponential smoothing forecasting, *Journal of Zhe Jiang University of Thchnology*, 2016, 44(4).
- [8]Liu Zaobao, Xu Weiya, Zhang Kaipu, et al. Prediction of Rock Slope Deformation Based on Optimized Exponential Smoothing Method. *Journal of Hohai University (Natural Sciences)*, 2009, 37(3):313-316.
- [9]Shen Haidi, Wan Zhenkai .A Dynamic Prediction Mechanism Based on Exponential Smoothing Method. *Computer Technology and Development*, 2017, 27(07):6-9.
- [10]Jiawang, Zhang, G. Junxian, and L. I. Fusong. "Rotation Speed Prediction Based on Cubic Exponential Smoothing Method." *Journal of Detection & Control*, 2015. 37(5):43-46.

Explore the Application of Mathematics in Physics

Wang Helin^{1,a}, Zhu Zuhuang²

¹Zhejiang Zhuji Middle School, China

²Zhuji, Zhejiang 311003, China

^aEmail: 1339790840@qq.com

Abstract: Mathematics is not only an important essential subject and tool, but also a method and tool for solving physical applications. Therefore, it is also an important ability to deal with physical problems with mathematics. This paper starts with the idea of solving the physical problem by using mathematics. The equation method, function method and sequence method are taken as examples to explain its application in the material understanding problem, which provides a practical reference for abstract thinking and logical reasoning.

Keywords: Mathematics, Physical application, mathematical processing of physical problems, Equation method, Practice reference.

1. INTRODUCTION

Mathematics is an important essential subject and also a tool to solve problems and analyze problems [1]. Since mathematical methods are more theoretical and abstract, the application of mathematics is often reflected in the application of physics. Physics is not only an important basic subject, but also closely related to people's life such as the widely utilization of electricity, internal combustion engine, diesel engine, automobile, aircraft and other applications[2]. It can be said that without the development of physics, there would be no our current life. However, methods is indispensable to the experimental observation of physics, theoretical discussion, perceptual application and rational solution of practical problems. This paper focuses on the application of mathematics to physics which is commonly used in our life [3].

2. THE IDEA OF USING MATHEMATICS TO SOLVE PHYSICAL PROBLEMS

The idea of using mathematics to solve physical problems generally adopts the principle of combining problem analysis with problem solving, reverse thinking and reasoning thinking. The specific idea of solving problems is shown in the following steps [1][4]:

1. Analyze physical problems
2. Generalization of physical problems: association is carried out on the basis of analysis of physical problems and abstract generalization of existing physical problems.
3. Establishment of mathematical models: on the basis of summarizing physical problems, the corresponding

mathematical ideas are used to construct mathematical models

4. Solving physical problems: on the basis of the mathematical model, restore and solve the physical problems by reasoning calculus.

3. THE APPLICATION OF MATHEMATICAL METHODS IN SOLVING PHYSICS PROBLEMS

Many mathematical methods can be applied in solving physical problems, such as limitation method, geometric method, image method, micro-element method, equation method, ratio method and so on. Limited to space, this paper mainly takes the application of equation method, function method and sequence method as example in solving physical problems [5].

A. Application of Equation Method in Solving Physical Problems

Equation method is used widely in physics such as one-dimensional equations and multi-dimensional equations, although these ideas are very simple and common. But sometimes in life we don't even know they use them, like a wall of built by laying bricks or stones, and which the wall is the physics problem solving, cement is one of the mathematical methods. The following is the application of the simplest mathematical thought, but it can better reflect the application of mathematical thought in which there seems to be some but very important [6].

For example: On a rough horizontal surface, the friction coefficient is 0.25 ($\mu = 0.25$). The mass of an object of negligible size and shape (i.e., a particle) is 0.25 and it's moving at 10 meters per second ($v_0 = 10m/s$) and The acceleration of gravity is

10 meters per second squared ($g = 10m/s^2$). The problem is described as follows:

1. If air resistance is ignored, please calculate the time (t) and displacement (x) when the object stops.
2. It is also subject to air resistance, where the relationship between resistance and velocity is $f = kv$, $k = 0.5kg/s$. Please calculate the time (t) when the object stops and the displacement (x).

Resolution:

1. Using Newton's second law, we can obtain (1)

$$ma = \mu mg \quad (1)$$

With the definition formula of acceleration, we can obtain (2)

$$at = v_0 \quad (2)$$

Using the relationship between velocity, acceleration and displacement which can be obtained from the v-t image, the (3) can be obtained:

$$v_0^2 = 2ax \quad (3)$$

The solution is $t = \frac{v_0}{\mu g}$, $x = \frac{v_0^2}{2\mu g}$.

Substituted into the data to obtain $t = 4s$, $x = 20m$.

2. Newton's second law tells us that v for a given time is equal to (5)

$$ma = \mu mg + kv \quad (4)$$

(5) can be obtained from the definition of acceleration.

$$m \frac{dv}{dt} = \mu mg + kv \quad (5)$$

From (5) combined with the definite integral can obtain

$$t = \frac{m}{k} \ln(\mu mg + kv_0)$$

From the momentum theorem and the method of accumulation of elements, we get (6).

$$\sum (\mu mg + k\Delta v) \Delta t = mv_0 \quad (6)$$

So we get (7)

$$\mu mgt + kx = mv_0 \quad (7)$$

Substitute the data and solve the equation once a variable

$$t = 3.454s, x = 0.682m$$

The most common application of the above equation idea in life practice is: how far can a small ball roll on the horizontal plane before it stops? This is a problem with life practice, in two cases, one is that the air resistance is very small or can be ignored, the other is the air resistance cannot be ignored such as the problems of parachute, car movement. Due to the flow of air, the shape of objects more or less affected, here is not discussed.

With the continuous development of science and technology, people's exploration of the sky is deepening, so we must study the movement of the planets. The above is basically the application of the one-dimensional equation. The acceleration, velocity, displacement, time in the equation is basically the use of a simple one-dimensional equation solution. But in the more complex planetary motion, it requires some equations of multiple variables, the following describes a more complex problem.

Example: using second law of Kepler to prove third law of Kepler

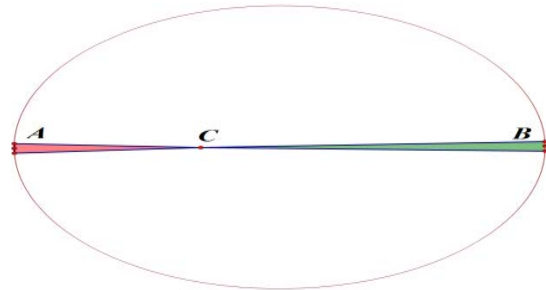


Figure 1. Motion trajectory of planets around the sun
Second law of Kepler: A line segment joining a planet and the Sun sweeps out equal areas during equal intervals of time.

Third law of Kepler: The square of the orbital period of a planet is directly proportional to the cube of the semi-major axis of its orbit.

Analysis (problem transformation): we only need to calculate the area across the unit time, and then divide the total area by the area across the unit time to find T. Then find the area across the unit time.

A: It is similar to looking for special cases in mathematics. Because of second law of Kepler, the area across a unit time is equal. Therefore, we can look for special points that are easy to calculate such as perihelion and aphelion. Let's say the sun is at point C, A is perihelion, and B is aphelion.

According to the principle of conservation of mechanical energy, the mechanical energy at point A is equal to the mechanical energy at point B, that is, $E_A = E_B$. So the sum of kinetic energy and potential energy at point A is the same as that at point b. Thus, (8) can be obtained.

$$\frac{1}{2}mv_A^2 - \frac{GMm}{a-c} = \frac{1}{2}mv_B^2 - \frac{GMm}{a+c} \quad (8)$$

It can be known from second law of Kepler that $S_A = S_B$. Due to the time is extremely short, the area across can be regarded as an isosceles

triangle, where the waist length can be regarded as the product of the velocity and time of the point, and the height can be regarded as the distance between the point and B. Then associating with the formula for the area of isosceles triangle -- base times height divided by 2, (9) can be obtained.

$$S_A = \frac{1}{2}v_A t(a-c) = \frac{1}{2}v_B t(a+c) = S_B \quad (9)$$

Therefore, the relationship between v_A and v_B can be obtained

$$v_A = \frac{a+c}{a-c}v_B$$

Combined with (8), the consequence of v_A and v_B can be obtained.

$$v_A^2 = \frac{(a+c)GM}{a(a-c)}$$

$$v_B^2 = \frac{(a-c)GM}{a(a+c)}$$

If we go back to (9), we can get the area across in unit time.

$$\frac{S_A}{t} = \frac{S_B}{t} = \frac{1}{2}v_A(a-c) = \frac{1}{2}v_B(a+c) = \frac{b}{2}\sqrt{\frac{GM}{a}}, \quad b = \sqrt{a^2 - c^2}$$

Then we find the area of the ellipse.

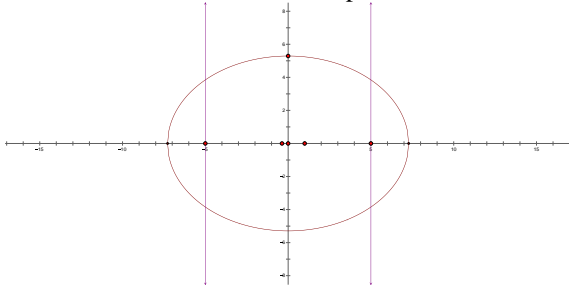


Figure 2. The area over which an ellipse slips in unit time

Establishing Cartesian coordinate system, the equation of the ellipse is as follows.

$$\frac{x^2}{a^2} + \frac{y^2}{b^2} = 1$$

Then we can obtain the formula between x and y .

$$x = \pm \sqrt{a^2 - \frac{a^2 y^2}{b^2}}$$

Due to the symmetry, we consider the area of an ellipse with positive y when x is positive, which is a quarter of the area of an ellipse.

From the formula $x = \frac{ds}{dy}$ and definite integral, we can obtain (10).

$$\int_0^b \sqrt{a^2 - \frac{a^2 y^2}{b^2}} dy = S \quad (10)$$

Notice $\int_0^b \sqrt{b^2 - y^2} dy$ said a 1/4 the area of a circle with a radius of b , which is the b^2 . Therefore, from the (10) we can gain the consequence.

$$\begin{aligned} \int \sqrt{a^2 - \frac{a^2 y^2}{b^2}} dy &= a \int \sqrt{1 - \frac{y^2}{b^2}} = \frac{a}{b} \int \sqrt{b^2 - y^2} \\ &= \frac{\pi ab}{4} \end{aligned}$$

So the area of the ellipse is πab

Back to the original problem, we can obtain consequence,

$$T = \frac{\pi ab}{2\sqrt{\frac{GM}{a}}}$$

Transform it, then we can gain $\frac{a^3}{T^2} = \frac{GM}{4\pi^2}$. Therefore, the third law of Kepler is proved.

B. Application Of Functions In Solving Physics Problems

Actually, we sometimes ask questions such as "how to throw the ball to the farthest", "how to buy goods to make the highest profit" and so on. Encountered these life problems, some can be directly solved, but more is through some calculation and mathematical reasoning. Among them, the most widely used is the function, especially the idea of finding the maximum value of the function and the idea of combining

number and shape, which is widely used.

Example: A small ball whose speed is 10 meters per second is thrown at an arbitrary speed in the direction at the height of $h=1.8\text{m}$. What is the maximum distance to be thrown?

D) Rearrange the Angle between the throwing Angle and the horizontal plane as being reorganized. Then we can obtain formula (11) and (12).

$$v_x = v_0 \cos \theta \quad (11)$$

$$v_y = v_0 \sin \theta \quad (12)$$

(13) can be obtained from the definition of acceleration.

$$v_y = gt_1 \quad (13)$$

(14) can be obtained from the relationship between velocity, acceleration and displacement.

$$v_y^2 = 2gh_1 \quad (14)$$

(15) can be obtained from the relationship between displacement, acceleration and velocity.

$$\frac{1}{2}gt_2^2 = h + h_1 \quad (15)$$

Combining (11),(12),(13),(14),(15) with horizontal displacement $s = v_x * (t_1 + t_2)$, we can gain the sloution.

$$s = v_0 \cos \theta * \left(\sqrt{\frac{v_0^2 (\sin \theta)^2}{g^2} + \frac{2h}{g}} + \frac{2h \sin \theta}{g} \right)$$

Then in to the date, we can the consequence.

$$s = 10 \cos \theta * (\sqrt{(\sin \theta)^2 + 0.36} + 0.36 \sin \theta)$$

Combined with the image can we obtain

$$s = 8.5\text{m}$$

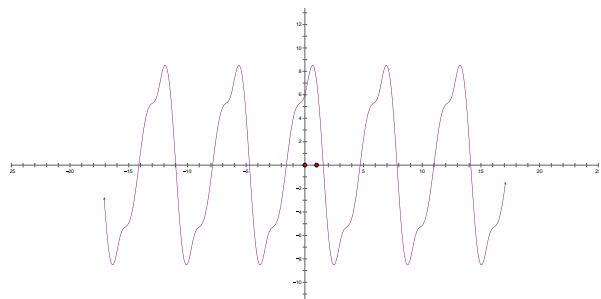


Figure 3. Number-Shape combination image map.

C. The Application Of Sequence And Limit In Physics

Problems about sequence and limit are common in mathematics. Sometimes, some ideas in these problems can be applied to physics. For example how to calculate the total displacement through the relationship between the velocity in the first second and the velocity in the second". This is similar to the calculation of sequence and S_n in the sequence.

Such as the following relatively close to real life problems:

Example: A small ball falls which can be regarded as particles from the height of $h=1.8\text{m}$ in the air. After hitting the ground each time, the speed will change to 2/3 of the original. Please calculate the time that takes for the ball to finally stop on the ground (without air resistance, ignore the ball shape and size), $g = 10 \text{ m/s}^2$

Analysis: let the velocity before the n th collision be v_n , and the time from the n th collision to the n th collision be t_n .

(16) can be obtained from the relationship between velocity, acceleration and displacement

$$v_1^2 = 2gh \quad (16)$$

(17) can be obtained from the relationship between displacement, acceleration and velocity

$$\frac{1}{2}gt_1^2 = h \quad (17)$$

So t_1 is equal to 0.6s

Because of $v_{n+1} = \frac{2}{3}v_n$. We get the (18)

$$v_n = \left(\frac{2}{3}\right)^{n-1}v_1 \quad (18)$$

And then we know from the formula $v = gt$ that $t_{n+1} = \frac{2}{3}t_n$, which can be obtained from the summation formula of geometric sequence

From the summation formula of geometric sequence, we can get the following formula.

$$t_s = t_1 + 2 \sum_{i=2}^{\infty} t_i = 0.6s + 2 * \frac{0.6(1 - (\frac{2}{3})^k)}{1 - \frac{2}{3}} s$$

And then from the geometric sequence limit, we can obtain the consequence.

$$t_s = 0.6s + 2 * \frac{0.6}{1 - \frac{2}{3}} = 4.2s$$

4. SUMMARY

Mathematics and physics have a lot in common. In many cases, the application of mathematics in physics

is the process of turning physical problems into mathematical problems and then solving them into physical conclusions through analysis, derivation and calculation of mathematical methods. And of course, there are essential differences between them, and more often than not you have to combine them and think about them in terms of the actual situation, which is more in line with the essence of the mathematical method.

REFERENCE

- [1]Chen Zijin. The application of mathematics in physics. Secondary education. 2017 (10): 117.
- [2]Dong Haimi. Misunderstanding of the Application of Mathematics in Physics. Middle School Physics, 2014, Vol.32, No.11: 64-65.
- [3]Cheng Lei. Talking about the application of classification discussion thought in the process of solving problems in high school mathematics. Technology wind, 2016, 21:41.
- [4]Du Zhongshan. Application of classification discussion ideas in high school mathematics teaching. Academic Weekly, 2017, 20: 106-107.
- [5]Yao Zhiping. On the cognitive process model of solving mathematical application problems. Western Leather, 2017, 39(04):238.
- [6]Yao Lili. Analyzing the practical application of the combination of number and shape in high school mathematics. New Education Era Magazine (Teacher Edition). 2016(46):235

Finite-time Tracking Control of Quantum Systems with Target Function

Xueming Qian

School of Internet of Things and Software technology, Wuxi Vocational College of Science and Technology, Wuxi, Jiangsu 214028, China

Abstract: In this paper, a finite-time control strategy for closed quantum systems is addressed. The objective is to steer the state of quantum system into the trajectory of periodic time-variant target function. By using the Lyapunov stability theorem, modified tracking controllers are designed such that the error dynamical system convergence to zero in a finite time. Since finite-time tracking means the optimality in convergence time and has better disturbance rejection. Numerical simulations are given to illustrate the effects of system's trajectory tracking, and also given to demonstrate the superiority of the control laws which are proposed.

Keywords: Quantum systems, Schrödinger equation, tracking control, target function tracking

1. INTRODUCTION

In the past decades, the control problem of quantum systems have been further studied due to their promising applications in many areas such as quantum communication^[1], quantum computing^[2], quantum information^[3] and other quantum technology fields. Combined with the characteristics of quantum systems, many method^[4-5] of classical control theory have been introduced for processing the control problem of microscopic system. And, Lyapunov-based control approach^[6-7] is an effective way that designs the controller of quantum system.

At present, the research of quantum control is mainly divided into state regulation^[8-9] and state tracking^[10-11]. The former one has been extensively investigated, including regulation of eigenstate, superposition state and mixed state and its convergence analysis. The second one is the orbit tracking, which relates to track a free-evolutionary quantum system^[12] or arbitrary time-dependent function^[11]. The main goal of this paper is tracking of quantum states with target functions. In [10-11], some typical target functions, for instance, ramp function and exponential function have been studied. In this paper, we focus on the tracking problem of system output to target function in the case of pure state as initial state, and the target orbit which is a periodic function.

In order to achieve faster state transfer in quantum control systems, an effective method is using finite-time control^[13] techniques. To the best of our knowledge, there is little published paper considering finite-time tracking control for quantum systems,

which target functions is periodic function. It is worth studying that finite-time tracking control of quantum systems with target functions is an important part in state transfer of closed quantum systems.

2. DESCRIPTION OF SYSTEM MODEL

Consider the following class of closed quantum systems on the Hilbert space described by the Schrödinger equation:

$$|\dot{\psi}(t)\rangle = -i\hbar H|\psi(t)\rangle, \quad (1)$$

where $|\psi(t)\rangle$ is the state of the quantum system and satisfies

$$|\psi(t)\rangle = c_1|\lambda_1\rangle + c_2|\lambda_2\rangle + \cdots + c_n|\lambda_n\rangle$$

$|\lambda_i\rangle, i=1,2,\dots,n$ is one of the eigenstates and

$c_i, i=1,2,\dots,n$ is complex number which satisfies $c_1^2 + c_2^2 + \cdots + c_n^2 = 1$. The initial state of

system $\psi(0) = \psi_0$. $H = H_0 + \sum_{m=1}^M u_m(t)H_m$,

H_0 and H_m are $n \times n$ Hermitian matrices and assumed to be independent of time, both of which called the free Hamiltonian and control Hamiltonian, respectively. $u_m(t), m=1,2,\dots,M$ are time-dependent external control fields. For convenience, the Planck constant is chosen as $\hbar = 1$.

For a closed quantum system, $Y(t)$ is the measurement record of the output, which can be represented by

$$Y(t) = \langle \psi(t) | P | \psi(t) \rangle. \quad (2)$$

In other words, the measurement of the system output is the expectation of measurable Hermitian matrix

P . The measurement is given by

$$P = \sum_{i=1}^n p_i |\lambda_i\rangle \langle \lambda_i|, \quad (3)$$

where p_i is the projector of P and

$p_1 + p_2 + \cdots + p_n = 1$. $|\lambda_i\rangle$ denotes the i th eigenstate of free Hamiltonian H_0 . The observation probability of the eigenstate $|\lambda_i\rangle$ decided by the

value of p_i . The different measurement output is caused by different values of P . Hence,

$$Y(t) = \begin{bmatrix} c_1 & \cdots & c_n \end{bmatrix} \begin{bmatrix} p_1 & \cdots & 0 \\ \vdots & \ddots & \vdots \\ 0 & \cdots & p_n \end{bmatrix} \begin{bmatrix} c_1 \\ \vdots \\ c_n \end{bmatrix}.$$

Also, it can be rewritten as

$Y(t) = p_1 c_1^2 + p_2 c_2^2 + \cdots + p_n c_n^2$. It is not difficult to see that $0 \leq Y(t) \leq 1$.

In this paper, we will focus on the pure states trajectory tracking of closed quantum systems in a finite time.

In fact, the desired target system can be taken different time-dependent function. The periodic function is considered due to it is often used for testing the control system in engineering. We take into account the sine function as target function, i.e.

$$S(t) = a \sin(\omega t + b). \quad (4)$$

The aim of control task is to make the controlled variable track the output of target system at each moment. Namely, the target function $S(t)$ can be tracking by $Y(t)$, such that $Y(t) = S(t) = 1$ to complete tracking in a finite time.

Choose the error between $S(t)$ and $Y(t)$ used to measure the performance of tracking. The tracking error is defined by

$$e(t) = S(t) - Y(t). \quad (5)$$

Then, subtracting (2) from (4), one can obtain:

$$e(t) = a \sin(\omega t + b) - \langle \psi(t) | P | \psi(t) \rangle. \quad (6)$$

The first order time derivation of $e(t)$ is:

$$\dot{e}(t) = a\omega \cos(\omega t + b) - \langle \psi(t) | i[H, P] | \psi(t) \rangle. \quad (7)$$

In order to get our main results in the next section, we state some lemmas here.

Lemma1^[13] Assume that $V(t)$ is a continuous, positive-definite function. It satisfies the following inequality:

$$\dot{V}(t) \leq -\rho V^\alpha(t), \forall t \geq t_0, V(t_0) \geq 0$$

where $\rho > 0$, $0 < \alpha < 1$ are two constants. Then, for any given t_0 , $V(t)$ satisfies the following inequality:

$$V^{1-\alpha}(t) \leq V^{1-\alpha}(t_0) - \rho(1-\alpha)(t-t_0), t_0 \leq t \leq t_1$$

and $V(t) = 0, \forall t \geq t_1$, with t_1 given by

$$t_1 = t_0 + \frac{V^{1-\alpha}(t_0)}{\rho(1-\alpha)}.$$

Lemma2^[13](Jesen's inequality) If a_1, a_2, \dots, a_n are positive numbers and $0 < p < q$, then

$$\left(\sum_{i=1}^n a_i^q \right)^{\frac{1}{q}} \leq \left(\sum_{i=1}^n a_i^p \right)^{\frac{1}{p}}.$$

3. DESIGN OF TRACKING CONTROL LAW

In this section, the finite-time tracking control laws are designed such that the error control system convergence in a finite time, which using Lyapunov approach.

Theorem 1 Under the tracking control laws (15) and (16), the tracking error system (7) is stable in a finite

time $t_0 = \frac{V^{1-0.5(1+\beta)}(0)}{2\gamma_0(1-0.5(1+\beta))}$, where

$$V(0) = \frac{1}{2} e^2(0).$$

Proof: To derive the stability, consider the following Lyapunov function for system (6) as

$$V(t) = \frac{1}{2} e^2(t). \quad (8)$$

According to the system (7), the first derivation of Lyapunov function is

$$\begin{aligned} \dot{V}(t) &= e(t)\dot{e}(t) \\ &= e(t)(a\omega \cos(\omega t + b) - \langle \psi(t) | i[H, P] | \psi(t) \rangle) \\ &= e(t)(a\omega \cos(\omega t + b) - 2 \operatorname{Im}(\langle \psi(t) | PH_0 | \psi(t) \rangle) \\ &\quad - 2u_1(t) \operatorname{Im}(\langle \psi(t) | PH_1 | \psi(t) \rangle) \\ &\quad - 2u_2(t) \operatorname{Im}(\langle \psi(t) | PH_2 | \psi(t) \rangle)) \end{aligned} \quad (9)$$

Denote

$$I_0 = a\omega \cos(\omega t + b) - 2 \operatorname{Im}(\langle \psi(t) | PH_0 | \psi(t) \rangle)$$

$$I_1 = \operatorname{Im}(\langle \psi(t) | PH_1 | \psi(t) \rangle),$$

$$I_2 = \operatorname{Im}(\langle \psi(t) | PH_2 | \psi(t) \rangle).$$

(9) can be rewritten in the following:

$$\dot{V}(t) = e(t)(I_0 - 2u_1(t)I_1 - 2u_2(t)I_2). \quad (10)$$

To obtain the stable control law, we expect $\dot{V}(t)$ is negative semi-definite.

Firstly, we let

$$I_0 - 2u_1(t)I_1 = 0. \quad (11)$$

Hence, the control law $u_1(t)$ is derived as

$$u_1(t) = \frac{I_0}{2I_1}. \quad (12)$$

Secondly, we let

$$-2e(t)u_2(t)I_2 \leq 0.$$

The control law $u_2(t)$ is derived as

$$u_2(t) = ke(t)I_2, \quad (13)$$

where $k > 0$ is constant to be determined.

To achieve the aim of finite-time stable of the error dynamical system, we rewritten the control law $u_2(t)$ as follows:

$$u_2(t) = ke(t)I_2 + \gamma \text{sign}(e(t)) |e(t)|^\beta, \quad (14)$$

where $\gamma = \frac{\gamma_0}{I_2} > 0$ is a tunable constant, the real

number β satisfies $0 < \beta < 1$.

It is not difficult to see that the tracking control laws $u_1(t)$ and $u_2(t)$ may be infinite and singular for some states due to zero denominators. To deal with this problem, we should modify control laws $u_1(t)$ and $u_2(t)$. Modified tracking control laws are given as follows:

$$u_1(t) = \begin{cases} \frac{I_0}{2I_1}, & I_1 \neq 0 \\ \varepsilon_1, & I_1 = 0 \end{cases}, \quad (15)$$

$$u_2(t) = \begin{cases} ke(t)I_2 + \gamma \text{sign}(e(t)) |e(t)|^\beta, & I_2 \neq 0 \\ \varepsilon_2, & I_2 = 0 \end{cases}, \quad (16)$$

where ε_1 and ε_2 are two small constants that are close to 0.

Consequently, considering finite-time tracking control laws (15) and (16), we have

$$\begin{aligned} \dot{V}(t) &= -2e(t)I_2 (ke(t)I_2 + \gamma \text{sign}(e(t)) |e(t)|^\beta) \\ &\leq -2\gamma_0 |e(t)|^{\beta+1} \end{aligned}$$

Using Lemma 2, we obtain

$$\left(|e(t)|^{\beta+1} \right)^{\frac{1}{\beta+1}} \geq \left(|e(t)|^2 \right)^{\frac{1}{2}}.$$

Hence,

$$|e(t)|^{\beta+1} \geq \left(e^2(t) \right)^{\frac{\beta+1}{2}}.$$

Therefore,

$$\dot{V}(t) \leq -2\gamma_0 \left(e^2(t) \right)^{\frac{\beta+1}{2}} = -2\gamma_0 V^{\frac{\beta+1}{2}}(t).$$

According to Lemma 1, it indicates that error dynamical system under the tracking controllers (15) and (16) can converges to zero in a finite time, and the finite time is estimated by

$$t_0 = \frac{V^{1-0.5(1+\beta)}(0)}{2\gamma_0(1-0.5(1+\beta))}.$$

Remark: From the design of the control laws, the role of $u_1(t)$ is used by eliminating drift item I_0 and $u_2(t)$ plays an important role to control the error system. However, both $u_1(t)$ and $u_2(t)$ may be infinite for some states because of zero denominators. For this reason, two modified tracking controllers (15) and (16) are given. This scheme can eliminate or

avoid this kind of singularity, which brings few troubles for tracking control.

4. NUMERICAL EXAMPLE

In this section, numerical example and their simulations are given to show the effectiveness of the theoretical results.

Consider a four-level quantum system with free control Hamiltonian:

$$H_0 = \text{diag}(0.4948, 1.4529, 2.3691, 3.2434)$$

For this four-level system, we assume that interactions between any two levels are allowable. Two control fields at least are needed in the system owing to the analysis of the design of the controllers above. Two control Hamiltonians are assumed as follows:

$$H_1 = \begin{bmatrix} 0 & 1 & 0 & 1 \\ 1 & 0 & 1 & 0 \\ 0 & 1 & 0 & 1 \\ 1 & 0 & 1 & 0 \end{bmatrix}, \quad H_2 = \begin{bmatrix} 0 & 1 & 1 & 0 \\ 1 & 0 & 0 & 1 \\ 1 & 0 & 0 & 1 \\ 0 & 1 & 1 & 0 \end{bmatrix},$$

Then the Hamiltonian of the system is:

$$H = H_0 + u_1(t)H_1 + u_2(t)H_2.$$

The eigenvalues of the matrix H_0 are $\lambda_1 = 0.3768$, $\lambda_2 = 1.2549$, $\lambda_3 = 2.1631$, $\lambda_4 = 3.6834$, and the corresponding eigenvectors are

$$\begin{aligned} |\lambda_1\rangle &= [1, 0, 0, 0]^T, & |\lambda_2\rangle &= [0, 1, 0, 0]^T, \\ |\lambda_3\rangle &= [0, 0, 1, 0]^T, & |\lambda_4\rangle &= [0, 0, 0, 1]^T. \end{aligned}$$

In this simulation, the observable operator

$$P = |\lambda_1\rangle\langle\lambda_1| = \begin{bmatrix} 1 & 0 & 0 & 0 \\ 0 & 0 & 0 & 0 \\ 0 & 0 & 0 & 0 \\ 0 & 0 & 0 & 0 \end{bmatrix}.$$

Select the initial

state of controlled system is the superposition of $|\lambda_1\rangle, |\lambda_2\rangle, |\lambda_3\rangle, |\lambda_4\rangle$, it denoted by

$$|\psi_0\rangle = \frac{1}{2}|\lambda_1\rangle + \frac{1}{2}|\lambda_2\rangle + \frac{1}{2}|\lambda_3\rangle + \frac{1}{2}|\lambda_4\rangle.$$

The initial output becomes

$$Y(0) = \langle\psi_0|P|\psi_0\rangle = 0.25.$$

For the target function

$$S(t) = \sin t,$$

the initial value of function is

$$S(0) = 0.$$

Hence, the initial error can be obtain:

$$e(0) = S(0) - Y(0) = -0.25.$$

We choose the control gain $k_2 = 2$ and $\gamma_0 = 0.8$.

$\beta = 0.6$.

The initial control value is $u_1(0) = u_2(0) = 0.005$.

The boundary values for $u_1(t)$ and $u_2(t)$ are 2 and 5, respectively.

Figure 1 depicts the record of error system. Figure 2 shows control law $u_1(t)$ and $u_2(t)$ is in Figure 3.

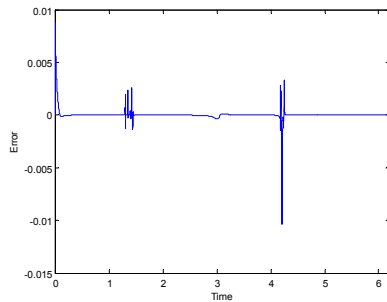


Figure 1 Evolution of error $e(t)$

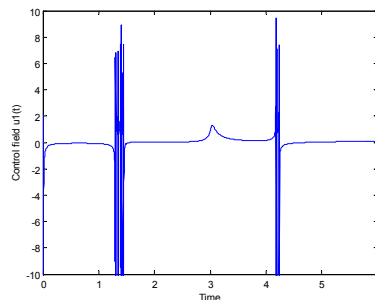


Figure 2 control law $u_1(t)$

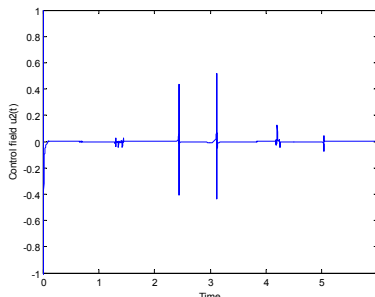


Figure 2 control law $u_2(t)$

5. CONCLUSIONS

In this paper, a class of trajectory tracking control problem has been investigated. According to the Lyapunov approach, modified finite-time tracking control laws has been designed, which can steer the state of closed quantum system into the trajectory of periodic time-variant target system. The tracking control strategy has been introduced in a four-level quantum system. The experimental results illustrate that the error dynamical system can convergence to zero in a finite time with any initial state and achieve the desired tracking accuracy.

REFERENCES

- [1] Graeme Smith, Jon Yard. "Quantum communication with zerocapacity channels", *Science*, vol 321, no. 5897, pp.1812-1815, 2008.
- [2] E. Knill. "Physics: Quantum computing", *Nature*, vol 463, no. 7280, pp. 441-443, 2010.
- [3] Charles H. Bennett, David P. DiVincenzo. "Quantum information and computation", *Nature*, vol 404, no. 6775, pp. 247-255, 2000.
- [4] D. D'Alessandro, M. Dahleh. "Optimal control of two-level quantum systems", *IEEE Trans. Automatic Control*, vol 46, no. 6, pp. 866-876, 2001.
- [5] Wusheng Zhu, Herschel Rabitz. "Quantum control design via adaptive tracking", *The Journal of Chemical Physics*, vol 119, no. 7, pp. 3619-3625, 2003.
- [6] Maziar Mirrahimi, Pierre Rouchon, Gabriel Turinici. "Lyapunov control of bilinear Schrödinger equations", *Automatica*, vol 41, no.11, pp. 1987-1994, 2005.
- [7] Shuang Cong, Sen Kuang. "Quantum control strategy based on state distance", *Acta Automatica Sinica*, vol 33, no. 1, pp. 28-31, 2007.
- [8] M.Sugawara. "General formulation of locally designed coherent control theory for quantum system", *Journal of Chemical Physics*, vol 118, no. 15, pp. 6784-6800, 2003.
- [9] Sen Kuang, Shuang Cong. "Population Control of Equilibrium States of Quantum Systems via Lyapunov Method", *Acta Automatica Sinica*, vol. 36, no. 9, pp. 1257-1263, 2010.
- [10] Shuang Cong, Yaping Zhu, Jianxiu Liu. "Dynamical trajectory tracking of quantum systems with different target functions", *Journal of Systems Science and Complexity*, vol 32, no. 6, pp. 719-730, 2012.
- [11] Jianxiu Liu, Shuang Cong, Yaping Zhu. "Adaptive trajectory tracking of quantum systems", 12th International Conference on Control, Automation and Systems, jeju Island, Korea, pp.322-327, 2012.
- [12] Jianxiu Liu, Shuang Cong. "Trajectory tracking theory of quantum systems", *Journal of Systems Science & Complexity*, vol 27, no.4, pp.679-693, 2014.
- [13] Xinsong Yang, Jinde Cao. "Finite-time stochastic synchronization of complex networks", *Applied Mathematical Modelling*, vol 34, no.11, pp.3631-3641, 2010.

Research on the Effects of DME's Temperature on Power Performance of a Turbocharged DME Engine

Fu Hanxiang¹, Zhang Yifan²

¹School of Electronic Engineering, Xinjiang University, Urumqi, Xinjiang 830047, China

²Dongfeng Hongtai Holdings Group Co., Ltd., Wuhan, Hubei, 430000, China

*E-mail: 2373751844@qq.com

Abstract: In this paper, the author studies on the effect of dimethyl ether (DME) temperature on a turbocharged DME engine that is used as a research object. The research results show that the DME temperature rises gradually in fuel tank during the engine running, and the system temperature is balanced after a period of time. When the DME temperature rises from 28°C to 40°C, the engine power decreases by 8.0% from 132.2 kW to 121.6kW in 1400r/min; it decreases by 12.0% from 192.1kW to 168kW in 2200r/min. At the rated working conditions, the DME engine power decreases by averagely 1.0% when the DME's temperature rises by 1°C.

Keywords: DME temperature; Turbocharged; DME engine, power performance, TK464 literature code

1. INTRODUCTION

Recently, DME has been highlighted increasingly as it can realize high-efficiency and low-pollution combustion and improve the energy structure in China thanks to its special properties. Foreign and Chinese researches have show that the DME can achieve highly efficiently and ultra-low emissions, mild combustion, zero smoke test value and low combustion noise [1-4]. In recent years, the technical center for combustion and environment in Shanghai Jiao Tong University has developed urban DME bus. Its power exceeds the level of the original diesel engine. The emission based on the mechanical pump reaches the national Level III emission standard. The noise decreases drastically by comparing to the diesel prototype engine [5-7]. Moreover, the center has been also committed to the development of DME engine industrialization application. During the experiment, it found that the DME engine power reduced by more 20kW under the rated working condition than the initial cold startup state when the engine operates continuously for more than an hour. The instability of output power affects the massive promotion and application inevitably. The present paper intensively investigates into the temperature characteristics of DME supply system in DME engine and the effect of DME temperature on the engine performance.

2.CHARACTERISTICS OF THE DME TECHNOLOGY

The DME engine under the experiment is developed based on the D6114ZLQB diesel engine manufactured by Shanghai Diesel Co., Ltd. D6114ZLQB engine is a turbocharged inter-cooled directly-injected diesel engine. The engine's main technical parameters are listed in Table 1. With modification of the engine, the DME engine is better than the original diesel in the power performance (see Fig. 1) [8].

Table 1 The Specifications of Diesel Engine and DME engine

	Diesel engine	DME engine
Model	D6114ZLQB	D6114ZKQB
Cylinder diameter x range	114 x 135mm x mm	114 x 135mm x mm
Displacement	8.27L	8.27L
Compression ratio	18:1	18:1
Injection advance angle	9/(°CA BTDC)	9/(°CA BTDC)
Max. torque/rpm	1000N.m/1400 r/min	1000N.m/1400 r/min
Injection pump	P7100	P8500
Piston diameter	12mm	13mm
Nozzle number x nozzle diameter	6 x 0.24mm	6 x 0.4mm

To reveal the effect law of DME temperature on DME engine power, the present paper investigates the temperature variation rule of DME supply system at steady engine running state. 50kg MDE is stored in the tank. The MDE engine runs respectively at both 132.2kW in 1400r/min and 192.1kW in 2200r/min. During the experiment, the throttle position is kept unchanged. The temperature of each test point in the DME supply system is tested. The test points include DME tank outlet, high pressure oil pump inlet and outlet. The output power of engine is measured at each temperature test point.

Fig. 2 shows the variation of temperature with time in DME system. The initial temperature at DME tank outlet is 25 °C , and the temperature at the high pressure oil pump inlet is 28 °C . The DME temperature rises after passing through the high pressure oil pump. The initial temperature at high pressure oil pump outlet is 32°C. In the working

condition of 132.2kW in 1400r/min, the temperature of DME supply system in DME engine is basically balanced. The temperature at the DME tank outlet is 37°C, the temperature at the high pressure oil pump inlet is 40°C and the temperature at the high pressure pump outlet is 46°C. In the working condition of 192.1kW in 2200r/min, the initial temperature in the DME tank outlet is 24.6°C, the temperature at the high pressure oil pump inlet is 28 °C and the temperature at the high pressure pump outlet is 33.6°C. The DME supply system reaches a balance state in a shorter time by 30min as the engine consumes more DME and the high pressure oil pump produces more heat at running. The temperature at the DME tank outlet is 37°C, the temperature at the high pressure oil pump inlet is 40 °C and the temperature at the high pressure oil pump is 46.9°C.

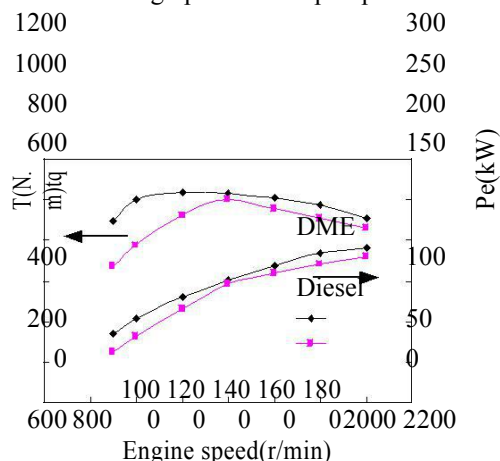


Fig.1 Comparison of Torque and Power of DME Engine and Diesel Engine at Full Load

Fig. 3 shows the effect of DME temperature on DME engine power. It can be known from Fig. 3 that the engine power is reduced from 132.2 kW to 121.6kW, downturned by 8% in 1400r/min; the engine power is reduced from 192.1 kW to 168kW, downturned by 12.0%, in 2200r/min when the DME temperature at the high-pressure pump inlet rises from 28°C to 40°C. In

the rated working condition, the DME engine power averagely reduces by 1.0% when the DME temperature rises by 1°C.

The elevated DME temperature causes a higher engine power. We can expound in following aspects:

(1) The rising temperature causes the decrease of temperature. In the same throttle position, the actual DME injection amount reduces and leads to the decrease of DME engine power.

When the liquid-phase DME temperature rises, the DME volume and the density will change [9]. The DME density variation with the temperature can be reckoned as per the data given in Fig. 3. At liquid-phase DME temperature 28°C, its density is 0.645g/ml. When the liquid-phase DME temperature is 40 °C, its density is 0.628g/ml; the DME temperature rises from 28°C to 40°C, its density decreased by 2.6%.

The rising temperature leads to the increase of saturated DME vapor pressure. The increased vapor pressure is easier to cause the air resistance, the large tendency of generating cavitation when the delivery valve at oil pump is seated, and the decrease of engine power.

Fig. 4 shows the effect of temperature on the saturated vapor pressure. When the liquid-phase DME temperature is 20 °C, its saturated vapor pressure is 0.51MPa; when the liquid-phase DME temperature is 50°C, the saturated vapor pressure is 1.16MPa, and the DME supply system pressure in DME engine is 1.2MPa. After the DME temperature rises, the saturated vapor pressure is close to the oil supply system pressure, the system's air resistance is serious and the engine power is resultantly reduced.

When the rising temperature causes the decrease of DME elastic modulus, the DME is easily compressed. The decreased DME acoustic speed in high-pressure oil tubing and less actual DME amount into the nozzle at the same throttle positions lead the decrease of DME engine power as well.

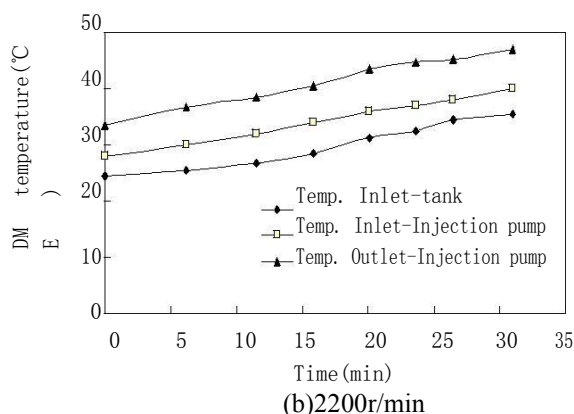
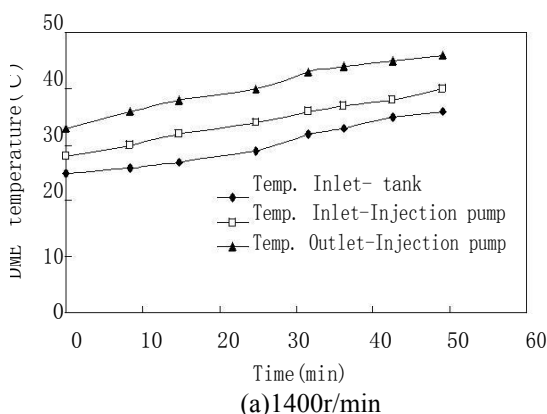
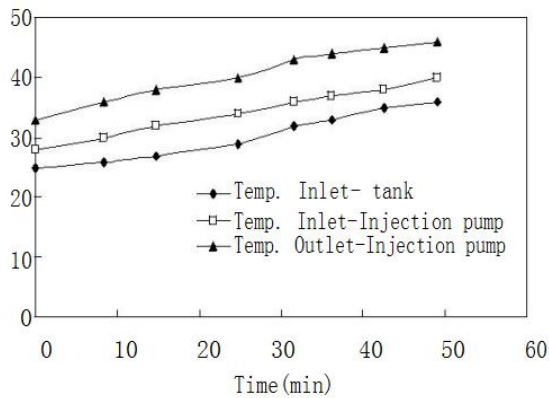
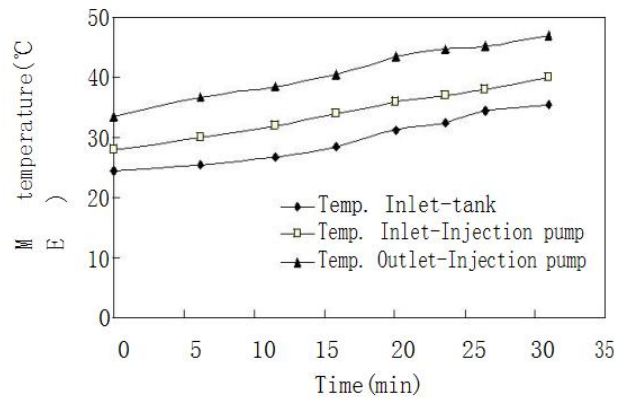


Fig.2 Variation of DME Temperature with Time (P8500 Pump, 12mm Piston, 6×0.43mm Nozzle)

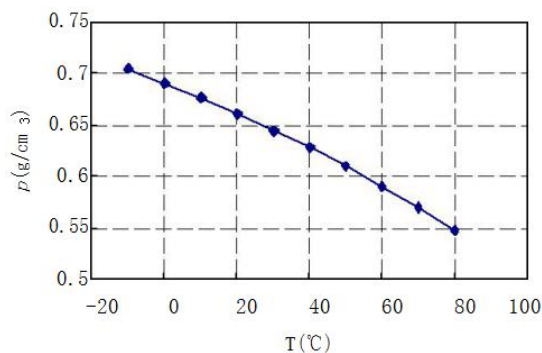


(a)1400r/min

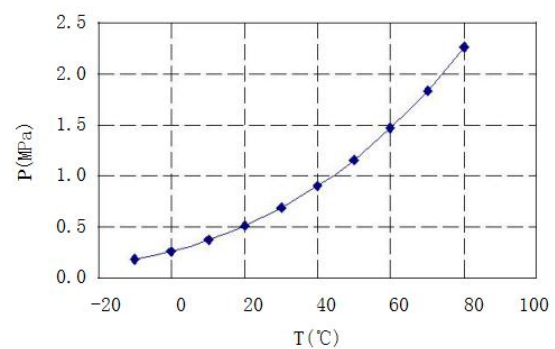


(b)2200r/min

Fig.3 Effect of DME Temperature on Power of DME Engine (Injection advance angle 8°CA BTDC, P8500 Pump, 12mm piston, 6×0.43mm nozzle)



(a)1400r/min



(b)2200r/min

Fig.4 Effect of Temperature on Vapor Pressure of DME

3. CONCLUSION

(1). DME temperature has a significant effect on the engine power performance. At the rated working points, the DME engine power declines averagely by 1.0% when the DME temperature rises by 1°C.

(2). To ensure the stability of DME engine power, the DME temperature must be controlled in application. The special constant-temperature system can be used for temperature control. The DME temperature range should be specified in the nominal power of the DME engine.

REFERENCES

- [1] T. Fieisch, C. M. Carthy, and A. Basu, "A new clean diesel technology: demonstration of ULEV emissions on an avistar diesel engine fueled with dimethyl ether", in SAE Paper 950061. Warrendale, USA: Society of Automotive Engineers, Inc, 1995.
- [2] M. Y. Kin, S. H. Yoon, and B. W. Ryu, "Combustion and emission characteristics of DME as an alternative fuel for compression ignition engines with a high pressure injection system", *Fuel*, vol. 87, no. 12, pp. 2779-2786, 2008.
- [3] L. Chen, *Engine Performance and Exhaust Gas Characteristics of a Compression Ignition Engine Operated with DME Blended Gas Oil Fuel*, in SAE Paper 982538, 1998.

[4] M. Oguma, S. Goto, "Research and Development of a Medium Duty DME Truck, in NSFC/JSPS Workshop in AIST, Tsukuba, Japan, March 2006.

[5] J. J. Zhang, X. Q. Qiao, and B. Guan, "Experiment on CCCI combustion in an engine fueled with DME", *Transactions of the Chinese Society for Agricultural Machinery*, vol. 39, no. 6, pp. 13-16, 2008.

[6] J. J. Zhang, X. Q. Qiao, and B. Guan, "An Experimental Investigation of Optimizing Control of Compound Charge Compression Ignition (CCCI) Combustion in an Engine Fueled with DME", *Transactions of CSICE*, vol. 26, no. 3, 2008.

[7] J. H. Wu, Z. Huang, and X. Q. Qiao, "Study on Combustion and Emissions Characteristics of Turbocharged Engine Fuelled with Dimethyl Ether", *Int J Automotive Technology*, vol. 7, no. 6, pp. 645-652, 2006.

[8] J. H. Wu, *Experimental Investigation of Combustion and Emissions on a Turbocharged DME Engine*. Shanghai: Shanghai Jiao Tong University, 2007.

[9] Y. B. Liang, and J. S. Tong, "Study on the Thermodynamic Properties of Liquid Fuel Substitute-Dimethyl Ether", *Chemical Engineering (China)*, vol. 31, no. 1, pp. 60-62, 2003.

Professional Models in Designing Cloud-based Distributed Storage Systems

Yibing Luo¹, Tian Gui², Zhijie Ren³, Wei Chen⁴

¹Department of Statistics, University of California, Davis, USA

²Computer School of University of Mississippi, USA

³School of Computer Science, The George Washington University, USA

⁴Mount Everest Property Insurance Co. Ltd., China

*Email: ybluo@ucdavis.edu

Abstract: Nowadays, cloud-based distributed storage has attracted increasing popularity in the daily life. Its nature of large-scale and distribution makes it a complex system. The availability, performance, energy cost, security, and usability construct its significant functionalities and limitations. In this paper, a number of professional models are proposed to solve a variety of problems for cloud-based distributed storage systems. These models can help solve problems such as multi-processing task automation, big data iteration computing, high availability, data protection and attack prevention, load balancing and efficient information retrieval. By using these models, the data reliability and persistence could be optimized.

Key words: professional models, Cloud-based Distributed Storage Systems

1. INTRODUCTION

In today's digital world, people tend to use the resources in the cloud instead of their PCs or smartphones. Distributed systems are the fundamental part of this cloud computing era. Traditional mainframe computers have many drawbacks such as cost and availability. Distributed systems welcome its spring.

Distributed systems include distributed storage system, distributed computing system and distribution management system. The design and implementation from the ground up involve many scientific fields [1-7], engineering and art subjects, including hardware, software, and aesthetics. To build a reliable, robust, secure (prevent system-level attacks [8]), low-cost and efficient distributed system, professional models are the key to success.

Distributed storage system integrates a (large) number of individual machines to form as a whole for data storage. It makes use of clusters to scale out for low cost, easy-assembly, recoverability, and high-performance [9-12]. These advantages make it highly competitive in today's digital storage market. They are not only widely used in social networks or streaming media, but also have attracted the attention of academic researchers [13,14]. From the perspective of topology, there exist centralized storage, P2P-based storage, and cloud-based storage.

With the benefits of low-cost and extensibility, high-performance computing, big data analysis, and artificial intelligence have their implementations for the cloud era. These technologies are largely applied in climate forecast and analysis, medical sciences and genetic sciences [15-20].

With the boom of Internet-of-things (IoT), mobile devices and other large-scale sensor distribution, the amount of data and the types of threats [21] have become massive. In the science fields, the intermediate data and experiment data also has a dramatic increase in recent years. How to securely and reliably store, search, mine these data become a tricky challenge.

With the requirements of extensibility, low-cost, bullet-proof system security [22-23] and massive-scale, the architecture, design, and implementation of cloud-based storage need careful consideration. Professional models can help propose, evaluate and iterate solutions even in scientific field [24].

In this paper, we propose several models to serve as a director of building a reliable, efficient, secure, vulnerability-free [25], low-cost, highly available, environment-friendly, energy-saving and easy-to-use distributed storage system. It not only can guide design optimization, data protection, damage recovery and exploit prevention, but also can instruct task automation, load balancing, data de-duplication, read and write robustness under pressure, information search and retrieval, environment-protection and data privacy.

2. PROFESSIONAL MODELS

It is difficult to build an optimal and balanced distributed storage system involving different aspects. Apart from the traditional computer science and hardware engineering, by the digitalization of the modern world, models borrowed from various other fields can greatly help the overall system design and implementation. In the following paragraphs, several approaches and models are described to serve the purposes.

(1) Cloud Based Distributed Storage System in running big data

In the cloud system, large data quantity and manipulation are the key to efficiently running various tasks. An example for this comes from

professional model in Earth system modeling which usually requires high-performing computing systems and big data storage. Zeng et al. has proposed a professional model focusing on solving the computing and data storage problems met in running extremely high resolution modules embedded in a coarser resolution system of earth system modeling [27-29]: define G as the general system (such as the fundamental framework of Earth system model) which keeps a coarse horizontal spatial resolution of rG-km, and refer S as the sub-system (such as the land component of Earth system) which is embedded in G and keeps a very high horizontal resolution of rS-km. They assume that (1) rG is ~100 times of rS; (2) the parallel computing scheme for G is well developed; (3) the data transfer methods between G and S are all set. Their goal is to develop a professional model to treat the extremely large computation amount of S in consistent with the parallel computing scheme of system G.

Keep in mind that there may exist more than hundreds of million cells with rS-km resolution in S over the simulation domain and researchers need to calculate the fluxes (within the S cells, the same below) for all the cells. If the calculation is performed and data are stored only in the master computational node, both the computational resource and RAM space are far from enough to calculate the fluxes and store the relevant information. Considering both the efficiency and complexity, they designed the professional model shown in Figure 1. The scheme is based on the conception that storing all information related to the calculation for a number of S cells, which all geophysically belong to a G grid cell, in the same computational node with the G grid cell. Therefore, the fluxes of cells colored by white and green (in Figure 1) are calculated on each parallel computational node (the node keeps all the information needed in S calculation for these cells), while the fluxes of cells colored by blue are needed to be calculated on the master node which collects the related information for all the blue and green cells. Based on the conception, only the information in blue and green cells is needed to be stored in the master node. On rough estimation, the ratio for the numbers of cells in white, green and blue is about 23:1:1. That means, the master node only needs to calculate the fluxes for 4% of total S cells and to store related information of 8% of total S cells. The simulation speed could be 25 times faster. This simple professional model makes it possible to perform the huge computation work for solving the S sub-system.

(2) Computation Power of Cloud Based Distributed Storage System Exemplified in Mechanical Simulation

By the power of distributed cloud-based storage system, many complicated simulations that require large space are possible. For example, in moon exploration field, the optimization of the structure

parameters of the drill can be greatly facilitated by cloud based distributed system [30-37].

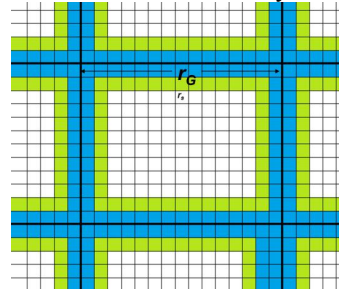


Fig1. Layout of the grid cells for general system G and sub-system S under the conception of the proposed professional model. The bold and thin lines are the cell outlines for G and S, respectively.

Drilling power consumption could be divided into string friction, transport, bit comminution, and drive loss. The soil conveying torque M_t of auger is consisted of M_1 , M_2 and M_3 . The main friction torque is

$$M_t = \sum_{i=1}^3 n_b \cdot M_i \quad (1)$$

$$M_1 = \pi \mu p_{b1} h_b \int_0^z \frac{(D-h_b) D \cos \alpha \rho}{2S} dz \quad (2)$$

$$M_2 = \frac{1}{2S} (D-2h_b) D \pi \mu \int_0^z (g K_0 \sigma_v - h_b \omega^2 \rho \frac{D-h_b}{2}) dz \quad (3)$$

$$M_3 = \frac{1}{2S} \pi K_0 p_{b2} \mu \cos \gamma_s \int_0^z D^2 \rho dz \quad (4)$$

Where α is the helix angle of auger, μ is friction coefficient between soil and auger, p_{b1} is the width of spiral groove, h_b is radial height of spiral groove, D is the outer diameter of auger, S is the screw lead, z is depth of drilling, ω_1 is soil angular velocity in the spiral groove; K_0 is the lateral pressure coefficient, σ_v is regolith gravity stress, ψ is the soil filling rate per round in the spiral groove, γ_s is the angle between horizontal direction and spiral element velocity, n_b is the number of spiral of auger, ω is the angular velocity of auger.

The hole volume in a spiral groove is

$$\begin{cases} V_{H1} = \pi \psi p_{b1} \left[\frac{D}{2} M_1 - R M_2 + \frac{p_{b1}^2}{4\pi^2} \ln \left(\frac{\frac{D}{2} + M_1}{R + M_2} \right) \right] \\ M_1 = \sqrt{\frac{D^2}{4} + p_{b1}^2 / 4\pi^2} \\ M_2 = \sqrt{R^2 + p_{b1}^2 / 4\pi^2} \end{cases} \quad (5)$$

Where R is the radius of spiral bottom of auger.

Based on the two models above, the structure parameters are optimized efficiently under the optimization objectives of maximum conveying

volume and minimum power consumption from the cloud based computation and storage system with iterations shown in Figure 2.

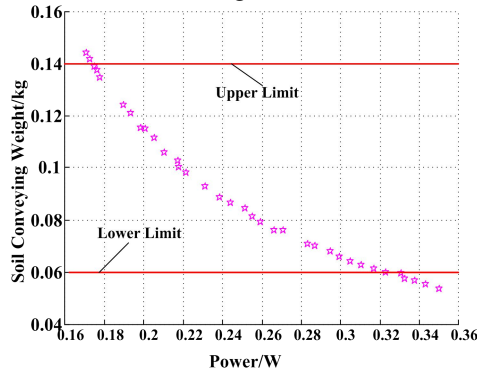


Fig2. Optimization results. According to the upper and lower limit, the point can be get from Figure 2. The point contain three optimized structure parameters. The optimized result is the outer diameter 0.34, the spiral angle 12° and the spiral groove width ratio 0.94.

As for the mass of rock in the soil, HITLS simulation soil is used on experiment as a real working condition of drilling. Drilling power consumption changes rapidly at the certain depth of rock placed. When the sample is obtained, it should be sealed and packed in a container. Then, the container is transformed to earth environment.

Based on the limit equilibrium principle of soil, the equations for the limit equilibrium principle of soil can be expressed as

$$\sum F_x = 0, P_c \sin(\alpha + \delta) = R_c \sin(\beta + \varphi) + \frac{\tau_c w_c d \cos \beta}{\sin \beta} \quad (6)$$

$$\sum F_y = 0, P_c \cos(\alpha + \delta) + R_c \cos(\beta + \varphi) = \frac{\gamma d w_c}{2} + \frac{\tau_c w_c d \sin \beta}{\sin \beta} + q w_c \quad (7)$$

The total horizontal cutting force is

$$H = H_h + H_l$$

$$= \frac{\sin(\alpha + \delta) + \cos(\beta + \varphi)}{\sin(\alpha + \beta + \delta + \varphi)} \cdot \left\{ \frac{\gamma d w_c}{2} \left[1 + \frac{2r}{3w_c} \sin \rho' \right] + \tau_c d w_c \left[1 + \cot \beta \cot(\beta + \varphi) \right] \left[1 + \frac{r}{w_c} \sin \rho' \right] + q w d \left[1 + \frac{r}{w_c} \sin \rho' \right] \right\}$$

To verify the proposed theory computed out from cloud-based system, a cutting speed test was conducted with a cutter of fixed structure parameters. The soil cutting process is shown in Fig. 15. For curves with different velocity as shown in Figure 3. The no-load cutting force is 15.2 N. The average and the calculated values can be expressed in Figure 4: the test values coincide closely with the calculated values.



Fig3. SLC cutting soil process

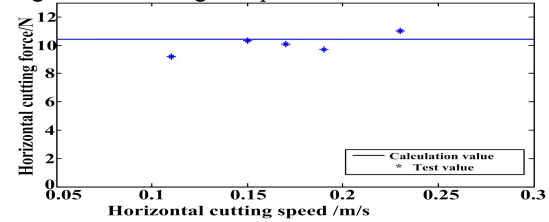


Fig4. Calculated and test values

(3) Applications of Cloud Based Distributed System in Scientific Fields

In the biomedicine field, cloud based system offers great assistance in rational designing of microorganism metabolics [38-42] and anti-cancer drugs [43-48], refining protein-DNA based electron density models [49,50], as well as finding carcinogenic mechanisms across big data bases [51]. A new trend using cloud based system has been seen in the field of energy chemistry [52, 53]:

Fuel cells have been demonstrated to be promising power generation devices to address the current global energy and environmental challenges. One of the many barriers to commercialization is the cost of precious catalysts needed to achieve sufficient power output. Platinum-based materials play an important role as electrocatalysts in energy conversion technologies. To improve catalytic efficiency and facilitate rational design and development of new catalysts, understanding structure-function relationships that underpin catalytic activity must be at a fundamental level. Therefore, researchers employed a combination of empirical potential simulations and DFTB calculations to investigate structure-function relationships of small PtN (N = 2-80) clusters on model carbon (graphene) supports [52,53]. Due to the conveniences from the cloud-based computing and storage system, the simulation of the catalysis can be achieved with great ease [54,55]:

Formally, the total energy, E , of a tight-binding system can be expressed within the DFTB approximation as

$$E = E_{bs} + E_{Coul} + E_{rep}$$

The potential function, is treated as an empirical function that is to be determined by fitting to experimental data and/or data from higher-level electronic structure calculations on the cloud systems. The quality of DFTB parameterization is

tested by comparing cluster formation energies calculated using both DFTB and DFT as shown. The formation energy for a Pt_mRu_n cluster (on a per atom basis) is defined as

$$E_f = [E(\text{Pt}_m\text{Ru}_n) - m E_{\text{Pt}} - n E_{\text{Ru}}]/(m + n),$$

where $E(\text{Pt}_m\text{Ru}_n)$ is the total energy of the cluster, and E_{Pt} and E_{Ru} are the energies per atom of bulk FCC Pt and HCP Ru, respectively. Test geometries for each size and composition are based on cluster morphologies from previous study on Pt nanoclusters. Test geometries for each size and composition are based on cluster morphologies from previous study on Pt nanoclusters.¹⁸ Both are contributed by cloud calculation. Ru and PtRu clusters are simply generated by replacing Pt atoms in these clusters and subjecting them to structural relaxation. In general, researchers see that for both homo-elemental as well as alloy clusters, the DFTB formation energies faithfully represent the target DFT data. Indeed, in addition to R-squared values being very close to one, indicating small statistical scatter, the slopes of the fits are also close to unity, indicating excellent one-to-one correspondence in the DFTB and DFT formation energies. Based on this successful parameterization, researchers further pursued next a few examples of GA-based morphological optimization of PtRu alloy clusters. As an example application, they have employed the validated DFTB parameter set within a Genetic Algorithm for structural optimization of PtRu clusters and showed that the procedure correctly captures surface segregation of Pt in PtRu nanoclusters. The cloud based storage system application facilitates greatly in the optimization: the low-energy structures predicted by the DFTB-based GA can serve as good starting points for future investigations of electronic properties and catalytic activity with higher-level DFT calculations. More broadly, the new DFTB parameter set for Pt-Ru interactions presented in this work opens up avenues for detailed investigation of structure–function relationships in this important class of catalytic materials.

3. SUMMARY

With the rise of cloud computing and big data, distributed storage systems have been witnessed in a rapid increase for its scale as well as its precision in calculation [56–58]. The proposed professional models can help the design, implementation and deployment of distributed storage systems at various aspects [59, 60], including system reliability, security [61, 62], efficiency, availability, cost, usability and processing capacity.

REFERENCES

[1] ZENG Y, XIE Z, YU Y, et al. Ecohydrological effects of stream–aquifer water interaction: a case study of the Heihe River basin, northwestern China.

Hydrology and Earth System Sciences, Copernicus GmbH, 2016, 20(6): 2333–2352.

[2] Baiyu Chen, Guilin Liu, 2017, Zhagn jianfang et al., A calculation method of design wave height under the three factors of typhoon: China, ZL 2016 1 0972118.X. Patent, 2016-10-31.

[3] WANG L-P, CHEN B-Y, CHEN C, et al. Application of linear mean-square estimation in ocean engineering. China Ocean Engineering, Chinese Ocean Engineering Society, 2016, 30(1): 149–160.

[4] Liping Wang, Liu Guilin, baiyu Chen et al., et al., Typhoon influence considered method for calculating combined return period of ocean extreme value: China, ZL 2010 1 0595807.6. Patent, 2013-03-20.

[5] Guilin Liu, Zheng Zhenjun, Liping Wang, et al., Power-type wave absorbing device and using method thereof: China, ZL 2015 1 0575336.5. Patent, 2017-11-03.

[6] KOU Y. Structural and Kinetic Study of N7-methyl, N7-benzyl and C8-chloro Guanine Lesions Using Human DNA Polymerase [beta]. 2015.

[7] XIE Z-H, ZENG Y-J, XIA J, et al. Coupled modeling of land hydrology–regional climate including human carbon emission and water exploitation. Advances in Climate Change Research, 2017, 8(2): 68–79.

[8] Chen Y, Wang Z, Whalley D and Lu L. Remix: On-demand live randomization. In Proceedings of the Sixth ACM Conference on Data and Application Security and Privacy (pp. 50–61). Mar, 2016. ACM.

[9] CHEN B, ESCALERA S, GUYON I, et al. Overcoming Calibration Problems in Pattern Labeling with Pairwise Ratings: Application to Personality Traits. Computer Vision – ECCV 2016 Workshops. Springer, Cham, 2016: 419–432.

[10] WANG L-P, CHEN B, ZHANG J-F, et al. A new model for calculating the design wave height in typhoon-affected sea areas. Natural Hazards, Springer Netherlands, 2013, 67(2): 129–143.

[11] PONCE-LÓPEZ V, CHEN B, OLIU M, et al. ChaLearn LAP 2016: First Round Challenge on First Impressions - Dataset and Results. Computer Vision – ECCV 2016 Workshops. Springer, Cham, 2016: 400–418.

[12] CHEN B, YANG Z, HUANG S, et al. Cyber-physical system enabled nearby traffic flow modelling for autonomous vehicles. 36th IEEE International Performance Computing and Communications Conference, Special Session on Cyber Physical Systems: Security, Computing, and Performance (IPCCC-CPS). IEEE, 2017.

[13] ESCALANTE H J, PONCE-LÓPEZ V, WAN J, et al. ChaLearn Joint Contest on Multimedia Challenges Beyond Visual Analysis: An overview. 2016 23rd International Conference on Pattern Recognition (ICPR). 2016: 67–73.

- [14] CHEN B, LIU G, WANG L. Predicting Joint Return Period Under Ocean Extremes Based on a Maximum Entropy Compound Distribution Model. *International Journal of Energy and Environmental Science*, 2017,2(6): 117-126. 2017.
- [15] ANTHONY BARRS, CHEN BAIYU, How Emerging Technologies Could Transform Infrastructure. <http://www.governing.com/gov-institute/voices/col-hyperlane-emerging-technologies-transform-infrastructure.html>.
- [16] Zhang SF, Shen W, Li DS, Zhang XW, Chen BY, Nondestructive ultrasonic testing in rod structure with a novel numerical Laplace based wavelet finite element method. *Latin American Journal of Solids and Structures*, 2018, 15(7):1-17, e48.
- [17] Zeng Y, Xie Z. Projection and evaluation of the land-atmosphere coupling strength over China by CMIP5 models. *Climatic and Environmental Research*, 2015, 20 (3): 337–346.
- [18] JIA B, XIE Z, ZENG Y, et al. Diurnal and seasonal variations of CO₂ fluxes and their climate controlling factors for a subtropical forest in Ningxiang. *Advances in Atmospheric Sciences*, Science Press, 2015, 32(4): 553–564.
- [19] Liu S, Xie Z, Zeng Y. Discharge Estimation for an Ungauged Inland River in an Arid Area Related to Anthropogenic Activities: A Case Study of Heihe River Basin, Northwestern China. *Advances in Meteorology*, Hindawi, 2016.
- [20] Kou Y, Koag M-C, Lee S. Structural and kinetic studies of the effect of guanine-N7 alkylation and metal cofactors on DNA replication. *Biochemistry*, 2018.
- [21] Chen Y, Zhang Y, Wang Z, Xia L, Bao C and Wei T. Adaptive android kernel live patching. In *Proceedings of the 26th USENIX Security Symposium (USENIX Security 17)*. Aug, 2017.
- [22] Wang X, Chen Y, Wang Z, Qi Y and Zhou Y. SecPod: a Framework for Virtualization-based Security Systems. In *USENIX annual technical conference* (pp. 347-360). July, 2015.
- [23] Zhou Y, Wang X, Chen Y and Wang Z. Armlock: Hardware-based fault isolation for arm. In *Proceedings of the 2014 ACM SIGSAC Conference on Computer and Communications Security* (pp. 558-569). Nov, 2014. ACM.
- [24] Lei X, Shi H, Kou Y, et al. Crystal Structure of Apo MEF2B Reveals New Insights in DNA Binding and Cofactor Interaction. *Biochemistry*, 2018, 57(28): 4047–4051.
- [25] Chen Y, Khandaker M and Wang Z. Pinpointing vulnerabilities. In *Proceedings of the 2017 ACM on Asia Conference on Computer and Communications Security* (pp. 334-345). Apr, 2017. ACM.
- [26] Liping Wang, Liu Guilin, baiyu Chen et al., Typhoon based on the principle of maximum entropy waters affect the design wave height calculation method: China, ZL 2010 1 0595815.0[P]. Patent, 2015-08-19.
- [27] ZENG Y, XIE Z, YU Y, et al. Effects of anthropogenic water regulation and groundwater lateral flow on land processes. *Journal of Advances in Modeling Earth Systems*, 2016, 8(3): 1106–1131.
- [28] ZENG Y, XIE Z, LIU S. Seasonal effects of irrigation on land-atmosphere latent heat, sensible heat, and carbon fluxes in semiarid basin. *Earth System Dynamics*, Copernicus GmbH, 2017, 8(1): 113–127.
- [29] ZENG Y, XIE Z, ZOU J. Hydrologic and Climatic Responses to Global Anthropogenic Groundwater Extraction. *Journal of climate*, American Meteorological Society, 2016, 30(1): 71–90.
- [30] Deng Z Q, Tian Y, Tang D W, et al. (2013). Research on new structure coring bit for extraterrestrial bodies exploration. *Chin. J. Mech. Eng.*, 49(19), 104–110
- [31] TIAN YE, DENG ZONG-QUAN. Coring Bit with Enhanced Structural Parameters for Improved Lunar Soil Sampling and Reduced Mechanical Disturbance. *Journal of aerospace engineering*, American Society of Civil Engineers, 2016, 29(4): 04016015.
- [32] TIAN Y, DENG Z-Q, TANG D-W, et al. Drilling Power Consumption Analysis of Coring Bit in Lunar Sample Mission. *Journal of aerospace engineering*, American Society of Civil Engineers, 2017, 30(5): 04017055.
- [33] TIAN Y, SUN Z H, ZHANG L. Analysis of Structural Parameters of Flexible Spiral Conveyor Blades and Study of its Transmission Power. *Ammonia Plant Safety and Related Facilities*, 2012, 200: 455–458.
- [34] TIAN Y, TANG D, DENG Z, et al. Drilling power consumption and soil conveying volume performances of lunar sampling auger. *Chinese Journal of Mechanical Engineering*, Chinese Mechanical Engineering Society, 2015, 28(3): 451–459.
- [35] Tian, Y., Deng, Z. Q, and Tang, D. W. (2012). Structure parameters optimization and simulation experiment of auger in lunar soil drill-sampling device. *Chin. J. Mech. Eng.*, 48(23), 10–15 (in Chinese).
- [36] Ye Tian, Panpan Yuan, Fei Yang, et al. Research on the Principle of a New Flexible Screw Conveyor and Its Power Consumption. *Applied Sciences*. 2018, 8(7): 1038-1045.
- [37] Tian, Y., Deng, Z.Q, Tang, D.W., et al. Power consumption of lunar subsurface coring driller and earth environment stimulant experiments. *Journal of Jilin University Engineering and Technology* Edition.2016
- [38] CHEN J, GOMEZ J A, HÖFFNER K, et al. Spatiotemporal modeling of microbial metabolism. *BMC systems biology*, 2016, 10: 21.

- [39] PHALAK P, CHEN J, CARLSON R P, et al. Metabolic modeling of a chronic wound biofilm consortium predicts spatial partitioning of bacterial species. *BMC systems biology*, 2016, 10(1): 90.
- [40] CHEN J, GOMEZ J A, HÖFFNER K, et al. Metabolic modeling of synthesis gas fermentation in bubble column reactors. *Biotechnology for biofuels*, 2015, 8: 89.
- [41] CHEN J, HENSON M A. In silico metabolic engineering of *Clostridium ljungdahlii* for synthesis gas fermentation. *Metabolic engineering*, 2016, 38: 389–400.
- [42] CHEN J, DANIELL J, GRIFF D, et al. Experimental testing of a spatiotemporal metabolic model for carbon monoxide fermentation with *Clostridium autoethanogenum*. *Biochemical engineering journal*, 2018, 129: 64–73.
- [43] KOU Y, KOAG M C, CHEUN Y, et al. Application of hypiodite-mediated aminyl radical cyclization to synthesis of solasodine acetate. *Steroids*, 2012, 77(11): 1069–1074.
- [44] KOU Y, CHEUN Y, KOAG M C, et al. Synthesis of 14',15'-dehydro-ritterazine Y via reductive and oxidative functionalizations of hecogenin acetate. *Steroids*, 2013, 78(2): 304–311.
- [45] CHEUN Y, KOAG M C, KOU Y, et al. Transesterification-mediated E-ring opening and stereoselective “Red-Ox” modification of furostan. *Steroids*, 2012, 77(3): 276–281.
- [46] KOAG M C, CHEUN Y, KOU Y, et al. Synthesis and structure of 16,22-diketocholesterol bound to oxysterol-binding protein Osh4. *Steroids*, 2013, 78(9): 938–944.
- [47] CHEUN Y, KOU Y, STEVENSON B, et al. Synthesis of C17-OH-north unit of ritterazine G via “Red-Ox” modifications of hecogenin acetate. *Steroids*, 2013, 78(7): 639–643.
- [48] KOU Y, LEE S. Unexpected opening of steroidal E-ring during hypiodite-mediated oxidation. *Tetrahedron letters*, 2013, 54(31): 4106–4109.
- [49] KOAG M-C, KOU Y, OUZON-SHUBEITA H, et al. Transition-state destabilization reveals how human DNA polymerase β proceeds across the chemically unstable lesion N7-methylguanine. *Nucleic acids research*, 2014, 42(13): 8755–8766.
- [50] KOU Y, KOAG M-C, LEE S. N7 methylation alters hydrogen-bonding patterns of guanine in duplex DNA. *Journal of the American Chemical Society*, 2015, 137(44): 14067–14070.
- [51] LEI X, KOU Y, FU Y, et al. The cancer mutation D83V induces an α -helix to β -strand conformation switch in MEF2B. *Journal of molecular biology*, 2018.
- [52] GASPER R, SHI H, RAMASUBRAMANIAM A. Adsorption of CO on Low-Energy, Low-Symmetry Pt Nanoparticles: Energy Decomposition Analysis and Prediction via Machine-Learning Models. *Journal of Physical Chemistry C, American Chemical Society*, 2017, 121(10): 5612–5619.
- [53] SHI H, KOSKINEN P, RAMASUBRAMANIAM A. Self-Consistent Charge Density-Functional Tight-Binding Parametrization for Pt-Ru Alloys. *The journal of physical chemistry. A*, 2017, 121(12): 2497–2502.
- [54] SHI H, AUERBACH S M, RAMASUBRAMANIAM A. First-Principles Predictions of Structure–Function Relationships of Graphene-Supported Platinum Nanoclusters. *Journal of Physical Chemistry C, American Chemical Society*, 2016, 120(22): 11899–11909.
- [55] SHI H, MIGUES A N, AUERBACH S M. Ab initio and classical simulations of the temperature dependence of zeolite pore sizes. *Green chemistry: an international journal and green chemistry resource: GC, The Royal Society of Chemistry*, 2014, 16(2): 875–884.
- [56] CHEN B, WANG B. Location Selection of Logistics Center in e-Commerce Network Environments. *American Journal of Neural Networks and Applications, Science Publishing Group*, 2017, 3(4): 40–48.
- [57] WANG L, XU X, LIU G, et al. A new method to estimate wave height of specified return period. *Chinese journal of oceanology and limnology = Zhongguo hai yang hu zhao xue bao / edited by the Chinese Society of Oceanology and Limnology, Science Press*, 2017, 35(5): 1002–1009.
- [58] LIU G, CHEN B, WANG L, , et al. Wave Height Statistical Characteristic Analysis. *Journal of oceanology and limnology*. 2018, 36(4):1123–1136.
- [59] Zeng Y, Xie Z, Liu S, et al. Global land surface modeling including lateral groundwater flow. *Journal of Advances in Modeling Earth Systems*. 2016, 10.
- [60] Xie Z, Liu S, Zeng Y, et al. A high-resolution land model with groundwater lateral flow, water use, and soil freeze-thaw front dynamics and its applications in an endorheic basin. *Journal of Geophysical Research: Atmospheres*. 2018, 123.
- [61] Chen, Y., Khandaker, M. and Wang, Z., Secure in-cache execution. In *International Symposium on Research in Attacks, Intrusions, and Defenses* (pp. 381–402). Sep, 2017. Springer, Cham.
- [62] Song, J.; Feng, Q.; Wang, X.; Fu, H.; Jiang, W.; Chen, B. Spatial Association and Effect Evaluation of CO₂ Emission in the Chengdu-Chongqing Urban Agglomeration: Quantitative Evidence from Social Network Analysis. *Sustainability* 2019, 11, 1

Research and Construction of Practical Teaching System of Software Engineering Specialty Based on CDIO

Yan Yang*, Sai Wang

Computer School, Central China Normal University, Wuhan, 430079, China

*E-mail: ms_yangyan@163.com

Abstract: With the continuous development of modern information technology, software engineering majors in colleges and universities are facing enormous challenges and opportunities. In order to train more applied talents of software engineering specialty and meet the needs of enterprises for talents, innovative teaching methods should be introduced into software engineering specialty in colleges and universities. The purpose is to improve students' practical ability and practical innovation ability, so that students can master more professional knowledge and skills through practice. Based on this, this paper takes the CDIO innovation education concept as the starting point, and makes a detailed analysis of the construction strategy of practical teaching system of software engineering specialty based on CDIO, which provides a reference for software engineering teaching in the future.

Key words: CDIO; Software Engineering; Practical Teaching

1. INTRODUCTION

With the continuous development of computer software industry, the demand for related talents is increasing day by day. Although there are many graduates of software engineering majors in colleges and universities every year, there are not many fresh students who can really meet the actual needs of talents in enterprises. The main reason for this phenomenon is that the training of schools does not meet the actual development needs of enterprises. Mainly because of the impact of the social environment, the various costs of enterprises are rising, especially the cost of human resources. Enterprises hope that the staff they recruit can immediately take up their posts. This will save a lot of training costs for enterprises, but schools mostly focus on the theoretical training of students, which is contrary to the needs of enterprises. On the other hand, the curriculum of software engineering specialty in colleges and universities is too old, and there is a gap between the talents trained and the actual needs of enterprises [1-3].

Table 1 Practical Teaching System for Software Engineering Majors

Title		Semester	Credit	Duration
In-class Experimental Courses	Introduction to Computer Science	1	0.25	8 class hours
	High-level Language Programming	2	1	32 class hours

The CDIO mode is a mode with conception, design, implementation and operation as its core content, mainly taking product life cycle as its main line, so as to realize the engineering teaching concept. It is mainly used to guide specific teaching. It can systematically put forward the syllabus of training ability. It includes four kinds of first-level ability, 17 groups and two groups of ability, 73 kinds of specific ability, including students' basic engineering ability, personal quality level, cooperation and communication ability, engineering adaptability and regulation ability. Among them, the CDIO mode systematically and comprehensively puts forward specific operational testing standards. In a word, CDIO mode is a competency-based training mode, which is quite different from the traditional knowledge-based training mode [4-5]. The application of CDIO-based teaching may help software engineering majors to get better achievements, and also plays an important role in the cultivation of their professional qualities.

2. TIME ALLOCATION OF PRACTICAL TEACHING SYSTEM IN SOFTWARE ENGINEERING SPECIALTY

The content of programming course design is started from the freshman year of the students. In every specialized course, there are relevant experimental training and practical exercises. Practice is usually arranged after the end of theoretical courses, and each important professional course has a long practice time, so that the theoretical knowledge learnt by students in class can be well applied, but also conducive to students' full mastery of theoretical knowledge. The design of practical training course provides a chance for students to establish correlation between knowledge points comprehensively. If knowledge theory and experiment are added, the content that students master is not deep enough, lacking a comprehensive and in-depth understanding, which affects students' comprehensive application ability. Improve the practical course of computer and enhance students' hands-on ability. Details are shown in Table 1 below.

	Data Structure	3	1	32 class hours
	Digital Logic	3	0.5	16 class hours
	Object-Oriented Programming	3	0.5	16 class hours
	Java Language Programming	4	0.5	16 class hours
	Principle of Database	4	0.5	16 class hours
	Design and Analysis of Algorithms	4	0.5	16 class hours
	Principle of Computer Composition	4	0.5	16 class hours
	Principle of Operating System	5	0.5	16 class hours
	Computer Network	6	0.5	16 class hours
	Course Design of Database	5	1	32 class hours
	Software Engineering Course Design	7	1	32 class hours
	Software Test Management	6	0.5	16 class hours
	Course Design of Software Testing and Quality Assurance	6	1	32 class hours
	Embedded System Development Technology	7	0.5	16 class hours
Out-school Production Practice		6-7	16	12 weeks
Probation		4-5	2	2 weeks
Graduation Design and Thesis Writing		8	6	6 weeks
Other Practical Activities	Summer comprehensive training	Summer	6	6 weeks
	In-school production practice	6-7	8	8 weeks

3. THE CONSTRUCTION STRATEGY OF PRACTICAL TEACHING SYSTEM OF SOFTWARE ENGINEERING SPECIALTY BASED ON CDIO

3.1 Reforming the Content of Theory Course

Because the time of practice increases and the time of theory decreases relatively, it is likely to cause some students' theoretical foundation is not solid, so when explaining theoretical knowledge, we must clear up the basic content, key and difficult points of theory, and strengthen students' pre-class preparation work arrangement. At the same time, when explaining theoretical knowledge in class, teachers can use more modern technology teaching tools, such as multimedia, micro-class and other forms, and integrate network resources so that they can serve the theoretical teaching of students.

3.2 Construction of Practical Teaching System

Software engineering specialized curriculum design is a good supplement to practical teaching for software engineering majors. Students can master the theoretical knowledge with deepened and expanded understanding. The professional theoretical knowledge and practical projects will be integrated to maintain the application-oriented characteristics, so that students can use what they have learned to master the ability to develop practical systems innovatively. Therefore, when constructing the practical teaching system of software engineering specialty, we should consider not only the students' acceptance of the basic contents of the specialty, but also the students' practical operation ability. Therefore, referring to the basic requirements of IT industry for applied talents and CDIO engineering teaching system, the practical teaching system of software engineering specialty is divided into three aspects: professional basic knowledge ability, professional engineering application ability and professional comprehensive quality ability.

3.2.1 Professional Basic Knowledge Ability

Professional basic knowledge ability refers to the content of curriculum design and curriculum design in the process of professional basic theory teaching, and enables students to master basic computer application technology in the course of curriculum design and independent training, and have corresponding ability.

3.2.2 Construction of Engineering Application Ability
Professional engineering application ability is mainly to simulate the development model of IT industry and to conduct practical training in schools. The purpose is to enable students to develop and design some simple application systems according to the specific requirements of software engineering, and to enable students to master the most basic system analysis and design capabilities, and to be able to apply professional knowledge and tools for practical activities.

3.2.3 The Construction of Vocational Comprehensive Literacy Ability

The construction of vocational comprehensive literacy competence is mainly through post-oriented, engineering school comprehensive training, enterprise practice, and team-based engineering development model. The purpose is to focus on training students' quality in future vocational work, constantly improve students' ability to use professional technology comprehensively, and lay a good foundation for them to solve practical problems in their work.

3.3 Innovation of Practical Teaching Model

In order to train more applied talents, CDIO engineering education concept is introduced into the practical teaching system of software engineering specialty. Innovating the past teaching methods and models to ensure the implementation and perfection of CDIO education concept in the actual teaching process.

CDIO teaching mode advocates "learning in engineering projects" which is also to comply with the "case-oriented, project-driven" practice teaching mode. When using this theory for specific teaching, teachers should first set up a task to be completed, then let students complete it, and put the teaching content in this task. In order to accomplish this task, students need to put forward feasible solutions by themselves, and then find a group to solve the problem together. In the process of completion, the students usually combine the actual project of the enterprise with the actual content of the teaching. After treatment, in the teaching practice class, the students combine into a project team to complete all the analysis, design, coding, testing, development and maintenance of the project. In this way, students will be placed in the team, in order to better complete the task, students will do their part, in the actual team cooperation to enhance the team spirit of students and solve practical problems.

Based on CDIO's professional accomplishment training and team cooperation ability training, combined with the actual software development scenario, team is the basic unit to carry out. With the leader of the team as the main core, team members are organized to make projects. Team members can work in a division of labor and collaboration, or they can work together to accomplish tasks at a certain stage. In practical teaching, if there are problems, we can let the advanced nature between team and group discuss, analyze and solve. If it cannot be solved, then teachers can give appropriate guidance. Teachers' guidance is very important, and they shoulder the important mission of answering questions and solving puzzles. Teachers encourage students to accomplish tasks through teamwork, but they also need to put forward corresponding suggestions for specific situations. With the help of this way of students' collaboration, students' team cooperation ability will be improved, and students' individual thinking ability and ability to solve practical problems will be enhanced, which will ultimately help students form good creative thinking.

3.4 Strengthen communication between teachers and students

The common communication between teachers and students is not only embodied in the classroom, but also outside the classroom. Teachers and students can also use modern communication tools, such as WeChat and Weibo, to carry out after-class communication. Due to the excessive teaching pressure and the rigid demand of learning progress, it is impossible for teachers to take every student into account in class. Teachers can only take the form of random checks or questioning in order to detect

students' classroom attendance or task completion. But with the widespread use of modern network communication tools, students are very fond of these network communication tools, coupled with students' higher acceptance of new things. By using this communication mode to strengthen the communication between students and teachers, students and teachers can have more opportunities to communicate after class, maintain the friendly relationship between teachers and students, and close the distance between students and teachers.

4. CONCLUSION

Through continuous exploration and analysis, the practical teaching system of CDIO software engineering specialty has been continuously improved in the specific use of software engineering specialty, and the traditional theory-based practical teaching mode has been greatly improved. A comprehensive engineering-oriented practical course has been set up, which provides students with a systematic opportunity to operate their practical abilities and greatly improves their comprehensive abilities, thus realizing a good teaching idea of "learning by doing". Through the analysis of CDIO teaching mode, we strictly implement the specific requirements of IT enterprises for school personnel training in each practical teaching segment, so that students can grow into new engineering applied talents. The application of CDIO-based teaching help software engineering majors to achieve better results, and also plays an important role in the cultivation of their professional qualities.

Reference

- [1] Wang Ping. Construction and Implementation of Practical Teaching System for Computer Science and Technology Specialty [J]. Computer Knowledge and Technology, 2018, 14 (15): 152-153.
- [2] Jiang Yaoyao. Construction and Implementation of Applied Practical Teaching System for Computer Science and Technology Specialty [J]. Computer Knowledge and Technology, 2018, 14 (14): 131-132.
- [3] Su Bingjun, Li Lin. Construction and Implementation of Applied Practical Teaching System for Computer Science and Technology Specialty [J]. E-commerce, 2017 (12): 76-77+85.
- [4] Xie Wenge, Zhou Jun, Tong Yujun, Jiadan. Research on the practical teaching system of Computer Engineering Specialty Based on CDIO [J]. Modernization of education, 2017, 4 (41): 235-236.
- [5] Zhou Jing. Case Study on the Construction of Innovative Practical Teaching System for Computer Major [J]. Computer Education, 2017 (08): 155-158+162.